SAPIENZA
UNIVERSITÀ DI ROMA

ENS

arXiv:1601.01713v1 [cond-mat.soft] 7 Jan 2016

Following the evolution of metastable glassy states under external perturbations: compression and shear-strain

Scuola di Dottorato Vito Volterra - École Doctorale 564 *Physique en Île-de-France*

Dottorato di Ricerca in fisica – XXVIII Ciclo

Candidate

Corrado Rainone

ID number 1207913

Thesis Advisors

Prof. Giorgio Parisi

Dr. Francesco Zamponi

A thesis submitted in partial fulfillment of the requirements
for the degree of Doctor of Philosophy in physics

October 2015

Thesis defended on 21 December 2015
in front of a Board of Examiners composed by:

Prof. Francesco Sciortino (chairman)

Prof. Federico Ricci-Tersenghi

Prof. Giulio Biroli

Dr. Marco Tarzia

Prof. Giorgio Parisi

Dr. Francesco Zamponi

Following the evolution of metastable glassy states under external perturbations: compression and shear-strain

Ph.D. thesis. Sapienza University of Rome - École Normale Superiéure, Paris

© 2015 Corrado Rainone. All rights reserved

This thesis has been typeset by LaTeX and the Sapthesis class.

The research leading to these results has received funding from the European Research Council under the European Union's Seventh Framework Programme (FP7/2007-2013)/ERC grant agreement n° [247328].

Author's email: corrado.rainone@weizmann.ac.il

Alla mia famiglia,
e ai miei amici a Roma, a Parigi,
e ovunque altro li porterà la vita.

Acknowledgments

The research work reported in this thesis has been performed over the course of a jointly-supervised PhD which has taken place both in the École Normale Supérieure of Paris and the University of Rome La Sapienza. First of all, I want to thank my supervisor in Paris, Francesco Zamponi, for suggesting this PhD arrangement which has allowed me to work with some of the best people in the field, and to live an experience of both great scientific and personal growth. I thank my supervisor in Rome, Giorgio Parisi, for always providing an interesting, instructive and original point of view, even on the apparently simplest of problems. I thank both my supervisors for directing and following my work during these years and for many useful teachings which have greatly helped my scientific growth.

I wish to thank all the collaborators that I've worked with during these years (among them Patrick Charbonneau, Yuliang Jin, Manuel Sebastian Mariani, Beatriz Seoane Bartolomè, Hajime Yoshino) for their hard work and invaluable contributions. I thank in particular Pierfrancesco Urbani for many stimulating discussions, and for giving me precious advice on many occasions, not only on scientific matters. I thank as well all the people that I had inspiring discussions with over the course of my PhD (among them Marco Baity-Jesi, Giulio Biroli, Chiara Cammarota, Ulisse Ferrari, Hugo Jacquin, Luca Leuzzi, Andrea Ninarello, Itamar Procaccia, Federico Ricci-Tersenghi, Tommaso Rizzo, Gilles Tarjus, Matthieu Wyart), in particular I wish to thank Francesco Turci for a very stimulating discussion during a workshop in Mainz. I take the occasion to thank the organizers of all the conferences, workshops and schools that I've taken part to over the course of my PhD.

I wish to thank all the friends that I've met in Paris, who have pretty much been my family during my stay there, for the many beautiful moments spent together: Tommaso Brotto, Tommaso Comparin, Matteo Figliuzzi, Silvia Grigolon, Alberto Guggiola, Eleonora De Leonardis, Martina Machet, Elena Tarquini, Gaia Tavoni, and all the others.

And finally, a special thank to my family. I would have never been able to do all this without their love and support.

Contents

Introduction **xi**

1 Supercooled liquids and RFOT **1**
1.1 The glassy slowdown . . . 1
1.1.1 The calorimetric glass transition . . . 2
1.1.2 Fragility and the Vogel-Fulcher-Tammann law . . . 4
1.1.3 Two-step relaxation . . . 5
1.1.4 Real space: the cage . . . 9
1.1.5 Real space: cooperativity . . . 11
1.2 From the slowdown to RFOT . . . 13
1.2.1 The foundations of RFOT . . . 14
1.2.2 Dynamics: MCT and Goldstein's picture . . . 16
1.2.3 Complexity: Kauzmann's paradox . . . 22
1.2.4 Summary of RFOT: for T_{MCT} to T_K. . . . 25
1.2.5 Beyond mean field: scaling and the mosaic . . . 28
1.3 Other approaches . . . 31
1.3.1 Dynamic facilitation theory . . . 31
1.3.2 Frustration limited domains . . . 33

2 Metastable glasses **37**
2.1 Thermodynamics and aging . . . 37
2.1.1 Protocol dependence . . . 39
2.1.2 Ultrastable glasses . . . 41
2.1.3 The jamming transition . . . 44
2.1.4 Theoretical approaches to aging . . . 47
2.2 Driven dynamics and rheology . . . 53
2.2.1 Athermal startup shear protocols . . . 56
2.2.2 The yielding transition . . . 59
2.2.3 Theoretical approaches . . . 61

3 The State Following construction **65**
3.1 The real replica method . . . 65
3.1.1 Quenching: the threshold . . . 67
3.1.2 Annealing: isocomplexity . . . 68
3.1.3 Summary . . . 68
3.2 The two-replica Franz-Parisi potential . . . 69

3.3 Beyond two replicas: the replica chain and pseudodynamics 72

4 The replica symmetric ansatz 75
4.1 Computation of the FP potential 75
4.1.1 Perturbations 76
4.1.2 The replicated entropy and the RS ansatz 77
4.1.3 Final result for the entropy of the glassy state 80
4.1.4 Saddle point equations 80
4.1.5 Physical observables 81
4.2 Stability of the RS ansatz 82
4.2.1 The unstable mode 84
4.3 Results 85
4.3.1 Special limits 86
4.3.2 Compression-decompression 88
4.3.3 Shear strain 92
4.4 Discussion 95
4.4.1 The Gardner transition 95

5 The full replica symmetry breaking ansatz 97
5.1 The potential 97
5.1.1 The fRSB parametrization 98
5.1.2 Expression of the potential and the observables 99
5.2 Results 100
5.2.1 Phase diagrams and MSDs 100
5.2.2 Critical slowing down 103
5.2.3 Fluctuations 105
5.2.4 Shear moduli 107
5.3 Discussion 108
5.3.1 Yielding within the fRSB ansatz 109

6 Numerics in the Mari-Kurchan model 111
6.1 Model 111
6.2 Results 113
6.2.1 Isocomplexity 113
6.2.2 State Following and the Gardner transition 114

7 Conclusions 123
7.1 Summary of main predictions 123
7.2 Strengths and weaknesses of our approach 124
7.2.1 The current status of RFOT 125
7.3 Proposals for further research 126
7.3.1 The Gardner transition in shear 127
7.3.2 State following in AQS protocols 127
7.3.3 Avalanches 127
7.3.4 Yielding 128
7.3.5 Non-linear rheology 129

A The infinite-d solution of hard spheres **131**

B Computation of the replicated entropy in the RS ansatz **135**
B.1 Entropic term . . . 135
B.2 Interaction term . . . 136
B.2.1 General expression of the replicated Mayer function . . . 136
B.2.2 Computation of the interaction term for a RS displacement matrix . . . 138

C Computation of the replicon mode **141**
C.1 The structure of the unstable mode . . . 141
C.2 Entropic term . . . 144
C.3 Interaction term . . . 145

D Computation of the replicated entropy in the fRSB ansatz **149**
D.1 Entropic term . . . 149
D.2 Interaction term . . . 154
D.3 Simplifications for $m = 1$ . . . 157

E Variational equations in the fRSB ansatz **159**
E.1 Lagrange multipliers . . . 159
E.2 A different equation for $G(x)$ . . . 162
E.3 Scaling analysis near jamming . . . 163
E.3.1 Scaling form of the equations . . . 163
E.3.2 Asymptotes and scaling of $\widehat{P}$ and $\widehat{f}$ . . . 164

Bibliography **167**

Introduction

This thesis is about glass. As stupid as this assertion looks, it is indeed important to state this fact loud and clear, at the very beginning.
Why is such an assertion necessary or even appropriate? The glass transition is one of the great unresolved problems in condensed matter physics (as the introduction of pretty much every work on the subject loves to remind) and it has been so for decades. And for decades, research has been produced, and still is, to investigate its nature. A thesis in the field of the physics of the glass transition which says about itself "this thesis is about glass" is therefore stating an obvious tautology, at the very best. The aim of this introduction is to have the reader understand that it is not so, and that indeed the theoretical research on the properties of glasses (as opposed to the huge amount of experimental and numerical work that has been done, and is still being done) is a relatively new subject that we are beginning to explore now.
But a pressing question then arises: what were those "decades of research" referred to above, about? The answer is: not glasses. Or rather, there has been, yes, a ponderous amount of *experimental* research about glasses over the last decades (Tool's works about fictive temperature are an example), which we will reap and use in this thesis. But the *theoretical* research, the research aiming to describe glass-related phenomena at first principle level, has not been very concerned with glass itself. Rather, most of the theoretical efforts carried out up to now are about supercooled liquids, that is, about *equilibrium* properties of glass formers.

This distinction is very important, and yet oftentimes forgotten. Despite this, it is indeed pretty obvious from an intuitive point of view. Every research article about the glass transition will at some point or another contain a sentence of the sort "...it is impossible to obtain data in this regime due to the extremely large time needed to equilibrate the sample...", and indeed, the reason why the glass problem is still open lies mainly in the fact that data in the deeply supercooled regime are, to state it in an unambiguous way, impossible to obtain. And yet, in everyday life, glasses are just everywhere and are indeed quite easy to manufacture; they are not a rare and exotic commodity. But despite this, the impression that one gets from the literature is that getting new data to better understand the glass problem is always sort of a struggle.
The distinction above makes it clear why: what researchers have been, and still are, mostly concerned about is the supercooled liquid. And supercooled liquids, unlike glasses, are indeed very rare and very valuable objects. It is indeed a fact that the various theories about the glass transition that are on the table today (Random First Order, Dynamic Facilitation, Frustration Limited Domains etc.) were conceived

first and foremost as theories about supercooled liquids rather than glasses, and their most defining predictions concern the supercooled regime; this is the reason why it is into that hard-to-reach regime that those much needed data are to be searched for. In such a scenario, the glass is at best seen as an enemy (interestingly, much like the crystal) who sneaks in during your simulation/experiment and ruins your day by pushing out of equilibrium your precious supercooled liquid sample.
In this thesis, we are concerned with glasses.

The problem with formulating a theory about glass lies in the fact that a glass is an intrinsically *out of equilibrium* object, as opposed to the supercooled liquid. This simple fact is at the origin of all problems that are commonly encountered when trying to conceive a theory of glasses. If the theorist is aiming for a first-principle theory, then the obvious starting point is of course statistical mechanics, as in all other branches of theoretical condensed matter physics. But statistical mechanics is a framework mainly concerned with the properties of *equilibrium* systems, whose thermodynamic state is stable, and whose lifetime is infinite. Glass has no such property, as we enunciated before: its properties depend of the time t and a glass does not live forever, but only until the glass former is able to relax and flow again like a liquid. There are theoretical tools conceived for the treatment of out-of-equilibrium scenarios, but they are all meant to deal with situations wherein the system is subject to a drive of some sort (say, an AC current), and they are meant for systems with long-range order. Glass is amorphous, and is out of equilibrium because it did not have enough time to relax, not because we are perturbing it in some way. So those tools are not suitable for our problem.
At this point, it looks like a meaningful theory of glass cannot make do without a time-based description, a view which the Dynamical Facilitation Theory (DFT), for example, embraces heartily; however, the dynamics of generic many-body systems, and in particular glass formers, does not enjoy a unified and commonly accepted first-principles framework such as the one that statistical mechanics is able to provide for systems in thermodynamic equilibrium. We will see over the course of this thesis that this weakness is manifest within DFT, whose models are necessarily phenomenological in nature and never start from a microscopic, first-principles description of the glass-forming liquid. So, it looks like one is between the proverbial rock and hard place: to have a first-principles theory, one must try to rely on dynamics; but to rely on dynamics, the theoretician necessarily has to sacrifice something in terms of microscopic description (like in DFT) or simplifying assumptions (like in Mode Coupling Theory).

However, if one actually looks at how the properties of a glass change over time (for example, its internal energy U as a function of time, or any other convenient observable), one can see that the dependence on t is actually pretty simple, i.e. the dynamics looks like a *quasi-equilibrium* process wherein the observables of the system remain stable over very long time periods, of the order of the impossibly long equilibration time needed to observe the supercooled liquid. This picture of glass as a system in quasi-equilibrium (or *restricted equilibrium*, as we will say more often) is at the root of the Random First Order Theory (RFOT) of the glass transition that this thesis is based on.
The RFOT posits that the glass transition is, yes, a dynamic phenomenon, but that it has a static origin. This origin comes in the form of a *Free Energy Land-*

scape (FEL), which is essentially a very rough landscape (think of a golf course, for example) of valleys (minima) separated by ridges (saddles), wherein single point, representing the glass former, has to navigate towards the bottom of the lowest valley in order to attain equilibration. The dynamics of the system then unfolds as a series of downhill jumps over the ridges (an *activation event*) separated by long persistence times within the valleys (referred to as *metastable states*). The large times needed for activated jumps to take place delay the onset of equilibration and cause the system to behave in a "glassy" manner, and as a result of this, the persistence times are so large that the system is effectively trapped (or equivalently, equilibrated) inside a metastable state for all times which are relevant for experimental and practical purposes.

What is most important about the FEL is that it is a *static* object, in the sense that it is uniquely determined by the equilibrium properties of the system, with no dynamics or time in play. Despite the fact that it prominently affects the dynamics of the glass former, it can be in principle studied with suitable static tools. This scenario opens the possibility that the whole phenomenology of glass could be in principle described by focusing on the study of the valleys (minima) that the system is trapped into during the time regime before equilibration, when the glass exists. In particular, since the system is equilibrated within a metastable state, one could in principle construct a *restricted thermodynamics* by defining a Gibbs measure which only accounts for the micro-configurations which are visited by the system as it vibrates inside this single minimum. From such a measure one could then compute a partition function, a thermodynamic potential, and finally, physical observables. Such a construction is referred to as *State Following* construction within the theory of generic systems (not only structural glasses) with a rough FEL and a consequent RFOT-like behavior. In this thesis we present and apply this construction to a realistic model of glass former, namely Hard Spheres (HS). We show how it allows to construct a fully analytic theory of glass, entirely from first principles, without the need to resort to dynamical tools; we show how it allows to obtain results for physical observables which are in agreement with the established phenomenology of glasses, and we show how it is also able to provide new insights into, and predictions about, the nature of the glass phase.

This thesis is organized as follows: in chapter 1, we give the fundamentals of the glass problem (with emphasis on the central phenomenon of the glassy slowdown) as a way to properly introduce RFOT and its physical picture; in chapter 2, we review the phenomenology of glasses as measured in experiments and simulations, in particular Differential Scanning Calorimetry and quasi-static shear strain, corresponding to adiabatic changes of the temperature T and of the strain parameter γ, respectively; in chapter 3 we present and review in detail the state following construction, along with some of the other tools which can be used within RFOT to approach the problem of metastability in general; in chapter 4 we perform the state following computation for the HS model in the mean-field limit, assuming the simplest possible structure for a glassy minimum (i.e. a simple paraboloid), and present the results so obtained; in chapter 5 we dispense with this last assumption and perform a more general computation for a arbitrarily complicated structure of the glassy minima, and present the results so obtained; in chapter 6 we provide some comparison with numerics in a simple, modified HS model which allows for a

simple analytical treatment and is also very easy to simulate; finally, in chapter 7, we summarize our conclusions and provide some suggestion for further research in the field of glass physics.

The results presented in this thesis have been for the great part already published, but here we present them in a coherent and hopefully self-contained manner. We refer the interested reader to

- Chapter 4: [1] C. Rainone, P. Urbani, H. Yoshino, F. Zamponi, "Following the Evolution of Hard Sphere Glasses in Infinite Dimensions under External Perturbations: Compression and Shear Strain", *Phys. Rev. Lett.* **2015**, *114*, 015701.
- Chapter 5: [2] C. Rainone, P. Urbani, "Following the evolution of glassy states under external perturbations: the full replica symmetry breaking solution", *ArXiv e-prints* **Dec. 2015**.
- Chapter 6: [3] M. S. Mariani, G. Parisi, C. Rainone, "Calorimetric glass transition in a mean-field theory approach", *Proceedings of the National Academy of Sciences* **2015**, *112*, 2361–2366; and [4] P. Charbonneau et al., "Numerical detection of the Gardner transition in a mean-field glass former", *Phys. Rev. E* **2015**, *92*, 012316.

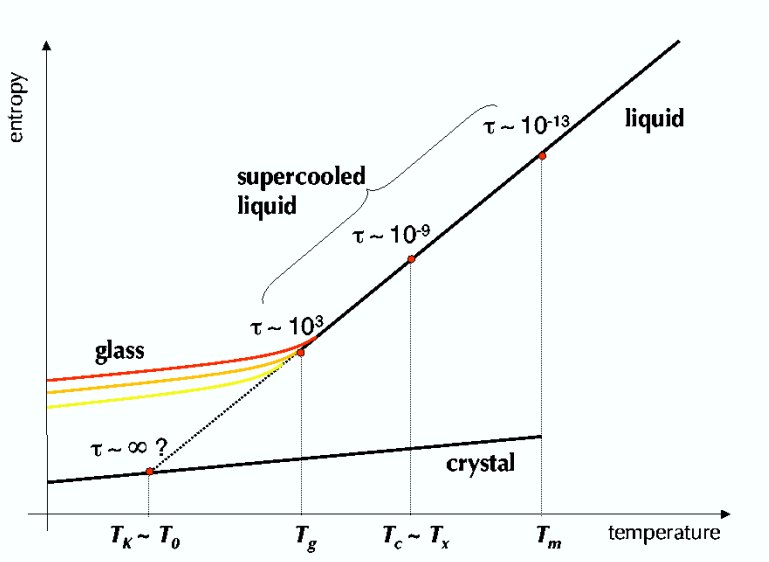

Figure 0.1. The equations of state of a prototypical glass former. We can distinguish the crystalline branch, the supercooled branch and, in color, the various metastable glass branches. As a guide, in this thesis we will mainly focus on cooling protocols wherein one moves down the supercooled branch and then into the glassy branches, down to $T = 0$. We will not be concerned with the deeply supercooled branch (dashed line). Reprinted from [5].

Chapter 1

Supercooled liquids and RFOT

In this first chapter we focus on the supercooled and deeply supercooled branches in figure 0.1, as a way to properly introduce the phenomenon of the glassy slowdown, the fundamental notion of *metastable glassy state*, and discuss the Random First Order Theory of the glassy slowdown upon which this thesis is based. We start by reviewing the basic phenomenology of the glass transition, with emphasis on the increase of the relaxation time, along with the manifestation of two-step relaxation. From there, we introduce the basics of RFOT, which posits that the slowdown of the dynamics in the glassy regime can be explained in terms of the insurgence of a great number of *metastable glassy states*, which trap the dynamics and hamper structural relaxation, thereby forcing the glass former in a metastable, out-of-equilibrium glass. We proceed by giving some arguments in support of the RFOT picture, in light of the phenomenology of the glassy slowdown discussed earlier. We then review summarily the RFOT picture over the course of a conceptual cooling experiment on a generic glass former, also discussing the possibility of an ideal glass transition. We conclude the chapter with a brief review of some other approaches to the glass problem.

1.1 The glassy slowdown

Most liquids (although not all of them [5]) crystallize upon cooling at a certain *melting temperature* T_m. However, it is always possible, employing some caution, to *supercool* a liquid below its melting point, avoiding crystallization and producing a *supercooled liquid*.
There are multiple ways to accomplish this. In experiments and industrial applications, one usually cools the liquid fast enough that the nucleation and growth of the crystal takes place on times much longer that the experimental time t_{exp} at which measurements are performed. In simulations, the crystal is usually "killed" by introducing polydispersity, i.e. by considering a liquid whose constituents can have different physical shapes (for example spheres with different diameters), so that an ordered, crystalline arrangement of the particles is inhibited. We do not delve into this issue and refer the reader to the detailed discussion of [5].

Once one has managed to obtain a supercooled liquid, it is possible to lower the temperature further, always minding the possibility of crystallization. On doing so,

one can then observe a dramatic increase of the relaxation time (we denote it as τ_R) (see figure 1.1) over a fairly short range of temperature. Besides this sharpness, this sudden growth is also impressive for its generality: it manifests in systems that range from atomic liquids, to molecular ones, to colloidal compounds and even metallic alloys [6]: any liquid can form a glass if supercooled fast enough [7]. This is already a hint to the fact that the glassy slowdown is a fairly general phenomenon, independent of the actual nature of the glass former under consideration.
We remind the reader that the relaxation time can be defined in terms of the viscosity by Maxwell's relation [5, 8]

$$\eta = G_\infty \tau_R, \tag{1.1}$$

(where G_∞ is the infinite frequency shear modulus) so that the glass former becomes more and more sluggish as the temperature is lowered. This relation is useful since it allows us to pass from a subtle observable like τ_R to a much more tangible physical property like the viscosity.

1.1.1 The calorimetric glass transition

When the viscosity of a liquid is so high, its ability to flow is severely hampered: it takes a time of order τ_R to relax any excitation (for example shear) the glass former is submitted to. This means that on experimental timescales $t_{exp} < \tau_R$ the glass former will effectually respond to an external perturbation as if it were an elastic solid, i.e. it will present a *shear stress* proportional to the strain [8]

$$\sigma = G_\infty \gamma. \tag{1.2}$$

Indeed, if we simply define a solid as any substance that has an elastic response, the glass former is effectively a solid on timescales such that $t_{exp} < \tau_R$. We stress the fact that this has absolutely nothing to do with the glass transition *per se*. The fact that a liquid can respond to shear like a solid on short enough timescales is completely general: solidity is indeed a timescale-dependent notion [9]. However, if we put this together with the glassy slowdown, we see that the time we would have to wait to see a liquid-like response to shear becomes rapidly so large that it becomes effectively impossible to do so. When this happens, we get the *calorimetric glass transition*, defined as the point where the equilibration time of the glass former becomes longer than the experimental time, thereby making it a solid from the point of view of the experimentalist. We have then the following implicit definition for the calorimetric glass transition temperature T_g

$$\tau_R(T_g) \equiv t_{exp}. \tag{1.3}$$

This definition of T_g is the one we are going to follow in the rest of this thesis. However, it can be immediately seen that this definition has a problem, namely the fact the t_{exp} depends on how our particular experiment (i.e. our *protocol*) is designed. It is actually more correct to talk about glass transition temperatures, with a plural; but in order to establish a standard, the convention is to set t_{exp} to

10^2 (sometimes 10^3) seconds[1]. This corresponds to having for the viscosity

$$\eta(T_g) \simeq 10^{13}\text{Poise}, \tag{1.4}$$

To put this number into perspective, water has a viscosity of about 0.01 Poise, and honey's is about between 20 and 100 Poise. A 10cm tall cup containing a liquid with a viscosity of 10^{13} Poise would take about 30 years to empty itself [7], so this value corresponds by all reasonable standards to a solid-like response.

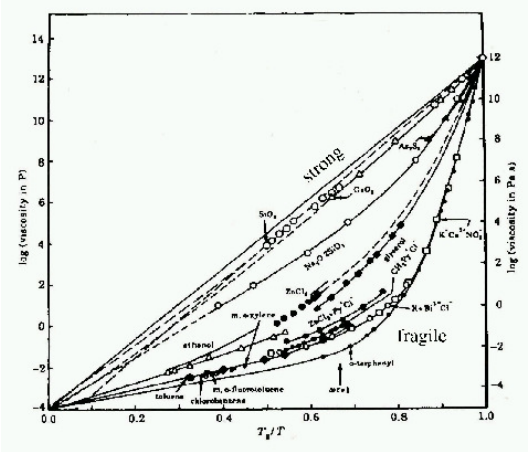

Figure 1.1. Angell's plot. When the (T/T_g) ratio is reduced by just one half, the most fragile glass formers show an increase of the viscosity (and thus the relaxation time) of almost 16 decades, and the viscosity of the strongest ones increases anyway of about 10 decades. This stunningly sharp growth is one of the most impressive phenomenons in all of low energy physics. Reprinted from [6].

The definition of T_g allows us to better appreciate the growth of τ_R at the onset of the glassy slowdown. We can plot on a logarithmic scale the viscosity versus the ratio T/T_g for various glass formers. What we get is the plot in figure 1.1, called *Angell's plot*. From Angell's plot we can clearly see that the growth of the viscosity (and so of τ_R) is at least exponential in T, and for some glass formers is even sharper. This is remarkable especially if one considers that the increase of the viscosity at the melting point T_m is much milder [5].

The definition of the calorimetric glass transition also allows us to introduce a problem which underlies the physics of glasses in general: namely the fact that everything has to be defined in a very anthropocentric way. It is true, as discussed in [5], that the increase of τ_R is so sharp that the actual value of t_{exp} doesn't effectively change matters. But this does not deny the fact that the only reason why we talk about a calorimetric glass transition lies in the fact that we are not patient (or long-lived for that matter) enough to observe the equilibration of the glass former below T_g. One reason for the success of the RFOT theory we are going to discuss lies in the fact that it brought all this dynamical, time-based phenomenology back to a critical phenomenon with a well defined transition temperature, which of course

[1]Indeed, the increase of τ_R is so sharp that the actual choice of t_{exp} does not make much of a difference.

is very appealing to physicists. Nowadays, the actual presence of an underlying critical phenomenon is not perceived anymore as a necessity within RFOT (an avoided transition would be just as good, as we are going to discuss), but it certainly contributed to shaping up the debate in the early days.
Nevertheless, we must stress a point: the calorimetric glass transition is not a transition, and the only relevant phenomenon is the increase of the relaxation time, i.e. the glassy slowdown. This is why this section bears its title.

1.1.2 Fragility and the Vogel-Fulcher-Tammann law

Let us go back to Angell's plot, figure 1.1. As we already said, some glass formers have an exponential increase of τ_R, while some others have an even sharper behavior. When we say "exponential", we can't help but immediately think about Arrhenius' law

$$\tau = \tau_0 \exp\left(\frac{\Delta}{k_B T}\right), \tag{1.5}$$

which gives the time needed, for a system at temperature T, to overcome an energy barrier of height Δ. The fact that the τ_R vs. T dependence is well described by Arrhenius' law already points toward the fact that relaxation in supercooled liquids must have something to do with barrier crossing. This is the first brick we need to introduce the concept of metastable state.
Glass formers which have an Arrhenius-like behavior are referred to as *strong* glass formers in glass physics. The champion of strong glass formers is undoubtedly Silica (SiO_2), namely the ordinary window glass. Conversely, those that have a *super-Arrhenius* behavior are dubbed *fragile* glass formers. Examples of this class are toluene and orto-terphenyl. We remark that the distinction between the two types is not very clear-cut (in figure 1.1 we can see a variety of behaviors rather than two sharply distinct classes), but it's anyway useful.

Because Arrhenius' law is not ok for fragile glass formers, it is automatic to ask how we could fit the $\tau_R(T)$ dependence for fragile glasses. One possible answer has been known, indeed, for quite a long time and is the Vogel-Fulcher-Tamman (VFT) law [10–12]

$$\eta(T) = \eta_\infty \exp\left(\frac{A}{T - T_0}\right). \tag{1.6}$$

The VFT law is purely phenomenological in nature, nothing more than a fit law with three parameters (τ_0, A and T_0) for viscosity data. However, it does a very good job for a great variety of glass formers (see for example [13, 14] for systematic tests of its validity). We can also see that it gives back a pure Arrhenius' law when $T_0 = 0$, so it also allows to interpolate nicely between fragile and strong behavior.

However, we immediately notice that the VFT law says something big: namely, that the relaxation time diverges at a temperature $T = T_0$. This is a very strong statement, as a divergence of the relaxation time would imply that at T_0 there is a phase transition. Not a "calorimetric" transition with a conventional, blurry definition. But a real critical phenomenon with a real critical temperature. Such a statement cries for an experimental, unambiguous validation.
Unfortunately, no such unambiguous validation exist. Although the good job done by the VFT law makes it at least reasonable that a divergence exists (and in the

following we will provide some more arguments in support of its existence), we must not forget that the VFT law is just a fit, meant to interpolate data. And below T_g, by definition, there are no such data. If we follow the convention $t_{exp} = 100s$, take for good the VFT law, and choose reasonably $t_{exp} \approx 10^{14}\tau_0$, $A \approx 10T_0$, we can immediately see that one cannot approach the putative critical point more than $\Delta T \approx \frac{1}{3}T_0$ without falling out of equilibrium first. So, since the VFT law is just a fit, using it to predict a divergence located so far from the region where there are any data to fit looks like an audacious over-stretching. As a matter of fact, choosing the "best" fit is always a very messy affair. There are indeed alternative laws, like Bässler's law [15]

$$\tau_R(T) = \tau_0 \exp\left[K\left(\frac{T^*}{T}\right)^2\right], \tag{1.7}$$

which anyway does a comparably good job and contains no divergence whatsoever. One could even argue that Arrhenius' law is all we need, since even the η vs. T of the most fragile glass formers is approximately a straight line if T is close enough to T_g, which means that it can be fitted to an Arrhenius' law if the range of temperatures is small enough. And there is at least one experiment in the literature [16] wherein, after producing very low-temperature supercooled liquid samples using new techniques[2], no super-Arrhenius behavior is actually observed at all.
In summary: extrapolations, however appealing they may appear, are insidious. The presence or not of a divergence at T_0 (see [17] for a very critical point of view) remains a point of contention to this day.

1.1.3 Two-step relaxation

The growth of τ_R (or equivalently η) around and below T_g has up to now been described with such adjectives as "dramatic", "stunning", and "impressive", and one can easily verify that the whole literature on the subject tends to use similarly grand words when it comes to Angell's plot.
When we consider something to be remarkable, it happens because it exceeds our expectations. And when we talk about physical quantities, having an expectation means having a *scale*, which in our case is t_{exp}. However, as we said before, t_{exp} is not a fundamental scale in any way, but rather a totally anthropocentric and conventional choice. If we were beings with a lifetime such that choosing a timescale of, say, 10^{13} seconds were reasonable, the growth of τ_R would certainly not have appeared as impressive (unless we take a leap of faith and believe that a singularity is present at T_0), and from a qualitative point of view, a glass former would just appear to us as a perfectly normal, flowing liquid. So it looks like the phenomenon of the glassy slowdown looks exciting merely because we look at it with a built-in timescale that the fundamental laws of nature do not share[3].

[2] Namely, vapor deposition. We shall discuss it later when we introduce ultrastable glasses.

[3] My Bachelor's thesis advisor was fond of saying "There only two numbers that matter in physics: zero and one". The reason for this is that we can always choose a scale for the phenomena in study and use it to measure the quantities involved. This statement applies very well to Angell's plot: nothing forbids us to choose a scale such that $\eta(T) \approx O(1)\ \forall T$. And why should a constant curve be of any interest for a physicist? From his point of view, literally nothing is going on, unless it goes to zero or infinity somewhere.

This view seems to be corroborated by the fact that the sudden sluggishness does not seem to be accompanied by any structural change whatsoever. If we look at the structural properties of a glass former around T_g, usually through its *static structure factor* $S(\mathbf{q})$ [18], no relevant change with T is observed [5, 19] (as one can see in figure 1.2), while its relaxation time grows of some 10 orders of magnitude in the same temperature range: if we take a snapshot of a glass former near T_g, which is what the $S(\mathbf{q})$ does, it looks exactly like a liquid, with no long-range order or Bragg peaks. This fact is dismaying from a physicist's point of view, considering that the

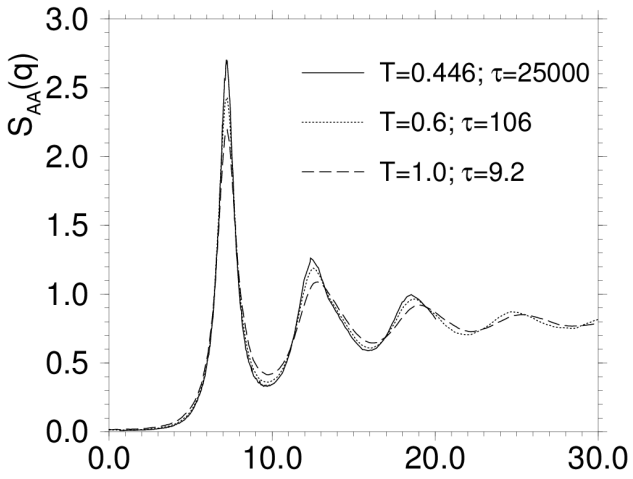

Figure 1.2. The static structure factor of a Lennard-Jones liquid for three different temperatures in the slowdown region. No qualitative changes are observed on lowering T. Reprinted from [19].

wisdom from the theory of critical phenomena suggests that a long relaxation time always comes together with a long correlation length (i.e. *critical slowing down*) [20]. It looks more and more like the glass transition is a problem for chemists and material scientists only, certainly not for physicists. In this paragraph we explain why it is not so, by showing a qualitative fingerprint of glassiness: the two-step relaxation.

Let us consider a model glass former made of N particles. Let us also consider a generic time-dependent observable $\mathcal{O}_i(t)$ relative to particle i. We can define a *dynamical correlation function*

$$C(t,t') = \frac{1}{N}\sum_{i=1}^{N} \langle \mathcal{O}_i(t)\mathcal{O}_i(t') \rangle \,. \tag{1.8}$$

Where $< \bullet >$ denotes an average over the initial condition at $t = 0$. Let us focus on liquids which are approaching the glass transition, but are still equilibrated. In that case the average is carried out using the canonical distribution and the dynamics

depends only on the difference $t - t'$. This is Time Translational Invariance (TTI) [21].
For particle glass formers the observable $\mathcal{O}_i(t)$ is usually the density fluctuation (in Fourier space) relative to particle i

$$\delta\rho_i(\mathbf{q}, t) \equiv \int d\boldsymbol{x}\ e^{-i\mathbf{q}\cdot\boldsymbol{x}}\delta(\boldsymbol{x} - \boldsymbol{x}_i(t)) = e^{-i\mathbf{q}\cdot\boldsymbol{x}_i(t)}. \tag{1.9}$$

With this choice, $C(t, 0)$ coincides with the intermediate scattering function $F_s(\mathbf{q}, t)$ usually measured in inelastic neutron scattering experiments [18].
Since to our knowledge the system has only one timescale τ_R, we would expect for the correlation function a form such as

$$F_s(\mathbf{q}, t) \simeq e^{-\frac{t}{\tau_R}}. \tag{1.10}$$

in principle different $\mathbf{q}$s may correspond to different τ_Rs, but the variations should only amount to a trivial rescaling that leaves intact the VFT dependence on T. So we expect a slower and slower, but nonetheless exponential decay on approaching T_g.

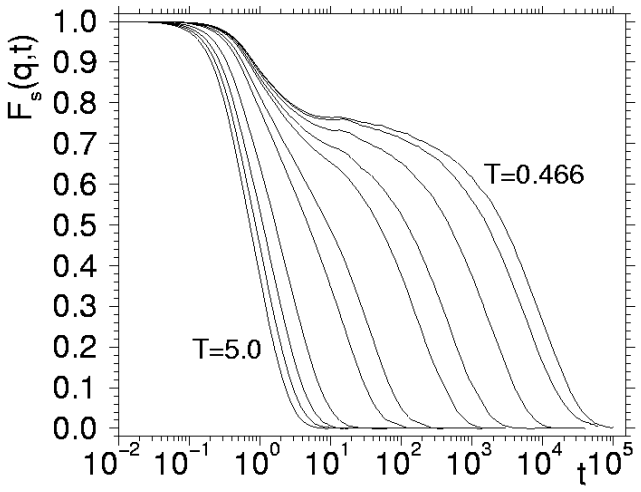

Figure 1.3. The intermediate scattering function obtained from simulation data of a Lennard-Jones liquid in the vicinity of T_g. As the temperature is lowered, two distinct relaxations appear, separated by a plateau of rapidly growing length. Reprinted from [22].

But this is not what is observed, see figure 1.3. For high T, we get the expected exponential relaxation. However, as we approach T_g we can see that the correlator changes shape and the relaxation proceeds in two steps: firstly a fast relaxation (remember that we are watching things in log time) to a plateau with a height C^* different from zero takes place. This first part of the relaxation is not very sensible to the onset of the glassy slowdown. Then, after another time which grows sharply as the temperature is lowered, we get the final structural relaxation. Fittingly, this pattern of decay is called *two-step relaxation* and unlike the simple (however

impressive) growth of τ_R, it is indeed a *qualitative* landmark of glassiness, one that will stay there even if we change our choice of t_{exp}.

So, after all, we were wrong in assuming that the system has only one timescale. Indeed, there are two of them, and only one of the two ultimately causes the slowdown of the dynamics and the growth of τ_R. This means that inside our system there is a well defined separation between *fast* processes, which yield the initial decay on the plateau and are weakly dependent on T, and *slow* processes which are on the contrary deeply affected by the onset of glassiness. The two different steps are called β relaxation (for fast processes) and α relaxation (for slow ones), and each of the two has its associated timescale, τ_β and τ_α respectively. Since structural relaxation is of course dominated by the *slowest* processes, we have

$$\tau_R \simeq \tau_\alpha, \tag{1.11}$$

so that the α-relaxation timescale is the one relevant for equilibration.

The presence of two-step relaxation is our second (an perhaps most important) building block towards the concept of metastable state: the presence of the two well-separated relaxations, with a long, flat plateau in the middle, seems to suggest that a glass can be thought of as a glass former which is *partially* equilibrated (β-relaxation has taken place) but still has to undergo complete equilibration (α-relaxation), whereupon it becomes a supercooled liquid again. This idea of *restricted equilibrium* is the fundamental concept behind the State Following construction.
The presence of partial relaxation is also important for another reason: if the relaxation was a simple (however slow) exponential with a single timescale, then every measurement (even of just one-time observables like, say, the pressure) made on a timescale $t_{exp} \ll \tau_\alpha$ would have shown a dependence on t, thereby dooming to fail any idea that glasses can be described by an equilibrium (i.e. with no dependence on t) approach. The fact that the relaxation of the system is effectively frozen on timescales as long as τ_α, however, saves us from this problem: there is, of course, a dependence of even one-time observables on t (i.e. *aging* [5, 21]), but we have to wait a very long time to observe it, and before that, one-time quantities are effectively constant on timescales which are long, but anyway much shorter than $\tau_\alpha \simeq \tau_R$ [1, 5].
Now, we can finally be more specific in our glass-supercooled liquid distinction. From now on, when we talk about glass, we will mean that we are looking at properties of a glass former, below T_g, on a timescale such that

$$\tau_\beta \ll t_{exp} \ll \tau_\alpha, \tag{1.12}$$

which means that we are looking at the plateau regime. Supercooled liquid instead means that we are looking at properties of a glass former when

$$t_{exp} \gtrsim \tau_\alpha. \tag{1.13}$$

Needless to say, and as we anticipated in the introduction, glasses are much easier to look at.

1.1.4 Real space: the cage

How does the relaxation of a glass former *actually* look like? If we take a look at the actual movement of the particles, in real space, during equilibration, what do we see?
In the next two paragraphs we answer this question. Let us define a new observable, the *mean square displacement* (MSD) of a tagged particle:

$$\langle r^2(t)\rangle \equiv \frac{1}{N}\sum_{i=1}^{N}\left\langle |\boldsymbol{x}_i(t)-\boldsymbol{x}_i(0)|^2\right\rangle, \tag{1.14}$$

which measures how much a particle is able to move from its initial position as time passes. We would expect, for short times, a ballistic regime where $r^2(t)\simeq t^2$, followed then by a diffusive regime [5, 23] with $r^2(t)\simeq D\,t$, where D is the *diffusion coefficient* [5]. However, since we already know that structural relaxation takes place in a two-step manner, we actually expect to see something more interesting.

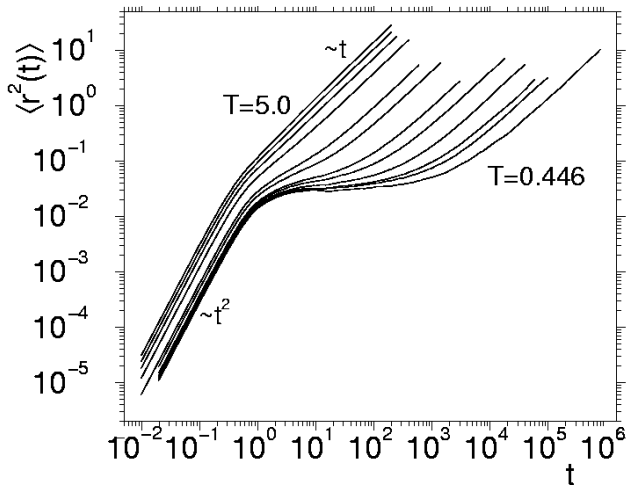

Figure 1.4. The MSD obtained from simulation data of a Lennard-Jones liquid in the vicinity of T_g. At high temperature, a crossover from ballistic to diffusive regime is observed. At the onset of glassiness, a plateau regime in which particles are caged appears. Reprinted from [24].

And we are not disappointed, see figure 1.4. At high temperature, the expected crossover from ballistic to diffusive behavior is observed. As the glassy slowdown sets in, a plateau regime, in which particles cannot move, manifests between the ballistic and diffusive regimes, similarly to what happens for the intermediate scattering function, figure 1.3. Indeed, the timescale necessary to observe diffusion coincides with the α-relaxation time τ_α [24].
This provides a picture of two-step relaxation in real space: on a fast timescale τ_β, the system undergoes an initial relaxation as particles move ballistically. After this, the particles remain stuck for a long time and they ability to move is suppressed: this is the *cage effect*[5, 23]. Particles cannot move away because they are confined

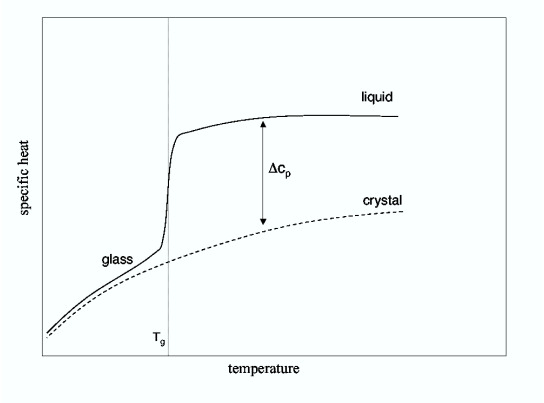

Figure 1.5. Specific heat at constant pressure of a prototypical glass former around the calorimetric glass transition. The liquid has a much higher c_p, but a sharp drop to the crystalline value is observed as the system becomes glassy. Reprinted from [5].

by their neighbors, and thus only vibrate (or rattle) inside their respective cages. These vibrations are very small: the MSD in the plateau regime is in the range of $10^{-2} - 10^{-1}$ particle diameters, and the Lindermann ratio, than compares the amplitude of vibrations with the intermolecular distance, is only about 10% in molecular glass formers [25].
This is how a glass looks like when viewed in real space: a system made of particles that only vibrate around equilibrium positions which have a disordered arrangement in space [5, 7]. A glass is, indeed, an *amorphous solid*. It is *solid* because particles are not free to move, but rather they can only vibrate around equilibrium positions, like they would do in a crystal. But it is also *amorphous* because the equilibrium positions have a disordered arrangement in space.
This picture is supported by specific heat measurements performed on glass formers, see figure 1.5. At high temperature (that is $T_g < T < T_m$), the specific heat of the supercooled liquid is a lot higher than the one of the corresponding crystalline solid; this is no surprise, since the constituents of the liquid are free to move around and thus they can store much more energy than the constituents of the crystal. But when T_g is crossed and the glass is formed (remember that we are working at $\tau_\beta \ll t_{exp} \ll \tau_\alpha$), the specific heat drops and becomes almost equal to that of the crystal [5]: this clearly indicates that the relevant excitations in a glass are not too different from the excitations found in crystals[4]. On timescales τ_α, particles will then be able to leave their cages and flow will be restored, bringing back the supercooled liquid.

To sum it up, the picture of a glass as a crystal with an amorphous lattice is certainly appealing: it is supported by a real-space description of the early relaxation in glass formers, and it is also elegant and easy to grasp. Nevertheless, we must again take some precaution: first of all, talking about "getting out of the cage" makes it look as if it were a single-particle process, while is really a cooperative

[4] Although they are not the same. We will come back to this when we discuss soft modes.

process (as we will see in the next paragraph): all particles are caged and the only way to get out is through cooperative motion. Second, a crystal is a stable state of matter, while a glass is not: it only lives on timescales much shorter than τ_α, after which diffusion sets in and the supercooled liquid comes back.

1.1.5 Real space: cooperativity

We focus now on timescales of the order of τ_α, when caging breaks down and structural relaxation is reached. Again, how does this process look like in real space?
We focus again on density fluctuations, but this time in real space:

$$\delta\rho(\boldsymbol{x},t) \equiv \sum_{i=1}^{N} \delta(\boldsymbol{x}-\boldsymbol{x}_i(t)) - \rho, \tag{1.15}$$

where ρ is the number density N/V of the liquid. We want to understand how correlated is the motion of particles in the system as relaxation sets in, so we have to study how much the correlation in time of the density fluctuations, in a certain region of space, is in its turn correlated with the same observable, in another point in space. If the correlation is high, it will mean that structural relaxation in the first point has to come together with relaxation in the other point, which is the definition of cooperativity. To sum it up, we have to study the correlations in space of correlations in time.
We already know that the correlation in time at a certain point $\boldsymbol{x}$ is given by the dynamical correlation function

$$C(\boldsymbol{x},t) \equiv \langle \delta\rho(\boldsymbol{x},0)\delta\rho(\boldsymbol{x},t)\rangle\,, \tag{1.16}$$

so we just take this definition one step further, but in space, and we define a new correlation function, the *four-point correlation function* $G_4(\boldsymbol{x},t)$

$$G_4(\boldsymbol{x},t) \equiv \langle \delta\rho(0,0)\delta\rho(0,t)\delta\rho(\boldsymbol{x},0)\delta\rho(\boldsymbol{x},t)\rangle - \langle \delta\rho(0,0)\delta\rho(0,t)\rangle \langle \delta\rho(\boldsymbol{x},0)\delta\rho(\boldsymbol{x},t)\rangle\,, \tag{1.17}$$

which essentially encodes the fluctuations of the dynamical correlation function. It is a four-point function because it looks at the correlation between two different points in space at two different points in time, rather than just two points in space as two-point, ordinary correlation functions do.
The necessity of using multi-point correlation functions to detect cooperativity in disordered systems was indeed first appreciated in the context of spin glasses (we will return to this issue later), rather than supercooled liquids. An early discussion about this point can be found in [26]. The first study of the G_4 in that context is reported it [27], although no interesting results were found at the time. From the G_4 we can define a *dynamical susceptibility* in the following way

$$\chi_4(t) = \int d\boldsymbol{x}\; G_4(\boldsymbol{x},t), \tag{1.18}$$

so that the χ_4 corresponds to the average volume of the regions wherein dynamics is cooperative. As those regions grow in size, and the G_4 has thus a slower decay

in space, the $\chi_4(t)$ is supposed to grow. So, if a maximum of the χ_4 shows up at a certain time, say t^*, then we will know that t^* is the time when the relaxation is cooperative the most. Studies of the χ_4 in numerical simulations (see for example [28], and [29] for a review) and even experiments [30] have indeed confirmed these expectations, as shown in figure 1.6. If one superimposes the dynamic correlation

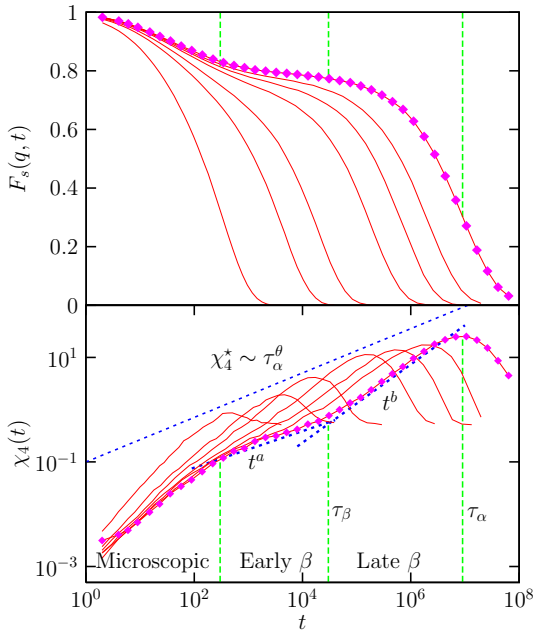

Figure 1.6. The $C(\boldsymbol{x},t)$ (top panel) and the respective $\chi_4(t)$ (lower panel) at various temperatures for a supercooled Lennard-Jones mixture in the various relaxation regimes. The lowest temperature is highlighted with symbols. The maximum of the $\chi_4(t)$ occurs when the $G_4(\boldsymbol{x},t)$ is long-ranged the most, which indicates high cooperativity. Unsurprisingly, relaxation is the most cooperative at $t^* \simeq \tau_\alpha$. Moreover, the peak of the χ_4 shifts up as T is lowered. Reprinted from [23].

function and its corresponding χ_4, it can be seen clearly that the maximum of the χ_4, which is the fingerprint of cooperativity, manifests during the α-relaxation regime. As it was reasonable to expect, the decaging process is highly cooperative and requires all particles (or a least an extensive fraction of them) to move, destroying the amorphous lattice which had caused the slowdown in the earlier phases of relaxation. In addition to this, the value $\chi_4(t^*)$ at the maximum shifts up with decreasing temperature (one can in fact see that $\chi_4(t^*) \simeq (\tau_\alpha)^\theta$ [23, 29]), indicating that as temperature is lowered, more and more cooperativity is required for the system to attain relaxation and flow. This again is no surprise, since more cooperativity requires more time, producing the glassy slowdown. This qualitative behavior is remarkably general [29].

Once the time t^* whereupon cooperativity manifests the most is known, one can take the corresponding $G_4(\boldsymbol{x}, t = t^*)$ and define a *lengthscale* ξ_d, called the *dynamical* lengthscale, which gives the average size of clusters of cooperative motion in the system. This is a more difficult task than the study of the χ_4 since finite-size effects can spoil the result unless sufficiently large systems are considered [23, 31,

32], but it can be carried out nonetheless, see for example [28, 31, 32].

The study of the phenomenology of these clusters, called *dynamical heterogeneities*, is a very rich and active field that reaches far beyond the glass transition problem. But it being a feature of the α-relaxation regime (and thus, of the supercooled liquid), it is pretty tangential to our subject and we will not cover it in this thesis. For the interested reader, we can refer to a review on the subject [33] and a book [34].

At the end of this section, we hope that the reader has been convinced of the fact that relaxation in glasses happens on two well-defined timescales, and that he has a clear visual representation of how these two phases unfold in real space. First, a fast relaxation (β-relaxation) whereupon particles are caged and only vibrate around equilibrium positions arranged in an amorphous fashion. Then, on timescales $t^* \simeq \tau_\alpha \simeq \tau_R$, a second relaxation ($\alpha$-relaxation) whereupon particles decage and the whole structure rearranges cooperatively.

1.2 From the slowdown to RFOT

In the preceding section we have detailed the main signatures of the glassy slowdown. Of course a lot more could be said (stretched exponential relaxation, Stokes-Einstein violation, etc.), but all these things tend to happen in the supercooled liquid, that is on timescales such that $t \simeq \tau_\alpha$ and so they are out of our scope. For the interested reader we reference the pedagogical review of [5], the more technical one of [23], along with some more reviews and textbooks [7, 19, 35–39]. We will balance this lack of focus on the supercooled liquid with a more detailed treatment of the actual glass, when $\tau_\beta \ll t \ll \tau_\alpha$.

The problem of formulating a theory of the glassy slowdown has been open for at least three decades, and by all appearances is still far from being solved. There are at least two reasons for this. The first one, of course, is that experiments, simulations and the like are very hard to perform because of the impossibly large experimental time which would be needed. As we said in the introduction, the theories of the glass transition which are in competition today were born as theories of supercooled liquids, and so their most relevant predictions, where with "relevant" we mean *predictions that could actually enable us to validate one theory and falsify the others*, always kick in inside a deeply supercooled regime which is experimentally and numerically unreachable. A second reason, which is more subtle, is that it is not even very clear what a theory of glass transition is actually supposed to do. Since the main phenomenon is the glassy slowdown, a theory has at least to explain why the slowdown happens and propose a coherent theoretical picture for it. So it has, at the very least, to allow one to get back the VFT law, or some alternative law, like Bässler's, to fit the Angell's plot with. Already at this point we can see how fishy the situation is: there is not even agreement on which predictions the theory is supposed to produce; fits are just fits, after all. As a result of this, competition between the various theories is mainly based on criteria of theoretical consistency and predictive power [23], rather than quantitative, stringent tests that are impossible to perform and, even when they are performed, always leave some room for interpretation wherein incorrect theories could settle and thrive (the debate on the VFT law is a

good, but definitely not the only, example).
If the aim of the theorist is to formulate a "universal" theory *à la Landau* (which is the declared goal and philosophy of RFOT, for example), then there is only one universal quantity that such a theory can be able to predict: namely, a critical exponent. Unfortunately, apart from the critical exponents of MCT [40] (which are anyway relative to a nonexistent dynamical arrest transition, as we are going to discuss), no such critical exponent has ever been measured, and indeed, since the glass transition is no transition at all, one even wonders where to look for such an exponent. As a matter of fact, the greatest, recent success of RFOT consisted in the prediction of the critical exponents of the jamming transition in hard spheres [41], the jamming transition [42–44] being a problem which initially was not related to glass forming liquids, if not in a tangential manner. The RFOT, as all other theories of the glass transition, was initially conceived as something that lives on the equilibrium, supercooled branch in figure 0.1. And yet it had to go all the way to $T = 0$ on the glassy branches (from a very pedestrian standpoint, the jamming transition is basically what happens to a large class of glasses when they are quenched down to zero temperature) to produce a quantitative, falsifiable prediction of an exponent.
This strange fact can however teach us a lesson: theories on the glass transition *can* make falsifiable predictions, if only one bothers to look at the actual glass, which is the *only* thing we are actually able to look at, and that we can experiment on. One of the aims of this thesis is to convince the reader that, even tough RFOT struggles (as all other theories do), to affirm itself when it must describe supercooled liquids, it is definitely superior to (and has a lot more potential than) other theories when it comes to the treatment of the metastable glass. In the following we will explain RFOT with added focus on the central concept of metastable state, as a way to get this point across.

1.2.1 The foundations of RFOT

The Random First Order Theory of the glass transition is based on three conceptual pillars:

1. The glassy slowdown is caused by the emergence, at low temperature, of a large collection of metastable states. The dynamics has to proceed as a series of activated barrier jumps between those states, causing the slowdown.

2. These states have a thermodynamic origin, in the sense that they can be identified with the minima of a static free-energy functional.

3. These states are exponentially many in the system size N, with their number given by $\mathcal{N} = e^{\Sigma N}$, where Σ is a static quantity called *configurational entropy* or *complexity*.

Summarizing, RFOT says that the slowdown of the relaxation dynamics of a liquid close to glassiness is due to the fact that it takes place in a very rough *free energy landscape* (FEL), characterized by the presence an exponential number of minima. RFOT started essentially as a mean-field approach to the study of the free-energy landscape in generic disordered systems [23].

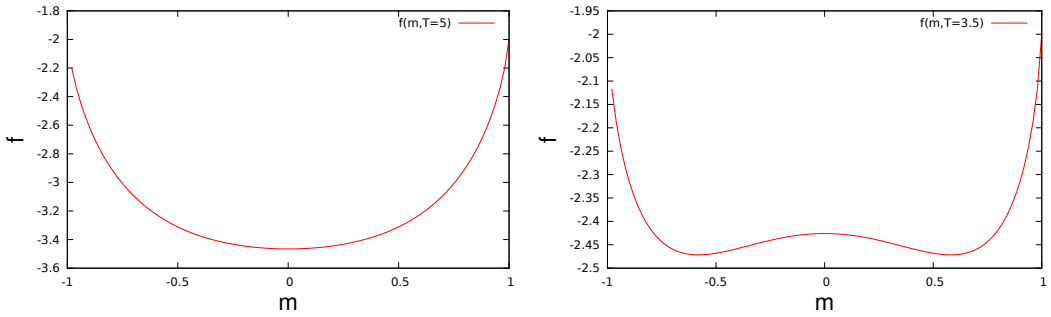

Figure 1.7. Gibbs free energy as a function of the magnetization m for the ferromagnetic Curie-Weiss model above (left) and below (right) T_c.

To fix ideas, let us consider the topical example, namely the Curie-Weiss theory of ferromagnetism. In that context, one is able to compute the Gibbs Free energy $f(m,T)$ of the system, as a function of the global magnetization m [45]. The Helmoltz free energy at zero external magnetic field is the Legendre transform of the f, so it will be given by the Gibbs free energy evaluated in its stationary points m^*, $f(m^*(T),T)$. At high temperature, only one minimum with zero magnetization is present and the system is paramagnetic and ergodic, i.e. it can visit all of the microscopic configurations that are allowed by conservation laws. But below a certain temperature T_c (see figure 1.7), the paramagnetic minimum splits in two distinct minima with $m^* \neq 0$, which correspond to two different *states* with opposite magnetizations. A phase transition takes place: in the thermodynamic limit, the system cannot go from one state to the other because it would have to surmount extensively ($\sim N$) large barriers to do so, and ergodicity is broken. From now on, the expressions "minimum of the energy landscape" and "metastable state" are to be considered interchangeable.

RFOT follows this basic nucleus, with only one (but very game-changing) modification. Since we are considering a disordered system, the Gibbs free energy gets replaced with a more complicated free energy functional which is a function of a *local* order parameter, rather than a global one. In the case of spin systems, it will be a function of all the single-site magnetizations m_i and is referred to as Thouless-Anderson-Palmer (TAP) free energy [46]. In the case of liquids, it is usually a functional of the local density profile [18]. For a lattice gas we can for example define the Landau potential [23]

$$\Omega(\{\mu_i\},T) \equiv -\frac{1}{\beta}\log\sum_{n_i}\exp\left[-\beta H(\{n_i\}) - \beta\sum_{i=1}^{N} n_i\mu_i\right], \tag{1.19}$$

where n_i is the site occupation number, H is the Hamiltonian and μ_i a local chemical potential. The free-energy functional $F(\{\rho_i\})$ will then be the Legendre transform of the Ω with respect to all the μ_is:

$$F(\{\rho_i\},T) = \Omega(\{\mu_i^*\}) + \sum_{i=1}^{N}\mu_i^*\rho_i, \tag{1.20}$$

with the μ_i^*s determined by the condition

$$\frac{\partial \Omega}{\partial \mu_i} + \rho_i = 0. \tag{1.21}$$

This definition can be generalized to the case of a density profile $\rho(\boldsymbol{x})$ in the continuum [18, 45], as we are going to see in the following. The FEL is the hyper-surface obtained by scanning the $F(\{\rho_i\})$ over all possible values of the local order parameters ρ_i.
Its stationary points, in particular, have cardinal importance. As the F is the Legendre transform of the Ω, this means that

$$\Omega(\{\mu_i = 0\}, T) = \min_{\{\rho_i\}} F(\{\rho_i\}, T), \tag{1.22}$$

which means that the thermodynamics of the system in absence of external chemical potentials is given by the free energy functional computed on its stationary points (as it happens if the Curie-Weiss model where the Helmholtz free energy is given by the Gibbs free energy computed in its stationary points in m).
With these definitions, the analogy with magnetic systems is clear: if we consider local density fluctuations

$$\delta\rho_i \equiv \rho_i - \rho, \tag{1.23}$$

where ρ is again the number density, we can see that the homogeneous, high temperature liquid ($\delta\rho_i = 0$) corresponds to the paramagnet, while the glass, with its amorphous nature, would correspond to a disordered ferromagnet with a rough free energy landscape. A crystal would not be homogeneous, but it would anyway have a periodic $\delta\rho_i$ profile, so it would be analogous to an anti-ferromagnet [45]. We can appreciate how the idea of a glass as a system with a rough free energy landscape is indeed very reasonable (see for example [47–50]).

We now proceed to explain why the three tenets of RFOT are coherent with the phenomenology presented in the preceding section.

1.2.2 Dynamics: MCT and Goldstein's picture

Let us start with points 1 and 2. Since those points make assertions about dynamics, we consider the theory that has been, up to very recently, the only first-principles theory for the dynamics of glass formers: the Mode Coupling Theory (MCT) [40, 51, 52].

Mode Coupling Theory and the p-spin

The aim of Mode Coupling Theory is to write a closed equation for the intermediate scattering function (or equivalently, the dynamical structure factor) $F_s(\mathbf{q}, t)$ for an equilibrated liquid close to glassiness. Let us consider the Newtonian (deterministic, without noise) dynamics of a generic liquid made of N particles with positions $\boldsymbol{x}_i$ and momenta $\mathbf{p}_i$. Every macroscopic, time-dependent observable for such a system will be a function of the positions and momenta, $A(t) \equiv A(\{\boldsymbol{x}_i(t)\}, \{\mathbf{p}_i(t)\})$, like the

density fluctuations in equation (1.15). From Hamilton's equations, one can derive the equation of motion for a generic observable $A(t)$

$$\frac{dA}{dt} = \{A(t), H\} \equiv i\mathcal{L}A(t), \tag{1.24}$$

where $\{A, B\}$ is the Poisson bracket

$$\{A, B\} = \sum_{i=1}^{N} \left(\frac{\partial A}{\partial \boldsymbol{x}_i} \cdot \frac{\partial B}{\partial \mathbf{p}_i} - \frac{\partial B}{\partial \boldsymbol{x}_i} \cdot \frac{\partial A}{\partial \mathbf{p}_i} \right), \tag{1.25}$$

and we have defined the Liouville operator

$$\mathcal{L}(\bullet) \equiv -i\{\bullet, H\}. \tag{1.26}$$

We want to write an equation of motion for a correlator $C(t) \equiv \langle A(t)A(0)\rangle$, where $A(t) = \delta\rho_i(\mathbf{q}, t)$, and $\langle\bullet\rangle$ denotes an average over the initial conditions $\boldsymbol{x}_i(0)$ and $\mathbf{p}_i(0)$ carried out with the canonical distribution. The original derivation of MCT carries out this program using Zwanzig's projection operator formalism [53] (although field-theoretic derivations are available, see [54]). We skip directly to the final result

$$\frac{d^2F(\mathbf{q}, t)}{dt^2} + \frac{\mathbf{q}^2 k_B T}{mS(q)} F(\mathbf{q}, t) + \frac{m}{Nk_B t} \int_0^t du \ \langle R_{-\mathbf{q}} R_{\mathbf{q}}(t)\rangle \frac{d}{dt} F(\mathbf{q}, t-u) = 0, \tag{1.27}$$

where

$$R_{\mathbf{q}}(t) = \frac{dJ^L_{\mathbf{q}}}{dt} - i\frac{i|\mathbf{q}|k_B T}{mS(\mathbf{q})}\delta\rho_{\mathbf{q}}.$$

and $J^L_{\mathbf{q}}$ is the longitudinal current [55]. This result is exact and does not require any simplifications. The nucleus of MCT consist in two uncontrolled approximations that are made on the memory kernel $\langle R_{-\mathbf{q}} R_{\mathbf{q}}(t)\rangle$ in order to get a closed, soluble equation. For the sake of brevity, we do not discuss them here and refer the interested reader to [55]. space of bilinear density products, and the second in expressing the resulting four-point dynamical correlation function as a product of two two-point functions $F_s(\mathbf{q}, t)$ [23, 55]. At the end of the day, one gets for the memory kernel

$$\frac{m}{Nk_B t} \langle R_{-\mathbf{q}} R_{\mathbf{q}}(t)\rangle = \frac{\rho k_B T}{16\pi^3 m} \int d\mathbf{k} \ |\tilde{V}_{\mathbf{q}-\mathbf{k},\mathbf{k}}|^2 F(k, t) F(|\mathbf{k}-\mathbf{q}|, t), \tag{1.28}$$

where the vertex $\tilde{V}_{\mathbf{q}-\mathbf{k},\mathbf{k}}$ has the definition

$$\tilde{V}_{\mathbf{q}-\mathbf{k},\mathbf{k}} \equiv \{(\hat{\mathbf{q}} \cdot \mathbf{k}) c(|\mathbf{k}|) + \hat{\mathbf{q}} \cdot (\mathbf{q}-\mathbf{k}) c(|\mathbf{q}-\mathbf{k}|)\}, \tag{1.29}$$

and $c(|\mathbf{q}|)$ is the direct correlation function [18]. With this expression, one can get a closed integro-differential equation for the intermediate scattering function, which can be solved easily once the static structure factor $S(\mathbf{q})$ is known. MCT is thus capable of predicting the relaxation patterns of glass formers from exclusive knowledge of static information. Despite the fact that the approximations involved are uncontrolled (which means that still today there is no idea as to what we are

actually discarding in imposing them), this is anyway a remarkable result and MCT has enjoyed a lot of success since its inception.

The main prediction of MCT is undoubtedly the one of *dynamical arrest*: at high temperature the dynamical correlator decays exponentially to zero, as one would expect from the discussion in subsection 1.1.3. However, at a certain temperature T_{MCT} (sometimes denoted simply as T_c), the correlator, after an initial fast relaxation, will remain stuck on a plateau and the system will never attain equilibrium: an ergodicity breaking takes place. At temperatures $T \gtrsim T_{MCT}$, one can observe a two-step decay reminiscent of the one discussed in section 1.1.3 (see figure 1.8). In fact, the length of the plateau, which as we already know corresponds to the α-relaxation time, goes to infinity on approaching T_{MCT} as

$$\tau_\alpha \propto \frac{1}{(T - T_{MCT})^\gamma}, \tag{1.30}$$

where the γ exponent can be computed from the memory kernel. This sharp transition can be interpreted as one from liquid to solid, and since no information about a crystalline state was used in the derivation, the solid the system freezes into must be non-crystalline, i.e., a *glass* [55].

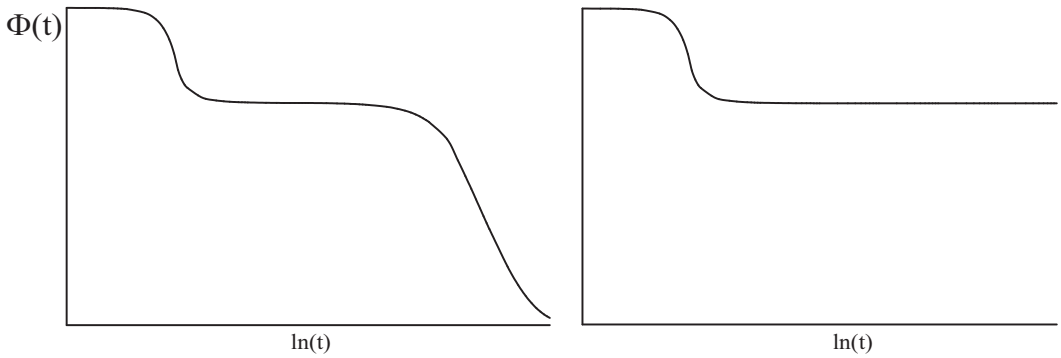

Figure 1.8. The various relaxation patterns predicted by MCT, near the MCT transition (left panel) and below it (right panel). Notice the logarithmic scale in t. Reprinted from [55].

This looks amazing: we have a first principles theory for the dynamics of glass formers which is able to predict the two-step relaxation patterns observed in simulations and experiments, and also predicts a sharp transition, with ergodicity breaking and divergence of the relaxation time, at a certain temperature. There is only one small problem, namely that, in pretty much all cases

$$T_{MCT} > T_g,$$

so one can easily go and see if the transition is actually there, and this is not the case: the α-relaxation time does grow sharply, but it stays finite and the system remains ergodic at temperatures below T_{MCT}. The MCT transition does not exist in real glass formers and must therefore be an artifact of the theory and its approximations [5, 23].

The reason for such a spectacular discrepancy would have been apparent some years after. Already in the original papers of Bentgzelius *et al.* [51] and Leutheusser [52], the authors proposed a "schematic" approximation of the MCT equation, which consisted in simplifying the wave vector dependence of the memory kernel, replacing the integral over $\mathbf{k}$ with its value at a certain wave vector $\mathbf{k}_0$ where the static structure factor has a strong peak. With this simplification one gets the "schematic" MCT equation

$$\frac{d^2\phi(t)}{dt^2} + \Omega_0^2\phi(t) + \lambda \int_0^t du\ \phi^2(t-u)\dot{\phi}(u) = 0. \tag{1.31}$$

This equation happened to have the same form as the equation that would have been derived in [56] for the equilibrium dynamics for a certain class of schematic models of disordered ferromagnets, i.e. spin glasses (SG)[57]. The generic Hamiltonian for these models was first introduced in [58] and has the form

$$H = \sum_{i_1<i_2<\cdots<i_p} J_{i_1,\ldots,i_p}\sigma_{i_1}\sigma_{i_2}\ldots\sigma_{i_p}, \tag{1.32}$$

where the couplings $J_{i_1,\ldots,i_p}$ are identically, independently distributed random variables (usually with a Gaussian probability distribution). They are called p-spin spherical models (PSMs) because of the p-body interaction involved (with $p > 2$), and because the spins are soft spins which must obey the spherical constraint

$$\sum_{i=1}^{N} \sigma_i^2 = N \tag{1.33}$$

Indeed, it was this analogy between MCT and the dynamics of p-spin SG that gave the original impulse for the formulation of RFOT as a theory for describing the glass transition [56, 59–62].

The PSM, although idealized and decidedly far from being a realistic model of a glass former, has numerous advantages: both its statics [63] and dynamics [64] can be exactly solved and the properties of its free-energy landscape can be studied in great detail. In particular, the presence, in a certain range of temperatures, of a great number of metastable minima with nonzero magnetization and free energy higher than the paramagnetic one (as postulated by RFOT) can be proven analytically [65] (see [66] for a review).

If one looks at the Hamiltonian (1.32), in can be seen immediately that all spins interact with one another: the model is *fully connected* and has no space structure, so it is a mean field (MF) model in the traditional sense. Because of this, the barriers between minima in the free-energy landscape scale as the system size N; in the thermodynamic limit, N goes to infinity and barriers become in turn infinite: the system is unable to nucleate from one state to the other and remains forever stuck in the one it started from, producing an hard ergodicity breaking like the one observed in MCT [66].

This invites us to rationalize the ergodicity breaking predicted by MCT as a MF-born artifact: in the real world, barriers are always finite and the system can always escape from the state is in, even though an extremely large time, of the order of τ_α, is needed to do so. Because of this, the glass former spends as extremely long

time partially equilibrated inside a metastable state (and a plateau regime is consequently observed), but it eventually escapes and relaxes, restoring ergodicity and bringing back the supercooled liquid. But if we accept MCT to have a mean-field nature, because of the analogy with the dynamical equations for a MF model (where activated barrier crossing is forbidden by construction), then this activated scenario cannot take place: as soon as the system finds itself in a state, it cannot escape and ergodicity is broken. Today, the status of MCT as a mean-field theory of glassy dynamics, although not apparent from direct inspection of the MCT equations, is pretty much an accepted and established fact [5, 23]. Furthermore, the recent derivation of the dynamics of hard spheres in the limit of infinite spatial dimensions (which as we are going to see corresponds to the MF limit) [67] has shown that the *exact* dynamical equations do have an MCT-like form. We refer to [68, 69] for further reading on the MF nature of MCT.

Goldstein's picture

As a matter of fact, the idea of the equilibrium dynamics of glass formers as a process dominated by activation was not very new even back then (even the exponential form of the $\tau_R(T)$ growth points towards this), as it had already been formulated by Goldstein [70] in 1969. Goldstein pictured the dynamics as taking place in the *potential energy landscape* (PEL) of the liquid, i.e. the hyper-surface obtained by scanning the interaction potential of the system over all values of particle coordinates. We can visualize is as a very rugged landscape of hills separated by narrow valleys [21], at the bottom of which lie the minima of the potential energy of the system, called *inherent structures* [5]. Adding thermal energy (i.e. raising the temperature) can be seen as a flooding of this landscape, with the level of the water higher the higher the temperature and the system can be seen as a boat that has to navigate the landscape [21].
When the temperature is low, only a few, disconnected lakes of water are present, and to sail them all ergodically, the boat must be transported by land over the ridges that separate the lakes: this is an activation event, ruled by Arrhenius' law. Goldstein postulated that energy minima differed only by a change of a subextensive number n of degrees of freedom, and thus could be surmounted by a system equipped with a thermal energy of order k_BT. This way, the system as a whole (as described by a single point in configuration space) would always have been in the process of transition, but on the local level the jumps would have been separated by a timescale that would grow in temperature in an (at least) Arrhenius fashion as required by an activation-dominated mechanism. Thus Goldstein's picture provided a good explanation for the two-step relaxation observed in glass formers and for the exponential growth of the relaxation time: the short β-relaxation would correspond to our boat sailing inside a single lake on a short timescale, while the α-relaxation would correspond to a much longer transport by land of the boat, over a ridge and down into the next lake.
What happens if we keep flooding? Pictorially speaking, at a certain point the flood should become so severe that the water arrives at the level of the highest ridges which separate the valleys i.e. at the level of *saddles*, that is stationary points which have at least one unstable direction. When this happens, the boat only sees a large body

of water wherein it is able to sail ergodically without the need for land transport: activation ceases to be the main mechanism of relaxation and Goldstein's scenario breaks down. This should happen for an high enough temperature T_x, and analogy with MCT suggest the identification

$$T_x \sim T_{MCT}$$

which has indeed been verified both in simulations [71] and experiments [72]. This identification bolsters the picture of glassy dynamics below T_{MCT} as an activation-dominated process.
The idea of the glass transition as a phenomenon ruled by a topological change in the energy landscape has indeed been very fruitful. In the PSM it can be proven analytically [73] that the stationary points of the energy landscape are minima (i.e. they have no unstable directions) only up to a certain threshold energy E_{th}, above which saddles take over. It can be also seen that T_{MCT} corresponds to the temperature such that the typical stationary points visited by the system are exactly those with $E = E_{th}$, thereby providing an exact realization of Goldstein's scenario. In real glass formers, analytic calculations of the sort are not possible and one must rely on numerics. Nevertheless, multiple studies (see for example [74–76] and the discussion in [5]) seem to confirm this picture. These results are very welcome, since they prove that even though in real liquids the MCT transition is wiped out by activation mechanisms, the topological transition is still present and fuels the fundamental analogy with the PSM even for out of MF glass formers.
Since the MCT temperature is the one where a crossover to activated dynamics takes place, and metastable states responsible for the slowdown appear, it is commonly taken as the reference temperature where the onset of "glassiness" is located, also because it has a fundamental and unambiguous definition, contrary to T_g. From now on, when we say "low temperature", we mean that we are below T_{MCT}.

There is however an important warning to give: potential energy landscapes and free energy landscapes are not the same thing and one must not confuse the two: the energy landscape is defined in the configuration space of the liquid and is independent of the temperature, while the free energy landscape is defined in the space of local order parameters and changes when the temperature is varied. Of course the two are the same when $T = 0$, and it could make sense to keep the identification as long as the temperature is very low, but attention must always be paid and the idea of identifying states with minima in the potential energy landscape is just plain wrong [5, 23, 77].

At the end of this paragraph, we hope that the reader is convinced that the two-step relaxation observed in glass formers is reasonably interpreted as originated by the appearance, in the free energy landscape of the system, of a collection of metastable minima (states) which exert a trapping effect on the dynamics for a stretch of time $t \simeq \tau_\alpha$ and keep the liquid from attaining relaxation and flowing. And that the identification of these states with minima of the free energy landscape appears reasonable in light of the analogy between MCT and the dynamics of the PSM, and by the presence of a topological transition in the PEL in both cases. Summarizing, we hope that he now believes that the two first tenets of RFOT appear at least a reasonable starting point for a theory of the glass transition.

1.2.3 Complexity: Kauzmann's paradox

Let us now turn to point 3. We have to ask ourselves the question "how many states can one have?"
How can we label a state? As we said, a state is a minimum of the FEL identified by a set $\{\rho_i^*\}$ of local densities (in liquids), or a set $\{m_i^*\}$ of local magnetizations (in spin models). Thus a glassy state in a realistic glass former corresponds to an amorphous density profile the liquid is frozen into. We had already encountered this picture when discussing caging: particles can only vibrate around equilibrium positions arranged in an amorphous structure, thus every state corresponds to such a structure.
Since these structures are amorphous, we can already surmise that a lot of them should exist. There are not many ways of arranging particles in an ordered structure, but there sure are a lot of possible disordered arrangements. Intuitively, the number of such arrangements should be equal to the number of configurations the liquid has at its disposal, divided by the number of configurations visited by the glass during the vibration around the amorphous structure.
The thermodynamic potential that logarithmically counts the configurations available to the system is the entropy, and we already know from the discussion in section 1.1.4 that the vibrational excitations of particles in a glass are not too different from the ones found in crystals. We could thus hope to count the number of amorphous structures by taking the supercooled liquid entropy and subtracting from it the entropy of the corresponding crystal, as a reasonable proxy for the vibrational entropy of the glass[5]. This leads to the definition of the *excess entropy*

$$S_{exc}(t) \equiv S_{liq}(T) - S_{cr}(T), \tag{1.34}$$

which we can measure by exploiting the relation between entropy and specific heat [5]

$$\frac{dS}{dT} = \frac{c_p(T)}{T}. \tag{1.35}$$

In figure 1.9 we show the excess entropy as a function of the temperature for salol, a fragile glass former. We can see that the excess entropy freezes at T_g to the value it had in the supercooled liquid: this is due to the fact that there is no latent heat at the glass transition (differently from what happens at the melting point T_m, see figure 0.1) , so the entropy is continuous at T_g. On further cooling, the excess entropy stays pretty much constant. This is of no surprise, as its derivative is proportional to the difference between liquid and crystalline specific heat, and we already mentioned in section 1.1.4 that $c_p^{liq} \simeq c_p^{cr}$. Nevertheless, the excess entropy at T_g is of the order of $3k_B$ per molecule, which is large [25]: the number $\mathcal{N}$ of possible amorphous configurations scales exponentially with the size of the system

$$\mathcal{N} \simeq e^{\Sigma N} \tag{1.36}$$

[5] A justification is that vibrational contributions are given by an harmonic expansion around a potential energy minimum, and the fact that the minimum corresponds to an ordered (crystal) or disordered (glass) arrangement of the particles should not change matters much. This is reasonable, but it does not make sense for systems where a harmonic expansion does not exist, like hard spheres [5].

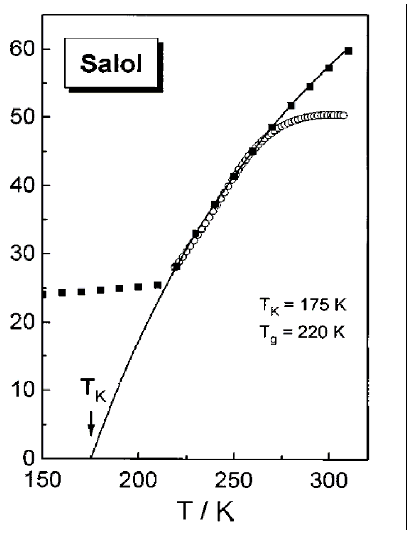

Figure 1.9. Excess entropy as a function of temperature for salol, in $kJ/(K \times \text{mol})$. Dots are experimental data, while the line is a fit of the form $S_{exc}(T) = A(1 - T_K/T)$. Reprinted from [25].

where Σ is the *complexity* (some prefer to call it *configurational entropy* and denote it S_c or s_c, but it is a matter of taste), and is the central static quantity of RFOT. In glass formers, the presence of an exponentially large number of metastable glassy states (and thus the possibility to define a configurational entropy) is a reasonable hypothesis (at least we hope that this discussion made it easier to accept), but it is an incontrovertible fact in the PSM, where the complexity can be analytically computed [65, 66] starting directly from the stationary points of the TAP free energy [46]. Again the PSM furnishes us with a setting wherein the basic ideas of RFOT are exactly realized.

Kauzmann's entropy crisis

If we look closely at figure 1.9, we can see a curious thing. The extrapolation of the excess entropy to temperatures below T_g goes to zero at about 175 K, a value far above absolute zero. So there is a finite temperature where the entropy of the supercooled liquid would become equal to that of the crystal, a very counter-intuitive phenomenon. We would expect the liquid entropy to be always above the crystalline one (a liquid is disordered, a crystal is not) for any finite temperature.
This vanishing of the excess entropy for finite temperature had indeed been known for quite some time, as it was first described by Kauzmann in 1948 [78]. What Kauzmann did was to extrapolate below T_g the data for various observables (enthalpy, free volume, energy, etc.), including the excess entropy. From figure 1.10, we can observe that the excess entropy seems to vanish for temperature different from zero in various glass formers. This temperature has been christened T_K in honor of Kauzmann, and the vanishing of the excess entropy is referred to as *Kauzmann's paradox*, or *Kauzmann's entropy crisis*.

We must immediately state a fact: Kauzmann's paradox was a paradox only

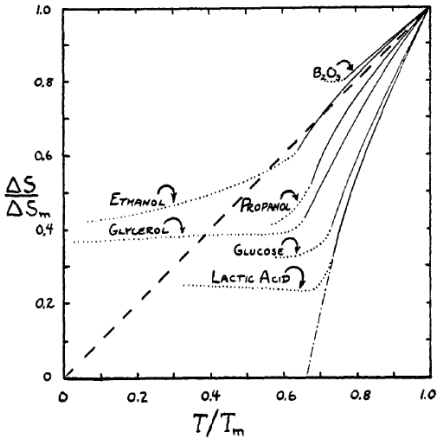

Figure 1.10. The original figure from Kauzmann's paper. For various glass formers, the temperature seems to vanish at $T = T_K$, $T_K \neq 0$. Reprinted from [78].

back then. As strange as the vanishing of the excess entropy can appear, there is no law of nature that actually forbids it. The crystallization transition in hard spheres for example is precisely due to the fact that the crystalline entropy becomes larger than the liquid one at high enough density [79], so nowadays we know that the entropy crisis does not violate any fundamental laws and its presence is not a serious problem. Nevertheless, it appeared paradoxical back then, and Kauzmann himself, in his paper, was eager to find a way out of it.
There are two possible interpretations. If we believe the fact that the excess entropy is a proxy for the configurational entropy Σ, and that it is possible, at least in principle, to equilibrate the supercooled liquid down to T_K, then a phase transition must be located there. If the configurational entropy vanishes linearly at T_K as figure 1.10 suggests, then the corresponding specific heat has a step at T_K, signature of a second-order transition [23]. This transition has been dubbed the *ideal glass transition* (sometimes *Kauzmann transition*).
Kauzmann himself did not believe this, and he proposed an alternative argument: it is not possible to equilibrate the supercooled liquid down to T_K, because the relaxation time grows so much that, in the end, it becomes larger than the crystal nucleation time. So either the glass former goes out of equilibrium and forms a glass, or nucleation will kick in and crystallize our sample. In any case, the supercooled liquid ceases to exist and the paradox at T_K is avoided. We refer to [5] for a discussion on this point.

Is the ideal glass transition necessary?

Unsurprisingly, the interpretation of T_K as the locus of a phase transition had a lot more fortune. The idea that the glassy slowdown is a manifestation of an underlying critical point at T_K is indeed very appealing and conceptually elegant. It also brings back the glass problem to a context, the one of critical phenomena, that physicists

are very familiar with, and for which a lot of theoretical tools are at their disposal. An argument in favor of this idea is that the temperature T_K is always very near to the temperature T_0 where the VFT fit has a divergence, and this applies to glass formers which have T_gs that vary from 50K to 1000K (see [80] for a compilation of data and [81] for a discussion). The coincidence is indeed remarkable, so much that for many proponents of RFOT, it cannot be a coincidence and they see it as incontrovertible proof that the ideal glass transition exists. However, there are glass formers where T_K and T_0 can differ as much as 20 % [82], so such unshakable certainty is ill-advised, at least for now.

The idea of an ideal glass transition at T_K is indeed so powerful and fascinating, that over the years it has come to be identified as the main prediction of RFOT. This is so much true, that most research articles that go and try to disprove RFOT focus on disproving the existence of the ideal glass transition (see for example [83] and [84]). This misunderstanding is also probably due to the fact that most models used in RFOT theory do have an ideal glass transition, starting from the paradigmatic PSM [66].

We argue here that identifying the ideal glass transition (and also the VFT law) with RFOT means missing the point: none of the three tenets that we formulated at the beginning of this section has anything to do with the ideal glass transition. For the RFOT picture to hold, we only need that the insurgence of metastable states cause the glassy slowdown, and that those metastable states have a *static* origin in the sense that they can be identified with the minima of a suitable free energy functional. This scenario can unfold independently from the presence or not of an ideal glass transition at finite temperature.

In summary, we argue that even an avoided transition ($T_K = 0$) is good enough for RFOT [23].

1.2.4 Summary of RFOT: for T_{MCT} to T_K.

In the preceding sections we have provided enough (at least we hope) arguments to convince the reader that the RFOT theory of the glass transition is a good starting point for a description of the physics of glass formers. Let us now give a more unified perspective, and summarize what happens during a cooling experiment of a glass former according to RFOT.

To be completely general, we focus on a generic system whose micro-configurations are denoted as $\mathcal{C}$ and has a Hamiltonian $H(\mathcal{C})$. The partition function is

$$Z = \int d\mathcal{C}\ e^{-\beta H(\mathcal{C})}. \tag{1.37}$$

From the discussion of 1.1.4 we know that states can be visualized as "patches" of configurations, namely those configurations which are visited by the system as particles vibrate around the amorphous structure that identifies the state. Assuming that each configuration can be unambiguously assigned to a single state, and that the "tiling" so generated covers the whole space of configurations[6], we can write the

[6] This is a very strong assumption, but it can be rigorously proven to be true in the PSM, see [85].

partition function as

$$Z = \sum_{\alpha} \int_{\mathcal{C}\in\alpha} d\mathcal{C}\ e^{-\beta H(\mathcal{C})} = \sum_{\alpha} e^{-\beta N f_\alpha}. \tag{1.38}$$

Where α is an index that identifies a state, and we have defined the intensive free energy f_α of a state. We can transform the sum over α in an integral using Dirac delta functions

$$\sum_{\alpha} e^{-\beta N f_\alpha} = \int df\ \sum_{\alpha} \delta(f - f_\alpha) e^{-\beta N f}. \tag{1.39}$$

We now notice that

$$\sum_{\alpha} \delta(f - f_\alpha) = \mathcal{N}(f) = e^{N\Sigma(f,\beta)}, \tag{1.40}$$

so that we are able to easily introduce the f-dependent complexity, which logarithmically counts the number of states with have the same in-state free energy f, or equivalently, the number of minima in the FEL who have the same height f. We get

$$Z = \int df\ e^{-\beta N[f - T\Sigma(f,\beta)]}. \tag{1.41}$$

In the thermodynamic limit, we can evaluate this integral with the saddle-point (or steepest-descent) method [86], getting

$$Z = e^{-\beta N[f^* - T\Sigma(f^*,\beta)]}, \tag{1.42}$$

where f^* is determined by the condition

$$\frac{d\Sigma}{df} = \frac{1}{T}, \tag{1.43}$$

which means that the partition function is dominated by the states with $f = f^*$ only, while the others do not have any impact on the thermodynamics of the system. The states with $f = f^*$ are referred to as *equilibrium states* for this reason, and the complexity of those states

$$\Sigma(f^*(\beta), \beta) \equiv \Sigma(\beta), \tag{1.44}$$

is accordingly called the *equilibrium complexity*, the one that is measured in experiments and simulations.

The typical form of the complexity for a system with an RFOT-like FEL is shown in figure 1.11. Let us now perform an infinitely slow cooling (such that the system is always equilibrated) and discuss the various regimes that take place as the system scans different regions of the FEL while $f^*(T)$ changes with temperature.

- $\mathbf{T > T_{MCT}}$: At high temperature, the minimization of the the free energy functional yields only the homogeneous solution $\rho_i^* = \rho\,\forall i$, with the corresponding free-energy $F(\{\rho\}) = F_{liq}$. The system is ergodic and liquid.
- $\mathbf{T_K < T < T_{MCT}}$: At $T = T_{MCT}$, $f^* = f_{MCT}$, states start to have an impact on the system and the relaxation time starts to increase. Those states are metastable since $f^* > F_{liq}$, but one can see that $F = f^* - T\Sigma(f^*, T) = F_{liq}(T)$ for every T in this interval, and that the free energy is analytic at T_{MCT}.

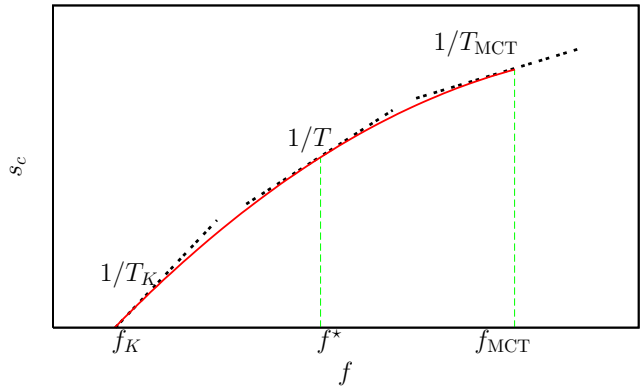

Figure 1.11. The typical form of the complexity as a function of the in-state free energy f. It is a monotonically increasing function in an interval $[f_{min}, f_{MCT}]$, and zero otherwise. For $f > f_{MCT}$, the FEL is dominated by unstable stationary points and the complexity is accordingly zero, as it happens in the PEL for $E > E_{th}$. At f_{MCT} stable minima, which can be found everywhere in the interval $[f_{min}, f_{MCT}]$, start to appear. At f_{min}, the complexity vanishes continuously as the number of minima becomes subexponential. The states with $f = f_{min}$ and those with $f = f_{MCT}$ correspond to the typical equilibrium states visited by the system at $T = T_K$ and $T = T_{MCT}$ respectively. Reprinted from [23].

This can be interpreted as follows: for $T_K < T < T_{MCT}$, the equilibrium liquid splits up in a collection of states, each identified by an amorphous structure and a set of vibration modes around it. On timescales $\tau_\beta < t < \tau_\alpha$, the system remains trapped in one of the equilibrium states with $f = f^*$, producing the plateau regime observed in the dynamics. When at $t \simeq \tau_\alpha$ relaxation approaches, the system starts to visit the other equilibrium glassy states gaining an entropic advantage in the form of $-T\Sigma(f^*, T)$, bringing back the supercooled liquid with its free energy $F_{liq}(T) = f^* - T\Sigma(f^*, T)$. This way, although states appear at T_{MCT}, they only impact the dynamics of the system and its equilibrium state remains always the supercooled liquid (as experimentally observed). In fact, if we compute the probability, at equilibrium, to find the system in one particular equilibrium state α, we get

$$P_\alpha = \frac{\int_{\mathcal{C}\in\alpha} d\mathcal{C}\ e^{-\beta H(\mathcal{C})}}{\int d\mathcal{C}\ e^{-\beta H(\mathcal{C})}} = \frac{e^{-\beta N f^*}}{e^{-\beta N(f^* - T\Sigma(f^*))}} = e^{-N\Sigma(f^*)} \underset{N\to\infty}{\longrightarrow} 0, \qquad (1.45)$$

so the system "hops" seamlessly between all possible equilibrium states.
On lowering T, f^* will decrease and the system will sample states in lower and lower regions of the energy landscape. We stress the fact that such a protocol is very difficult to realize in practice as the relaxation time starts to grow sharply below T_{MCT}. If one performs an infinitely rapid quenching dynamics (like the MCT one), the system will not have time to descend in the FEL and will remain stuck in the highest states with maximal complexity.
Of course, an hopping process like the one we described can take place only in real systems. In MF models, once the system is blocked in a state, it can never get out, as MCT predicts.

- $\mathbf{T \leq T_k}$ At $T = T_K$, the equilibrium states become the ones with $f = f_{min}$ and the complexity vanishes. We have still $f_{min} - T\Sigma(f_{min}) = F_{liq}$, and the total entropy $\Sigma + s_{vib}$ is continuous, but the specific heat ($c_p = \frac{dS}{d\log T}$) has a jump induced by the vanishing of Σ: the entropy vanishing scenario of Kauzmann is realized and the ideal glass transition takes place.
  Below T_K, the number of states becomes sub-exponential and the system can now be found, at equilibrium, inside a single glassy state, thus yielding a stable, thermodynamic glass.

This is how the glassy slowdown happens according to RFOT. One must admit that the picture is quite elegant and brings together nicely many different inputs and observations, from MCT to excess entropy to Kauzmann's paradox. Needless to say, the PSM realizes this scenario exactly [66].

1.2.5 Beyond mean field: scaling and the mosaic

We mentioned at the start of this section that a theory of the glass transition has at least to describe well the glassy slowdown, which means that it has to reproduce the VFT fit (or some other fit) of the τ_R vs. T dependence. Within RFOT, this means that we need to compute τ_α as a function of T, and to do so, we must focus on the dynamics, in particular on long timescales comparable with τ_α, when relaxation occurs.
But this brings to the surface the great weakness of RFOT [23], namely its reliance over the concept of metastable state, and consequently on a mean-field description. The MF nature of RFOT models (starting from the PSM, but there are many others) makes it, on one side, an ideal playground to study metastability: states are sharply defined, they have an infinite lifetime, and their properties can be studied analytically even for realistic models of glass formers as we are going to see in the following of this thesis. But on the other side, the failure to take into account activation mechanisms and non-MF effects in general, means that the theory is found wanting when attempting to describe the regime wherein non-MF effects come into play, which is also the regime wherein relaxation occurs (remember the wrong MCT prediction of a transition at T_{MCT}). This difficulty in going beyond MF (see for example [87] for a dynamics-based attempt) is the great weakness of RFOT and a solution to this problem does not seem to be forthcoming [23]. As a result of this, the connection between RFOT and the dynamics of the system on long ($t \simeq \tau_\alpha$) timescales comes from a bundle of phenomenological scaling arguments, which goes under the name of *mosaic theory* [25, 60, 62, 88], and was essentially conceived as a reworking of the old Adam-Gibbs theory [89] to include the notion of complexity.

Mosaic theory is an attempt to bring out of MF the MF-based concept of metastable state: in the real world, the τ_α timescale is always finite, so the concept of metastable state must become local in time. Indeed, since metastable states are, well, metastable, they are intrinsically out-of-equilibrium objects and so any attempt at a rigorous definition must start from the dynamics (see for example [90, 91]). Another problem comes from the fact that states, being MF objects, do not take into account at all the notion of *real space*. In MF models, there is

no space structure, so it makes sense to talk about the system globally being in a "state" and hopping to another global state at the onset of relaxation as we said in the preceding paragraph. Once real space comes into play, this picture clearly makes no sense: hopping from on state to another takes place through a nucleation mechanism which can only be *local* in space: as soon as a sufficient time passes for activation to happen, droplets will start to form at certain points in the sample, and each of them will be in a certain "state". There is absolutely no reason for them to be all in the same state, since all states with $f = f^*$ (including the one the system is about to leave) have the same free energy and thus they are completely degenerate. a free energy gain in passing from one state to another, it would mean that the system is not at equilibrium, in contrast to the RFOT picture which asserts that the equilibrated, liquid system is restored by the seamless hopping process between states. Thus, we can expect that the original state will break up in a collection of tiles (a mosaic), each of them in a different state. The fact that rearrangements must be local should not come as a surprise, considering that the local nature of rearrangements in glass formers had been already pointed out by Goldstein [70]. In summary, states must be defined locally both in space and time, i.e. they are characterized both by a *timescale* τ_α and a *lengthscale* ξ.

We are interested in computing the timescale as a proxy for τ_R. What we can do is work out the lengthscale, get from it an estimate of the barrier size to rearrangement, and get from it the timescale using Arrhenius' formula. Since we have said that rearrangement should take place through nucleation, let us assume that our glass former is in a state γ. When a time $t \simeq \tau_\alpha$ has passed, thermal fluctuations will form a droplet of linear size R, typically in another state δ. On the boundary, the mismatch between the two states will induce a free energy *cost* in the form of a surface tension

$$\Upsilon R^\theta, \tag{1.46}$$

where theta is a generic exponent, $\theta \leq d-1$. Usually it is equal to $d-1$ (where d is the dimension of space) since it represents a surface term, but this not need be the case in general [5]. This free energy price has to be balanced by a free energy *gain* of some sort. In nucleation theory it is usually given by the free energy difference between the two coexisting phases, but in this case the two states have the same free energy $f = f^*$. Thus the complexity comes into play: the droplet can be found in $\mathcal{N} = e^{R^d \Sigma(T)}$ different states, so it is of course invited to explore them all and gain an entropic advantage in the form of $-T\Sigma(T)R^d$ rather than staying in state γ. The total energy barrier for forming the droplet is

$$\Delta F = \Upsilon R^\theta - T\Sigma(T)R^d, \tag{1.47}$$

which means that large droplets will tend to survive, while small ones will tend to go back to the background state. The crossover between the two happens at a lengthscale ξ which can be obtained by setting ΔF to zero. We get:

$$\xi = \left(\frac{\Upsilon}{T\Sigma(T)}\right)^{\frac{1}{d-\theta}}. \tag{1.48}$$

Now, following [62], we fix the barrier height Δ as

$$\Delta \equiv \max_R \Delta F(R) = \frac{\Upsilon^{\frac{d}{d-\theta}}}{[T\Sigma(T)]^{\frac{\theta}{d-\theta}}}, \tag{1.49}$$

and using Arrhenius' formula we get

$$\tau_R = \tau_0 \exp\left(\frac{\Upsilon^{\frac{d}{d-\theta}}}{k_B T[T\Sigma(T)]^{\frac{\theta}{d-\theta}}}\right). \tag{1.50}$$

Now we know that near to T_K

$$\Sigma(T) \simeq A(T - T_K), \tag{1.51}$$

so we can plug this into the formula for τ_R, getting

$$\tau_R = \tau_0 \exp\left(\frac{\Upsilon^{\frac{d}{d-\theta}}}{k_B T[AT(T - T_K)]^{\frac{\theta}{d-\theta}}}\right), \tag{1.52}$$

so we get a law which looks like the VFT one, although not the same. However, in [62] it was claimed that $\theta = d/2$, which would give for τ_R

$$\tau_R = \tau_0 \exp\left(\frac{\Upsilon^2}{k_B T[AT(T - T_K)]}\right) \underset{T\to T_K}{\simeq} \tau_0 \exp\left(\frac{B}{T - T_K}\right), \tag{1.53}$$

exactly the VFT law. We must however state again that the VFT law is just a fit, not a fundamental law or the result of a first-principles computation, so perhaps it is not worth it to fiddle with θ and make assumptions about its value just for the sake of getting it back. Using the (1.52) with θ as a fitting parameter would probably do an even better job than the VFT and there are alternative laws which provide anyway a good fit of the data.

Summarizing, even if we had to use some arguments (and some common sense) to get the results, RFOT indeed passes the test, in the sense that it does provide a good explanation for the super-Arrhenius increase of τ_R, in the form of the *complexity*: the barrier size scales with the inverse of a power of Σ and thus increases when T_K is approached, causing a sharper increase that the simple Arrhenius' one (where the barrier would be constant).

There is an alternative formulation of the mosaic theory which does not use nucleation and is conceptually more robust than the one we just presented, we refer to [92] and [5] for details. In [92], the authors also propose a method to measure the lengthscale ξ, through the definition of a special correlation function, the *point-to-set* correlation function. The measurement of ξ using this tool has indeed given encouraging results and a growth of ξ on supercooling is observed [93], so the mosaic picture, and RFOT with it, does seem to be on the right track when it comes to the description of supercooled liquids. We refer to [5] for an in-depth discussion on the point-to-set lengthscale.

We conclude here our exposition of RFOT, and we hope that we managed to make it looks at least as a reasonable starting point for a theory of glasses. For further reading, we refer to [5] for a pedagogical approach, to [23] for a more technical point of view, and to [25] for a critical assessment. We refer also the reviews [94], [88], and a book [95].

1.3 Other approaches

A much beloved quote by prof. D. Weitz says "There are more theories of the glass transition than there are theorists who propose them". While it is certain that prof. Weitz was a little exaggerating, it is true that there are indeed many different theoretical pictures for the glassy slowdown. This is not necessarily a bad thing, since it shows that this field of research has still many open problems, there is still a lot of work to do, and the debate is fluid and lively (tellingly, prof. Weitz's quote is much beloved by glass theorists themselves), so there it no shortage of "other approaches" that we could talk about.
However, since they are so many, we will focus here only on the ones that are most popular at the moment, and that are more suitable of an analytic, statistical-mechanical treatment. Reviews on the approaches we will leave out can be found for example at [7, 96, 97], and we refer to section IV.A of [23] for more references.

1.3.1 Dynamic facilitation theory

The Dynamic Facilitation Theory (DFT) [98–100] picture is in many ways completely specular to the RFOT approach. Whereas RFOT posits a static explanation (in the form of metastable states) for the glassy slowdown, DFT favors a completely dynamical approach and postulates that thermodynamics plays absolutely no role. While RFOT relies mainly on MF-born concepts (like global metastable states and the FEL) and on MF models, DFT is firmly rooted in real space and its paradigmatic models all are finite-dimensional. While RFOT is at pain when it comes to link its thermodynamic foundations to dynamics, in DFT dynamics is the very cornerstone of the approach.
These stark differences between the two approaches come from their differing views about what is the distinguishing phenomenological fingerprint of glassiness. For RFOT, the fingerprint of glassiness is activation, *à la Goldstein*, so RFOT naturally stages itself into the FEL, and as a result of this it naturally relies on a static MF description of the FEL. According to DFT, the fingerprint is *cooperativity*, which takes place during the dynamics of the system when viewed in real space. So DFT, accordingly, stages itself in real space and naturally relies on dynamical tools [5].

The philosophy of DFT is that diffusion and relaxation can only be achieved through cooperativity: for a particle to escape its cage, all particles around it must also decage and move away, and this in turn will stimulate other particles to move [101]. So, we can see decaging process as the creation of a new *defect* (a cluster of mobile particles), which is in turn susceptible of inducing (*facilitating*) mobility in nearby regions, creating other defects. This picture is undoubtedly reasonable, as we have seen in paragraph 1.1.5 that facilitation does play a role in the dynamics of glass formers close to T_g. It looks even more reasonable in light of the fact that it is possible to define models based exclusively on the idea of dynamic facilitation, called Kinetically Constrained Models (KCMs) [99].

Kinetically Constrained Models

KCMs can come in different flavors, but they all have two things in common: their thermodynamics is trivial, and their dynamics is constrained by rules which mimic

the facilitation picture. A first example is the Kob-Andersen (KA) lattice gas [102], wherein a particle can hop from one site to the other only if i) it is empty, and ii) if there are less than m neighbors around it ($m = 6$ on a cubic lattice would correspond to the unconstrained gas). It is basically a model that enforces the notion of caging in a strict sense, and can be studied for various values of m and different lattice topologies, from cubic to Bethe [99].
Another champion of KCMs is the Fredricksen-Andersen (FA) model [103], which opts for a specular philosophy to the one of the KA model, focusing on holes rather than particles. Each site on the lattice can be mobile $n_i = 1$ or not $n_i = 0$. The Hamiltonian, again, contains no interaction

$$H_{FA} = J \sum_i n_i \tag{1.54}$$

and $\langle n_i \rangle \propto \exp(-\beta J)$, so that mobility is suppressed at low temperatures (as one would expect). The dynamics, for its part, takes place with the usual Glauber rules, but a site can make a transition from mobile to non-mobile only if there are at least other k neighboring mobile sites. A variation on the FA is the East model [104], where only sites on the left in each space dimension can facilitate the dynamics.

Strengths and weaknesses

The main advantage of DFT lies in the fact that dynamics is the very core of the approach, so, for example, their predictions on the relaxation time can be easily obtained. Some models show a strong, Arrhenius-like behavior, like the FA with $k = 1$, while others have a more fragile character. The East model for example has $\log \tau_\alpha \simeq \frac{1}{T^2}$, which quite reminisces Bässler's law, eq. (1.7), and the FA on a square lattice with $k = 2$ (the original version of the model from [103]) is even more fragile, with $\tau_\alpha \simeq \exp[\exp(c/T)]$. The great majority of KCMs do not predict a divergence of the relaxation time at finite temperature, but it is possible to define a KCM in such a way that a divergence is present [105]. Despite this, their predictions for τ_α can be shown to fit experimental viscosity data quite well, see for example [14, 17]. So DFT does pass the test, perhaps in an even more convincing manner than RFOT.

Another great advantage of KCMs lies in the fact that they naturally reproduce the phenomenon of dynamical heterogeneities [106, 107], so much that some studies on dynamical heterogeneities were actually motivated by their observation in the context of KCMs. They also give the possibility to study in great detail multi-point correlation functions (like the G_4), even enabling researchers to get rigorous scaling relations between susceptibilities, lengthscales and timescales [29, 108]. The DFT picture provides also a natural explanation of the violation of the Stokes-Einstein relation for viscosity and diffusion [109]. We stress that all these predictions come easily from DFT, while a dynamics-based formulation of RFOT is still lacking (see [67] for a possible starting point), so there is no denying that the DFT picture is clearly superior to RFOT when it comes to the study of dynamics in the supercooled liquid regime.

However, there are some weaknesses. The biggest, conceptual weakness lies in the exclusive role attributed to facilitation, which is seen as the *only* possible

mechanism for relaxation. To make this more clear, this means that mobility and defects cannot be created in any way: a region of the system which is not mobile cannot relax unless a drifting defect visits it, and no spontaneous motion is possible (mobility is conserved). This is a very strong assumption, which may not be true, see for example [110].
On the other hand KCMs cannot make do without the assumption of mobility conservation, or at least without assuming that violations to this assumption become more and more rare when T is lowered. If mobility can be created and destroyed, KCMs immediately become trivial models and their glassy phenomenology is wiped out [23], which is a huge and undefended weak point.

In addition to this, as much as RFOT suffers from an over-reliance on MF-based statics, DFT seems to suffer from an over-reliance on dynamics. In particular, the fact that KCMs all have a trivial thermodynamics does not even seem a necessity, and it constitutes no proof that glass formers share this feature. Moreover, there is a subtle point, namely the fact that having a trivial thermodynamics does not mean that all the RFOT based phenomenology of metastable states cannot take place in KCMs. The thermodynamics of RFOT models is indeed trivial, in a way, since from T_{MCT} down to T_K equilibrium is always given by the supercooled liquid; and indeed, the presence of metastable states cannot be detected using standard statistical mechanical tools, requiring to use of the TAP approach [46] or the replica method [45]. In summary, we argue that the triviality of the standard thermodynamics of KCMs does not imply the triviality of their replica-based (or state-following based) thermodynamics.

A less severe and more taste-related weakness is the one of predictive power. Intuitively, for a theory to be very predictive we should have to put a few things into it, and get a lot in return. DFT, as we just detailed, does give you a lot, but it also requires you to put a lot inside. As interesting as KCMs are, there is at present no way of linking them to microscopic models of glass formers [23]. Their dynamical rules in particular are just imposed from the outside without any microscopic of first-principles justification, and they cannot be generally derived (see [111] for an exception) from an interaction Hamiltonian.
This means that in order to get quantitative predictions about real glass formers, KCMs must usually be suitably "tuned" using experimental or numerical data, which is unpleasant. We will return to this point in the following when discussing the DFT approach to metastable glasses. We will see that, while DFT needs extensive tuning to work well, the RFOT-based state following construction enables us to get predictions from first principles, at the only price of an Hamiltonian.

1.3.2 Frustration limited domains

According to the Frustration Limited Domains (FLD) [112] picture, the fingerprint of glassiness is disorder and the amorphous nature of the glass phase, which is rationalized as a consequence of geometric frustration. Frustration can be broadly defined as the incompatibility between a *locally* preferred arrangement, and the symmetry of the space it finds itself in, thereby rendering the local structure incapable of tiling the whole space forming a global periodic structure.
A pedagogical example is a triangle of spins with anti-ferromagnetic interactions:

the local preferred structure would be a +1 spin and a -1 spin at the end of each bond, but the triangular topology renders this arrangement impossible: at least one bond is not satisfied (which means that the relative energy cannot be minimized), and as a result there are three possible (and equivalent) optimum frustrated arrangements. This example illustrates how the frustration is caused by geometry: on a square lattice, there would have been no problem. Moreover, it also illustrates how frustration is also a source of degeneracy and multiplicity, an important ingredient in the context of amorphous materials. This ideas can also apply to particle systems. It is for example known that the local preferred order for packings of spheres in $d = 3$ is the icosahedral one, which is however incompatible with periodic ordering [113].

According to FLD, the glassy slowdown is a manifestation of a second-order critical point at a certain temperature $T^* > T_m$, which is destroyed by frustration [114]. When the liquid is cooled down, it starts to form locally preferred structures (LPS) in preparation for the transition at T^*, but those structures are incapable of tiling the whole space due to frustration, so they end up forming domains of size ξ separated by topological defects, where a surface tension will be located due to the mismatch. The rearrangement of these domains, not much differently from what happens in the mosaic picture, will then have to proceed by activation [114], producing a slowdown of the dynamics like the one observed in glass formers [115].

Models

The scenario suggested by FLD can be implemented in statistical-mechanical models. A particularly elegant realization in the case of spheres is the one proposed by Nelson [116]: the idea is to embed the spheres in a spherical manifold with $d = 3$, in such a way that the local icosahedral order is now compatible with extension in space. The energy of the system can then be minimized and a "reference" configuration obtained. The curvature of space is then reduced, up to the point when the euclidean flat space is recovered. This way one can observe how the ordered configuration on the sphere changes to a disordered configuration rife with FLDs, separated by a complex network of defects. However, this approach is also technically very hard to implement and it is almost impossible to get quantitative predictions [23].

There are two other possible ways: either a phenomenological scaling treatment, like the one implemented in [114], or coarse grained lattice models. The Hamiltonian of such models is always made up of two terms: one that reproduces the unfrustrated system and yields the second-order transition at T^*, and another which acts as a source of frustration. A paradigmatic Hamiltonian is

$$H = -J \sum_{\langle ij \rangle} S_i S_j + Q \sum_{i \neq j} \frac{S_i S_j}{|x_i - x_j|}, \tag{1.55}$$

where we can clearly see the competition between ferromagnetic, local interaction (which will tend to favor local ordering) and the long-ranged Coulombic interaction which acts as a frustrating term. Models of this sort can be defined with soft spins, Ising spins, $O(N)$ spins and Potts variables. In the case of $O(N \to \infty)$ and soft spins one can see that the transition is killed as soon as $Q \neq 0$ [117], while in the case of Ising spins the transition becomes first order [118]. Anyway, in both cases,

a disordered phase is found at low T wherein dynamics is slowed down in a glassy manner [112]. The size ξ of FLDs in particular is found to have the scaling

$$\xi \simeq \sqrt{\frac{J}{Q}}\xi_0^{-1}, \tag{1.56}$$

where ξ_0 is the correlation length of the avoided transition at T^*. Since it decreases as the system is cooled below T^*, the size of FLDs is found to increase on lowering T, which in turn means that the barrier to rearrangement of the FLD must increase upon supercooling. So FLD theory passes the test as RFOT and DFT, since it does provide a good explanation for the super-Arrhenius increase of the relaxation time. We can also observe from the (1.56) that more frustration means bigger FLDs. This is reasonable, since frustration keeps the FLDs from tiling the whole space, so having more of it should correspond to smaller domains. This in turn implies a direct relation between fragility and frustration, which is probably the most original prediction of FLD theory. As a result, FLD can account for a wide range of different behaviors, from strong to fragile, just by tuning suitably the strength of frustration.

Strengths and weaknesses

FLD theory has the great merit of actually posing deep questions about the nature of cooperative regions seen in glassy systems. RFOT just postulates them as originated by an underlying disordered FEL, and DFT only focuses on how they move. FLD instead describes them explicitly, in a very practical and very grounded way, and proposes a coherent and elegant picture for their origin. FLD has also the merit of bringing back the attention of researchers on a fact so obvious it is often forgotten: glasses behave like solids, and the rigidity of solids is indeed due to structure, not dynamics, so perhaps it is too soon to rule out the existence of any structure in glassy materials: they may actually hide more order than we think (see for example [119]).

This grounded and real-space bound description of FLD theory is, however, also its weakness: as of now there have not been any direct observations of FLDs [5, 23]. We have focused before on how the static structure factor $S(\mathbf{q})$ does not seem to capture anything unusual on crossing T_g, although the fragmentation in FLDs could be so severe that the residual order eludes a bulk tool like the $S(\mathbf{q})$. In principle it could be possible to observe FLDs and their related LPSs through numerical simulations, but this is more complicated than it looks [120], and there is not even agreement on which is the locally preferred order one should look for. For example in [121], the growth of icosahedral order is found to be more pronounced in fragile liquids as expected from the FLD approach, but in [122] it is argued that everything can be understood in terms of bond-orientational order, rather than icosahedral, so that the situation looks very convoluted.

Moreover, one would also appreciate to go beyond scaling arguments and coarse-grained models like the one defined in equation (1.55), and perform calculations on microscopic models of glass formers, but this does not look easy. It is indeed possible to implement numerically a Nelson-like treatment for a Lennard-Jones mixture [123] with very encouraging results, but at present there is no apparent way of translating this into a statistical-mechanical calculation. As a matter of fact, models like the

one in equation (1.55), when treated with the replica method, show a Kauzmann transition like the one predicted in RFOT (see for example [124]), so it could very well be that a first-principles treatment of FLD will end up giving back RFOT results, which could be a very interesting turn of events.

Chapter 2

Metastable glasses

In this chapter we focus on the glassy branches in figure 0.1, when our glass former is frozen, for a time τ_α, in an amorphous solid called a glass. We will mainly focus on two different experimental designs: in the first one, the preparation of the glass is followed by a waiting time during which the glass is left at rest to age, followed by experimental measurements of its thermodynamic properties; in the second one, the glass is prepared and then subjected to an external mechanical drive, during which its response to the drive is characterized. In both cases we will present the usual phenomenology as observed in simulations and experiments, and also the theoretical tools up to now used to approach the problem. The aim of this chapter is to detail how glasses, despite being out of equilibrium systems, are anyway long-lived states of matter endowed with well defined physical properties, that can be measured and hopefully computed from a first-principles theory.

2.1 Thermodynamics and aging

In the preceding chapter we have discussed the properties of glass formers, as observed in experiments and simulations designed in such a way that

$$t_{exp} \gtrsim \tau_\alpha,$$

on a range of temperatures which goes roughly from T_K (we do not care if T_K is zero or not) to T_{MCT}. This range of temperature corresponds to the one wherein the glassy slowdown takes place, and phenomenology beyond the one observed in simple liquids can manifest.
In this chapter, on the other hand, we talk about glasses. This means that the typical experiment/simulation will be designed so that

$$\tau_\beta \ll t_{exp} \ll \tau_\alpha.$$

Let us be more specific, and perform an idealized experiment of length t_{exp} on a glass former. The simplest possible experiment consist of at least two phases: first a preparation of the sample, which takes a time t_{prep}, and then a measurement of some sort, carried out at t_{exp}. The time that elapses between the end of preparation and the experimental time will be called the *waiting time*, and denoted as t_w. The

simplest preparation protocol one can consider is a very rapid quench of the glass former down to a target temperature T, $T_K < T < T_{MCT}$ [125]. This is actually the process by which glasses are canonically made, and we will refer to such procedures as *quenching protocols*; however, one could also consider more creative protocols. For example, one could equilibrate the glass former down to a temperature T_f, $T_K < T_f < T_{MCT}$ (the notation will be clear later), *then* quench it rapidly down to a target temperature T [126] and perform measurements. Such a protocol will be referred to as an *annealing protocol*.
To equilibrate the system at T_f, one can choose any convenient protocol; the most straightforward one is a step-like quench down to T_f, after which the sample is left at rest until equilibrated. The annealing time needed for such a protocol is then

$$t_{ann} = \tau_R(T_f) = \tau_0 \exp\left(\frac{A}{T_f - T_0}\right) \tag{2.1}$$

so it obviously grows very rapidly with T_f. Of course, in a real laboratory it is impossible to achieve infinite quench rates (the thermal conductivity of any substance is finite) and more complicated protocols could be needed in order to avoid crystallization [5], but since the sample is equilibrated at T_f, the actual protocol used does not matter: the system loses memory of its history once equilibrated and its properties do not depend on time, a situation referred to as *Time Translational Invariance* (TTI), as we already discussed [21]. Once the annealing phase has been completed, we quench the glass down to T, a process which will take a time t_{qu} such that $t_{ann} + t_{qu} = t_{prep}$, and then wait a time t_w before performing our measurements. After $t = t_{ann}$ the system is out of equilibrium, so from T_f downward its equation of state will deviate from the supercooled liquid one as shown in figure 0.1: T_f is the temperature whereupon the system forms a glass. This temperature has been defined by Tool in [127] and called the *fictive temperature*. In any reasonable experimental setting it is practically equal to the glass transition temperature T_g, so we will consider them as being interchangeable from now on.

One can easily understand the difference between the two protocols we described in light of the summary of RFOT we made in section 1.2.4: in the first protocol we do not let the system equilibrate in any way, so it remains arrested in the threshold states in the highest regions of the FEL (corresponding to $f = f_{th}$ such that $\Sigma(f, T)$ is maximized[1]), and will still be there when we perform our measurement at t_{exp}, unless the waiting time is very long. In the second protocol, the system remains anyway blocked in the threshold states, but then we give it enough time $t_{ann} \simeq \tau_R(T_f)$ to descend in the FEL (thanks to activation), down to the equilibrium states with $f = f^*$ determined by the condition (1.43) with $T = T_f$. This way, when we will quench it again down to T, the system will remain trapped in one of the equilibrium states selected at T_f, and again, it will still be there when we perform our measurements at t_{exp}.

[1] Technically, the definition of threshold state it that of a minimum which is infinitesimally near to being a saddle. However, it is reasonable that such stationary points will be in the highest part of the FEL (ridges are always located higher than valleys) and thus have maximal complexity, as long as the complexity is a monotonously increasing function of f. If these conditions are met, the identification between threshold and maximal complexity is safe (and is rigorously true in the PSM).

In summary, having a lower temperature T_f (and thus a longer protocol) means that the phenomenology observed at t_{exp} will be ruled by deeper and deeper minima in the FEL.

2.1.1 Protocol dependence

From the description we just gave of the simplest protocols for glass preparation, the reader can immediately understand that glass is an intrinsically *out of equilibrium* object. In practical terms, this means that a typical glass has not had enough time to forget its history and so the properties measured at t_{exp} can depend, in principle, both from the preparation protocol, and on the time that has passed between the end of preparation and the measurement. In summary, any measurable observable $\mathcal{O}$ can depend on t_{ann}, t_{qu} and t_w, and on the details of whatever happened during these time periods.

We already said that the dependence on t_{ann} is no big deal: the system is left at rest until equilibration sets in at T_f (or T_g), so it has forgot all its past history, including the annealing protocol employed to get at T_g, which is effectively the only trace left of the past history of the glass. The dependence on t_w is very weak as well, at least for one-time observables: in the case of quenching protocols, power laws with small exponents or even logarithmic laws, such as

$$\mathcal{O}(t_w) = \mathcal{O}_\infty + \left(\frac{\tau_0}{t_w}\right)^\alpha, \tag{2.2}$$

$$\mathcal{O}(t_w) = \mathcal{O}_\infty + \log(1 + \tau_0/t_w), \tag{2.3}$$

are usually reported [125]. The dependence should be even weaker for the annealing protocols that reach deeper and more stable states in the FEL. This also implies that the dependence on t_{qu} is as well weak: a rapid quenching protocol followed by a long waiting time is the exact same thing as a long quench followed by a short t_w. In summary, the properties measured in a glass annealed at a temperature T_g and then quenched at a temperature T do not depend much on the protocol needed to get from T_g to T[2], and only depend on the temperature T_g (or equivalently T_f), and on t_{ann} through it:

$$\mathcal{O}(t_w, t_{ann}, t_{qu}) \longrightarrow \mathcal{O}(T_g, T).$$

which was indeed Tool's original idea for T_f [127]. Despite the fact that a glass is not at equilibrium, its one-time properties are effectively independent of time (at least until it relaxes again on an impossibly long timescale $\tau_\alpha(T)$): it actually makes sense to talk about a thermodynamics of glasses.

To detect actual signatures of aging, one must focus on two-time quantities, like the already mentioned dynamical correlation functions. In an out of equilibrium, aging scenario, they will depend on both times t and t'

$$C(t', t) \longrightarrow C(t_w, t_w + \tau). \tag{2.4}$$

[2]This is true as long as the glassy metastable state the system is in does not undergo any further in-state phase transition (like the minimum splitting in two or more sub-minima). We will see that this is exactly the case with the Gardner transition.

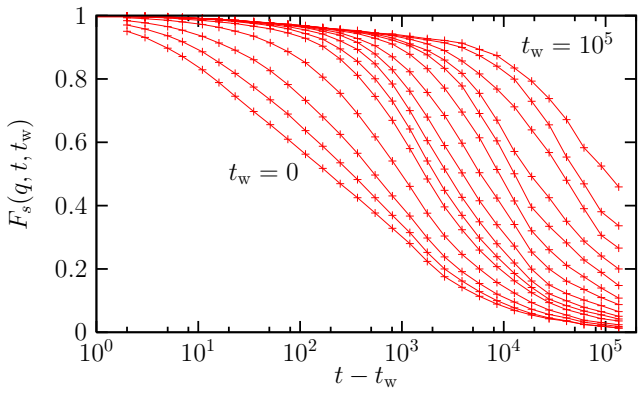

Figure 2.1. The intermediate scattering function of a prototypical glass former after a quenching protocol, in an aging situation. We can see how the relaxation time τ_0 increases when the waiting time increases, a typical aging effect. A quasi-equilibrium regime is observed at small times. Reprinted from [23].

In figure 2.1 we show a typical aging-like relaxation pattern for the dynamical correlator, plotted for various waiting times after a quenching protocol. At small times the curves are almost superimposed and the dependence on t_w is weak, so that TTI is restored. At longer times, a stronger dependence on t_w is observed, and the correlator decays to zero on a timescale τ_0 which depends strongly on t_w. This dependence on t_w, which can also be seen as the *age* of our glass, is the definition of aging [21, 23].

The fact that τ_0 increases with t_w may seem counter-intuitive: the system has to eventually decorrelate on a fixed timescale $\tau_\alpha(T)$, so one would naively expect $\tau_0(t_w) = \tau_\alpha - t_w$. This however is wrong: the system has first to relax inside a steady state, and then decorrelate again. When $t_w = 0$ is zero, the preparation of the sample has just ended and the system has not yet had time to settle it its new state. So when we observe it after an interval τ, is has decorrelated significantly as part of this partial equilibration process. But if we wait a time t_w, take a snapshot of the system, and then take another at $t_w + \tau$, we will observe less decorrelation, since part of the process has taken place before the first snapshot at t_w: the more we wait, the less decorrelation we observe, until at $t_w \simeq \tau_\alpha$ the dynamics crosses over to the equilibrium one where TTI is valid again, an *interrupted aging* scenario [21].

All this phenomenology seems well tailored to RFOT: at T_g, the system is at equilibrium, visiting a great number of degenerate states whose free energy f^* only depends on T_g through equation (1.43). When the system is quenched down to T, is has not enough time to equilibrate again, but it can equilibrate inside the state with a relaxation time of order τ_β weakly dependent of the temperature, generating a TTI dynamics on short timescales. After this, the system will stay equilibrated inside the state and its observables will reach a restricted equilibrium value, independent of time and dependent only on the thermodynamics (and so on T) of the metastable state. Of course, if the experimental time is comparable to τ_α, one can actually observe aging effects, as the glass relaxes and its observables go

back to their equilibrium, supercooled liquid values. But this is possible only when $T \simeq T_g$, very near to the equilibrium line, so those effects are effectively negligible.

2.1.2 Ultrastable glasses

The protocol dependence properties of glasses open exciting scenarios, wherein one could manufacture materials whose physical properties could be "tuned" just by changing their preparation protocol. However, such a program is not easy to realize, at least until recently: the time t_{ann} needed to get a low T_g grows very steeply with T_g (equation (2.1)), so only a very limited range of T_gs is within practical reach. This is the reason why the brutal quenching protocols like the one described at the beginning of this chapter have been for much time the standard for studying glasses [125]: doing better is very time-consuming and difficult.
However, in recent years, a new experimental and numerical protocol has allowed researchers to get, in a few hours, glasses with T_gs that would correspond to canonical preparation protocols up to decades long, allowing us to go much beyond T_{MCT}. The glasses so produced are fittingly called *ultra-stable* glasses [16, 128–133] .

Ultrastable glasses are prepared via a special protocol that goes under the name of *vapor deposition*: the glass former is slowly deposited onto a substrate whose temperature is controlled by a thermostat, and is of course lower that the calorimetric glass transition temperature defined in section 1.1.1. In such a setup, the particles near the free surface enjoy enhanced mobility and are able to look for equilibrated configurations much faster than they would in the bulk of the sample, as it would happen in a canonical annealing protocol. This creates, layer by layer, glasses which are exceptionally stable and correspond to ordinary glasses with impossibly long annealing times (around 40 years for some samples described in [129]). This procedure can be implemented both in experiments [129, 133] and simulations [130, 132], and can be shown to work well both for fragile and strong glass formers [133].

Once the sample has been prepared, it can be studied and characterized in a variety of ways. In experiments, Differential Scanning Calorimetry (DSC) is usually employed: heating and cooling scans are performed on the sample and its properties (heat capacity at constant pressure and enthalpy in the case of [129]) are measured as a function of T (see figure 2.2).

The cooling scans in the right panel of figure 2.2 correspond essentially to the equations of state in figure 0.1: the enthalpy branches away from the liquid EOS at a fictive temperature T_f which depends on the preparation protocol. In addition to this, one can also perform an heating scan, wherein the sample is prepared and then (rapidly) heated up. In this case, hysteresis is observed: the enthalpy becomes lower than the liquid one, up to an onset temperature T_{on} whereupon the glass melts back into the liquid.
The stability of the glass is characterized by the two temperatures T_f and T_{on}: lower T_f and larger T_{on} correspond to higher stability (and a larger hysteresis cicle). A lower T_f means that the glass is arrested in lower minima in the FEL, and correspondingly, more thermal energy must be supplied to the system to dislodge it from these minima and melt it back into the liquid, yielding a higher onset temperature [129].

In numerical simulations [130], one has access to positions and momenta of all

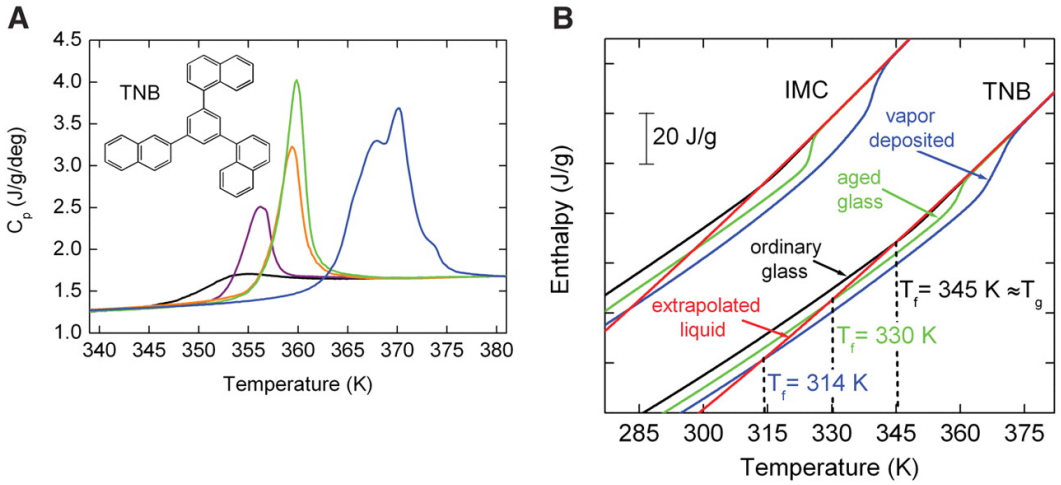

Figure 2.2. *(Right panel)*: enthalpy for an ultrastable glass (blue), a glass with an annealing time of 15 days (green) and an ordinary glass produced by cooling the liquid at about 40K/min (black). In a cooling scan, the enthalpies branch away from the liquid value at the fictive temperature T_f, and remain always higher than the liquid enthalpy (since $C_p^{gl} < C_p^{liq}$ as we already mentioned). In a heating scan, the enthalpy of the glass becomes lower than the liquid enthalpy, up to a temperature T_{on} when the glass melts back into the liquid and the enthalpy regains its liquid value. Both T_f and T_{on} quantify the stability of the corresponding glass. *(Left panel):* heat capacity at the onset transition. A maximum is observed, which separates the glass at low T from the liquid at high T. Obviously $C_p^{gl} < C_p^{liq}$ as expected. Reprinted from [129].

particles, allowing a more refined analysis. In particular, the properties of the PEL that underlies the liquid can be studied. Such a study can be carried out in the following way: one takes an equilibrium configuration (essentially a set of $3N$ positions) of the supercooled liquid at a certain temperature T below T_{MCT}. One can then minimize the potential energy of the liquid, using for example a gradient descent method [5], using the equilibrium configuration as a starting point for the algorithm. This procedure (which essentially corresponds to a sudden quench to zero temperature) will produce a configuration corresponding to a minimum of the potential energy (an inherent structure) with a certain energy E_{is}, which will be one of the minima that the system typically vibrates around at temperature T [97]. As we mentioned in section 1.2.2, lower minima of the PEL can only be reached through activation, so they correspond to larger annealing times and thus to higher stability.

In figure 2.3 we show some results from [130], for a glass produced by vapor deposition *in silico* of Lennard-Jones particles: one can see that a lower substrate temperature allows the system to reach lower minima in the PEL, as expected. This provides one more way to quantify the stability of the glasses produced by vapor deposition. In particular, the glass with the lowest E_{is} corresponds to an optimal substrate temperature approximately equal to the Kauzmann temperature for the glass former in study [130], a very intriguing coincidence.

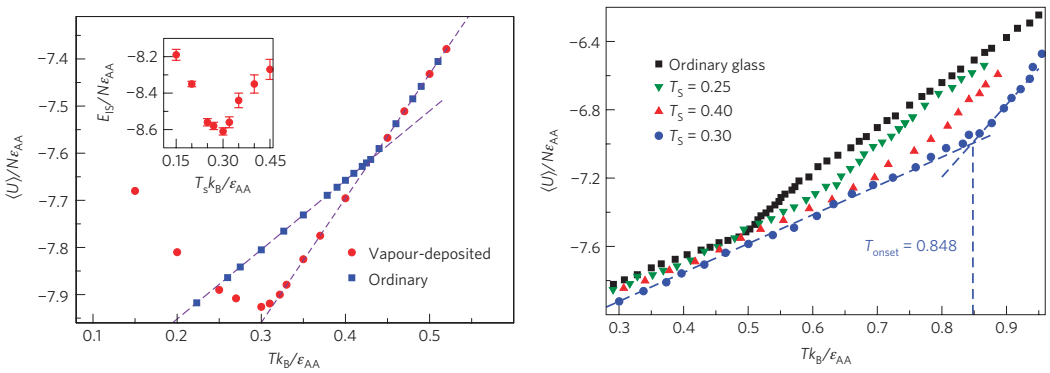

Figure 2.3. *(Left panel)*: Average potential energy $\langle U \rangle$ of the vapor-deposited glasses (red symbols) as a function of the substrate temperature T_s, compared with the same observable for an ordinary glass (blue symbols). The vapor-deposited glasses show supercooled liquid behavior (which means that $T_f = T_s$) for temperatures much below the glass transition temperature for the ordinary glass, with a lower limit at $T_s \simeq 0.3$, about the value of T_K for this system. In the inset, the inherent structure energy is plotted as a function of T_s: a minimum is observed, again at $T = 0.3$, corresponding to optimal substrate temperature. *(Right panel)*: heating and cooling scans on glasses with three different substrate temperatures, with $T_f = T_s$ for all the glasses, except for the one with $T_s = 0.25$ (as one can see in the left panel). Again an onset transition is observed, with T_{on} shifting up for more stable glasses. All data are plotted in Lennard-Jones units. Reprinted from [130].

In addition to this, one can also study the average potential energy $\langle U \rangle$ as a function of T, and perform cooling and heating scans similarly to [129]. Again, an onset transition is observed, with higher T_{on} corresponding to higher stability as expected. In numerical simulations one can also study very precisely the structural properties of the glass, for example employing Voronoi tesselation. We do not delve into the details, but we summarize that the more stable glasses do show structural peculiarities, with a homogeneous (albeit always amorphous) structure almost totally devoid of defects (such as polycrystallites), in contrast with ordinary glasses which present bigger defects, and in larger number [130]. This is in agreement with the fact that ultrastable glasses also show suppressed diffusion properties with respect to ordinary glasses [129], another index of enhanced stability.

In summary, ultrastable glasses are certainly going to be studied more and more in the next years: they are relatively easy to produce and allow researchers to bypass annealing protocols which would be decades long, one of the big difficulties in the study of the glass transition. Moreover, we mentioned in the introduction and in section 1.2 that most of the relevant predictions of theories of the glass transition are found at temperatures much lower than T_{MCT}, so that only experiments performed at those temperatures, on an *equilibrated* glass former, can hope to unveil "smoking gun" evidence in favor of one particular approach. Ultrastable glasses seem to give a big help in this direction, so a new influx of experimental and numerical data from their study is to be expected in the future.

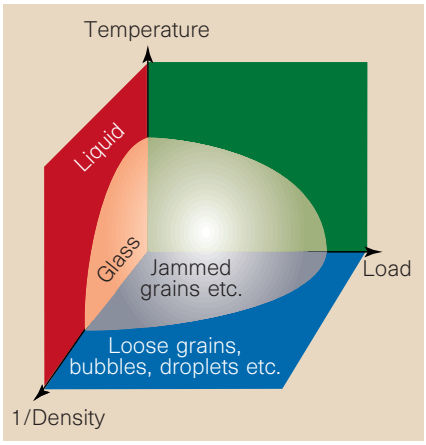

Figure 2.4. The proposed unified phase diagram for the glass and jamming transitions. Reprinted from [43].

2.1.3 The jamming transition

Let us now make a detour to talk about a phenomenon which at first glance is completely unrelated to glasses: the jamming transition [42–44]. The aim of this paragraph is to convince to reader that it is not at all a detour, at least within RFOT.

The jamming transition is probably one of the most ubiquitous phenomena one can conceive. The canonical example of jamming system is a fistful of sand: when it is not compressed, it responds to stresses by flowing, more or less like a liquid would. However, if we clench our fist, at a certain point we will not be able to squeeze the sand anymore and the response will be solid-like: the grains of sand are mechanically in contact, forming an amorphous, tight packing. The jamming transition is a transition between a loose, liquid-like system to a jammed, solid-like one.

This may look like a calorimetric glass transition, but it is not the same thing. In the glass transition the solid that originates from the glass former is due to caging and vibrations inside the cage, which render it capable of bearing loads and respond like a solid; however, the system is still compressible and pressure is finite. In the jamming case, there is no temperature and the solid-like behavior is due to the forming of a network of mechanical contacts between the grains; and if those grains can be reasonably modeled as mechanically undeformable, hard particles, the resulting solid is incompressible: its pressure is infinite.

To study jammed packings, one usually constructs them using a certain protocol (the choice of words is not casual). In experiments, one can for example throw the grains in a shaking box one at a time until the packing jams [134]. In simulations, a very popular algorithm is the one by Lubachesky and Stillinger [135] (LS), wherein the packing is created by inflating the spheres at a fixed rate γ during a molecular dynamics run. Another possibility is to consider soft particles with a potential that vanishes outside the particles (tennis balls, essentially): one starts from a random configuration, compresses it, then minimizes the potential energy, and then

compresses it again, until a zero energy configuration cannot be found anymore [136, 137]. The jamming problem can then be formulated as: *"Given a procedure to construct an amorphous packing, what are the properties of the packing so obtained? First of all, what is its jamming density φ_j[3]? How does the contact network behave? Which properties depend on the actual procedure, and which ones do not?"*. A ponderous research effort has ensued, in the last years, to answer these questions.

Luckily for us, this effort has been successful (see for example the reviews [138, 139]), at least for frictionless spherical particles, so we can reap and summarize the most relevant results:

1. The jamming density φ_j does depend on the protocol used. In the paradigmatic case of the LS algorithm for hard spheres, it can be seen that a lower rate γ corresponds to a lower φ_j [140, 141]. In $3d$, an fcc crystal is produced for small rates ($\varphi_j = \varphi_{FCC} \approx 0.74$), while for a fairly large range of intermediate rates an amorphous packing with $\varphi_j = \varphi_{GCP} \approx 0.68$ is produced[4]. For even higher rates, φ_j goes down smoothly with γ.

2. *All* amorphous packings of frictionless particles at the jamming threshold φ_j are *isostatic* [142, 143], which means that the average number of contacts z in the packing is just the one needed to ensure mechanical stability, $z_{iso} = 2d$[5], in agreement with Maxwell's criterion [144].

3. The probability distribution of the absolute value of forces in a packing $P(f) \equiv \sum_{i=1}^{N_c} \delta(f - f_i)$ (where N_c is the number of contacts) has a power-law behavior (a pseudogap) for small forces, $P(f) \simeq f^{\theta}$, where the exponent θ is apparently the same for every $d \geq 2$ [145–147].

4. The pair distribution function $g(h)$[18], $h \equiv (r - D)/D$ (where D is the diameter of a sphere) is singular at small h: $g(h) \simeq h^{-\gamma}$, with the exponent γ again independent of dimension [140, 145, 146]. Indeed a scaling relation can be derived to link γ with θ [145, 148].

5. The Debye-Waller factor (or equivalently the MSD) of a packing of hard spheres subject to agitation (like in the LS algorithm), and near the jamming threshold, scales with the reduced pressure[6] as $\Delta \simeq p^{-\kappa}$ [41, 149].

6. The density of states (DOS) $D(\omega)$ of vibrational modes in a jammed packing of spheres (soft or hard) has a plateau down to zero frequency [137, 150], a property referred to as *marginality*. It can be shown that this property is intimately connected with isostaticity, as the frequency ω^* that delimits the plateau at low frequencies can be shown to obey the scaling $\omega^* \simeq z - z_{iso}$ [151]. This means that the packing is mechanically stable (is in a stationary point of the PEL where no negative modes can be found), but only marginally so: it can be destabilized without paying an energy cost.

[3] φ is defined as the fraction of volume occupied by the particles, $\varphi \equiv \frac{N}{V_{par}} V = \rho V_{par}$.

[4] We mention that this numerical estimate is subject to an error of about 10%, so caution is advised, as always.

[5] d is the dimension of space.

[6] $p \equiv \frac{\beta P}{\rho}$, where P is the pressure.

In summary, jammed packings surprisingly show properties with a remarkable degree of universality, in the sense that they are both protocol-independent, and also apparently independent of the dimension d of space as long as $d \geq 2$. The isostaticity and marginality of jammed packings point toward the fact that the jamming transition may be a phenomenon governed by a critical point in the Landau sense (albeit at $T = 0$), with an associated set of critical exponents. As a matter of fact, a whole scaling description of the jamming transition can be derived just by assuming marginality [145, 148, 152]. Moreover, we point out the fact that these critical properties can be measured and characterized very accurately, differently from what happens in the case of glasses where no transition is present and everything is built around elusive, subtle observables, like the complexity Σ.

What do jammed packings have in common with glasses? They have in common the most important thing, namely the characteristic that makes them both hard to approach theoretically: protocol dependence.
Glasses are protocol dependent because they are not able to equilibrate on human timescales, while jammed packings are protocol dependent because they are *athermal* systems made of macroscopic objects, such that the relevant energy scale is far above $k_B T$. In both cases, the system is unable to forget its history and treating it with the usual tools of statistical mechanics is impossible. But at the end of the day, the jamming problem ("*Given a procedure to construct an amorphous packing, what are the properties of the so obtained packing?*") and the glass problem (*"Given a protocol to produce a glass, what are the properties of the so obtained glass?"*) have the exact same nature, which is the reason why we put them in the same chapter.

The idea that the protocol dependence of glasses and jamming systems could be treated on the same footing was first introduced in [43], where a unified phase diagram was proposed, see figure 2.4. In this picture, jamming systems could be viewed as glasses of repulsive particles[7] quenched down to zero temperature and then compressed until mechanically rigid. This would allow for a unified treatment of the two problems.
Within the RFOT approach, the implementation of this program consist in identifying jammed packings with the endpoints of metastable glassy states at $T = 0$, $\varphi = \varphi_j$, and infinite pressure (see figure 2.5). This is more easily done in the celebrated hard sphere (HS) [18] model where temperature plays no role and the only control parameter is the packing fraction φ, although it is possible to apply it also to soft harmonic spheres. This approach to the jamming transition was first reviewed in [153], and allows one to treat jammed packings in a purely static fashion, thanks to the static nature of metastable glassy states which is at the very heart of RFOT. In last few years, this line of research has produced remarkable results. It was shown in particular that the HS model could be solved exactly in the infinite dimensional, MF limit $d \to \infty$ [154], employing the replica method which is the natural tool for treating RFOT models [45, 94] (more on this in the following), and that this exact solution could accurately predict the critical exponents γ, θ and κ along with the isostaticity property of packings [41, 154–156]. All these results were obtained only from first principles and to this date embody the greatest accomplishment of

[7] The presence of an at least soft-core repulsion is of course necessary to induce a jamming transition.

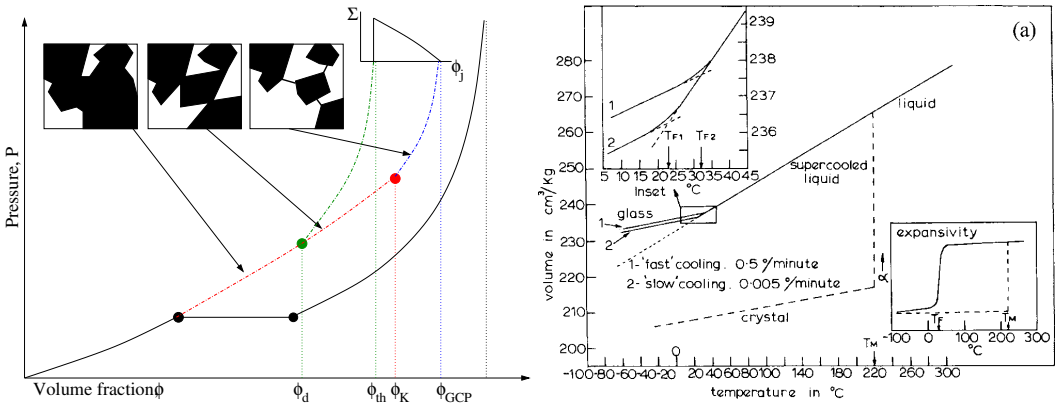

Figure 2.5. *(Left panel)*: pressure vs. packing fraction phase diagram of hard spheres as proposed in [153]. The slowest compression rates lead to a crystalline packing with maximal density φ_{FCC}. Higher, but still fairly low rates allow one to go into the "supercooled" regime all the way down to the Kauzmann transition, and then to φ_{GCP} which is the jamming point for the ideal glass and corresponds to the maximal density for an amorphous packing. Higher rates select a glassy state between φ_d (analogous to T_{MCT}) and φ_K in analogy with an annealing protocol for a glass, and these states have jamming densities in a continuous interval between $\varphi_{th} = \varphi_j(\varphi_d)$ and $\varphi_{GCP} = \varphi_j(\varphi_K)$. *(Right panel)*: specific volume vs. temperature phase diagram of a generic glass former. The similarity with the left panel is manifest if one identifies $1/\varphi = v$ and $P = 1/T$. Reprinted from [7].

RFOT, showing that the initial conjecture of Kikpatrick, Thirumalai and Wolynes [56, 59–62] is indeed realized in a strong sense in the MF limit.

Since the jamming transition and the RFOT predictions about it concern the properties of metastable glassy states at infinite pressure, we are going to talk more, and with more detail, about them in the following.

2.1.4 Theoretical approaches to aging

As we mentioned in the previous paragraph, a satisfactory "theory of aging" must be able, given a certain preparation protocol, to predict the properties of the glass so produced. Since a glass is out of equilibrium, using standard statistical mechanics would only give back trivial results relative to the equilibrated supercooled liquid, which means that one must in principle resort to off-equilibrium dynamical tools. In this case, to predict the properties of an aged glass, one must

1. Write the equations for the dynamical process that reproduces the protocol under consideration,

2. solve them and compute the values of observables from the solution.

Specifying to our case, in the case of brutal quenching protocols [125] one needs to study a dynamical process starting from a random initial configuration, while in the case of the annealing protocols (like those employed for ultrastable glasses) [126] one must consider a dynamics starting from an initial configuration equilibrated at T_f [21].

This program does not look easy, especially considering the fact that a theory for the dynamics of glass formers is still lacking. MCT is by construction a theory for equilibrium dynamics, so it cannot be employed in this setting, and the recently proposed MF approach of [67] is still in its infancy. Nevertheless, something has been done, and we review briefly those efforts.

RFOT

We mentioned in section 1.2.2 that the MCT equations are formally identical to the equations for the equilibrium dynamics of the PSM [66]. However, while the MCT equations are derived assuming equilibrium *ab initio*, in the case of the PSM the derivation is completely general, which means that so obtained dynamical equations have general validity and can be employed for aging studies.
Those equations read [66]

$$\begin{aligned}\frac{\partial C(t,t_w)}{\partial t} &= \mu(t)C(t,t_w) + 2TR(t_w,t) + \frac{p}{2}\int_{-\infty}^{t_w} dt'\ C^{p-1}(t,t')R(t_w,t') \\ &\quad + \frac{1}{2}p(p-1)\int_{-\infty}^{t} dt'\ R(t,t')C^{p-2}(t,t')C(t',t_w), \end{aligned} \tag{2.5}$$

$$\begin{aligned}\frac{\partial R(t,t_w)}{\partial t} &= \mu(t)R(t,t_w) + \delta(t-t_w) \\ &\quad + \frac{1}{2}p(p-1)\int_{t_w}^{t} dt'\ R(t,t')C^{p-2}(t,t')R(t',t_w), \end{aligned} \tag{2.6}$$

$$\mu(t) = T + \frac{p}{2}\int_{-\infty}^{t} dt'\ C^{p-1}(t,t')R(t,t'), \tag{2.7}$$

where the correlation function C and *response function* R have been defined

$$C(t,t_w) \equiv \frac{1}{N}\sum_{i=1}^{N}\overline{\langle\sigma_i(t)\sigma_i(t_w)\rangle} \qquad R(t,t') \equiv \frac{1}{N}\sum_{i=1}^{N}\frac{\delta\overline{\langle\sigma_i(t)\rangle}}{\delta h_i(t')}, \tag{2.8}$$

($h_i(t)$ is a space and time dependent perturbing magnetic field) and $\overline{(\bullet)}$ denotes an average over the quenched disordered couplings [66]. In an equilibrium situation, the correlation and response functions are linked by the fluctuation-dissipation theorem (FDT) [21]

$$R(t,t_w) = \frac{1}{T}\frac{\partial C(t,t_w)}{\partial t_w}, \tag{2.9}$$

while in an aging situation they have to be treated separately. The solution for these equations in the aging regime was first described in [157] and is reviewed in great detail in [21], so here we just summarize the most relevant points.
The solution exhibits an aging phenomenology just like the one reported in figure 2.1: at short times $\tau = t - t_w$, the dynamics is TTI and the FDT holds. On intermediate timescales the dynamics remains arrested around a plateau whose height can be shown to be equal to the "size" of the threshold states at temperature T [157], after which the system then decorrelates on a timescale $\tau \simeq \tau_0(t_w)$. However, one can also observe that the length of the plateau $\tau_0(t_w)$ increases indefinitely with t_w, so that the system is effectively aging forever and the dynamics never crosses over

to an equilibrium one (which would require that $\tau_0(t_w)$ saturate to a t_w independent value, restoring TTI). This is no surprise, since the system needs activation the leave the threshold level in the FEL, which is forbidden by construction in the PSM. In fact, the aging dynamics of [157] corresponds to the slow descent of the system towards a threshold minimum in the FEL [158], which however is reached only asymptotically in t_w. The system descends effectively forever, moving along ridges and visiting stationary points with a lower and lower number of unstable directions, thereby slowing down more and more as time passes, causing the increase of τ_0 with t_w.
The most relevant prediction of the aging dynamics defined above consists in the fact that, on timescales much larger that t_w, a generalized version of the FDT holds [157]. One can define a *fluctuation-dissipation ratio* (FDR) in the following way [23]

$$R(t, t_w) = \frac{X(t, t_w)}{T} \frac{\partial C(t, t_w)}{\partial t_w}. \tag{2.10}$$

This can be done in general, but in MF spin glass models like the PSM, one can observe that

$$X(t, t_w) \simeq x(C(t, t_w)) \tag{2.11}$$

where x is a generic function. Since in the case of the PSM (and RFOT systems in general) the decay of the correlator is two-step, the function x effectively reduces to two numbers: $x = 1$ when C is large and both TTI and the FDT are valid, and $x = X_\infty$ when C is small and decorrelation sets in. This invites us to define an *effective temperature*

$$T_{\text{eff}} = \frac{T}{X_\infty}, \tag{2.12}$$

so that the aging system can be visualized as a system at equilibrium, only with a temperature T_{eff} different from the bath temperature T [159, 160].

To measure the FDR, one can define a susceptibility

$$\chi(t, t_w) \equiv \int_{t_w}^{t} dt' \; R(t, t'), \tag{2.13}$$

which together with the (2.9) would imply

$$T\chi(t, t_w) = C(t, t) - C(t, t_w), \tag{2.14}$$

so that a plot of $\chi(t, t_w)$ vs. $C(t, t_w)$ is a straight line with slope -1. If the FDT is not valid, but an effective temperature can be defined, one would expect to see a slope of $-X_\infty$ when C is small. This prediction has been validated in numerical simulations of realistic models of glass formers, see for example [161, 162] and figure 2.6.

The temperature defined through the (2.10) can be shown to have a lot more physical meaning that one could assume at first sight. In particular, it can be shown to possess all the properties required from a temperature as a state variable: it can be measured with a suitable thermometer and controls the direction of heat flows, as a "real" temperature is supposed to do [159]. Moreover, a whole thermodynamics for metastable glasses can be in principle built around the concept of effective

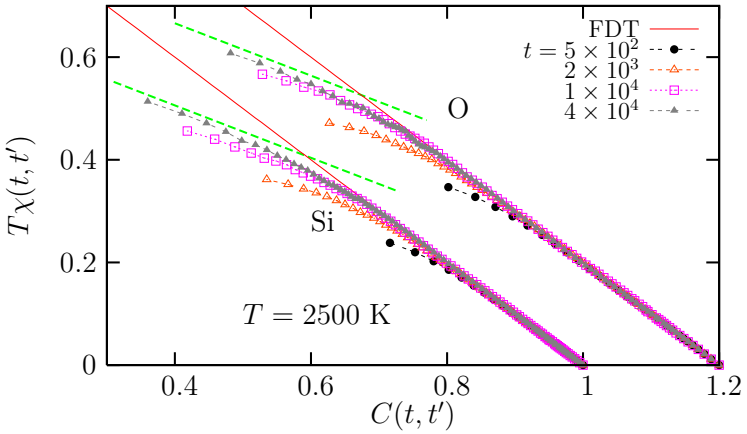

Figure 2.6. Susceptibility vs. correlation plot for a simulated SiO_2 glass. For large times, the numerics for both atomic species converge smoothly to a two straight-line plot with $X_\infty \approx 0.51$, which yields $T_{\text{eff}} \approx 4900K$. Reprinted from [162].

temperature, see [39].
The presence of an effective temperature is intimately linked with the presence of two relevant timescales for equilibration: the fast degrees of freedom are able to equilibrate (on a timescale τ_β), with the bath at temperature T, but the slow degrees of freedom are unable to do so since their equilibration time τ_α is too large. However, they can be conceived as "quasi-equilibrated" at T_{eff} [163]. We will see that the replica method allows one to give more solidity to the notion of effective temperature.

This effective temperature approach has been for much time the standard RFOT approach to aging (we refer to [164] for a review), but it clearly suffers from some problems. First of all, not all experiments reveal the presence of a well-behaved effective temperature (see for example [165]), and we will also see that the presence of activation mechanisms can lead to negative effective temperatures, a clearly paradoxical result.
However, the biggest weakness is of conceptual nature: since activation is prohibited, the system is always and forever stuck at the threshold level, without ever being able to penetrate below it. This means that this kind of dynamics is only capable of reproducing brutal quenching protocols, and fails completely when one tries to describe annealing protocols such as the ones we defined in section 2.1. A satisfactory theory of aging must be able to account for those protocols and the appearance, in recent years, of ultrastable glasses analogue to glasses prepared with very slow annealing protocols [129, 130] now makes it even more of a mandatory task, for models and theorists, to go "beyond the threshold" [21].

Since within RFOT the system cannot go beyond the threshold by itself, we must put it there ourselves, namely we must consider a dynamics whose initial configuration is not random, but sampled from the canonical Boltzmann-Gibbs distribution at T_f. This program can actually be implemented in the case of the PSM, wherein the equations for such a dynamics have been derived in [166]. Their solution shows, unsurprisingly, an equilibrium dynamics (with FDT and TTI both

valid) much like the MCT one, with the only difference that the system relaxes inside a single metastable state selected by the (1.43) instead of equilibrating in the ergodic supercooled liquid. The system of course never gets out (since activation is forbidden), so one has a well-defined plateau regime for long times, from which the interesting in-state observables can be computed[8].
This is exactly what we want, but anyway there is a problem, namely that implementing the program of [166] in real liquids looks like a difficult task. In principle a generalization of the formalism employed in [67] could be developed, but it doesn't look at all easy, since the derivation of [67] for just an equilibrium, MCT-like dynamics is already quite computationally heavy. In this thesis we propose a much simpler, but equally predictive alternative.

DFT

The aging dynamics of KCMs has been extensively reviewed in [168], so we will be brief. As we mentioned before, they have the big advantage of being well defined models which can be treated analytically and have a real space structure, and yet exhibit a remarkably rich phenomenology. In particular, they provide an ideal playground to study activation mechanisms.
The possibility of activation in the dynamics of KCMs can lead to very interesting results in terms of FDT violation. The case of the FA model, equation (1.54), in particular, has been extensively studied [169]. The dynamical correlations considered in the FA are the Fourier transforms of the local mobility correlation functions

$$C_q(t,t_w) = \sum_i \sum_j \langle n_i(t) n_j(t_w) \rangle_c \, e^{-iq(r_i - r_j)}. \tag{2.15}$$

That for $q = 0$ correspond to the dynamical correlation function of the energy [169]

$$C_0(t,t_w) \propto \langle H(t) H(t_w) \rangle_c \,. \tag{2.16}$$

Remarkably, the structure of FDT violations is again found to be very simple. In particular, one has, for $d > 2$ and $q = 0$, a well-defined long-time FDR X_∞, see figure 2.7. Notice how the FDR depends on the wave-number (and thus on the lengthscale) considered, an effect which could not be observed in MF models where space plays no role. Unsurprisingly, to find a well defined FDR one must consider the $q = 0$ limit, corresponding to global observables.
However, one can see from figure 2.7 thet

$$X_\infty = -3,$$

for every $d \geq 2$. This yields a negative effective temperature, quite a paradoxical result.
Despite being apparently paradoxical, a simple argument [169] shows that this behavior is indeed to be expected, due to the possibility of activation. As we said before, the $C_0(t,t_w)$ is related to the fluctuations of the energy, whose conjugated variable is temperature. If one raises the temperature of the system, the timescale

[8] The quenching and annealing dynamics can be treated in a unified manner within the dynamical TAP formalism, see [167].

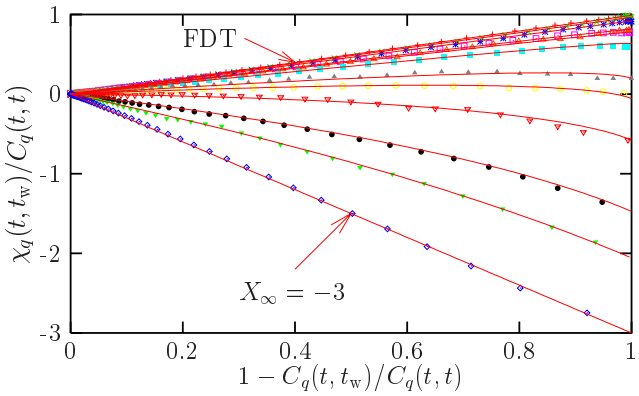

Figure 2.7. Susceptibility vs. correlation plots for the FA model in $d = 3$. Symbols are numerical data while lines are theoretical calculations. Wave-numbers decrease from top to bottom, with the bottonmost corresponding to $q = 0$. A negative FDR is observed. Reprinted from [169].

for activation goes down following Arrhenius' law, equation 1.5, speeding up relaxation and allowing the system to descend in the PEL. So the response of the energy to a temperature step is negative, causing the negative FDR observed in [169]. This example shows how the effective temperature is a MF-bound concept, and how it may not be viable for the description of aging in real glassy systems (especially strong ones) wherein activation is expected to play a role. This view is corroborated by the fact that relaxation mechanisms of KCMs seem to be a lot more mean-field like for more "fragile" KCMs, like the East Model [104]. In that case it can be seen that the relaxation proceeds in a step-like manner with multiple time sectors, each of whom can be associated to an effective temperature [168], as argued in [163].

Besides the description of activation mechanisms, Dynamical Facilitation Theory can also well describe the properties of glasses in the plateau regime. In particular, it has not remained silent after the appearance of ultrastable glasses: in [170], the non-equilibrium dynamics of the East model for a cycling temperature protocol is studied, with the express purpose of reproducing the results of [129] (in particular the left panel of figure 2.2) and DSC experiments in general. We report a sample of the results in figure 2.8. A very good agreement between theory and experiment is found, but we warn that this comes at a price: a rigorous mapping between actual glass formers and KCMs is still lacking, so to obtain an agreement like the one in figure 2.8 the East model must be "tuned" suitably. In particular, the values the energy scale J for mobility, the onset temperature T_0 whereupon the glassy slowdown starts to manifest, the microscopic relaxation time τ_0 and the fractal dimension of heterogeneities d_f must all be fixed by hand, either from reversible transport data [14] or from atomistic simulation results; and even at that point, an additional optimization over one remaining free parameter is required [170].

In summary, KCMs do have a more true-to-life nonequilibrium dynamics with respect to the RFOT approach, but they also suffer from their nature of effective models, whose physics is imposed from the outside instead of being derived from

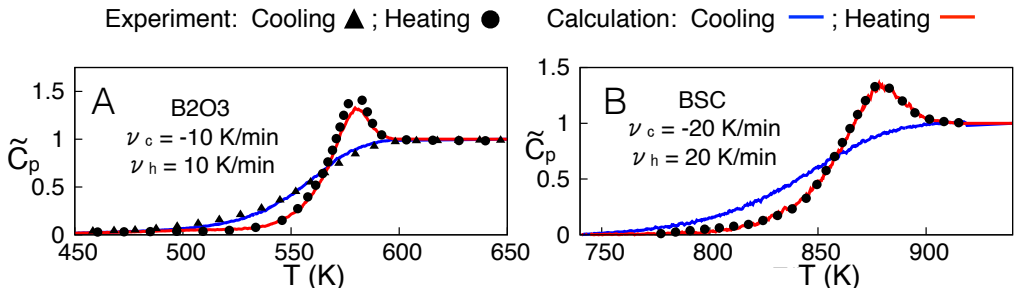

Figure 2.8. Heat capacities of fragile glass formers (boron oxide in the left panel, borosilicate in the right panel) measured from DSC experiments, compared with predictions from the non-equilibrium dynamics of the East model [104]. $\nu_{c/h}$ are the cooling/heating rate respectively. A very good agreement between experiment and theory can be observed. More plots can be found in [170].

first principles. Our state following approach, by contrast, can produce qualitatively accurate results starting just from the microscopic interaction potential of a glass former of choice, without the need for phenomenological arguments or scaling treatments.

2.2 Driven dynamics and rheology

After a glass has been prepared, one can of course do a lot more than just let it age. Namely, one can also perturb the glass with some external drive and measure its response to such a drive. There is no shortage of drives one could supply to a glass: electric currents, electromagnetic fields, scattering particles etc., but here we are concerned with mechanical drives, the simplest being shear strain. The study of the rheology of glasses, especially for low temperatures deep in the metastable glass phase ($T \ll T_g$), ties with the study of mechanical response and plasticity in amorphous solids in general (see for example [171–176]) and also in pastes, foams, colloids etc. [8], so it goes without saying that it is a field relevant for multiple engineering and material science applications.

Since we are focusing on glasses, which are solids, let us consider a cube of glass, and apply a shear displacement on its topmost face, along the x-axis. Every point $\boldsymbol{x}$ in the cube is transformed in another point $\boldsymbol{x}'$ the following way

$$\begin{aligned} x' &= x + \gamma y, \\ y' &= y, \\ z' &= z, \end{aligned} \tag{2.17}$$

Where $\gamma = \Delta x/L$, i.e. the displacement of the topmost face divided by the side L of the cube. The difference $\boldsymbol{x}' - \boldsymbol{x}$ is a vector field, called the *displacement field* [8] and denoted as $\mathbf{u}(\boldsymbol{x})$. One then has

$$\frac{\partial u_x}{\partial y} \equiv \gamma_{xy} = \gamma \tag{2.18}$$

where $\gamma_{\alpha\beta}$[9] is the *strain tensor*. Such a shear geometry is referred to as *simple shear*, and corresponds to the simplest possible structure of the strain tensor

$$\gamma_{\alpha\beta} = \begin{pmatrix} 0 & \gamma & 0 \\ 0 & 0 & 0 \\ 0 & 0 & 0 \end{pmatrix} \tag{2.19}$$

Of course, one could apply deformations in many different ways, each corresponding to a different choice of shear geometry (a very popular one is the Couette geometry [177]) and more complicated displacement fields, which in turn requires a full tensorial description of the strain [8], but in this thesis we focus on simple shear.
If our material is a solid, we reasonably expect from it an *elastic response* when the shear is small enough: the material responds to the displacement with a *shear stress*[10] proportional to the strain [8]

$$\sigma_{xy} = \sigma = \mu\gamma, \tag{2.20}$$

which is essentially Hooke's law cast in a shear-strain setting. The quantity μ is called the *shear modulus* or *elastic modulus*.
All these relations are valid at equilibrium. To be general, and remembering the discussion of section 1.1.1 and [9], we can include time into the description and write

$$\sigma(t) = G(t - t')\gamma, \tag{2.21}$$

where t' is the time whereupon the strain is applied, and we have defined a response function $G(t)$. With this definition we can treat both fluids and solids: in a fluid, the $G(t)$ will vanish after some time (intuitively, the relaxation time τ_R) and the fluid will absorb the stress (think of honey), while for a solid one will have a nonzero limit for large times, $\lim_{t\to\infty} G(t) = \mu$.
Let us now assume that we perform an experiment with time-dependent strain. We approximate this strain as formed by a succession of strain steps, each one at a time t_i, $\delta\gamma(t_i) \equiv \gamma(t_{i+1}) - \gamma(t_i)$, so that

$$\sigma(t) = \sum_i G(t - t_i)\delta\gamma(t_i) \simeq \sum_i G(t - t_i)\dot{\gamma}(t_i)\delta t_i \tag{2.22}$$

which in the continuum limit becomes

$$\sigma(t) = \int_0^t G(t - t')\dot{\gamma}(t')dt', \tag{2.23}$$

where $\dot{\gamma}(t)$ is the *strain rate*. This relation was derived in the elastic, low-strain limit, and fittingly has a strong linear response flavor. In the general case, the stress response will be a more complicated functional of the shear rate

$$\sigma(t) = \mathcal{F}[\dot{\gamma}(t)]. \tag{2.24}$$

[9] In the following we will denote space directions with Greek indices $\alpha, \beta, \gamma, \delta \ldots$ and particles with Latin indices $i, j, k \ldots$.

[10] In reality, the independent variable is actually the stress (essentially the force we supply to the material), and the displacement (essentially the strain) depends on it. Most simulations are however performed under strain control, although stress control can in principle be employed, see for example [178].

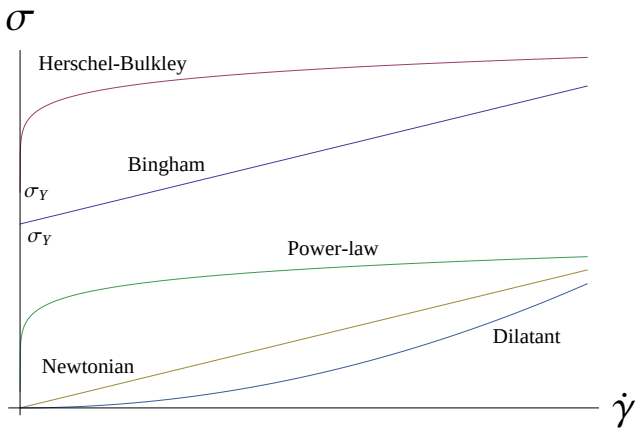

Figure 2.9. The most common models of flow in fluids and plastics. Plastics (Herschel-Bulkley and Bingham) are distinguished by the presence of a *yield stress* σ_Y, namely a finite level of stress that must be supplied to the system in order to observe flow, while fluids flow for any value of the stress.

This last relation is called a *constitutive equation*. The aim of a rheology experiment (theory) is to measure (compute) the constitutive equation for a given material, given a shear protocol $\dot{\gamma}(t)$ [8, 177].
In the case of steady shear $\dot{\gamma} = const$ in particular, one gets

$$\sigma(t) = \dot{\gamma} \int_0^t G(t')dt', \tag{2.25}$$

and the ratio of shear stress over shear rate is just the viscosity η, so in the long time limit one has [8]

$$\eta = \frac{\sigma}{\dot{\gamma}} = \int_0^\infty G(t)dt. \tag{2.26}$$

This linear relation is valid in the limit of small rates. In general the curve $\sigma(\dot{\gamma})$, called the *flow curve*, will have a non-linear form. See figure 2.9 for the most common flow curves found in plastics and fluids [177].
The flow curve characterizes the rheology of the material in the long time steady state [8]: for every value of the stress (essentially the force we supply to the material) the flow curve tells us the shear rate (essentially the velocity of flow) obtained with that stress. Most glasses and amorphous materials in general exhibit a *Herschel-Bulkley* [177] flow curve, namely

$$\sigma(\dot{\gamma}) = \sigma_Y + K\dot{\gamma}^n, \tag{2.27}$$

with an exponent n close to $1/2$ [175, 179, 180]. Since the flow curve exists only for $\sigma > \sigma_Y$, a glass has a finite *yield stress*: it flows only when the stress is high enough to deform it. For lower stresses, it responds elastically like a solid [172].
If then one remembers that $\eta(\dot{\gamma}) = \sigma(\dot{\gamma})/\dot{\gamma}$, we can see that glass formers typically exhibit *shear thinning*: viscosity (and thus the relaxation time) goes down with the shear rate [8], a behavior common to a vast class of fluids [23]. Another model with yield-stress behavior is the *Bingham plastic* [177], where $n = 1$ and viscosity is constant.

2.2.1 Athermal startup shear protocols

Most experiments and simulation on glasses employ a *startup shear* protocol, where a simple shear strain is quasi-statically applied to the glass and the stress response is measured, until the glass reaches the yielding point whereupon it starts to flow steadily. Interestingly, the steady state usually depends only on the driving, which means that the material has forgotten its history and aging has stopped, a process referred to as *rejuvenation* [23, 181].

To be more specific, the glass is typically prepared by quenching an equilibrated configuration down to zero temperature, dropping the system in an inherent structure. Once preparation is complete, a strain is applied in small steps, either by implementing a transformation like the (2.17) on particle coordinates, or by keeping the glass former between two walls moving in opposite directions [172, 182]; in both cases, the strain acts as an effective deformation of the PEL. After each step, the potential energy is minimized and the system allowed to settle in a new inherent structure (which may or may not be different from the initial one), before applying shear again. Such a protocol is called an Athermal Quasi Static (AQS) protocol since thermal fluctuations play no role and the system is allowed to equilibrate in the PEL after each step ($\dot{\gamma} \to 0$) [174].

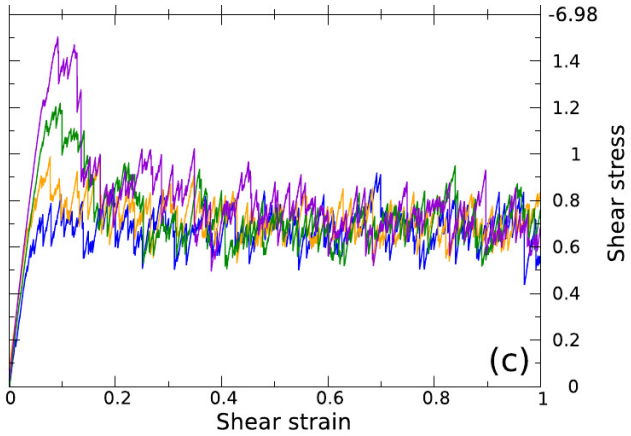

Figure 2.10. Stress-strain curve for a Lennard-Jones system with Wahnström parameters in an AQS protocol. The quench rates, in Lennard-Jones units, are 2×10^{-2} (blue), 2×10^{-3} (yellow), 2×10^{-4} (green), 2×10^{-5} (violet). A linear regime is observed for small strain, followed by a stress overshoot and then a steady flow. A slower quench corresponds to higher shear modulus and a more prominent stress overshoot. Reprinted from [172].

The observed stress-strain curves are reported in figure 2.10. One can observe, for small strain, a linear regime wherein response is elastic and a shear modulus can be defined, followed by an overshoot in stress, and then a flowing steady state [172, 183]. The magnitude of the overshoot[172, 182] and the shear modulus [172, 184] both increase when the quench is slower, which is reasonable: slower quenches correspond to deeper minima in the PEL and thus more stability and rigidity. This qualitative behavior is remarkably general [172, 174, 182]: it has been observed in systems that range from polymer glasses [185] to colloidal gels [184] to metallic

glasses [186]. Moreover, in granular materials a phenomenon referred to as *dilatancy* is observed: even though shear strain transformations such as the (2.17) are supposed to preserve volume (and thus pressure), the pressure is found to increase quadratically with the strain [187, 188].

The origin of the stress overshoot can be better understood if one looks more closely at the stress-strain curves in figure 2.10. We report such a "close up" in

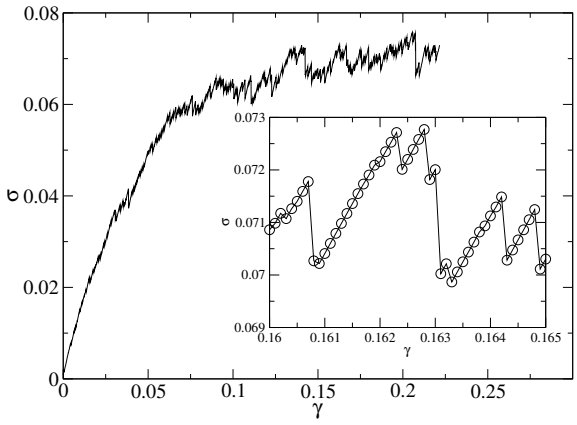

Figure 2.11. Stress-strain curve for a simulated system of harmonic disks. In the inset a "zoom in" is reported, wherein one can observe that the curve is really made up of roughly linear, elastic segments separated by plastic events, or avalanches. Reprinted from [174].

figure 2.11. One can see that a typical AQS stress-strain curve is actually made up of short segments, wherein the response is almost perfectly linear and elastic energy is loaded into the material; these segments are separated by catastrophic events whereupon the stress drops down sharply and the energy is dissipated; these are called *plastic events*, or *avalanches*. In a PEL perspective, one can visualize the elastic part as a deformation of the inherent structure the system is in, which however maintains its identity. At a certain point, the inherent structure opens up along an unstable mode, stability is lost, and the system is kicked away, producing an avalanche until it finds a new minimum[11]. Interestingly, a stress overshoot is again observed at the end of elastic segments [174].

In the elastic segments, the system "follows" the inherent structure in strain, so the motion of particles will be generally made up of two contributions: the affine transformation due to the strain and the *nonaffine* contribution necessary to track the minimum and maintain mechanical stability [190]:

$$\boldsymbol{x}_i' = \boldsymbol{x}_i + \boldsymbol{\gamma} \cdot \boldsymbol{x}_i + \boldsymbol{y}_i, \tag{2.28}$$

[11] Such a process is referred to as *saddle node bifurcation* and is somewhat analogous to a spinodal point. Indeed, one can describe it using a simple cubic theory wherein the potential energy of the system is projected along the (almost) unstable mode, and interesting scaling predictions can be obtained, see [189].

where $\boldsymbol{x}_i$ are the coordinates of particle i in the unstrained inherent structure, $\boldsymbol{x}'_i$ its coordinates in the strained one, and $\boldsymbol{y}_i$ is the nonaffine contribution. Stability within the original minimum requires that the force on each particle i, $\boldsymbol{f_i} = -\frac{\partial V}{\partial \boldsymbol{x}_i}$ be zero. The nonaffine contributions can be worked out by requiring that the forces stay zero when the strain is applied, with corresponds to imposing

$$\frac{d\boldsymbol{f}_i}{d\gamma} = \frac{\partial \boldsymbol{f}_i}{\partial \gamma} + \frac{\partial \boldsymbol{f}_i}{\partial \boldsymbol{x}_j} \cdot \frac{d\boldsymbol{y}_j}{d\gamma} = 0. \tag{2.29}$$

Where the repeated indices are understood to be summed over. One can then define two quantities

$$\boldsymbol{\Xi}_i \equiv \frac{\partial \boldsymbol{f}_i}{\partial \gamma} \qquad \boldsymbol{v}_i \equiv \frac{d\boldsymbol{y}_j}{d\gamma}, \tag{2.30}$$

called the *mismatch force*[12] and the *nonaffine velocity*, respectively [190]. Interestingly, the nonaffine forces are nonzero only for amorphous inherent structure configurations [190], so they can be used as a measure of disorder. With these definitions one can solve for the nonaffine velocities:

$$\boldsymbol{v}_i = -\boldsymbol{\mathcal{H}}^{-1}_{ij} \cdot \boldsymbol{\Xi}_j \longrightarrow v_{i\alpha} = -\mathcal{H}^{-1}_{i\alpha j\beta} \Xi_{j\beta}, \tag{2.31}$$

where $\mathcal{H}_{i\alpha j\beta}$ is the Hessian matrix (or dynamical matrix), that we had already encountered in the context of jammed packings.
Once the nonaffine velocities have been determined, the coefficients of the elastic theory [191] for the glass can be readily obtained. Their expression is

$$\mu_n \equiv \frac{1}{n!}\frac{d^n}{d\gamma^n}\sigma(\{\boldsymbol{x}(\gamma)\}) = \frac{1}{n!}\left(\frac{\partial}{\partial \gamma} + \boldsymbol{v_i} \cdot \frac{\partial}{\partial \boldsymbol{x}_i}\right)^n \frac{dV(\{\boldsymbol{x}(\gamma)\})}{d\gamma}. \tag{2.32}$$

One can immediately observe that the presence of nonaffine velocities has no influence on the stress thanks to the minimum condition $\frac{\partial V}{\partial \boldsymbol{x}_i} = 0$. However it impacts all elastic coefficients, in particular the shear modulus:

$$\mu = \frac{\partial \sigma}{\partial \gamma} - \Xi_{i\alpha}\mathcal{H}^{-1}_{i\alpha j\beta}\Xi_{j\beta} = \mu_a - \mu_{na}, \tag{2.33}$$

where μ_a is the *Born term* for a pure affine deformation [192], and μ_{na} is the nonaffine contribution.

The presence of the shear overshoot can now be understood: a loss of stability is by definition associated with the appearance of a zero mode[13] in the Hessian matrix, whose inverse appears in the nonaffine contribution in the (2.33). So the nonaffine contribution will grow as the endpoint is approached, while the Born contribution stays always finite: at a certain γ the shear modulus will be zero (and the stress-strain curve flat) and then drop until it becomes infinitely negative at the endpoint, causing the stress to go down in a steeper and steeper manner. The stress overshoot is thus an inevitable consequence of the loss of stability.

[12] The mismatch force can be seen as the contribution of particle i to the shear stress, derived with respect to its position, $\boldsymbol{\Xi}_i = \frac{\partial^2 V}{\partial \gamma \partial \boldsymbol{x}_i}$.

[13] Obviously the Hessian will always contain zero modes associated to symmetries, i.e. Goldstone modes. But they can be identified and removed easily.

This is valid for the small segments associated with a single inherent structure as just described. In one wants to "coarse grain" this picture to the whole strain-stress curve, then one may argue that a basin containing different inherent structures (called a *metabasin* [193]) should replace the inherent structure, and then the yielding transition to the steady state would correspond to a loss of stability in the whole metabasin. This picture is easy to grasp at a pictorial level, but it is obviously difficult to translate in a theory: what does exactly mean that a metabasin loses its stability and opens up? Is there a zero mode somewhere again, relative to the whole metabasin? Can one define and compute the associated Hessian matrix? Does the loss of stability of the metabasin imply a loss of stability for all the inherent structures therein contained?
We will see that these notions can be made more precise within replica theory.

2.2.2 The yielding transition

The transition between the elastic regime and the steady state is referred to as "yielding transition" and has lately been the subject of extensive study (see for example [182, 189, 194–196]). We already notice the fact that there is no clear definition for the yielding transition (much like the glass transition, in fact). A rheology-bound definition would suggest to choose the maximum of the stress σ_Y and its associated γ_Y as the yielding point. Others opt for a definition in terms of onset of energy dissipation (and consequently, avalanches) [197], or for a definition in terms of qualitative changes in the structure of the PEL (namely, in the statistics of barriers between inherent structures) after the transition [195], but there is no general agreement. Even though it is evident, from figures 2.10 and 2.11, that there is a qualitative change in behavior between the "elastic" regime and the steady state, it is not easy to pin the exact point whereupon it happens.

In the next paragraph we will see that there are theoretical approaches that ensure a good *macroscopic* description of yielding, in the sense that they do reproduce flow curves (figure 2.9) with a yield-stress form. However, a "theory of yielding" has to to do more, in the sense that it has to provide a good *microscopic* (or mesoscopic, at least) description of the transition and the ensuing flow.
Nowadays, it is generally agreed upon that flow can be thought of as a sequence of elementary, mesoscopic rearrangements that take place at well-defined points in the sample, called Shear Transformation Zones (STZ) [198]. Such a shear transformation will then induce a stress that will propagate elastically in the sample, in analogy with the nucleation of an Eshelby inclusion [199], inducing other STZs in a cascade and producing an avalanche. This picture is confirmed by a normal mode analysis of the Hessian matrix: the eigenvector (which contains the particle displacements associated with the mode[14]) of the critical mode associated with the instability shows strong localization properties [200] and a quadrupolar angular symmetry [174, 201] (see figure 2.12), just like the displacement field induced by an Eshelby inclusion. Indeed, it has been argued in [200] that only low-lying localized modes contribute to plasticity, in the sense that they are the only ones that can produce divergencies in

[14] If one writes the inverse Hessian in spectral form, $\boldsymbol{\mathcal{H}}^{-1} = \sum_i |\boldsymbol{\psi}_i\rangle \frac{1}{\lambda_i} \langle \boldsymbol{\psi}_i|$, the solution for the nonaffine velocities (2.31) becomes $\boldsymbol{v} = -\sum_i |\boldsymbol{\psi}_i\rangle \frac{1}{\lambda_i} \langle \boldsymbol{\psi}_i| \boldsymbol{\Xi}\rangle$, so the nonaffine velocity is dominated by the term proportional to the critical mode when the system is near enough to the instability.

the coefficients of the elastic theory (2.32). This would exclude delocalized modes such as phonons from the excitations relevant for yielding, a very strong assertion.

The idea that flow is initiated in definite points is not new. The mechanism for

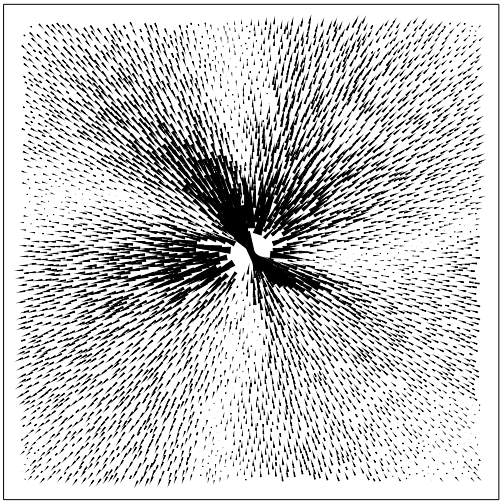

Figure 2.12. The (almost) critical mode associated with one of the instabilities (or equivalently, stress drops) in figure 2.11. The quadrupolar structure is clearly discernible. Reprinted from [174].

failure in crystalline solids is indeed ruled by a population of topological defects, known as dislocations [202], where structural failure manifests at the onset of flow. Amorphous solids, however, lack an analogue of dislocations because of their disordered nature, and as a result of this it is difficult (or perhaps impossible) to predict where failure occurs [203]. Indeed, most research on yielding focuses on finding a way to overcome this difficulty.

The first approach that comes to mind is a normal mode analysis of the Hessian, in particular of the soft modes at lowest frequency [204]: from an intuitive point of view, one would expect the perspective critical mode to be the lowest frequency one, unless the instability is too far away. One could then identify the mode, extract from it the polarization vectors of particles in the mode, and from it deduce where the ST will occur. Sadly, it is not that simple, as the dynamics of the modes as strain is applied is highly chaotic [204] and the critical mode coincides with the lowest frequency one just for a small interval of strains before the instability [174].

Another difficult point is the phenomenon of *shear banding*, namely the tendency of flow in amorphous materials to concentrate in well defined bands, leaving the rest of the material unperturbed [23]. This phenomenon is of great relevance since it is responsible for the brittleness typical of glasses: instead of deforming plastically, a glass usually breaks, because the flow at the onset of deformation concentrates

in bands, producing fractures. This behavior seems to depend on the amorphous nature of the glass and not on its actual chemical composition: metallic glasses [205, 206], for example, are usually brittle and have a strong tendency to shear band, while their crystalline counterparts do not [172].
Shear bands are nothing but a special form of dynamical heterogeneity [34], which points towards the fact that a real-space description is needed to characterize them, like shown in [207, 208]. This however looks like a challenging task, especially for MF-bound approaches like RFOT.

2.2.3 Theoretical approaches

We conclude the chapter with a brief review of some theoretical approaches to glassy rheology. A "perfect" theory or rheology, as we said before, would be a theory capable of predicting the constitutive equation for a generic shear rate protocol $\dot{\gamma}(t)$, and it goes without saying that such a program can be implemented only within a dynamical approach. This is usually very difficult, although not impossible.
However, one does not necessarily have to consider time-dependent shear protocols. For the purpose of determining the flow curve (and the yield stress σ_Y), just the capacity to treat steady shear protocols $\dot{\gamma} = const$ would anyway be sufficient. A startup shear protocol with quasi-static strain would enable us to obtain the shear modulus and the yield stress, and in principle it does not require to resort to dynamics, as we are going to see.

MCT

We mentioned before the fact that a glass subject to shear can rejuvenate, which means that its aging stops and ergodicity is restored [23]. Thanks to this fact, MCT does a lot better in the context of driven dynamics than it does in aging situations, and a lot of research efforts have been dedicated to the derivation of MCT-based rheological equations. The first of such derivations, for the steady shear case, was reported in [209], wherein a field-theoretic formalism was employed. A different derivation [210] uses the projection operator formalism, although the physics is the same in both cases. Above T_{MCT} the viscosity is found to obey the scaling law

$$\eta(\dot{\gamma}, T) = \eta(T)[1 + \dot{\gamma}/\dot{\gamma}_0]^{-\nu} \tag{2.34}$$

with $\nu = 1$, a shear thinning behavior. Below T_{MCT}, a Bingham plastic-type [177] behavior is predicted, with constant viscosity after the yielding point.
This approach can even be generalized to arbitrary shear protocols, as shown in [211, 212]. Again, in the liquid phase a shear-thinning behavior is predicted, with a flow curve more or less of the Herschel-Bulkley type [212]. If a step shear protocol is employed, $\dot{\gamma}(t) = \gamma\delta(t)$, one can again observe the usual stress overshoot, and the yield stress and shear modulus can be computed. The shear modulus is found to increase when temperature decreases, as reasonably expected. Oscillatory shear protocols have also been studied within the MCT approach, see for example [213].

In summary, MCT provides a good qualitative description of flow in glass formers, and is also remarkably flexible, allowing researchers to consider many different shear histories. All of this despite being a first principle (for much time, the *only*

first principle) approach to glassy dynamics, which is always a very welcome feature. However, one must not forget that MCT has an intrinsically MF nature, and as a consequence of this it predicts a nonexisting glass transition (as discussed in section 1.2.2) which renders it unable of providing a good description of glass-formers for temperatures much below T_{MCT}. As a result of this, the rheological variants of MCT do nor better nor worse than their equilibrium counterpart for temperatures deep in the glass phase.

RFOT

Within RFOT every equilibrium glass is associated to a glassy metastable state. As a result of this, properties relative to the state, before yielding occurs (first of all the shear modulus), can be computed from first principles without resorting to dynamics, see [214, 215], and [216] for a review. In [214], in particular, it is shown that the arrest of the system within a metastable state is associated with the appearance of a finite shear modulus that can be analytically computed from replica theory; to this day, this is the only first-principle prediction of the manifestation of a finite shear modulus (which we recall is the hallmark of solidity [9]) at the calorimetric glass transition.
However, the description of flow after yielding still requires a dynamical approach, which unsurprisingly relies again the analogy between MCT and PSM dynamics.

In [181] the dynamics of a PSM-like model is considered, which the addiction of a *driving force* which mimes the shear driving. The Langevin equation for a single spin is

$$\dot{\sigma_i}(t) = -\mu(t)\sigma_i(t) - \frac{\partial H}{\partial \sigma_i} + f_i^{\text{drive}}(t) + \eta_i(t), \tag{2.35}$$

with the driving force defined as

$$f_i^{\text{drive}}(t) = \epsilon(t) \sum^{*} \tilde{J}_i^{j_1,\dots,j_{k-1}} \sigma_{j_1}(t) \dots \sigma_{j_{k-1}}, \tag{2.36}$$

where

$$\sum^{*} \equiv \sum_{i<j_1<j_2<\dots j_{k-1}} + \sum_{j_1<i<j_2<\dots j_{k-1}} + \dots + \sum_{j_1<j_2<\dots j_{k-1}<i}, \tag{2.37}$$

and the couplings $\tilde{J}$ are quenched random variables symmetrical with respect to a permutation of the j indices, but uncorrelated with respect of permutations of the i index with any j index. As a result of this, this force cannot be written as the derivative of a potential.

The role of the shear rate is played by $\epsilon(t)$ and a steady flow with $\epsilon = const$ is considered in [181]. In the fluid phase above T_{MCT} a shear thinning behavior much like the one in equation (2.34) is found, although the exponent ν is now a function of the temperature, with $\nu(T_{MCT}) = 2/3$ and $\nu(T \to 0) \to 1$. In the glass one has

$$\eta(\dot{\gamma}, T) \simeq \dot{\gamma}^{-\nu(T)}, \tag{2.38}$$

so that the behavior is Herschel-Bulkley for all temperatures below T_{MCT}.

It's interesting to note that these results are different from the MCT ones, despite the fact that the two approaches are supposed to have the same physical

content. This may be due to the chosen form of the driving force, that despite being reasonable is still far away from being a description of a real, three dimensional flow. In any case, this approach suffers from the same shortcomings of the MCT approach in terms of MF-bound description.
Very little effort has been up to now dedicated to the description of flow beyond mean-field [23], even at the level of the scaling description provided by the mosaic (see [25] for a discussion and some first predictions). Anyway, this lack of focus is shared also by other approaches such as Dynamical Facilitation and Frustration Limited Domains [23].

Effective models

The rheology of glassy materials beyond MF has been up to now studied mainly through phenomenological models. The most popular of them is undoubtedly the Soft Glassy Rheology (SGR) model [217, 218], which consists in an adaptation of the trap models for aging originally proposed by Bouchaud [219, 220].
In this class of models the system is described as a single point that moves in a complex PEL through activation, just like in Goldstein's picture [70]. The PEL itself is idealized as a host of traps with a certain depth, described by a distribution $\rho(E)$ of traps depths, which in turn induces through Arrhenius' law a distribution $\rho(T, \tau)$ of persistence times within the traps. The distribution of times is usually chosen in such a way that its first moment diverges for low temperatures [23], so to reproduce ergodicity breaking.
The SGR model implements strain as an effective lowering of the barriers between traps [8]. We stress the fact that such a model has anyway a strong MF spirit, since only the PEL is considered and every detail regarding actual real space structure is neglected. However, the SGR model also allows activation, a trait which is not shared by the MCT and RFOT approaches, allowing the study of the interplay between activation and driving. It is also remarkably flexible: arbitrary shear protocols can be considered and the flow curve easily obtained: in particular, the model behaves as a Herschel-Bulkley plastic below the ergodicity breaking (glass transition) temperature, while in the fluid phase the behavior goes from Newtonian to power-law as the temperature is lowered [8].

Other phenomenological models have been defined over the years, mainly with the description of the yielding transition in mind. As a result of this, the all use STs as their building blocks, and mainly differ in how the interaction between STs is modeled. Two classes of such models exist: in the first class, the interaction between STs is modeled as thermal noise, in a MF kind of way [221, 222]. In the second class [223, 224], STs are put on a lattice (in a spirit similar to cellular automatons [196]) and their interaction is usually mediated by an elastic propagator of the form

$$\mathcal{G}(\phi, r) \simeq \frac{\cos(4\phi)}{r}, \tag{2.39}$$

which reproduces the quadrupolar structure shown in figure 2.12.

These models however have many shortcomings. The MF models, while exactly solvable, all suffer from their neglect of real space structure, a choice which seems to be very ill advised in the case of the yielding transition, whose phenomenology

possesses a strong characterization in real space as we discussed in paragraph 2.2.2. In addition to this, the modeling of interactions between STs as an effective thermal bath (a trait also shared by the SGR model, in fact) requires the definition of an associated "mechanical noise" effective temperature T_{eff}, whose nature is all but clear [8, 175, 181], and that of course suffers from all the shortcomings of effective temperatures in general as discussed in paragraph 2.1.4. We refer to [194] for a very critical point of view on the subject.
Elasto-plastic lattice models [223, 224], on the other hand, are more true-to-life and do take real space structure into account, but they are anyway idealized [225]: for example, they are limited to two dimensions, and usually do not take into account the displacement of STZs as the material is deformed (see [176]); besides this, they are not analytically solvable. As a result of these problems, usually they need some tuning to satisfactorily reproduce flow curves [176].

Chapter 3

The State Following construction

In the preceding chapter we have detailed how glasses are endowed with well defined and time-independent physical properties: they have a specific heat, a compressibility, a Debye-Waller factor, a shear modulus, etc.: our aim is to compute analytically those quantities from a first-principles theory. In this chapter we present some of the tools that can be used to approach the problem within RFOT, all of which rely in some way or another on the replica method originally developed in the context of spin glass theory. In particular we present the State Following construction that this thesis is based on, along with a possible generalization of it that could in principle allow to model more complicated protocols than the ones considered in this work. The reader should appreciate how all the computation schemes that we present in this chapter are centered around the aim of treating metastability in a purely static fashion, without having to solve the dynamics, in accordance with the RFOT picture of the glass transition as a phenomenon with a static origin.

3.1 The real replica method

We are interested in a metastable glass, be it obtained with a quenching [125] or an annealing protocol [126]. We want to compute its physical properties as they would manifest themselves in a DSC experiment (paragraph 2.1.2) or in a quasi-static simple shear experiment (paragraph 2.2.1). In both those cases, the perturbation (temperature change or shear) is applied adiabatically to the material, which means that the system is in *restricted equilibrium* inside a metastable state during the experiment. Within RFOT, as we mentioned, states have a *static* origin: they are not just born from the plateau regime in the dynamics, but they are minima of a suitable, static FEL. As a result of this, and differently from what happens in other approaches to the glass problem, they have a static free energy

$$f_\alpha(T,\gamma) = -\frac{1}{N\beta}\log\int_{X\in\alpha} dX\; e^{-\beta V_\gamma(X)} = F(\{\rho^\alpha(\beta,\gamma)\},\beta) \tag{3.1}$$

where $X \equiv (\boldsymbol{x})_{i=1}^N$ is a generic configuration of the glass former, F is the free-energy functional, ρ^α the amorphous profile that corresponds to the state, and γ

a generic perturbation that the glass is subjected to. This free energy rules the whole thermodynamics of the metastable state, and the physical observables of the system at restricted equilibrium can be computed from it using standard equilibrium thermodynamic relations, like Maxwell's: within RFOT, to study a metastable glass, we have to compute its free energy f_α.
It is however obvious that computing the f_α is not sufficient, because we also need to know which state the system is in, i.e. we need to know α. However, as we detailed in paragraph 1.2.4, this knowledge comes to us in the form of the *complexity*. If the glass has been prepared through a quenching protocol, the state will be one of the threshold states such that

$$f_\alpha = f_{th} : \max_f \Sigma(f,\beta) = \Sigma(f_{th},\beta), \tag{3.2}$$

while if the glass has been made with an annealing protocol down to a glass temperature T_g, the state will be selected by the condition (1.43), that we recall here

$$f_\alpha = f^* : \frac{1}{T_g} = \left.\frac{d\Sigma(f,\beta)}{df}\right|_{f=f^*}, \tag{3.3}$$

and the system will remain in this state during the quench down to the target temperature T. In both cases, knowledge of both the in-state free energy f and the complexity Σ is required to study the thermodynamics of state α.

In principle, the computation of the free energy and complexity would require starting from the free energy functional F: one has to compute the functional, then find its stationary points as a function of T, and then count them to get the complexity; quite a challenging program. This "hands-on" approach can nevertheless be implemented in the case of the p-spin spherical model (PSM), wherein the free energy is the TAP free energy [46] of all local magnetizations m_i as we already discussed (we refer again to [66] for further reading); but it is not viable in the case of real glass-formers, also considering the fact that the free energy functional in real liquids is usually a functional of the local density profile in the continuum [18] $\mathcal{F}[\rho(\boldsymbol{x})]$, unless we limit ourselves to lattice gases.
The solution to this problem was proposed in [226] and goes under the name of *real replica* method. The basic idea is to introduce m replicas of the original system, with the condition that they all live in the same metastable state. This can be accomplished, for example, by introducing a weak coupling ϵ between replicas [226]. The partition function for the replicated system reads then

$$Z_m = \sum_\alpha e^{-\beta N m f_\alpha}. \tag{3.4}$$

now we can again introduce the complexity

$$\frac{1}{N}\log\left[\sum_\alpha \delta(f-f_\alpha)\right] \equiv \Sigma(f,\beta),$$

and again we get

$$Z_m = \int df\ e^{-\beta N[mf - T\Sigma(f,\beta)]} = e^{-\beta N[mf^* - T\Sigma(f^*,\beta)]} \equiv e^{-\beta N \Phi(m,\beta)}, \tag{3.5}$$

where we have defined the free energy of the replicated system $\Phi(m,\beta)$ and the condition (1.43) on f^* has now been "upgraded" to

$$\frac{m}{T} = \left.\frac{d\Sigma(f,\beta)}{df}\right|_{f=f^*}. \tag{3.6}$$

Then one than easily prove that

$$f^*(m,\beta) = \frac{\partial}{\partial m}[\Phi(m,\beta)], \tag{3.7}$$

$$\Sigma(f^*(m,\beta),\beta) = m^2\frac{\partial}{\partial m}[m^{-1}\beta\Phi(m,\beta)]. \tag{3.8}$$

So, once we are able to compute the free-energy Φ of the replicated system and perform its analytic continuation to real values of m, the real replica method enables us to compute the free energy $f^*(m,\beta)$ of the equilibrium states fixed by the (3.6) and their complexity $\Sigma(f^*(m,\beta),\beta)$. The full complexity function can be then computed by inverting the (3.6) to get $m(f^*,\beta)$ and plugging it into the m-dependent complexity, equation (3.8)) to get $\Sigma(f,\beta)$ [45, 226, 227].
Summarizing, the basic idea of the real replica method is to introduce a parameter m conjugated to the in-state free energy f, allowing us to compute it just by taking a derivative of the replicated free energy, in a standard thermodynamic fashion [226]. From the (3.6), we can see that choosing a different m selects a different group of metastable states, which are different from the equilibrium states of the system unless $m = 1$: the presence of the parameter m allows us to choose f^* at our leisure, and study different groups of states according to our needs: within this formalism, choosing a dynamical protocol corresponds to choosing a function $m(T)$.
Indeed, observing more closely the (3.6) and comparing it with the (1.43), we are immediately prompted to define an effective temperature in the following way

$$\frac{1}{T_{\text{eff}}} = \frac{m}{T} = \left.\frac{d\Sigma(f,\beta)}{df}\right|_{f=f^*}, \tag{3.9}$$

which means that the states we select by choosing m at temperature T are effectively those that would be equilibrated at $T = T_{\text{eff}}$ defined in the (3.9): we can appreciate how the real replica method is nothing but a static (and more flexible) incarnation of the effective temperature picture [159, 160, 163].

3.1.1 Quenching: the threshold

In the case of a quenching protocol down to a target temperature T, the system will remain stuck in the threshold states fixed by the (3.2), so the function $m(T)$ will simply be $m(T) = m_{th}(T)$ such that

$$\frac{m_{th}}{T} = \left.\frac{d\Sigma(f,\beta)}{df}\right|_{f=f_{th}}, \tag{3.10}$$

and unsurprisingly, one has

$$\frac{m_{th}}{T} = \frac{1}{T_{\text{eff}}} \tag{3.11}$$

where T_{eff} corresponds [160] to the effective temperature computed from the dynamical solution [157]. The real replica method allows one to compute all interesting long-time observables relative to a generic quenching dynamics.

3.1.2 Annealing: isocomplexity

In the case of an annealing dynamics, things are more complicated. We know that the state of the system is selected at equilibrium through the (1.43), so we know that $m(T_g) = 1$ and $f_\alpha = f(1, T_g)$. However, we still need to determine the rest of the function $m(T)$ as the system is quenched below T_g and the original equilibrium state is "followed" in temperature. Summarizing, we need a criterion to choose a function $m(T)$ consistent with the requirement that the system remain in that same state as T changes [228].
Following [229], one can assume that, as T is changes, states do not coalesce, or merge, or cross. This means that the number (and thus the complexity) of states at each free energy level f is a conserved quantity, and can be used as a label for the states. This method is usually referred to as isocomplexity [228, 229]. The function $m(T)$ will be then determined by the condition

$$\Sigma(1, T_g) = \Sigma(m(T), T), \tag{3.12}$$

where Σ is the m-dependent complexity computed in the (3.8). In chapter 6 we will present some results on glassy state following obtained with the isocomplexity assumption.

3.1.3 Summary

The real replica method provides us with a set of tools to treat metastability without having to resort to the TAP approach. This method is thus well suited to the study of a quenching dynamics like the one considered in [157]. It constitutes a computational tool conceived for the treatment of all systems with an RFOT transition (from structural glasses, to spin glasses [57] and even optimization problems in computer science [230]). Because of this, it has been for much time the standard method for the treatment of structural glasses within RFOT, from the very first papers [231, 232] to the more recent efforts of the series [41, 154–156].

Nonetheless, as we detailed in the previous chapter, in recent years the experimental and numerical focus has moved away from quenching protocols; and within the real replica method, the only way to treat annealing protocols is the isocomplexity assumption, which despite being reasonable fails in all models except the PSM: the states do actually cross, merge and coalesce, so assuming that their number is conserved is just plain wrong. The isocomplexity assumption is thus, at best, an approximation of the real dynamics of the system, even at mean-field level.
This weakness should not come as a surprise considering how the real replica method is basically a static recasting of the effective temperature concept, which postulates that the typical configurations visited during a non-equilibrium, aging dynamics are just the configurations the system would visit if it were equilibrated at $T = T_{\text{eff}}$. This is a very strong assumption that is false in most cases: the configurations visited by the system during aging may very well have nothing to do with equilibrium ones, even at MF level, and as a result of this they may have a vanishing weight in the equilibrium probability distribution, and be missed completely by the real replica computation.
In summary, we need a more refined formalism to treat annealing dynamical protocols like the ones considered in [166]. In the following section we introduce that

formalism, and we refer to [45, 94, 227] for further reading on the real replica method.

3.2 The two-replica Franz-Parisi potential

Let us go back to the definition of the in-state free energy f_α

$$f_\alpha(T,\gamma) = -\frac{1}{\beta N}\log\int_{X\in\alpha} dX\ e^{-\beta V_\gamma(X)}. \tag{3.13}$$

We have detailed in paragraph 1.2.4 how states are essentially "patches" in the configuration space of the system (see figure 3.1), which in this case is the Nd-dimensional space of vectors X. We have to somehow find a way to make sure that only configurations belonging to state α are included in the partition function above, which means that we have to define a Gibbs measure somehow *constrained* inside the state.
According to the amorphous solid picture 1.1.4, the configurations belonging to state α will consist of the fixed amorphous configuration the particles vibrate around, which is given by a set of positions $R \equiv (\boldsymbol{r})_{i=1}^N$, and all configurations visited during the vibration. We can thus hope to implement the constraint in state α by accepting in the partition function only configurations which are not too far away from R. We can thus write

$$f(T,\gamma;R) = -\frac{1}{\beta N}\log\int dX\ e^{-\beta V_\gamma(X)}\theta[\Delta_r - \Delta(X,R)], \tag{3.14}$$

where $\Delta(X,R)$ is the rescaled MSD between X and R

$$\Delta(X,R) \equiv \frac{d}{N}\sum_{i=1}^{N}(\boldsymbol{x}_i - \boldsymbol{r}_i)^2 \tag{3.15}$$

and θ is the Heaviside theta function [233]. We have essentially chosen $\theta[\Delta_r - \Delta(X,R)]$ as the characteristic function of state α.
The $f(T,\gamma;R)$ is the free energy of the glass selected by the amorphous configuration R. However, it is clear that such a thing cannot be computed: on technical level, the presence of the constraint breaks translational invariance and prevents us from using standard statistical-mechanical methods; on a conceptual level, we do not know R.
To circumvent this difficulty we can assume that the properties of the glass do not depend much on the actual realization of the amorphous configuration R, i.e., that the observables of the glass possess a *self-averaging* [66] property. As a rule of thumb, this is usually true for extensive observables like the free energy. Thus we can average the f over all possible amorphous configurations R, which will be distributed with a certain probability distribution $P(R)$.
We then have to find out which is $P(R)$, but this is simple: the configuration R is by definition the last configuration visited by the system before falling out of equilibrium, so it will be distributed with the usual canonical distribution at $T = T_g$,

$$P(R) = \frac{e^{-\beta_g V(R)}}{Z(T_g)}. \tag{3.16}$$

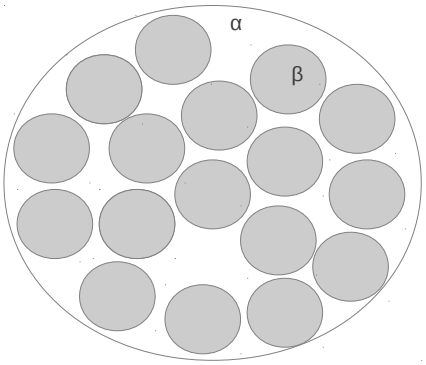

Figure 3.1. States as patches in the space of configurations of the glass-former.

So in the end we can define the free energy of the glass

$$f_g(T,\gamma;T_g) = \overline{f(T,\gamma;R)} = \int dR\ \frac{e^{-\beta_g V(R)}}{Z(T_g)} f(T,\gamma;R), \tag{3.17}$$

which is the free-energy of a glass at temperature T, subjected to a generic perturbation γ, and prepared through an annealing protocol such that the system falls out of equilibrium at T_g[1]: it allows us to follow a state in temperature from when it is selected by the (1.43) at T_g to a temperature T whereupon a measurement is performed. This free energy, dubbed the *Franz-Parisi potential* (FP), has been formalized in [235] in the context of spin glass models, with the express purpose of studying the long time limit of annealing protocols like the ones considered in [166], and is the centerpiece of State Following (SF) formalism. Up to now it has been only employed in the context of schematic spin glass models [236–239]; in this thesis we apply it, for the first time, to a realistic model of glass former.

This is exactly what we need, but there is clearly a missing ingredient: which is the value of Δ_r? We have to somehow fix its value in such a way that the whole glass state, and nothing more than that, is sampled.
To understand how to choose Δ_r, let us rewrite the (3.14) in the following way:

$$\frac{1}{Z}\int dX\ e^{-\beta V_\gamma(X)}\delta[\Delta_r - \Delta(X,R)] = \langle \delta[\Delta_r - \Delta(X,R)]\rangle \equiv e^{-\beta N(V(\Delta_r)-V(\infty))}, \tag{3.18}$$

wherein we have replaced the Heaviside theta with a Dirac delta[2] and used the fact

[1] We stress again that the self-averaging property is not true for all observables. In particular, it is not true for observables strongly related to the structure R of the glass, such as the refractive index: the structure R is sampled from the distribution $P(R)$, so it not uniquely determined by T_g, and as a result of this glasses with the same fictive temperature can have different refractive indexes as discovered in [234].

[2] In the thermodynamic limit, the two choices are completely equivalent: if the theta is the characteristic function of the state, then the delta is the characteristic function of its boundary. But in the thermodynamic limit the dimensionality of the configuration space goes to infinity, and the volume of any compact set inside it concentrates on its own boundary [158]. It is a purely geometrical fact.

that choosing $\Delta_r = \infty$ means considering the whole configuration space. The (3.18) is nothing but the probability[3] that, if we throw a random configuration X with the canonical distribution, we find it to be at a distance Δ_r from the configuration R, written in a large deviation form through the function $V(\Delta_r) \equiv f(T, \gamma; R)$.

How does $V(\Delta_r)$ behave? The probability to find the configuration X just on top of the configuration R is obviously zero, so one must have $V(\Delta_r = 0) = \infty$. Conversely, when $\Delta_r = \infty$, we are accepting all configurations, so the probability is one. Between these two values, we expect that at high temperature the probability will just monotonically increase (and $V(\Delta_r)$ decrease), since we are considering a larger and larger region of the space of configurations and the Boltzmann-Gibbs distribution is effectively a uniform distribution at high T.
However, this will not be true below T_{MCT}, whereupon glassy states appear (see figure 3.1). The configuration R will belong to one of the states and the probability will go up monotonically only as long as we consider through Δ_r a region contained within the state: when the region becomes bigger, one starts to sample configurations on the boundary, which are unlikely configurations that the system only visits when barrier crossings take place: the probability will start to go down and $V(\Delta_r)$ to increase. When Δ_r is increased further, other states are taken into consideration and $P(\Delta_r)$ will increase anew.
Summarizing, below T_{MCT}, the function $V(\Delta_r)$ will have a minimum for $\Delta_r^* \neq 0$, and that value of Δ_r will correspond to the optimal sampling of configurations inside the state. This picture is not changed by the introduction of the average over R (3.17): the $f_g(T, \gamma; T_g)$ must be minimized over Δ_r to obtain the free energy of the glass.

If one chooses $T = T_g$, then the FP potential corresponds to the free energy of an equilibrium state at T_g, the same one can compute from the real replica method. In that case, since $V(\Delta_r = \infty) = F_{liq}$, one has by definition

$$V(\Delta_r^*) - V(\infty) = T\Sigma(T) \tag{3.19}$$

as sketched in figure 3.2. From the 3.2 the reader can appreciate the first order character of the glass transition according to RFOT: T_{MCT} corresponds to the spinodal point whereupon metastable states lose stability; below T_{MCT}, a glassy minimum is present with $\Delta_r = \Delta_r^* \neq 0$, but always metastable with respect to the liquid minimum with $\Delta_r = \infty$, with a free energy gap between the two equal to $T\Sigma(T)$; at $T = T_K$, the glassy minimum becomes stable with respect to the liquid one and the ideal glass transition takes place.

In chapters 4 and 5 we present the results obtained applying the SF construction to hard spheres in the MF limit. We refer to [239] for a comparison of the isocomplexity and SF approaches in the context of p-spin glasses.

[3] We recall that the prescription to compute the probability distribution of a generic observable $\mathcal{O}(\mathcal{C})$ is $P(\mathcal{O}) = \langle \delta(\mathcal{O} - \mathcal{O}(\mathcal{C})) \rangle$.

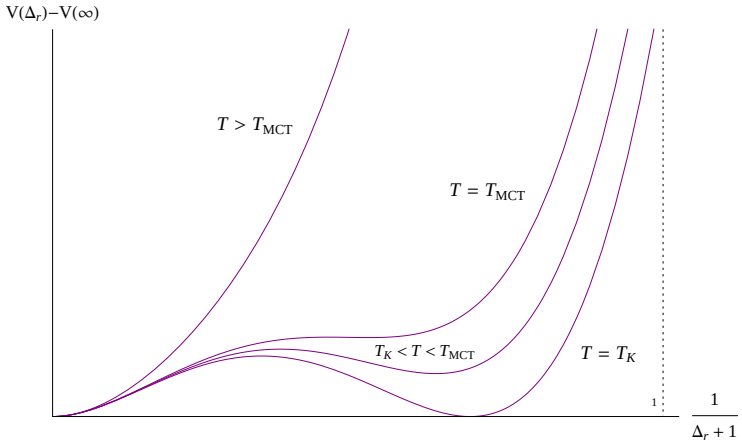

Figure 3.2. The FP potential as a function of Δ_r for $T = T_g$, as the temperature is lowered as detailed in paragraph 1.2.4.

3.3 Beyond two replicas: the replica chain and pseudo-dynamics

The FP construction can be generalized to larger numbers of replicas. Its generalization to three replicas was for example used in [240] to study barriers between metastable states, and its generalization to an arbitrary number of replicas was first sketched in [241].

Let us suppose that we have a generic system with configurations $\mathcal{C}$, $\mathcal{C}' \ldots$, a Hamiltonian $H(\mathcal{C})$ and a notion of "similarity" between configurations $q(\mathcal{C}, \mathcal{C}')$, which has to be conveniently chosen depending on the system. Above, we have used the MSD between configurations, but if one starts from a density-functional theory of a liquid, the choice could be [242]

$$q(\mathcal{C}, \mathcal{C}') = \int d\boldsymbol{x} d\boldsymbol{y}\ w(\boldsymbol{x} - \boldsymbol{y}) \rho_{\mathcal{C}}(\boldsymbol{x}) \rho_{\mathcal{C}'}(\boldsymbol{y}), \tag{3.20}$$

where $\rho_{\mathcal{C}}(\boldsymbol{x})$ is the density profile relative to the configuration $\mathcal{C}$ [18] and w a coarse-graining function whose details have no relevance. For spin models one usually uses [243]

$$q_{\mathcal{C}\mathcal{C}'} = \frac{1}{N} \sum_{i=1}^{N} \sigma_i^{\mathcal{C}} \sigma_i^{\mathcal{C}'}. \tag{3.21}$$

One starts from replica 1, which is chosen to be equilibrated at a temperature T_1

$$P(\mathcal{C}_1) = \frac{1}{Z} e^{-\beta_1 H(\mathcal{C}_1)}. \tag{3.22}$$

Replica 2 is chosen to be equilibrated at a temperature T_2, and constrained to be near to replica 1 by using the $q(\mathcal{C}_1, \mathcal{C}_2)$

$$P(\mathcal{C}_1, \mathcal{C}_2) = \frac{1}{Z(\mathcal{C}_1)} e^{-\beta_2 H(\mathcal{C}_2)} \delta(q(\mathcal{C}_1, \mathcal{C}_2) - C(1,2)) \frac{1}{Z} e^{-\beta_1 H(\mathcal{C}_1)}, \tag{3.23}$$

where

$$Z(\mathcal{C}_1) \equiv \int d\mathcal{C}_2 e^{-\beta_2 H(\mathcal{C}_2)} \delta(q(\mathcal{C}_1, \mathcal{C}_2) - C(1,2)). \tag{3.24}$$

This corresponds to the two-replica case; in general, one can define a transition probability

$$M(\mathcal{C}_{s+1}|\mathcal{C}_s) \equiv \frac{1}{Z(\mathcal{C}_s)} e^{\beta_{s+1} H(\mathcal{C}_{s+1})} \delta(q(\mathcal{C}_s, \mathcal{C}_{s+1}) - C(s, s+1)), \tag{3.25}$$

in such a way that the probability of a "trajectory" can be written as

$$P(\mathcal{C}_L, \mathcal{C}_{L-1}, \ldots, \mathcal{C}_1) = \prod_{i=1}^{L-1} M(\mathcal{C}_{s+1}|\mathcal{C}_s) P(\mathcal{C}_1). \tag{3.26}$$

for a chain of length L. The transition rate defined in the (3.25) defines a Markov stochastic process, and with it, a dynamics. Within this dynamics, the system samples the phase space with an equilibrium Boltzmann-Gibbs distribution at each step, so it is allowed to equilibrate, but not too far away from the configuration at the preceding step, because of the δ constraints: the replica chain defined above implements formally the RFOT idea of the dynamics of glass formers as a process made of activated jumps between states. Because the system equilibrates at each step, the dynamics defined in (3.25) is fittingly referred to as a *Boltzmann pseudodynamics* [243].

The replica chain can be interesting to study for a finite number L of bonds (for example, in [237, 244] it was argued that the two-replica potential may be not sufficient for following states adiabatically in the whole range of temperatures), but its most interesting application is in the limit $L \to \infty$ of infinite bonds and constant chain length. In that case, the values of the index i are promoted to continuous variables and the parameters $C(s, s+1)$ to functions $C(t, t')$. It can then be shown [243] that in this limit, and with $\beta_s = const = \beta$ one gets back, for the PSM, the slow part of the dynamical equations (2.5), (2.6) and (2.7) for a quenching dynamics. This is no surprise: in the pseudodynamics defined above, the system equilibrates within a state at each step, and as a result of this only the details of the slow part of relaxation are reproduced, while the fast part is neglected by construction. An annealing dynamics [166] can be modeled by choosing $\beta_1 = \beta_g$ and $\beta_s = \beta \ \forall s \neq 1$. The main advantage of the pseudodynamics approach is the usual advantage of RFOT tools in general (real replica method, FP potential, etc.): since the system is equilibrated at each step, the actual computation of the properties of the chain is completely *static* in nature, and corresponds, roughly, to the problem of computing the static properties of a replicated system, where each replica corresponds to a node in the chain. Again, details of the long-time dynamical properties of the system can be computed without ever touching the dynamics itself.

In [242] the replica chain is applied to a generic model of glass former in a liquid theory setting. Within liquid theory, the computation of the statics of a liquid typically reduces to the computation of its pair distribution function $g(r)$ [18]. To implement the chain formalism, one must consider a mixture of different particle species, each of them corresponding to one replica in the chain, with the pair distribution function generalized to $g_{ab}(r)$ where a and b are species-labeling

indexes. Within liquid theory for particle mixtures, the $g_{ab}(r)$ is related to the direct correlation function $c_{ab}(r)$ by the Ornstein-Zernike relation [18]

$$c_{ab}(\boldsymbol{x},\boldsymbol{y}) = h_{ab}(\boldsymbol{x},\boldsymbol{y}) - \rho \sum_c \int d\boldsymbol{z}\ h_{ac}(\boldsymbol{x},\boldsymbol{z}) c_{cb}(\boldsymbol{z},\boldsymbol{y}), \tag{3.27}$$

where $h_{ab}(\boldsymbol{x}) \equiv g_{ab}(\boldsymbol{x}) - 1$. To solve the statics of the mixture, one has to find another relation to link the $c_{ab}(\boldsymbol{x})$ with the $g_{ab}(\boldsymbol{x})$, so to get a closed system of integral equations, as per usual practice in liquid theory [18]. In [242], two closure schemes are studied: the first is the well known Hypernetted Chain (HNC) closure [18]:

$$\log[h_{ab}(\boldsymbol{x}) + 1] + \beta v_{ab}(\boldsymbol{x}) = h_{ab}(\boldsymbol{x}) - c_{ab}(\boldsymbol{x}), \tag{3.28}$$

where $v_{ab}(\boldsymbol{x})$ is the interaction potential between species a and b; the other is a closure scheme proposed by Szamel in [245]:

$$c_{ab}(k) = \int dq\ V(k,q) h_{ab}(q) h_{ab}(k-q), \tag{3.29}$$

where $V(k,q)$ is the MCT vertex defined in the (1.29). Very interestingly, once one imposes TTI and FDT, in both cases the slow part of the MCT equation is recovered [242]. This result bolsters the RFOT picture of dynamics as a hopping process between states.

The replica chain is not the main focus of this thesis so our treatment of it stops here. Up to now, it has only been used in the case $\beta_s = const$ which reproduces a quenching dynamics, but its potential goes far beyond that. On one hand, it could be interesting to consider general protocols wherein $\beta(t)$ is a full function of the time, but the most interesting application could come from its generalization to a shear strain situation, instead of simple aging. For example, it could be in principle used to get a complete RFOT-born rheological theory of glass formers for a generic shear protocol $\dot{\gamma}(t)$.

Chapter 4

The replica symmetric ansatz

In this chapter we perform the computation of the Franz-Parisi potential for the hard sphere (HS) model in the MF limit. As we anticipated, the perturbations we focus on will be adiabatic compression/decompression and quasi-static shear strain, and we compute the response of glassy states to these perturbations. As we detail in the following, the computation requires the formulation of an *Ansatz* about the structure of the metastable state the system is trapped in. In this chapter we focus on the so-called Replica Symmetric (RS) ansatz, which means that we assume the state to be a simple minimum of the FEL without any further internal structure. Since all calculations are performed with the saddle-point method [86], the results obtained from this ansatz and its relative saddle point must be checked for stability, i.e. the Gaussian fluctuations around the saddle point value of the integral must be negative. We verify that beyond a certain value of both the compression and the strain parameter, it is not so: the RS Ansatz is unstable and a more complicated structure manifests inside the glassy minimum in study, requiring a more complicated Ansatz.

4.1 Computation of the FP potential

We want to compute:

$$F_g(T,\gamma;T_g,\Delta_r) = \frac{1}{Z_m}\int dR^1\cdots dR^m\, e^{-\beta_g\sum_{a=1}^m V(R^a)} F(T,\gamma;R^1,\Delta^r), \tag{4.1}$$

with

$$F(T,\gamma;R,\Delta^r) \equiv -T\log\int dX e^{-\beta V_\gamma(X)}\delta(\Delta^r-\Delta(X,R)), \tag{4.2}$$

where to be general we average the F over m replicas instead of just one. This way, one can in principle take a state outside of the equilibrium line by choosing m appropriately as explained in section 3.1, a protocol which could for example correspond to a quench followed by an adiabatic perturbation. However, in this thesis we only focus on the equilibrium, $m = 1$ case, corresponding to an annealing protocol as previously discussed.
The average above defined can be computed using the *replica trick* [45, 66]. If one defines

$$Z_g \equiv \int dX e^{-\beta V_\gamma(X)}\delta(\Delta^r-\Delta(X,R)), \tag{4.3}$$

and

$$\begin{aligned} -\beta N F_{\rm FP} &= \log \int dR^1 \cdots dR^m dX^1 \cdots dX^s e^{-\beta_g \sum_{a=1}^m V(R^a) - \beta \sum_{b=1}^s V_\gamma(X^b)} \\ &= \log \int dX^1 \cdots dX^m e^{-\beta_g \sum_{a=1}^m V(X^a)} (Z_g)^s = \log[Z_m \overline{(Z_g)^s}] \ , \end{aligned} \tag{4.4}$$

then we have, at leading order for small s

$$\begin{aligned} -\beta N F_{\rm FP} &= \log \left[Z_m \overline{(Z_g)^s} \right] \sim \log \left[Z_m (1 + s \overline{\log(Z_g)} + O(s^2)) \right] \\ &= \log Z_m + s \, \overline{\log Z_g} + O(s^2) \\ &= -\beta F_m - s \beta F_g(T, \gamma; T_g) + O(s^2) \ . \end{aligned} \tag{4.5}$$

Therefore we have to compute the free energy of $m+s$ replicas; m "reference" ones and s "constrained" ones, that are at different temperature or density, and then we have to expand it around $s = 0$; the leading order gives the replicated free energy F_m [226], while the linear order in s will yield the FP free energy $F_g(T, \gamma; T_g)$ we want to compute.

4.1.1 Perturbations

The construction above can be performed for any model $V(X)$ of glass former. In the following, we focus only on the hard sphere (HS) [18] interaction potential, whose definition we recall here

$$v_{HS}(\boldsymbol{x}) \equiv \begin{cases} 0 & |\boldsymbol{x}| > D \\ \infty & |\boldsymbol{x}| \leq D \end{cases} \tag{4.6}$$

hence temperature plays no role and the packing fraction is the only relevant control parameter [18]. Furthermore, the energy is zero, therefore the free energy contains only the entropic term and $-\beta F = S$.
For technical reasons, it is convenient to fix the packing fraction through the sphere diameters, while assuming that the number density ρ be constant, as in the LS algorithm [135]. We consider the m reference replicas to have diameter D_g and packing fraction φ_g, while the s constrained replicas have the same number density but $D = D_g(1+\eta/d)$. Following [153, 154] we also define a rescaled packing fraction $\widehat{\varphi} = 2^d \varphi / d$ that has a finite limit when $d \to \infty$. Note that the packing fraction of the constrained replicas is therefore $\varphi = \varphi_g (D/D_g)^d \sim \varphi_g e^\eta$ and similarly $\widehat{\varphi} = \widehat{\varphi}_g e^\eta$.

Following [214–216], we also apply a shear strain γ to the constrained replicas, which is obtained by deforming linearly the volume wherein the system is contained. Following the discussion in section 2.2, we call x'_μ, with $\mu = 1, \cdots, d$, the coordinates in the original reference frame, in which the shear strain is applied. In this frame, the cubic volume is deformed because of shear strain. To remove this undesirable feature, we introduce new coordinates x_μ of a "strained" frame wherein the volume is brought back to a cubic shape. If the strain is applied along direction $\mu = 2$, then all the coordinates are unchanged, $x_\mu = x'_\mu$, except the first one which is changed according to

$$x'_1 = x_1 + \gamma x_2 \ , \qquad x_1 = x'_1 - \gamma x'_2 \ . \tag{4.7}$$

Let us call $S(\gamma)$ the matrix such that $\boldsymbol{x}' = S(\gamma)\boldsymbol{x}$. In the original frame (where the volume is deformed by strain), two particles of the slave replica interact with the potential $v(|\boldsymbol{x}' - \boldsymbol{y}'|)$. If we change variable to the strained frame (where the volume is not deformed), the interaction is

$$v_\gamma(\boldsymbol{x} - \boldsymbol{y}) = v(|S(\gamma)(\boldsymbol{x} - \boldsymbol{y})|) \ . \tag{4.8}$$

An important remark is that $\det S(\gamma) = 1$ meaning that the simple strain defined above does not change the volume and thus the number density $\rho = N/V$ of the system.

In summary, to follow a glass state under a compression and a strain, we have to compute the Franz-Parisi potential where the constrained replicas have a diameter $D = D_g(1 + \eta/d)$ and interact with a potential $V_\gamma(X) = \sum_{i<j} v_\gamma(\boldsymbol{x}_i - \boldsymbol{x}_j)$. The control parameter of the reference replica is their density φ_g, while the control parameters of the constrained replicas are the compression parameter $\eta = \log(\varphi/\varphi_g)$ and shear strain γ. The replicated entropy of this system can be computed through a generalization of the methods of refs. [154, 155], which we sketch below.

4.1.2 The replicated entropy and the RS ansatz

The *exact* expression of the replicated entropy of HS in the MF limit, and for a completely generic replica structure has been derived in [155]:

$$\begin{aligned} s[\hat{\alpha}] = 1 - \log\rho + d\log(m+s) + \frac{(m+s-1)d}{2}\log(2\pi e D_g^2/d^2) \\ + \frac{d}{2}\log\det(\hat{\alpha}^{m+s,m+s}) - \frac{d}{2}\widehat{\varphi}_g\,\mathcal{F}\,(2\hat{\alpha}) \ , \end{aligned} \tag{4.9}$$

where $\hat{\alpha}$ is a $(m+s)\times(m+s)$ symmetric matrix defined in appendix A and $\hat{\alpha}^{a,a}$ is the matrix obtained from $\hat{\alpha}$ by deleting the a-th row and column. We refer to appendix A for a sketch of the derivation of the ∞-dimensional solution.
As explained in appendix A, the matrix $\hat{\alpha}$ encodes the fluctuations of the replica displacements $u_a \equiv x_a - X$ around the center of mass of all replicas. Because $\sum_a u_a = 0$, the sum of each row and column of $\hat{\alpha}$ is equal to zero, i.e. $\hat{\alpha}$ is a *Laplacian* matrix. Here we used D_g as the unit of length, and for this reason D_g and $\widehat{\varphi}_g$ appear in eq. (4.9). We call the last term in Eq. (4.9) the "interaction term", while the one containing the determinant of $\alpha^{m,m}$ will be called the "entropic term". It is usually more convenient to use a different matrix, denoted as $\hat{\Delta}$

$$\Delta_{ab} \equiv \frac{d}{D_g^2}\left\langle (u_a - u_b)^2 \right\rangle = \alpha_{aa} + \alpha_{bb} - 2\alpha_{ab}, \tag{4.10}$$

which encodes the MSDs between replicas; the matrix $\hat{\Delta}$ has a more straightforward physical interpretation and is more suited to the definition of the parameter Δ^r in section 3.2, but it is completely equivalent to the $\hat{\alpha}$.

Following [155], the (4.9), once optimized over $\hat{\alpha}$ (or equivalently $\hat{\Delta}$), yields the entropy of the replicated system of hard spheres. We must then perform its analytic continuation to real s and then take the linear order in s to get the FP potential. In order to perform this computation, we must make a choice, an *ansatz*, for the

matrix $\hat{\Delta}$, which encodes the replica structure of the problem, and therefore its physical content in terms of structure of the FEL. The simplest choice is the replica symmetric (RS) ansatz, which reads

$$\hat{\Delta} = \begin{bmatrix} 0 & \Delta^g & \cdots & \Delta^g & \Delta^r & & \cdots & & \Delta^r \\ \Delta^g & 0 & \cdots & \Delta^g & & & & & \\ \vdots & \ddots & \ddots & \vdots & \vdots & & & & \vdots \\ \Delta^g & \cdots & \Delta^g & 0 & \Delta^r & & \cdots & & \Delta^r \\ \Delta^r & & \cdots & \Delta^r & 0 & \Delta & \cdots & & \Delta \\ & & & & \Delta & 0 & \cdots & & \Delta \\ \vdots & & & \vdots & \vdots & \vdots & \ddots & & \vdots \\ & & & & \Delta & \cdots & & 0 & \Delta \\ \Delta^r & & \cdots & \Delta^r & \Delta & & \cdots & \Delta & 0 \end{bmatrix} \tag{4.11}$$

where Δ^g is internal to the block of m replicas, Δ to the s replicas, and Δ^r is the relative displacement between the m-type and s-type replicas. We also define the parameter

$$\Delta^f \equiv 2\Delta^r - \Delta^g - \Delta. \tag{4.12}$$

Let us examine the (4.11). The m-block encodes the MSDs between the master replicas, the $s-$block of the slave replicas, and the off-diagonal blocks the MSDs between the master and slave replicas: the MSDs in the off-diagonal blocks are all equal to Δ^r as prescribed by the δ-constraint in the (4.2); as discussed before, we assume the replicas in the m-block to be at equilibrium in the liquid phase, so there is no reason for the MSDs between them to have any special structure.
The physical content of the RS ansatz is contained in the $s-$block. Suppose that we have a glassy minimum in the FEL, and we throw s replicas inside it at random using the Boltzmann-Gibbs distribution; those replicas probe the structure of the bottom of the glassy minimum as we follow it under compression or shear. If the minimum is just a plain paraboloid, there is no reason for the MSDs between any couple of the slave replicas to depend on the actual couple we choose: once they equilibrate inside the state, all replicas are equivalent and we can permutate them as we please without changing the physics of the problem: we are indeed in a replica symmetric scenario.
Let us now assume that bottom of the state actually contains three different sub-minima: the situation changes completely. For simplicity let us assume that $s = 9$, and replicas 1-3, 3-6 and 6-9 end up in minimum 1, 2 and 3 respectively: it is clear that the permutation symmetry between replicas has been broken; replicas inside the same sub-minimum (like replicas 1 and 3) will be close together and will have a low mutual MSD Δ_{13}, but replicas in two different sub-minima (for example replicas 3 and 5) will be farther apart and will have a MSD Δ_{35} higher than Δ_{13}: we are in a one-step replica symmetry broken (1RSB) scenario [45], and the $s-$block of matrix $\hat{\alpha}$ will have to contain two MSD parameters, Δ_2 for replicas inside the same sub-minimum and Δ_1 for replicas in different ones [246]. In figure 4.1 we represent pictorially the difference between the RS and 1RSB scenarios.
The breaking of replica symmetry described above can be iterated: the sub-minima

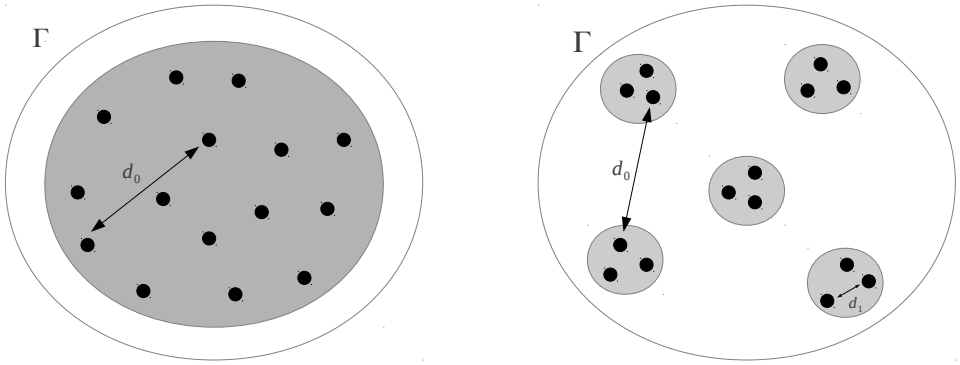

Figure 4.1. RS and RSB structures for the glassy state. Grey blobs are sub-states and black dots are replicas.

could contain sub-sub minima (2RSB) and so on. The process can in principle go on indefinitely, and we will see that in fact it does. However, in this chapter we limit ourselves to the simplest RS structure, encoded by matrix (4.11).

The entropy (4.9) must now be computed for the choice (4.11) of the matrix $\hat{\alpha}$ and then optimized with respect to Δ^g, Δ, and Δ^r. The computation in quite long and not particularly instructive, so we give the details in appendix B, and we skip directly to the final result. The entropic term is

$$\begin{aligned} s_{entr} &= \log\det\alpha^{m,m} = (1-m-s)\log 2 - 2\log(m+s) + (m-1)\log\Delta^g \\ &\quad + (s-1)\log\Delta + \log[ms\Delta^f + s\Delta^g + m\Delta], \end{aligned} \tag{4.13}$$

and for the interaction term one has

$$\mathcal{F}(\Delta^g,\Delta,\Delta^f) = \int \frac{d\zeta}{\sqrt{2\pi}} e^{-\frac{\zeta^2}{2}} \mathcal{F}_0\left(\Delta^g,\Delta,\Delta^f+\zeta^2\gamma^2\right) . \tag{4.14}$$

with $\mathcal{F}_0$ equal to

$$\begin{aligned} \mathcal{F}_0(\Delta^g,\Delta,\Delta^f) = \int dy\, e^y \Bigg\{ 1-\Theta\left(\frac{y+\Delta^g/2}{\sqrt{2\Delta^g}}\right)^m \\ \times \int dx\,\Theta\left(\frac{x+y-\eta+\Delta/2}{\sqrt{2\Delta}}\right)^s \frac{e^{-\frac{1}{2\Delta^f}\left(x-\Delta^f/2\right)^2}}{\sqrt{2\pi\Delta^f}} \Bigg\} , \end{aligned} \tag{4.15}$$

where we have defined

$$\Theta(x) \equiv \frac{1}{2}(1+\mathrm{erf}(x)), \tag{4.16}$$

and $\mathrm{erf}(x)$ is the error function [233]. We notice that the compression parameter η and the shear γ both enter only in the interaction term. This completes the computation of the entropy of the $m+s$ replicas.

4.1.3 Final result for the entropy of the glassy state

Now that we have obtained the replicated entropy, we have to expand it for small s and take the leading order in s, in order to get the Franz-Parisi entropy of the glassy state.
For $s \to 0$ we obtain the real replica entropy for m replicas [153, 154]:

$$\lim_{s\to 0} s[\hat{\alpha}] = s_m(\Delta^g) = 1 - \log\rho + \frac{d}{2}(m-1) + \frac{d}{2}\log m + \frac{d}{2}(m-1)\log(\pi\Delta^g/d^2) - \frac{d}{2}\widehat{\varphi}_g \int dy\, e^y \left[1 - \Theta\left(\frac{y+\Delta^g/2}{\sqrt{2\Delta^g}}\right)^m\right] . \tag{4.17}$$

The linear order in s gives, finally, the in-state entropy of the glassy state (Franz-Parisi entropy):

$$\lim_{s\to 0} \partial_s\{s[\hat{\alpha}]\} = s_g = \frac{d}{2} + \frac{d}{2}\frac{\Delta^g + m\Delta^f}{m\Delta} + \frac{d}{2}\log(\pi\Delta/d^2) + \frac{d\widehat{\varphi}_g}{2}\int \mathcal{D}\zeta \int dy\, e^y\, \Theta\left(\frac{y+\Delta^g/2}{\sqrt{2\Delta^g}}\right)^m \times \int dx\, \log\left[\Theta\left(\frac{x+y-\eta+\Delta/2}{\sqrt{2\Delta}}\right)\right] \frac{e^{-\frac{1}{2\Delta_\gamma(\zeta)}(x-\Delta_\gamma(\zeta)/2)^2}}{\sqrt{2\pi\Delta_\gamma(\zeta)}} , \tag{4.18}$$

where $\Delta_\gamma(\zeta) = \Delta^f + \zeta^2\gamma^2$ and we recall that $\mathcal{D}\zeta = \frac{d\zeta}{\sqrt{2\pi}}e^{-\frac{\zeta^2}{2}}$. It will be often convenient to make a change of variable $x' = (x - \Delta_\gamma(\zeta)/2)/\sqrt{\Delta_\gamma(\zeta)}$ in the integral, which leads to (dropping the prime for convenience):

$$s_g = \frac{d}{2} + \frac{d}{2}\frac{\Delta^g + m\Delta^f}{m\Delta} + \frac{d}{2}\log(\pi\Delta/d^2) + \frac{d\widehat{\varphi}_g}{2}\int dy\, e^y\, \Theta\left(\frac{y+\Delta^g/2}{\sqrt{2\Delta^g}}\right)^m \int \mathcal{D}\zeta\, \mathcal{D}x\, \log\left[\Theta\left(\frac{\sqrt{\Delta_\gamma(\zeta)}x + \Delta_\gamma(\zeta)/2 + y - \eta + \Delta/2}{\sqrt{2\Delta}}\right)\right] . \tag{4.19}$$

From this expression of the internal entropy, we can obtain the saddle point equations for Δ and Δ^f and study the behavior of glassy states. We notice that the parameter Δ_g is contained only in the (4.17), so its saddle point equation is independent of both η and γ and only depends on the glass transition density $\widehat{\varphi}_g$.

4.1.4 Saddle point equations

As already detailed, the FP entropy (4.19) must be optimized over Δ, Δ^f and Δ^g in order to get the entropy of the metastable glassy state. The equation for Δ^g is obtained by maximizing eq. (4.17). We have

$$0 = \frac{m-1}{m\Delta^g} + \frac{\widehat{\varphi}_g}{2}\int dy\, e^y \Theta\left(\frac{y+\Delta^g/2}{\sqrt{2\Delta^g}}\right)^{m-1} \frac{e^{-\frac{(y+\Delta^g/2)^2}{2\Delta^g}}}{\sqrt{2\pi\Delta^g}} \left(\frac{1}{2} - \frac{y}{\Delta^g}\right) . \tag{4.20}$$

For a fixed reference density $\widehat{\varphi}_g$ (and fixed m, here we are mostly interested in $m \to 1$), one can solve this equation to obtain Δ^g. Then, the entropy in eq. (4.19) must be maximized with respect to Δ and Δ^f to give the internal entropy of a glass state prepared at $\widehat{\varphi}_g$ (the value of Δ^g is the equilibrium one corresponding to $\widehat{\varphi}_g$) and followed at a different state point parametrized by η and γ. As usual in replica computations [57], the analytical continuation to $s \to 0$ induces a change in the properties of the entropy, and as a consequence the solution of the equations for Δ and Δ^f is not a maximum, but rather a saddle-point. However, the correct prescription is not to look at the concavity of the entropy, but to check that all the eigenvectors of the Hessian matrix of the $s[\hat{\alpha}]$ remain negative, as we discuss in the next section.

The equations for Δ and Δ^f are obtained from the conditions $\frac{\partial s_g}{\partial \Delta} = 0$ and $\frac{\partial s_g}{\partial \Delta^f} = 0$. Starting from eq. (4.19) and taking the derivatives, we get

$$\begin{aligned} 0 &= \frac{m\Delta - \Delta^g - m\Delta^f}{m\Delta^2} \\ &\quad + \frac{\widehat{\varphi}_g}{2} \int dy \mathcal{D}x \mathcal{D}\zeta \; e^y \frac{\Theta\left(\frac{y+\Delta^g/2}{\sqrt{2\Delta^g}}\right)^m}{\Theta\left(\frac{\xi}{\sqrt{2\Delta}}\right)} \frac{e^{-\frac{\xi^2}{2\Delta}}}{\sqrt{2\pi\Delta}} \left(1 - \frac{\xi}{\Delta}\right), \end{aligned} \tag{4.21}$$

$$0 = \frac{1}{\Delta} + \frac{\widehat{\varphi}_g}{2} \int dy \mathcal{D}x \mathcal{D}\zeta \; e^y \frac{\Theta\left(\frac{y+\Delta^g/2}{\sqrt{2\Delta^g}}\right)^m}{\Theta\left(\frac{\xi}{\sqrt{2\Delta}}\right)} \frac{e^{-\frac{\xi^2}{2\Delta}}}{\sqrt{2\pi\Delta}} \left(1 + \frac{x}{\sqrt{\Delta_\gamma(\zeta)}}\right), \tag{4.22}$$

with

$$\xi = \sqrt{\Delta_\gamma(\zeta)} x + \Delta_\gamma(\zeta)/2 + y - \eta + \Delta/2 \,, \tag{4.23}$$

wherein again $\Delta_\gamma(\zeta) = \Delta^f + \gamma^2\zeta^2$. In some cases, it might be useful to perform an additional change of variables from y to ξ. Those saddle point equations must be solved for varying η and γ, and the entropy (4.18) must be computed along the solution in order to get the physical observables of the glass that we compute in the next paragraph.

4.1.5 Physical observables

We now compute the pressure and the shear stress, that are the responses of the glassy state to compression and shear-strain, respectively. We recall that Δ and Δ^f are obtained by setting the derivatives of s_g with respect to them equal to zero, which means that when we take for example the derivative of s_g with respect to γ, it is enough to take the partial derivative instead of the total one.

For a system of hard spheres, the reduced pressure $p = \beta P/\rho$ is the response of the system to compression and is given by [18, 153]

$$p_g = -\widehat{\varphi} \frac{\partial s_g}{\partial \widehat{\varphi}} = -\frac{\partial s_g}{\partial \eta} \,, \tag{4.24}$$

and we get from eq. (4.19):

$$\frac{p_g}{d} = \frac{\widehat{\varphi}_g}{2} \int dy \mathcal{D}x \mathcal{D}\zeta \; e^y \frac{\Theta\left(\frac{y+\Delta^g/2}{\sqrt{2\Delta^g}}\right)^m}{\Theta\left(\frac{\xi}{\sqrt{2\Delta}}\right)} \frac{e^{-\frac{\xi^2}{2\Delta}}}{\sqrt{2\pi\Delta}} \tag{4.25}$$

recalling Eq. (4.23). The p_g/d vs. $\widehat{\varphi}$ (or $\eta = \log(\widehat{\varphi}/\widehat{\varphi}_g)$) curve is the equation of state of the corresponding metastable glass.

The response to a shear strain is given by the shear stress, which is defined as [215]

$$\beta\sigma = -\frac{\partial s_g}{\partial \gamma}, \tag{4.26}$$

and we get from eq. (4.19):

$$\frac{\beta\sigma}{d} = -\gamma\frac{\widehat{\varphi}_g}{2}\int dy\mathcal{D}x\mathcal{D}\zeta\; e^y \frac{\Theta\left(\frac{y+\Delta^g/2}{\sqrt{2\Delta^g}}\right)^m}{\Theta\left(\frac{\xi}{\sqrt{2\Delta}}\right)}\frac{e^{-\frac{\xi^2}{2\Delta}}}{\sqrt{2\pi\Delta}}\left(1+\frac{x}{\sqrt{\Delta_\gamma(\zeta)}}\right)\zeta^2\ . \tag{4.27}$$

Shear modulus and dilatancy

It is interesting to consider as a particular case the response of the glass to an infinitesimal strain, $\gamma \to 0$. In that case, we have that both $\Delta_\gamma(\zeta) \to \Delta^f$ and $\xi \to \sqrt{\Delta^f}x + \Delta^f/2 + y - \eta + \Delta/2$ become independent of ζ. We have thus

$$\frac{\beta\mu}{d} = \lim_{\gamma\to 0}\frac{\beta\sigma}{d\gamma} = -\frac{\widehat{\varphi}_g}{2}\int dy\mathcal{D}x\; e^y \frac{\Theta\left(\frac{y+\Delta^g/2}{\sqrt{2\Delta^g}}\right)^m}{\Theta\left(\frac{\xi}{\sqrt{2\Delta}}\right)}\frac{e^{-\frac{\xi^2}{2\Delta}}}{\sqrt{2\pi\Delta}}\left(1+\frac{x}{\sqrt{\Delta^f}}\right)\int\mathcal{D}\zeta\;\zeta^2 = \frac{1}{\Delta}\ , \tag{4.28}$$

where the last equality is obtained by noticing that $\int\mathcal{D}\zeta\;\zeta^2 = 1$ and using eq. (4.22) in the limit $\gamma \to 0$, where again the integral over ζ disappears because ξ and Δ_γ become independent of ζ. In this way we see that $\sigma/\gamma \to \mu$, where μ is the shear modulus of the glass and it is inversely proportional to the cage radius. This provides an alternative derivation of the results of [214, 215].

From eq. (4.28) we deduce that for small γ the physical entropy is

$$s_g(\eta,\gamma) = s_g(\eta,\gamma=0) - \frac{d}{2}\gamma^2\frac{1}{\Delta(\eta,\gamma=0)} + \cdots\ , \tag{4.29}$$

where $\Delta(\eta,\gamma)$ is the solution of eqs. (4.21)-(4.22). Therefore we have

$$\begin{aligned} p_g(\eta,\gamma) = &-\frac{\mathrm{d}s_g(\eta,\gamma)}{\mathrm{d}\eta} = p_g(\eta,\gamma=0) + \frac{d}{2}\gamma^2\frac{\mathrm{d}}{\mathrm{d}\eta}\frac{1}{\Delta(\eta,\gamma=0)} + \cdots \\ &= p_g(\eta,\gamma=0) + \gamma^2(\beta R(\eta)/\rho) + \cdots\ , \end{aligned} \tag{4.30}$$

from which we deduce the expression of the dilatancy R as

$$\frac{\beta R(\eta)}{\rho} = \frac{d}{2}\frac{\mathrm{d}}{\mathrm{d}\eta}\frac{1}{\Delta(\eta,\gamma=0)}\ . \tag{4.31}$$

4.2 Stability of the RS ansatz

In the preceding section we have detailed the computation of the replicated entropy and the FP potential, employing the simplest possible RS ansatz. The computation has been made with the saddle point, or steepest descent method [86], wherein an integral in the form $\int dx\; e^{Nf(x)}$ is approximated as $e^{Nf(x^*)}$, with x^* a point

of maximum of the $f(x)$. It can be shown that the error committed with this approximation vanishes in the limit $N \to 0$ as long as the point x^* is a maximum, i.e. if $\frac{d^2 f}{dx^2}\Big|_{x=x^*} < 0$.
We stress the fact that this is not only a mathematical problem, but also a physical one: in statistical mechanics, the function $f(x)$ is usually the Gibbs free energy as a function of the order parameter, like the Gibbs free energy $f(m)$ of the Curie-Weiss model as discussed in paragraph 1.2.1, and its stationary points x^* correspond to the possible phases the system can be found in. If the second derivative of the $f(x)$ becomes zero, this means that a phase transition is taking place: the stable phase (or equivalently, the saddle point) the system is in becomes critical (flat), an infinite susceptibility manifests, and below the transition the stable saddle point shifts to a different value x^*, while the stationary point that was stable above the transition ($m^* = 0$ in the case of the Curie-Weiss model) becomes unstable, as shown in figure 1.7 for the ferromagnetic transition.

In the case of the replicated entropy, we have a much more complicated "Gibbs free energy" $s[\hat{\alpha}]$ and "order parameter" $\hat{\alpha}$, but the spirit is exactly the same: checking the concavity of the replicated entropy $s[\hat{\alpha}]$ is one and the same with studying the behavior of the glassy state in terms of in-state phase transitions wherein the glassy minimum would "split" in sub-minima as in figure 1.7. In summary, we have to check that the saddle point given by equations (4.20), (4.21) and (4.22) is a maximum of the replicated entropy.

It is however clear that the question requires some caution. First of all, we have restricted ourselves to a fixed form of the matrix $\hat{\alpha}$, i.e. the RS one. As a result of this, checking the concavity of the replicated entropy with respect to Δ_g, Δ and Δ_f would only tell us if there is an instability within the RS ansatz, but would miss instabilities towards saddle points with more RSBs, which as we discussed before is the interesting case corresponding to a phase transition inside the minimum. As a result of this, the general Hessian matrix of the $s[\hat{\alpha}]$,

$$M_{a<b;c<d} \equiv \frac{2}{d} \frac{\delta^2 s[\hat{\alpha}]}{\delta \alpha_{a<b} \delta \alpha_{c<d}} \tag{4.32}$$

must be calculated, and only *then* we can compute it on the RS solution at the saddle point.
Another issue is the fact that the $s[\hat{\alpha}]$ is also a function of the parameter s, which we send to zero in the end to compute the FP potential. So we are considering the Hessian of a function of a matrix which has one block of size $s \times s$ with s going to zero, a clearly pathological situation. To illustrate the problems that one could have, a pedagogical example [57] is a $s \times s$ matrix with zeros on the diagonal and an off-diagonal parameter q

$$Q = \begin{pmatrix} 0 & q & q \\ q & 0 & q \\ q & q & 0 \end{pmatrix} \qquad s = 3 \tag{4.33}$$

And a function $s[Q]$ defined as

$$s[Q] \equiv -\mathrm{Tr}(Q^2) = -s(s-1)q^2. \tag{4.34}$$

As long as $s \geq 1$, it is clear that $q = 0$ is a maximum of s. But if we send $s \to 0$, it evidently becomes a minimum: changing the value of s can change the nature of stationary points of the $s[\hat{\alpha}]$, as we precedingly discussed. As a result of this, the usual prescription in replica theory is that the Hessian (4.32) must be computed for general s, and then one must verify that the analytic continuation of its eigenvalues for $s \to 0$ be negative, in order to check stability [57, 227].

4.2.1 The unstable mode

Now that we have settled these questions we can proceed with the calculation of the Hessian (4.32). If we observe it closely, we see that we are checking the fluctuations of the $s[\hat{\alpha}]$ with respect to all the elements in the $\hat{\alpha}$ matrix, i.e. we are considering fluctuations in all the blocks. But already from an intuitive point of view, it is clear that only fluctuations in the sector of slave replicas should matter: the s replicas are the ones that probe the bottom of the glass state as we follow it, while the m ones only select the state and remain at equilibrium in the liquid phase. Only the s replicas are able to detect a transition within the state like the one shown in figure 1.7 (this intuitive argument is made more formal in appendix C).
This means that we can focus just on the "reduced Hessian"

$$M^s_{a\leq b;c\leq d} \equiv \frac{2}{d}\frac{\delta^2 s[\hat{\alpha}]}{\delta\alpha_{a<b}\delta\alpha_{c<d}}, \qquad a,b,c,d \ \in [m+1, m+s]. \tag{4.35}$$

and compute it on the RS solution. This reduced Hessian enjoys the same exact replica permutation symmetries of the Hessians typically considered within the real replica method [64, 155, 247, 248], wherein the matrix $\hat{\alpha}$ is just an RS matrix without any block structure. In particular, one can show that because of replica symmetry, the Hessian M^s, when computed on the RS solution, must necessarily have the general form

$$M^s_{a<b;c<d} = M_1\left(\frac{\delta_{ac}\delta_{bd}+\delta_{ad}\delta_{bc}}{2}\right) + M_2\left(\frac{\delta_{ac}+\delta_{ad}+\delta_{bc}+\delta_{bd}}{4}\right) + M_3, \tag{4.36}$$

so it effectively depends only on three parameters M_1, M_2 and M_3. As shown in [64, 247], this operator has only three independent eigenvalues,

$$\lambda_R = M_1 \tag{4.37}$$
$$\lambda_L = M_1 + (s-1)(M_2 + sM_3) \tag{4.38}$$
$$\lambda_A = M_1 + \frac{s-2}{2}M_2 \tag{4.39}$$

called the *replicon*, *longitudinal* and *anomalous* modes, respectively. Each of these modes is relative to a subspace of the vector space the $s-$block of the matrix s lives in. Of these three modes, the replicon mode is the one which is linked to instabilities towards s-blocks with mode RSBs (the state splits up as in figure 1.7), while the longitudinal one, for example, gives information relative to spinodal points (the state opens up along an unstable direction and becomes a saddle), so it is linked to the MCT transition and threshold states [227], and also with yielding as we are going to see. However, here we are only interested in the replicon mode.

In summary, we must compute the replicon mode $\lambda_R = M_1$, perform its analytic continuation for $s \to 0$, and check its sign along the solution given by equations (4.21), (4.22) and (4.20). The computation of the replicon follows the same lines as the one performed in [155] with only a few modifications, so we skip, again, directly to the final result and refer to appendix C for the details. The replicon mode, for $s = 0$, is:

$$\lambda_R = \frac{1}{\Delta^2}(-16 - 8\widehat{\varphi}_g - 8\widehat{\varphi}_g\langle\Theta_0(\lambda)^{-1}\mathcal{L}_0(\lambda)\rangle), \tag{4.40}$$

With

$$\mathcal{L}_s(\lambda) = \left[\left(\frac{\Theta_1(\lambda)}{\Theta_0(\lambda)}\right)^2 - \lambda\frac{\Theta_1(\lambda)}{\Theta_0(\lambda)}\right]\left[(2-2\lambda^2) + (s-4)\left(\frac{\Theta_1(\lambda)}{\Theta_0(\lambda)}\right)^2 + (6-s)\lambda\frac{\Theta_1(\lambda)}{\Theta_0(\lambda)}\right], \tag{4.41}$$

and

$$\Theta_0(x) \equiv \Theta(-x/\sqrt{2}), \tag{4.42}$$

$$\Theta_1(x) \equiv e^{-\frac{1}{2}x^2}/\sqrt{2\pi}, \tag{4.43}$$

and the average $\langle\bullet\rangle$ is defined as

$$\langle O(\lambda)\rangle = \int_{-\infty}^{\infty} \mathcal{D}\lambda\, G(\lambda)O(\lambda) = \int_{-\infty}^{\infty} \mathcal{D}\lambda\bar{\mathcal{D}}_m\lambda'\, K(\lambda',\lambda)\, O(\lambda). \tag{4.44}$$

with the kernel $K(\lambda',\lambda)$ defined in the (B.22) and the measure $\bar{\mathcal{D}}_m\lambda'$ in the (B.20).

Now, we must solve the equations (4.21), (4.22) and (4.20) for varying η and γ, and then compute along the solution the pressure (4.25), the shear strain (4.27), and the replicon mode (4.40), which will allow us to draw phase diagrams for the glass like the ones measured experimentally in figures 2.2 and 2.10. In the following section we present the results so obtained.

4.3 Results

In this section we solve the saddle point equations derived above, and compute the observables of the glass. We proceed as follows: first we choose a planting density $\widehat{\varphi}_g$, and solve the (4.20) to get the cage radius Δ. We then solve the (4.21) and (4.22) for varying η and γ, and compute the value of observables along the solution. We treat separately the compression-decompression and shear strain case, and we repeat the procedure for different $\widehat{\varphi}_g$s, corresponding to different annealing protocols as discussed in paragraph 2.1.2.

The equations cannot be solved analytically in the general case, so a numerical algorithm is required. Our choice is to use the iteration method, and we compute numerically the integrals appearing in the expressions using the simplest rectangle method; the integrands (which are essentially error functions or suitable combinations of them) are implemented numerically using the Faddeeva Library for C++[1]. Before reporting the full solution, we first focus on two special limits wherein an analytical solution can be obtained, providing a check of the numerics.

[1] http://ab-initio.mit.edu/wiki/index.php/Faddeeva_Package

4.3.1 Special limits

Equilibrium limit

When $\eta = \gamma = 0$, the constrained replicas sample the glass basins in the same state point as the reference replicas. Therefore, it is reasonable to expect that eqs. (4.21) and (4.22) admit $\Delta = \Delta^r = \Delta^g$, hence $\Delta^f = 0$, as a solution.

To check this, we first analyze eq. (4.21). For $\eta = \gamma = 0$, $\Delta = \Delta^g$ and $\Delta^f = 0$, we have $\Delta_\gamma(\zeta) = 0$ and $\xi = y + \Delta/2$. Therefore the integrand does not depend on x and ζ and $\int \mathcal{D}x\mathcal{D}\zeta = 1$. Then it is clear that eq. (4.21) becomes equivalent to eq. (4.20) and is satisfied by our conjectured solution.

The analysis of Eq. (4.22) is slightly more tricky. Setting $\eta = 0$, $\gamma = 0$, $\Delta = \Delta^g$ we get, with a change of variable $x' = x\sqrt{\Delta^f} + \Delta^f/2$ (and then dropping the prime for simplicity):

$$\begin{aligned} -\frac{2}{\widehat{\varphi}_g \Delta} = & \int dy\; e^y \Theta\left(\frac{y+\Delta/2}{\sqrt{2\Delta}}\right)^m \\ & \times \int dx\; \frac{e^{-\frac{(x-\Delta^f/2)^2}{2\Delta^f}}}{\sqrt{2\pi\Delta^f}} \frac{1}{\Theta\left(\frac{x+y+\Delta/2}{\sqrt{2\Delta}}\right)} \frac{e^{-\frac{(x+y+\Delta/2)^2}{2\Delta}}}{\sqrt{2\pi\Delta}} \left(\frac{x+\Delta^f/2}{\Delta^f}\right) . \end{aligned} \tag{4.45}$$

We now observe that

$$\left(\frac{x+\Delta^f/2}{\Delta^f}\right) \frac{e^{-\frac{(x-\Delta^f/2)^2}{2\Delta^f}}}{\sqrt{2\pi\Delta^f}} = \left(-\frac{d}{dx}+1\right) \frac{e^{-\frac{(x-\Delta^f/2)^2}{2\Delta^f}}}{\sqrt{2\pi\Delta^f}} \xrightarrow[\Delta^f\to 0]{} -\delta'(x) + \delta(x) \tag{4.46}$$

where $\delta(x)$ is the Dirac delta distribution. Therefore eq. (4.45) becomes, with some manipulations

$$\begin{aligned} -\frac{2}{\widehat{\varphi}_g \Delta} &= \int dy\; e^y \Theta\left(\frac{y+\Delta/2}{\sqrt{2\Delta}}\right)^m \int dx\; \left[-\delta'(x)+\delta(x)\right] \frac{1}{\Theta\left(\frac{x+y+\Delta/2}{\sqrt{2\Delta}}\right)} \frac{e^{-\frac{(x+y+\Delta/2)^2}{2\Delta}}}{\sqrt{2\pi\Delta}} \\ &= \int dy\; e^y \Theta\left(\frac{y+\Delta/2}{\sqrt{2\Delta}}\right)^m \left(\frac{d}{dy}+1\right) \left[\frac{1}{\Theta\left(\frac{y+\Delta/2}{\sqrt{2\Delta}}\right)} \frac{e^{-\frac{(y+\Delta/2)^2}{2\Delta}}}{\sqrt{2\pi\Delta}}\right] \\ &= \frac{m}{m-1} \int dy\, e^y \Theta\left(\frac{y+\Delta/2}{\sqrt{2\Delta}}\right)^{m-1} \left(\frac{1}{2}-\frac{y}{\Delta}\right) \frac{e^{-\frac{(y+\Delta/2)^2}{2\Delta}}}{\sqrt{2\pi\Delta}} , \end{aligned} \tag{4.47}$$

So, also the equation for Δ_f becomes equivalent equivalent to eq. (4.20). We conclude that for $\eta = \gamma = 0$, the solution of Eqs. (4.21)-(4.22) is $\Delta^f = 0$ and $\Delta^g = \Delta$ for all m, which furnishes us with a starting point for the iteration algorithm.

A particularly interesting case is when $m = 1$. In this case the reference replicas are in equilibrium in the liquid phase, and the constrained replicas therefore sample the glass basins that compose the liquid phase *at equilibrium*, like in the real replica method 3.1. From eq. (4.25) it is quite easy to see that for $m = 1$, $\gamma = \eta = 0$, $\Delta^f = 0$, $\Delta^g = \Delta$, one has $\Delta_\gamma(\zeta) = 0$ and $\xi = y + \Delta/2$ and

$$p_g = \frac{d\,\widehat{\varphi}_g}{2} \int dy\, e^y \frac{e^{-\frac{(y+\Delta/2)^2}{2\Delta}}}{\sqrt{2\pi\Delta}} = \frac{d\,\widehat{\varphi}_g}{2} = p_{\text{liq}} . \tag{4.48}$$

Where we have used the fact that the equation if state of HSs in the MF limit is just the Van Der Waals one [18]. This shows in particular that the pressure of the glass *merges continuously with the liquid pressure* at $\widehat{\varphi}_g$, as it should be. 3. The difference $\Sigma = s_{\text{liq}} - s_g$ then gives the equilibrium complexity $\Sigma(\hat{\varphi})$ of the supercooled liquid.

The jamming limit

The other interesting limit is of course the jamming limit, whereupon the internal pressure of the glass state diverges as detailed in paragraph 2.1.3 and correspondingly its MSD $\Delta \to 0$ [153].
To investigate this limit, we specialize to the case $\gamma = 0$ and we consider the limit $\Delta \to 0$ of equations (4.21) and (4.22). Using the relation

$$\lim_{\mu\to 0} \Theta(x/\sqrt{\mu})^\mu = e^{-x^2\theta(-x)} \ , \tag{4.49}$$

the leading order of eq. (4.19) is

$$\begin{aligned} s_g &\simeq \frac{d}{2}\frac{\Delta^g + m\Delta^f}{m\Delta} - \frac{d\widehat{\varphi}_g}{4\Delta}\int dy\, e^y\, \Theta\left(\frac{y+\Delta^g/2}{\sqrt{2\Delta^g}}\right)^m \\ &\quad \times \int_{-\infty}^{\eta-y} dx\, (x+y-\eta)^2 \frac{e^{-\frac{1}{2\Delta^f}\left(x-\Delta^f/2\right)^2}}{\sqrt{2\pi\Delta^f}} \\ &= \frac{d}{2\Delta}\left\{\frac{\Delta^g}{m} + \Delta^f - \frac{\widehat{\varphi}_g}{2}\int dy\, e^y\, \Theta\left(\frac{y+\Delta^g/2}{\sqrt{2\Delta^g}}\right)^m \int_{-\infty}^{0} dx\, x^2 \frac{e^{-\frac{1}{2\Delta^f}\left(x-y+\eta-\Delta^f/2\right)^2}}{\sqrt{2\pi\Delta^f}}\right\}. \end{aligned} \tag{4.50}$$

Hence, we obtain that $s_g \sim C/\Delta + \log\Delta + \cdots$ when $\Delta \to 0$, where the term $\log\Delta$ is explicitly present in eq. (4.19). Next, we observe that:

- The coefficient C should vanish at jamming. This is because $s_g = \Delta^{-1}C + \log\Delta + \cdots$, hence the equation for Δ is $-\Delta^{-2}C + \Delta^{-1} + \cdots = 0$, or equivalently $-C + \Delta + \cdots = 0$, which shows that when $C \to 0$, also $\Delta = C \to 0$. The jamming point is therefore defined by $C \to 0$. Note by the way that this condition guarantees that $s_g \sim \log\Delta$ when $\Delta \to 0$, which is the physically correct behavior of the glass entropy because particles are localized on a scale Δ [153].
- The derivative of C with respect to Δ^f should also vanish, because it determines the equation for Δ^f at leading order in Δ.

The two conditions $C = 0$ and $dC/d\Delta^f = 0$ give two equations that determine the values of η and Δ^f at the jamming point, for a fixed glass (i.e. at fixed $\widehat{\varphi}_g, \Delta^g, m$). These two equations read

$$\begin{aligned} 0 &= \frac{\Delta^g}{m} + \Delta^f - \frac{\widehat{\varphi}_g}{2}\int dy\, e^y\, \Theta\left(\frac{y+\Delta^g/2}{\sqrt{2\Delta^g}}\right)^m \int_{-\infty}^{0} dx\, x^2 \frac{e^{-\frac{1}{2\Delta^f}\left(x-y+\eta-\Delta^f/2\right)^2}}{\sqrt{2\pi\Delta^f}} \ , \\ 0 &= 1 - \frac{\widehat{\varphi}_g}{2}\frac{d}{d\Delta^f}\int dy\, e^y\, \Theta\left(\frac{y+\Delta^g/2}{\sqrt{2\Delta^g}}\right)^m \int_{-\infty}^{0} dx\, x^2 \frac{e^{-\frac{1}{2\Delta^f}\left(x-y+\eta-\Delta^f/2\right)^2}}{\sqrt{2\pi\Delta^f}} \ . \end{aligned} \tag{4.51}$$

Note that one could get the same equations by taking directly the $\Delta \to 0$ limit of Eqs. (4.21) and (4.22). This system of two equations determines the values of the jamming density $\widehat{\varphi}_j = \widehat{\varphi}_g e^{\eta_j}$ and the corresponding Δ_j^f. Note that in general $C \sim |\eta - \eta_j|$ and therefore $\Delta = C \sim |\eta - \eta_j|$ vanishes linearly at jamming, as we will see.
Moreover, from the (4.25) one can see that in the jamming limit

$$p \simeq \Delta^{-1}. \tag{4.52}$$

This scaling of the pressure is predicted also by the real replica method [155], always with the RS ansatz. However, it does not coincide with the scaling $p \simeq \Delta^{-\kappa}$ reported in paragraph 2.1.3 and in [149]. This already points towards the fact that the simplest RS ansatz is not sufficient in the jamming limit and a phase transition to a more complicated internal structure of the state is present, as we will show in the following.

4.3.2 Compression-decompression

We report here the result for compression and decompression protocols, with varying η and $\gamma = 0$. This protocols mimic, for HSs, the DSC experiments discussed in paragraph 2.1.2.

Mean Square displacements

In figure (4.2) we report the evolution of the MSDs (or equivalently, Debye-Waller factors) Δ and Δ^f under compression ($\eta > 0$) or decompression ($\eta < 0$) at $\gamma = 0$. In decompression, we find that Δ^f increases quadratically from zero, while Δ also increases; this is reasonable, since the spheres in the glass become more free to move when the system is decompressed and Δ increases as a result. We observe that at low enough η a spinodal point is met, whereupon the solution disappears with a square-root singularity in both Δ and Δ^f; this behavior is the usual one for spinodal points. At this spinodal point, the glass ceases to exist and melts into the liquid phase: within our formalism we recover the onset transition discussed in paragraph 2.1.2 and reported in [129, 130].

Upon compression, again Δ^f increases quadratically while Δ decreases, as expected. If the planting density $\widehat{\varphi}_g$ is high enough, (see for example $\widehat{\varphi}_g = 8$ in figure 4.2), Δ vanishes linearly at η_j while Δ^f stays finite, as predicted by the asymptotic analysis of the preceding paragraph. The values of η_j and Δ_j^f coincide with the ones obtained from the equations in the jamming limit reported in section 4.3.1.
At low density, however (see for example $\widehat{\varphi}_g = 5$ in figure 4.2) another spinodal point is met (signaled again by a square root singularity) before jamming occurs (we mark it with a symbol in figure 4.2). We will see in the following that this spinodal point is unphysical (it does not correspond to a true loss of stability within the glass state), and it is an artifact of the theory, originated by the fact that we are using the RS ansatz in a region where it is unstable. This unphysical spinodal point has also been found in spin glasses in a similar setting, see [238].

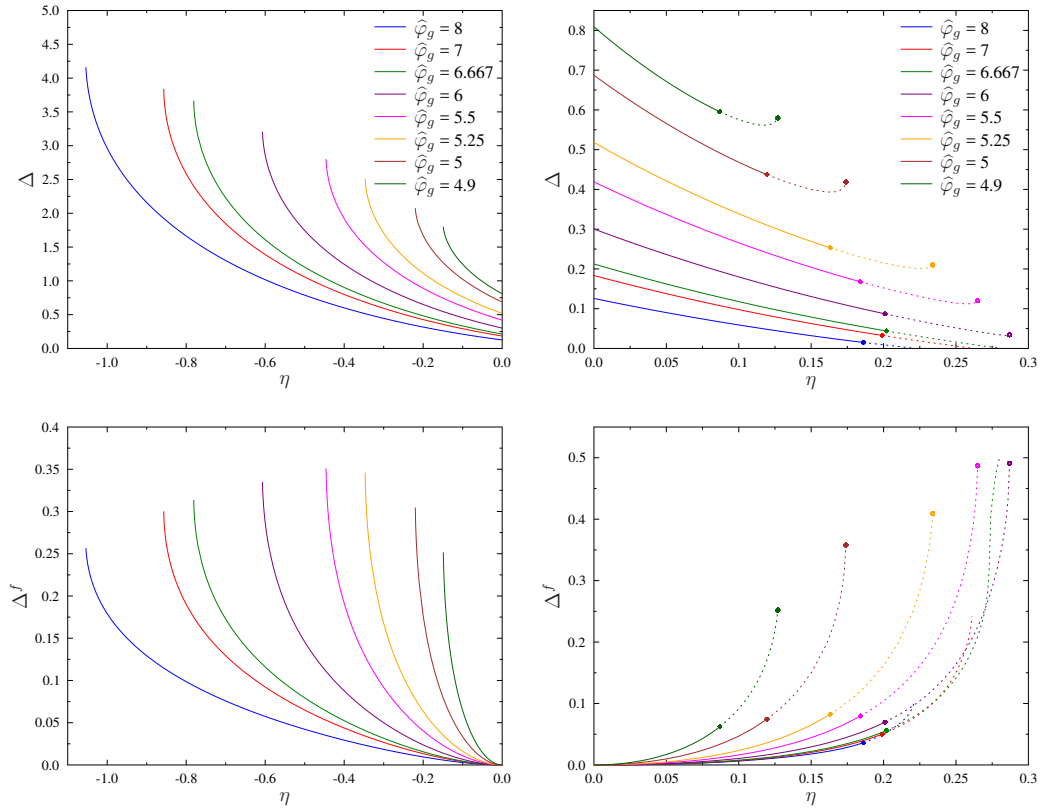

Figure 4.2. Δ (*top panels*) and Δ^f (*bottom panels*), solutions of eqs. (4.21)-(4.22), for different glassy states followed in decompression ($\eta < 0$, *left panels*) and compression ($\eta > 0$, *right panels*). We use separate scales to improve readability of the figures. The dashed lines indicate the unstable region wherein the replicon mode is positive (figure 4.3).

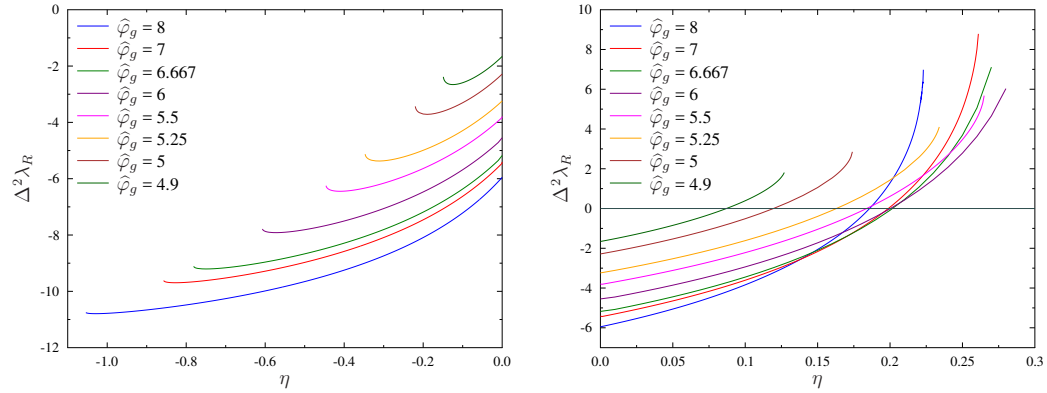

Figure 4.3. The replicon mode given by equation (4.40), for the same glasses as in figures 4.2 and 4.4. Upon decompression the replicon is always negative and the RS solution is always stable; upon compression, the replicon vanishes at the Gardner transition signaling an instability of the RS solution.

The replicon and the Gardner transition

We now focus on the replicon mode. We observe from figure 4.3 that upon compression, before either jamming or the unphysical spinodal point is reached, the replicon mode becomes positive, signaling that the glass state undergoes a phase transition as previously discussed, whereupon a more complicated structure of sub-minima manifests inside it [156, 249].
In principle, the structure appearing within the state could correspond to an arbitrary level of RSB, and one could check only *a posteriori* which is the correct number of steps of RSB of the ansatz corresponding to a stable solution. However, based on the analogy with spin glasses, and also the results of [41, 156] and the discussion of section C.1, we expect that replica symmetry is broken towards a fullRSB ansatz [250], corresponding to an infinite number of RSBs and a fractal hierarchy of sub-states appearing within the original glassy minimum. Such a transition had been discovered by Gardner in [249] in the context of spin glass models, and it is fittingly referred to as the *Gardner transition*. In paragraph 4.4.1 we discuss it in more detail. In all figures, we report the unstable part of the curves with a dashed line, to remember that the RS ansatz is unstable in that region.

Phase diagram and observables

We can finally report (figure 4.4) the phase diagram of HSs computed from the SF construction. The phase diagram in figure 4.4 is to be compared with phase diagrams like those shown in figures 0.1, 2.2, 2.3 and 2.5, and the reader can appreciate how the phenomenology is qualitatively well reproduced by the SF construction. The system is prepared at low density ρ and then particle volume V_s is slowly increased (or equivalently, container volume is decreased), and the reduced pressure p is monitored. We plot the reduced pressure $p = \beta P/\rho$ versus the packing fraction $\varphi = \rho V_s$, and they can be seen as playing the roles of the temperature and enthalpy for the purpose of comparison with figure 2.2. As long as the system is equilibrated, it follows the liquid equation of state (EOS), which in the MF limit is just the Van Der Waals EOS [18]. At the MCT transition density φ_{MCT} glasses appear, and the system can fall out of equilibrium, starting to age in a glass state selected by an equilibrium configuration at $\varphi_g > \varphi_{MCT}$.
The slope of the glass EOS at φ_g is different from that of the liquid EOS, indicating that when the system falls out of equilibrium at φ_g, the compressibility has a jump, as discussed in paragraph 2.1.2 in the case of the heat capacity. Following glasses in compression, the pressure increases faster than in the liquid (compressibility is smaller) and diverges at a finite *jamming* density $\varphi_j(\varphi_g)$. Before jamming is reached, the glass undergoes the Gardner transition [41, 249], and we can compute precisely the transition point $\varphi_G(\varphi_g)$ for all φ_g. Interestingly, the Gardner transition line ends at φ_{MCT}, i.e. $\varphi_G(\varphi_g = \varphi_{MCT}) = \varphi_{MCT}$. This implies that the first glasses appearing at φ_{MCT} (which are the easiest to probe experimentally) are marginally stable towards breaking into sub-states, while glasses appearing at $\varphi_g > \varphi_{\mathrm{d}}$ remain stable for a finite interval of pressures. Yet, all glasses undergo the Gardner transition at finite pressure before jamming occurs, in agreement with the results of [41].

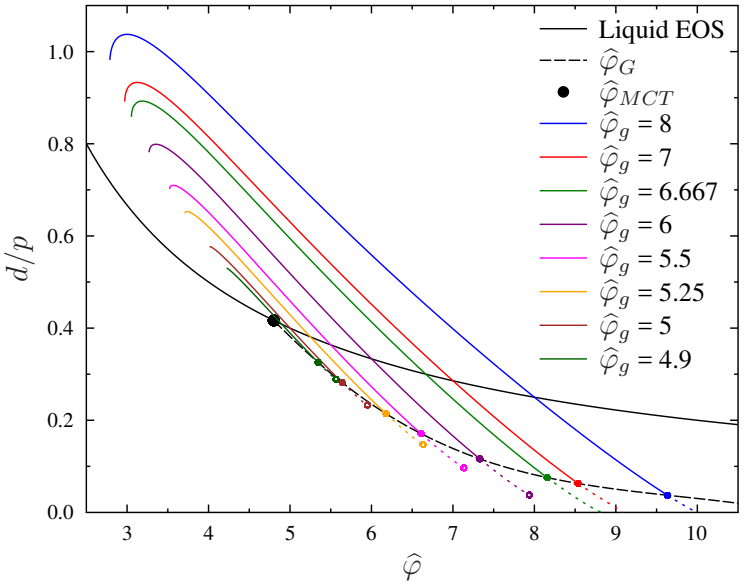

Figure 4.4. Following glasses in (de)compression. Inverse reduced pressure d/p is plotted versus packing fraction $\widehat{\varphi} = 2^d\varphi/d$. Both quantities are scaled to have a finite limit for $d \to \infty$. The liquid EOS is $d/p = 2/\widehat{\varphi}$. The MCT transition $\widehat{\varphi}_{MCT}$ is marked by a black dot. The glassy EOS are reported as full colored lines, that intersect the liquid EOS at the glass transition density (or equivalently, fictive density [127]) $\widehat{\varphi}_g$. Upon compression, a glass prepared at $\widehat{\varphi}_g$ undergoes a Gardner transition at $\widehat{\varphi}_G(\widehat{\varphi}_g)$ (full symbols and long-dashed black line); beyond $\widehat{\varphi}_G$ our computation is not correct and glass EOS are reported as dashed lines. For low $\widehat{\varphi}_g$, they end at an unphysical spinodal point (open symbol) before jamming occurs.
Upon decompression, the glass pressure falls below the liquid one, until it reaches a minimum, and then grows again until a physical spinodal point whereupon the glass melts into the liquid [129, 130].

A given glass prepared at φ_g can be also followed in *decompression*, by decompressing it a relatively fast rate t_{dec} such that $\tau_\beta \ll t_{\text{dec}} \ll t_{\text{exp}}$. In this case we observe hysteresis, again consistently with experimental results [7, 129, 130]. In fact, the glass pressure becomes *lower* than the liquid one, until the spinodal point whereupon the glass becomes unstable and melts into the liquid is met. Note that pressure "undershoots" (it has a local minimum, see figure 4.4) before the spinodal is reached [3], and the compressibility becomes infinite: this is a result of the MF nature of our approach. A Maxwell construction should be performed at the onset point in order to get the right finite-d behavior.

We also report results for the shear modulus, easily deduced from the results for Δ reported in figure 4.2 using equation (4.28), and we can also compute the dilatancy from eq. (4.31). The results are reported in figure 4.5. Note that $R/\rho = (1/2)\widehat{\varphi}\partial\mu/\partial\widehat{\varphi}$ as it can be deduced by combining equation (4.31) and (4.28). From this last relation one can easily notice that the singularities in the shear modulus also impact the dilatancy R, as pointed out in [188]. As a result of this, the dilatancy diverges both at the spinodal point whereupon Δ has a square-root singularity

(hence infinite derivative) and at the jamming point where $\Delta \to 0$.

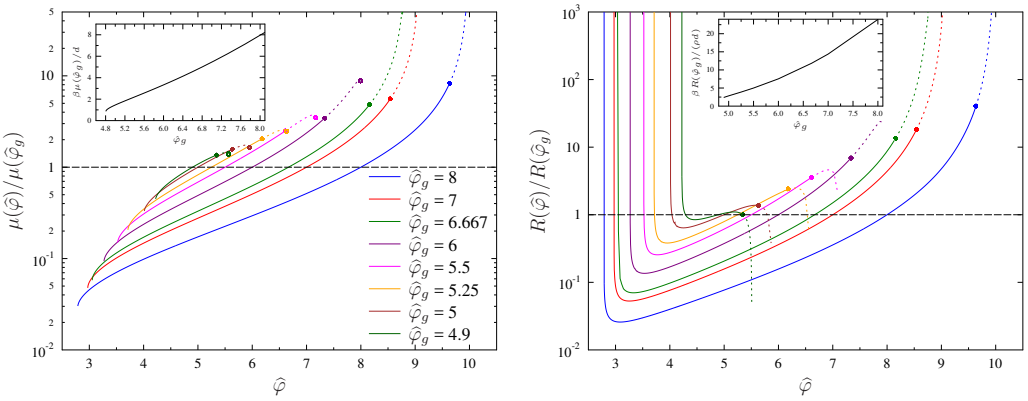

Figure 4.5. *Left panel*: Shear modulus versus density for different glasses. Same styles as figure 4.4. In the inset we report $\mu(\widehat{\varphi}_g)$ versus $\widehat{\varphi}_g$. Note that the dilatancy $R/\rho = (1/2)\widehat{\varphi}\partial\mu/\partial\widehat{\varphi}$ diverges both at jamming and at the low density spinodal point where the glass melts. *Right panel*: Dilatancy R as a function of density for different glasses. Recall that $R/\rho = (1/2)\widehat{\varphi}\partial\mu/\partial\widehat{\varphi}$. In the inset, the evolution of $R(\widehat{\varphi}_g)$ with $\widehat{\varphi}_g$ is reported. Note that the dilatancy diverges both at jamming and at the low density spinodal point whereupon the glass melts.

4.3.3 Shear strain

We now focus on shear-strain. Our typical protocol will be as follows: we again anneal the glass former down to a glass density $\widehat{\varphi}_g$, however, this time, we apply a simple shear strain to it instead of quenching it down to a target density $\widehat{\varphi} = \widehat{\varphi}_g e^{\eta}$. This is different from the athermal AQS protocols reviewed in paragraph 2.2.1, and we will discuss the differences in the final section.

Mean square displacements and replicon mode

We report the results for Δ and Δ^f in figure 4.6. We observe that upon increasing γ both Δ and Δ^f increase, until a spinodal point is reached, whereupon they both display a square root singularity, which is shared by both the shear stress σ and the glass pressure p_g (see figure 4.8). Interestingly, their behavior is somewhat specular to the one found in compression: Δ stays almost constant for a fairly long range of γs, while Δ_f immediately grows rapidly. This is reasonable, since the Δ is nothing but the Debye-Waller factor of the glass, so we do not expect it to change much upon shearing, shear strain being a volume-preserving perturbation.

However, before the spinodal is met, the replicon mode becomes positive again (figure 4.7) and the system undergoes, again, a Gardner transition. The fact that that Gardner transition is met when the system is subject to a shear strain might be surprising at first sight, because one would intuitively think that straining a glass state amount to a simple deformation of the state, without inducing its breaking into sub-states. Moreover, the effect of a mechanical drive should intuitively amount to injecting energy into the system (i.e., a heating or a decompression) as argued

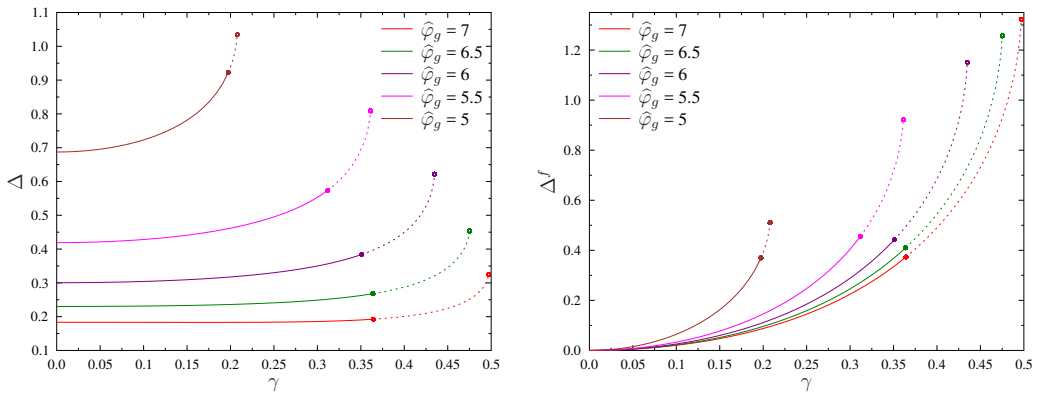

Figure 4.6. Values of Δ (*left panel*) and Δ^f (*right panel*) as functions of shear strain γ. The dashed lines again indicate the unstable region wherein the replicon mode is positive (figure 4.7).

for example in [181].
However, note first that on general grounds, the free energy landscape *can* change once perturbations are added [57]. Moreover, we also find (see figure 4.8) that the pressure of the glassy state increases when the shear strain is applied, because of dilatancy [187, 188]. This means that the particles in the glass basins may, upon shearing, become more constrained, triggering an ergodicity breaking inside the state, and with it a Gardner transition. We discuss further this issue in paragraph 4.4.1

Stress-strain curves

We can now draw the stress-strain curves of the glass. We report the behavior of shear-stress σ and pressure p versus γ, see figure 4.8, and observe how they well reproduce qualitatively the phenomenology shown in figure 2.10.
At small γ, we observe a *linear response* elastic regime wherein $\sigma \sim \mu\gamma$, as expected; the pressure increases quadratically above the equilibrium liquid value, $p(\gamma) \sim p(\gamma = 0) + (\beta R/\rho)\gamma^2$. Both the shear modulus μ and the dilatancy $R > 0$ increase with $\widehat{\varphi}_g$, indicating that glasses prepared by slower annealing are more rigid, as discussed in paragraph 2.2.1

Upon further increasing γ, glasses enter a non-linear regime, and undergo a Gardner transition at $\gamma_G(\varphi_g)$. As it happened in the compression protocol, we find $\gamma_G(\varphi_\mathrm{d}) = 0$, and γ_G increasing rapidly with φ_g. For $\gamma > \gamma_G(\varphi_\mathrm{d})$, the glass breaks into sub-states and the RS calculation becomes unstable, however, we can anyway keep following the state. Then, we notice that the RS computation correctly predicts the stress overshoot, followed by a spinodal point where the glass basin loses stability and disappears.
The spinodal point corresponds to the yielding point whereupon the glass starts to flow, as discussed in paragraph 2.2.2, so within the SF formalism we have ad unambiguous definition for the yielding point γ_Y; the values of yield strain γ_Y and of yield stress σ_Y are found to increase with φ_g, as expected. These results are qualitatively consistent with the experimental and numerical observations of [172,

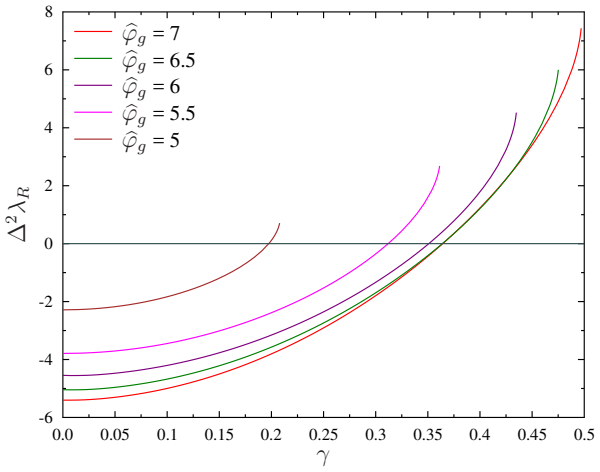

Figure 4.7. The replicon mode, eq. (4.40), for the same glasses as in figures 4.6 and 4.8. The replicon vanishes at the Gardner transition signaling an instability of the RS solution.

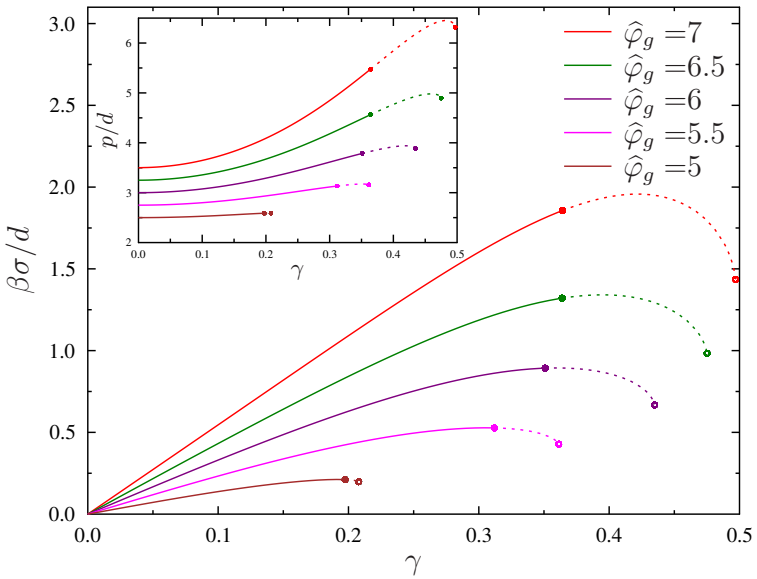

Figure 4.8. Following glassy states prepared at $\widehat{\varphi}_g$ upon applying a shear-strain γ. Shear-stress σ *(main panel)* and reduced pressure p *(inset)* as a function of strain for different $\widehat{\varphi}_g$. Same styles as fig. 4.4. Upon increasing the strain, the states undergo a Gardner transition at $\gamma_G(\widehat{\varphi}_g)$. For $\gamma > \gamma_G$ our RS computation is unstable but predicts a stress overshoot followed by a spinodal point.

182], and we will see in the next chapter that the fRSB computation gives similar results in terms of stress overshoot and yielding point.

4.4 Discussion

We have performed the computation of the Franz-Parisi potential (3.17), with the simplest RS ansatz. We show that the state following method is able to give predictions for many physical observables of experimental interest, and reproduces a quite large number of observations. These include: *(i)* the pressure as a function of density for different glasses (figure 4.4), which displays a jump in compressibility at φ_g [153, 251]; *(ii)* the presence of hysteresis and of a spinodal point in decompression in the pressure-density curves, whereupon we show that more stable glasses (those with higher φ_g) display a larger hysteresis, consistently with the experimental observations of [7, 129, 130]; the behavior of pressure and shear-stress under a startup shear perturbation (figure 4.8), where we show that *(iii)* the shear modulus and the dilatancy increase for more stable glasses (higher φ_g), and *(iv)* that the shear-stress overshoots before a spinodal (yielding) point is reached where the glass yields and starts to flow [172, 182]. Note however that the spinodal (yield) point falls beyond the Gardner transition and therefore its estimate, reported in figure 4.8, is only approximate. Furthermore, *(v)* we predict that glasses undergo a Gardner transition both in compression (fig 4.4) and in shear (fig 4.8), and we locate the Gardner transition point. Finally, we *(vi)* compute the dilatancy and the shear modulus everywhere in the glass phase (figure 4.5) and study their behavior close to the jamming transition.

4.4.1 The Gardner transition

Both in compression and shear strain, we detect an instability in the RS computation from the study of the replicon mode (4.40). This instability corresponds to a second order critical point which is referred to as *Gardner transition*, and corresponds to a breaking of the glassy state in a fractal hierarchy of micro-states, described by a fRSB ansatz [57, 250], in a spirit similar to the ferromagnetic transition in figure 1.7. It has been discovered in [249] in the context of the p-spin Ising model (essentially the Ising spin version of the PSM), and is essentially analogue to the transition found in the Sherrington-Kirkpatrick spin glass model [252] in presence of a magnetic field, by de Almeida and Thouless in [253]. The only difference is that in the SK model the state that undergoes the transition is the ergodic paramagnet, while for the Gardner transition it is a glass state dynamically selected by an annealing protocol as previously discussed. The relevant phenomenology is the same in both cases.

The presence of a Gardner transition in a realistic model of glass former is not a surprise, as it had been already reported in [41, 156], always for hard spheres. As of today, the nature of the Parisi fRSB solution is still not completely understood, but some of its phenomenology is well known. Without any doubt, the most physically relevant trait of the fRSB micro states is that they are *marginal* [247], which means that their replicon mode is zero everywhere in the fRSB phase [155].
This marginality of the fRSB solution has all kinds of implications. In [156], in particular, it was shown that the marginality condition of the fRSB solution directly implies the isostaticity property of jammed packings [142, 143], i.e. packings are *predicted* to be isostatic, with $z = 2d$. This way, the isostaticity property is recovered, within replica theory, as the manifestation of a critical mode (or equivalently,

an infinite susceptibilty), revealing the jamming transition as a critical phenomenon as anticipated in paragraph 2.1.3. Moreover, in [156], the fRSB ansatz is also show to be necessary to compute the critical exponents κ, γ, θ of the jamming transition (paragraph 2.1.3), while the RS ansatz would for example predict $\kappa = 1$ as mentioned before. These findings show the relevance of the Gardner transition for glasses at low temperatures and high pressure, at least within RFOT. We must however stress the fact that the "mechanical" marginality related to isostaticity in jammed packings, and the marginality of fRSB micro states related to the vanishing of the replicon are not the same thing, although it is clear that they must be connected in some way. Work is still ongoing to better understand their relation. The results of [156] were obtained within the real replica method [226] and the isocomplexity approximation, but in the next chapter we show that they can be more satisfactorily re-derived in the state following setting.

The presence of a Gardner transition in shear, however, is a novelty which deserves further investigation and may open new theoretical scenarios for the study of the yielding transition. As we mentioned, fRSB micro-states are marginal, which means that just a little perturbation will kick the system outside of a microstate to another, producing a very intermittent and rough response. This kind of physics looks well suited to the stress-strain curves in figures 2.10 and 2.11. For example, the fact that the interval $\langle \Delta\gamma \rangle$ before the first avalanche is met scales as N_{iso}^{β}, with N the system size and $\beta_{iso} < 1$ [195] (i.e. in the thermodynamic limit an infinitesimal strain will destabilize the system), could be well explained in terms of marginality. There is however a cardinal difference between the AQS protocols discussed in paragraph 2.2.1 and the ones reproduced here in the SF setting: in AQS protocols the system is quenched to zero temperature *before* strain is applied, which means that the glass is already in the fRSB phase, and fittingly, it immediately responds very roughly like in figures 2.10 and 2.11, while in figure 4.8 the strain is immediately applied after preparation at $\widehat{\varphi}_g$; as a result of this, the system is still equipped with thermal energy when subjected to strain, and the roughness of the PEL responsible for the intermittent response in AQS protocols is smoothed away by thermal fluctuations, producing a perfectly elastic response all the way to γ_G. This prediction is very relevant and should in principle be easily verifiable, although there is relative paucity of numerical results for shear of thermal amorphous systems. We will discuss this issue in more detail in section 7.3.

At the end of the day, though, the Gardner transition first and foremost implies that a fRSB computation must be performed, in order to follow the less dense glasses (which we recall are the easiest to prepare) down to the jamming limit, compute their jamming density, and the critical exponents of jamming. We also need it to check whether the phenomenology of yielding predicted by the RS ansatz remains the same when the fRSB one is employed.
In the next chapter we perform the fRSB computation in the state following setting.

Chapter 5

The full replica symmetry breaking ansatz

In the preceding chapter, we have computed the FP potential assuming the simplest possible replica symmetric ansatz for the slave replicas sampling the bottom of the followed glassy state. We have then used the so obtained thermodynamic potential to compute many quantities of interest, including equations of state for the glass, stress-strain curves, dilatancy and shear modulus, obtaining in all these cases a good qualitative agreement between the results of our computation and the phenomenology of glasses reviewed in the first chapters. However, we have also detected, for a sufficiently large value of both perturbations considered, a Gardner transition inside glassy states, rendering the RS ansatz unstable in a region of the phase diagram both in compression and strain. As a result of this, the approach is unable to provide predictions in a whole region of the phase diagram, as it happens for example for the EOS of the least dense glasses (corresponding, coincidentally, to shorter and thus easier to realize preparation protocols) in compression that terminate in an unphysical spinodal point before jamming can occur. And even where the RS equation of state exists, it can be at best considered an approximation of the results which must be derived with the correct ansatz. In this chapter we assume the "correct" ansatz to be the full replica symmetry breaking one, and perform again the computation of the FP potential and physical observables within this ansatz.

5.1 The potential

Our starting point is again the replicated entropy (4.9). The entropic and interaction (equations (B.15),(B.16)) terms have the same definition as before. The difference with respect to the previous chapter is that this time we choose a matrix $\hat{\Delta}_{ab}$ (or equivalently, $\hat{\alpha}_{ab}$) in the form

$$\hat{\Delta} = \begin{pmatrix} \hat{\Delta}^g & \hat{\Delta}^r \\ (\hat{\Delta}^r)^T & \hat{\Delta}^s \end{pmatrix}, \tag{5.1}$$

where the matrices $\hat{\Delta}^g$ and $\hat{\Delta}^r$ are defined as in the (4.11), and the matrix $\hat{\Delta}^s$ is now a matrix with an infinite number of RSBs [57, 250].

5.1.1 The fRSB parametrization

Let us sketch rapidly how a matrix with an infinite number of RSBs can be parametrized in practice. An RS matrix is parametrized by a single element Δ; as we said in paragraph 4.1.2, a 1RSB matrix corresponds to having two relevant parameters Δ_1 and Δ_2, one for each level in the hierarchy of states. Moreover, we also need to specify how replicas are grouped in the states, i.e. we need to say how many replicas s_1 of the total s we have, end up in the same state at the lowest level of the hierarchy; in paragraph 4.1.2 we had $s = 9$ and $s_1 = 3$, which would correspond to a matrix $\hat{\Delta}^s$

$$\Delta_{ab}^{1RSB} = \begin{bmatrix} 0 & \Delta_2 & \Delta_2 & \Delta_1 & \Delta_1 & \Delta_1 & \Delta_1 & \Delta_1 & \Delta_1 \\ \Delta_2 & 0 & \Delta_2 & \Delta_1 & \Delta_1 & \Delta_1 & \Delta_1 & \Delta_1 & \Delta_1 \\ \Delta_2 & \Delta_2 & 0 & \Delta_1 & \Delta_1 & \Delta_1 & \Delta_1 & \Delta_1 & \Delta_1 \\ \Delta_1 & \Delta_1 & \Delta_1 & 0 & \Delta_2 & \Delta_2 & \Delta_1 & \Delta_1 & \Delta_1 \\ \Delta_1 & \Delta_1 & \Delta_1 & \Delta_2 & 0 & \Delta_2 & \Delta_1 & \Delta_1 & \Delta_1 \\ \Delta_1 & \Delta_1 & \Delta_1 & \Delta_2 & \Delta_2 & 0 & \Delta_1 & \Delta_1 & \Delta_1 \\ \Delta_1 & \Delta_1 & \Delta_1 & \Delta_1 & \Delta_1 & \Delta_1 & 0 & \Delta_2 & \Delta_2 \\ \Delta_1 & \Delta_1 & \Delta_1 & \Delta_1 & \Delta_1 & \Delta_1 & \Delta_2 & 0 & \Delta_2 \\ \Delta_1 & \Delta_1 & \Delta_1 & \Delta_1 & \Delta_1 & \Delta_1 & \Delta_2 & \Delta_2 & 0 \end{bmatrix}; \tag{5.2}$$

and of course one has also the diagonal elements Δ_d, corresponding to considering the same replica, whose value depends on how the "similarity" between replicas is defined[1]. A generic $(k-1)$RSB matrix will then be parametrized by a set of MSD parameters $\Delta_d; \Delta_1, \Delta_2, \ldots, \Delta_k$ and a set of "block" parameters $s_1, s_2, \ldots, s_{k-1}$[2], with $s_k = 1$ and $s_0 = s$ by definition; every generic kRSB matrix can be reconstructed from knowledge of this set of parameters.
One can then construct a function $\Delta(x)$, $1 < x < s$, in the following way

$$\Delta(x) \equiv \Delta_k \quad \text{if} \quad x \in]s_{k-1}, s_k], \tag{5.3}$$

which essentially describes the profile of the first row of a generic hierarchical matrix. When the number of breakings k is finite, this function has a step structure. When k goes up, the function will more and more look like a continuous function, and in the limit $k \to \infty$ corresponding to the fRSB ansatz, the function will be a continuous function of x. In figure 5.1 we give a demonstrative cartoon of the function $\Delta(x)$ for $k = 4$ and $k = \infty$.
In summary, every hierarchical matrix, with finite or infinite k, will be parametrized by a couple

$$\{\Delta_d, \Delta(x)\}. \tag{5.4}$$

It can be shown [254] that this parametrization preserves all the properties of the algebra of hierarchical matrices, and formulas for the product and the inverse in terms of the parametrization (5.4) can be derived. We refer to [57, 156, 254] for further reading on the issue.

[1] For HSs one has $\Delta_d = 0$, while for spin glasses one would have $q_d = 1$.

[2] Obviously $s > s_1 > s_2 > \cdots > s_{k-1} > 1$ when $s > 1$, and conversely $s < s_1 < s_2 < \cdots < s_{k-1} < 1$ when s is analytically continued to real $s < 1$ [66].

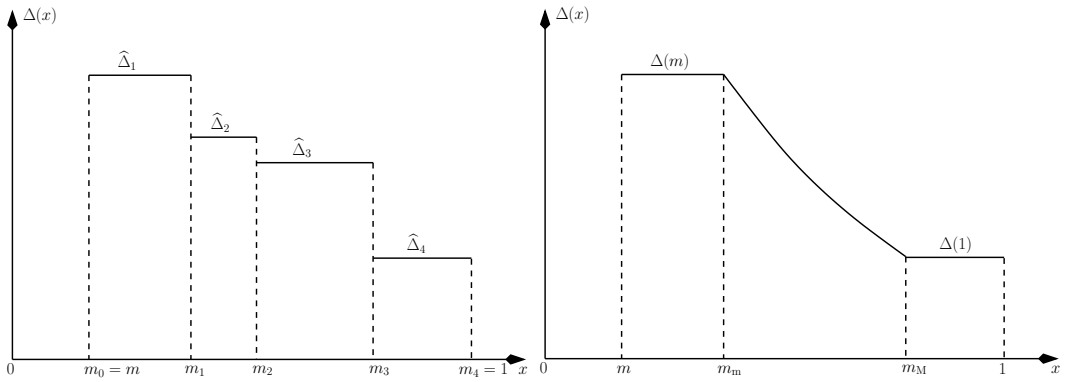

Figure 5.1. The function $\Delta(x)$ for $k = 4$ (*left*) and its expected form for $k = \infty$ (*right*). Reprinted from [156].

5.1.2 Expression of the potential and the observables

Now that we are equipped with a parametrization for the fRSB ansatz, we are ready to compute the FP entropy within the fRSB ansatz. As in the RS case, the computation is long and not very instructive, so we report it in appendix D, and skip, again, to the final result. The expression of the entropy of the followed state is

$$\begin{aligned} s_g[\alpha] = \frac{d}{2} + \frac{d}{2}\log\left(\frac{\pi\langle\Delta\rangle}{d^2}\right) - \frac{d}{2}\int_0^1 \frac{\mathrm{d}y}{y^2}\log\left(\frac{\langle\Delta\rangle + [\Delta](y)}{\langle\Delta\rangle}\right) + \frac{d}{2}\frac{m\Delta^f + \Delta^g}{m\langle\Delta\rangle} \\ + \frac{d\widehat{\varphi}_g}{2}\int_{-\infty}^{\infty}\mathcal{D}\zeta\int_{-\infty}^{\infty}\mathrm{d}h\,\mathrm{e}^h\Theta\left(\frac{h+\Delta^g/2}{\sqrt{2\Delta^g}}\right)^m \\ \times\int_{-\infty}^{\infty}\mathrm{d}x'\,f(0,x'+h-\eta+\Delta(0)/2)\frac{\mathrm{e}^{-\frac{1}{2\Delta_\gamma(\zeta)}(x'-\Delta_\gamma(\zeta)/2)^2}}{\sqrt{2\pi\Delta_\gamma(\zeta)}}, \end{aligned} \tag{5.5}$$

with the definitions

$$[\Delta](x) \equiv x\Delta(x) - \int_0^x \mathrm{d}y\,\Delta(y), \tag{5.6}$$

$$\langle\Delta\rangle \equiv \int_0^1 \mathrm{d}x\,\Delta(x), \tag{5.7}$$

$$\Delta^f \equiv 2\Delta^r - \Delta_g - \Delta(0), \tag{5.8}$$

and the function $f(x,h)$ obeys the Parisi equation [57]

$$\frac{\partial f}{\partial x} = \frac{1}{2}\frac{\mathrm{d}\Delta(x)}{\mathrm{d}x}\left[\frac{\partial^2 f}{\partial h^2} + x\left(\frac{\partial f}{\partial h}\right)^2\right], \tag{5.9}$$

with the boundary condition

$$f(1,h) = \log\Theta\left(\frac{h}{\sqrt{2\Delta(1)}}\right). \tag{5.10}$$

Again, this form is valid for a generic matrix (that is, a generic profile $\Delta(x)$) and must be optimized over $\Delta(x)$ and Δ^r as detailed in appendix E.
The definitions of the main observables, pressure and shear strain, are the same as before. For the pressure we have

$$\frac{p_g}{d} = \frac{\widehat{\varphi}_g}{2} \int dh\ e^{h+\eta-\Delta(0)/2} \int \mathcal{D}\zeta \Theta \left(\frac{h+\eta+\Delta_r+\zeta^2\gamma^2/2-\Delta(0)}{\sqrt{2(2\Delta_r+\zeta^2\gamma^2-\Delta(0))}} \right) f'(0,h), \quad (5.11)$$

and for the shear strain we get

$$\frac{\beta\sigma}{d} = \gamma \frac{\widehat{\varphi}_g}{2} \int dh\ e^{h-\Delta(0)/2} \int \mathcal{D}\zeta\ \zeta^2\ \frac{e^{-\frac{(h+\Delta_r(\gamma)-\Delta(0))^2}{2(2\Delta_r(\gamma)-\Delta(0))}}}{\sqrt{2\pi(2\Delta_r(\gamma)-\Delta(0))}} \left(\frac{\Delta_r(\gamma)-h}{2\Delta_r(\gamma)-\Delta(0)} \right) f(0,h), \quad (5.12)$$

with the definition

$$\Delta^r(\gamma) \equiv \Delta^r + \frac{\gamma^2\zeta^2}{2}. \quad (5.13)$$

In the following section we report the results obtained by solving the optimization equations for $\Delta(x)$ and Δ_r and computing the physical observables defined above.

5.2 Results

5.2.1 Phase diagrams and MSDs

Compression-decompression

We focus first on the compression-decompression phase diagram, as done in the preceding chapter. We report it in figure 5.2. We can now see that within the fRSB ansatz, glasses (including those with $\widehat{\varphi}_g = \widehat{\varphi}_{MCT}$) can be followed beyond the Gardner point, all the way to the jamming transition; the unphysical spinodal points that were predicted by the RS ansatz for the less dense glasses have now disappeared. So, at least for hard spheres, there is no need to use potentials with three or more replicas to prevent unphysical spinodal points from appearing within the theory, differently for what was argued in [237, 244]. In particular, we can now compute the jamming densities $\widehat{\varphi}_j$ for every glass; for the glasses prepared through an annealing down to $\widehat{\varphi}_g = \widehat{\varphi}_d$, corresponding to the shortest (and thus easiest) possible annealing protocols, one has

$$\widehat{\varphi}_j(\widehat{\varphi}_d) \simeq 7.30.$$

This is the value of the density of the least dense packings that can be constructed through an annealing protocol (or equivalently, the most dense that con be constructed without needing an exponentially long annealing time, eq. (2.1)). Less dense amorphous packings can in principle be obtained with procedures reproducing quenching protocols, but the computation of their jamming density cannot be performed within the SF setting, which is conceived for the study of annealing protocols. We will return to the issue in section 7.3.

It can also be interesting to study how the MSDs behave near the Gardner point. Up to the the Gardner transition, the state is a simple minimum and only a single

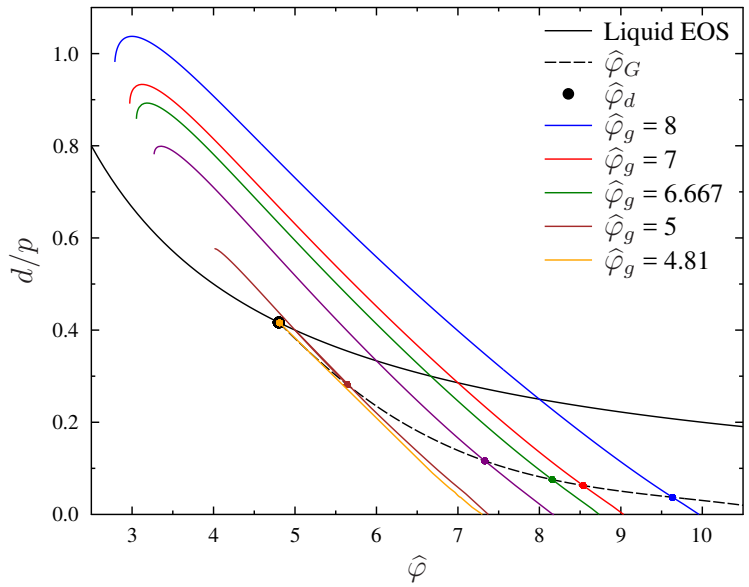

Figure 5.2. Following glasses in (de)compression within the fRSB ansatz. Glassy states can now be followed all the way to the jamming point, for all planting densities $\widehat{\varphi}_g$.

MSD Δ is present; afterwards, the fRSB structure manifests, the state becomes a metabasin of sub-minima, and the MSD becomes a more complicated object $\Delta(x)$, depending on how deep we go in the fRSB hierarchy as x is varied. In particular, $x = 0$ corresponds to the MSD $\Delta(0)$ of replicas which are farthest apart and sample the big glassy metabasin at the top of the hierarchy, while $\Delta(1)$ is the MSD of replicas which are in the smallest micro states at the bottom of the hierarchy; for historic reasons and the analogy with the fRSB solution of the SK model, it is commonly called Δ_{EA} [57]. The Δ_{EA} is the Debye-Waller factor of the glass in the fRSB phase.

In figure 5.3 we plot the MSD Δ up to $\widehat{\varphi}_G$, and then the values of $\Delta(0)$, Δ and $\langle\Delta\rangle$ (equation (5.7)). We can see how the three quantities bifurcate at the Gardner point, with Δ_{EA} decreasing in preparation for the jamming transition, whereupon the spheres enter in contact and $\Delta_{EA} \to 0$. We had mentioned in paragraph 2.1.3 and in the preceding chapter that the scaling of Δ_{EA} is that situation is supposed to be $\Delta_{EA} \simeq p^{-\kappa}$, where κ is a nontrivial exponent. In order to compute it, and the other two exponents of jamming γ and θ, one must perform a scaling analysis near jamming of the optimization equations in the fRSB ansatz (appendix E). The analysis itself is quite technical in nature and very similar to the one already performed in [156], so we refer the interested reader to section E.3 in the appendix, and here we limit ourselves to saying that the results of [156] are recovered. In particular, one has

$$\begin{aligned} \kappa &\simeq 1.41574 \\ \theta &\simeq 0.42311 \\ \gamma &\simeq 0.41269 \end{aligned}$$

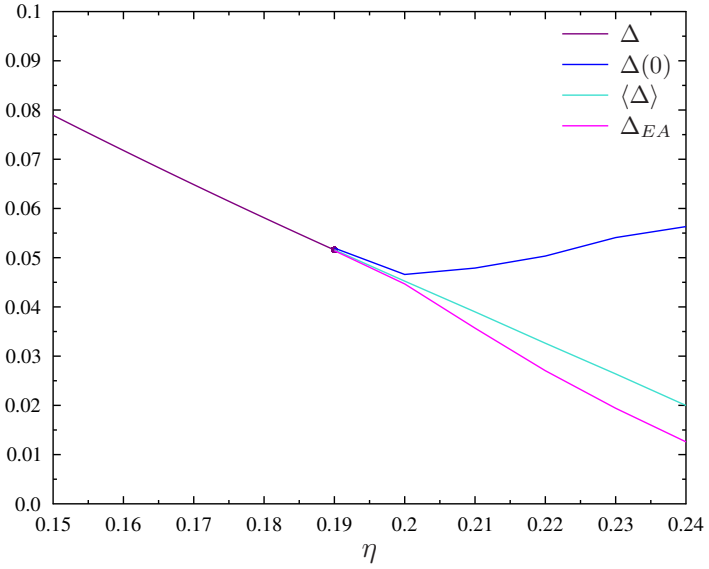

Figure 5.3. MSDs for the glass around the Gardner point for $\widehat{\varphi}_g = 6.667$.

as in [41, 156].

Shear strain

The phase diagram in strain is reported in figure 5.4. One can see that, with respect to the RS computation of the preceding chapter, the yielding point γ_Y is shifted to higher values of γ (we replot the RS solution with a dashed line for comparison), and again a stress overshoot is detected.

However, we are not able to follow glassy states all the way to the yielding point. The reason for this is that the code we use to solve the variational equations is unable to approach the yielding point, and it loses track of the solution beyond a certain value of γ thet we mark with an empty circle in figure 5.4. Differently from the spinodal points to the RS solution, which were a genuine artifact of the theory, we believe that this problem is only technical in nature, and can be in principle solved just by using a more refined code for solving the variational equations in shear. Nevertheless, we argue that the presence of a yielding point also within the fRSB ansatz is difficult to refute, despite the technical difficulties.

This view of things is corroborated by the behavior of the MSDs beyond the Gardner point, which we report in figure 5.5. We can see that, beyond the Gardner point, the MSD $\Delta(0)$ of the glassy metabasin shoots up very rapidly, signaling that the glassy state is being widened more and more by the shear. Despite this, the MSD Δ_{EA} of the micro states within it decreases, signaling that they become more tight. This is no surprise, since the pressure is actually increasing because of dilatancy as one can see in the inset of figure 5.4, and we already know that Δ_{EA} is supposed to be inversely proportional to the pressure p.

In summary, we argue that the yielding transition is always present in the fRSB

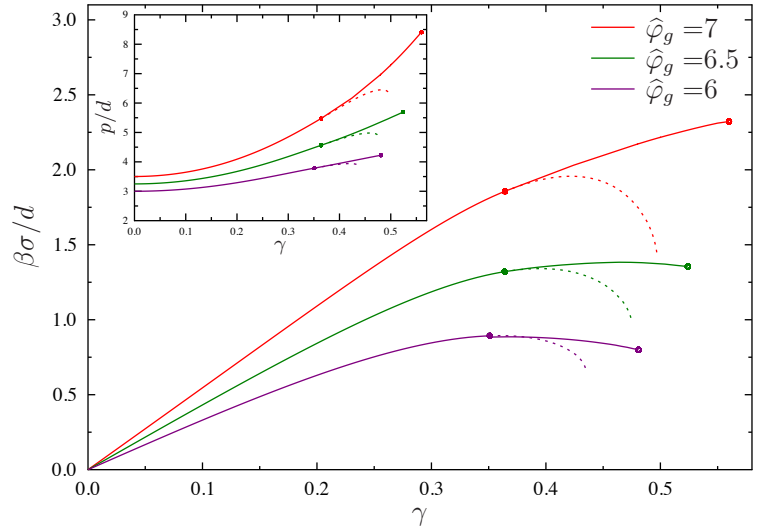

Figure 5.4. Following glassy states prepared at $\widehat{\varphi}_g$ upon applying a shear-strain γ. With respect to the RS computation (dashed lines) the yielding point γ_Y is shifted to larger values of the strain for all glasses. However, we are unable to follows states all the way to the yielding points due to instabilities in the numerical code for the solution of the variational equations. Despite this, the stress overshoot is still present (see $\widehat{\varphi}_g = 6$) and a yielding point, tough not approachable, is clearly present at higher values of the strain. An empty circle marks the end of curves beyond which the code is unable to follow the solution.

ansatz, and that the picture of yielding as a spinodal point that emerged from the RS computation remains true in this case, with the only caveat that is must be applied to *metabasin* level. The yielding transition corresponds to a loss of stability (or equivalently, a saddle node bifurcation) at the metabasin level as we had already surmised in paragraph 2.2.2. This means that the MSD $\Delta(0)$ is supposed to have, near the yielding point, the square-root behavior

$$\Delta(0) - \Delta(0)^{max} = -C\sqrt{\gamma_Y - \gamma}, \tag{5.14}$$

just like the MSD Δ at the onset transition. This however is true only for $\Delta(0)$. We argue that Δ_{EA} will stay finite (and with it, the pressure) at the yielding point γ_Y, as the plot in figure 5.5 seems to indicate.

5.2.2 Critical slowing down

The Gardner transition, despite its peculiarities, is still a second order critical point, whereupon a phenomenology typical of continuous transitions is supposed to manifest. First of all, suppose to perform a quenching dynamics with an initial condition within the state, as in [166]. We want to investigate how the dynamics relaxes towards equilibrium within the metastable state. In the stable glass phase the metastable state is ergodic (just like the liquid phase above the MCT transition density $\widehat{\varphi}_{MCT}$) and an exponential relaxation is consequently observed [3, 4, 166],

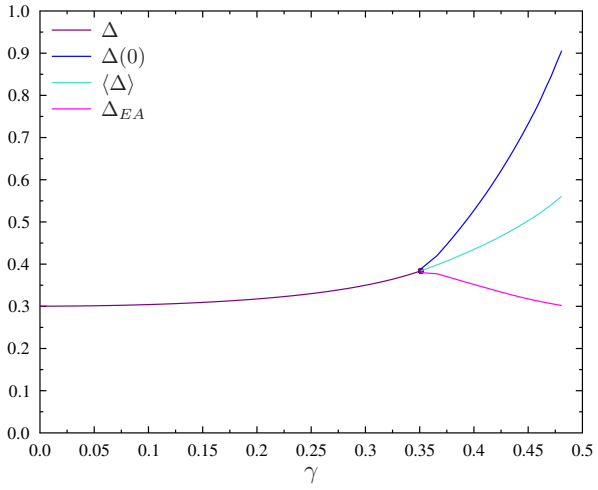

Figure 5.5. MSDs for the glass at $\widehat{\varphi}_g = 6$ as shear is applied. The MSD of the metabasin $\Delta(0)$ grows rapidly beyond the Gardner point, while the MSD of fRSB micro-states Δ_{EA} decreases.

as anticipated in paragraph 2.1.4. However as the Gardner point is approached, we expect a dynamical slow down due to the appearance of an internal structure of sub-states within the metastable basin. Indeed, at this transition point, the relaxation becomes power law instead of exponential, a phenomenon well known within the theory of critical phenomena and dubbed *critical slowing down* [20]. To fix ideas, let us define a dynamical mean square displacement

$$\Delta_D(t) = \frac{d}{N}\sum_{i=1}^{N} |x_i(t) - x_i(0)|^2 \tag{5.15}$$

being $x_i(t)$ the position of the sphere i at time t. At the Gardner transition point we have

$$\Delta_D(t) \sim \Delta - At^{-a} \tag{5.16}$$

being Δ the solution of the RS saddle point equations (4.20) to (4.22); the constant A is expected to be positive. This in turn implies that the relaxation time within the state obey the scaling [255]

$$\tau_\beta \propto (\widehat{\varphi}_G - \widehat{\varphi})^{-1/a} \tag{5.17}$$

as studied in [4].
We want to compute the exponent a. This is related to the so called *exponent parameter* λ [255]

$$\lambda = \frac{\Gamma(1-a)^2}{\Gamma(1-2a)}. \tag{5.18}$$

It has been shown in [255] that the exponent parameter can be computed from the replica approach. Indeed it is given by

$$\lambda = \frac{w_2}{w_1} \tag{5.19}$$

and w_1 and w_2 are two cubic terms in the expansion of the free entropy around the RS solution at the Gardner point, defined in [155]. As proven in paragraph C.3, all the expressions for quadratic and cubic terms reported in [155] can be reused in the state following setting, just by redefining suitably the integral measure for computing averages

$$\langle \mathcal{O}(\lambda) \rangle_{RS} \equiv \int d\lambda \; \mathcal{O}(\lambda) \frac{e^{-\frac{(\lambda+\sqrt{\Delta})^2}{2}}}{\sqrt{2\pi}} \longrightarrow \langle \mathcal{O}(\lambda) \rangle_{SF} \equiv \int d\lambda \; \mathcal{O}(\lambda) G(\lambda), \tag{5.20}$$

where $G(\lambda)$ is defined in equation (4.44). We can thus effortlessly write the expression for λ

$$\lambda = \frac{-8\widehat{\varphi}_g w_2^{(I)}}{16/\Delta^3 - 8\widehat{\varphi}_g w_1^{(I)}} \tag{5.21}$$

where $w_1^{(I)}$ and $w_2^{(I)}$ are defined in [155, Eq.(79)]. With some algebra (see [2]), we get the final result:

$$\lambda = \frac{-4\widehat{\varphi}_g A}{16 + 8\widehat{\varphi}_g (1+B)}, \tag{5.22}$$

with

$$A = \left\langle \Theta_0^{-1}(\lambda) \Gamma_2(\lambda, 0) \right\rangle, \tag{5.23}$$

$$B = \left\langle \Theta_0^{-1}(\lambda) \Gamma_1(\lambda, 0) \right\rangle, \tag{5.24}$$

and

$$\begin{aligned}
\Gamma_2(\lambda, s) = &\left[2\left(\frac{\Theta_1(\lambda)}{\Theta_0(\lambda)}\right)^3 - 3\frac{\Theta_1(\lambda)\Theta_2(\lambda)}{\Theta_0^2(\lambda)} + \frac{\Theta_3(\lambda)}{\Theta_0(\lambda)} \right] \left[2\lambda^3 + 2(s-6)\left(\frac{\Theta_1(\lambda)}{\Theta_0(\lambda)}\right)^3 + \right. \\
&\left. + 3\frac{\Theta_1(\lambda)}{\Theta_0(\lambda)} \left[4\lambda \frac{\Theta_1(\lambda)}{\Theta_0(\lambda)} - (s-4)\frac{\Theta_2(\lambda)}{\Theta_0(\lambda)} \right] - 6\lambda \left(\lambda \frac{\Theta_1(\lambda)}{\Theta_0(\lambda)} + \frac{\Theta_2(\lambda)}{\Theta_0(\lambda)} \right) + (s-2)\frac{\Theta_3(\lambda)}{\Theta_0(\lambda)} \right], \\
\Gamma_1(\lambda, s) = &\left[1 + \frac{\Theta_1^2(\lambda)}{\Theta_0^2(\lambda)} - \frac{\Theta_2(\lambda)}{\Theta_0(\lambda)} \right]^2 \left[(s - 3\lambda^2) + (s-6)\frac{\Theta_1^2(\lambda)}{\Theta_0^2(\lambda)} + 6\lambda \frac{\Theta_1(\lambda)}{\Theta_0(\lambda)} - (s-3)\frac{\Theta_2(\lambda)}{\Theta_0(\lambda)} \right],
\end{aligned} \tag{5.25}$$

and the $\Theta_k(\lambda)$ functions are defined as [155]

$$\Theta_k(x) \equiv \frac{1}{\sqrt{2\pi}} \int_x^\infty dy \; y^k \mathrm{e}^{-\frac{1}{2}y^2}. \tag{5.26}$$

The quantities A and B can be easily computed numerically; we report the results of the numerical evaluation of the exponents in table 5.1.

5.2.3 Fluctuations

Besides critical slowing down, another phenomenology typical of second order critical points is the manifestation of an infinite susceptibility, which as a rule of thumb is usually linked to the inverse of the zero mode that signals the transition [20] (in our case, the replicon).

$\widehat{\varphi}_g$	λ	$1/a$
4.8	0.702666	
4.9	0.560661	2.65122
5	0.509074	2.54665
5.25	0.437754	2.42661
5.5	0.393779	2.36344
5.87	0.351157	2.30848
6	0.339808	2.29475
6.667	0.295692	2.24461
7	0.280148	2.22805
8	0.246892	2.19440
10.666	0.204280	2.15441

Table 5.1. Our results for λ and $1/a$ for various planting densities $\widehat{\varphi}_g$.

In paragraph 1.1.5, we discussed the dynamical susceptibility $\chi_4(t)$ and how it reaches a maximum at a time $t^* \simeq \tau_\alpha$ corresponding to cooperative relaxation of the system. In the case of the Gardner point, the situation is similar but there is a very relevant difference, namely the fact that the transition is second order, and differently from the MCT transition, is not avoided: the susceptibility converges to a stable static value, $\lim_{t\to\infty} \chi_4(t) = \chi_4$, which goes to infinity as the transition is approached, $\lim_{\varphi\to\varphi_G^-} \chi_4 = \infty$. This divergence can be also used in practice to locate numerically the Gardner transition, see [4].
To fix ideas, let us define

$$\chi(t) = \langle \Delta^2(t) \rangle - \langle \Delta(t) \rangle^2 \,, \tag{5.27}$$

where the brackets are used to denote the average over the thermal history of the system. The $\chi(t)$ is a dynamical quantity, but we need to focus on its large time behavior when $\langle \Delta(t) \rangle \to \Delta$. In this case $\chi(t) \to \chi_4$, where χ_4 is a static susceptibility

$$\chi_4 = \langle \Delta_{ab}^2 \rangle - \langle \Delta_{ab} \rangle^2 \,, \tag{5.28}$$

already well known in the context of spin glasses, that can be computed from a static approach [256, 257].
Within a mean field theory, fluctuations like the (5.28) are encoded in the quadratic term (the so-called mass term) of the field theory that is obtained by expanding the free energy around the critical point (the Gardner point in this case) [20, 257]. Within this field theory, the order parameter field is Δ_{ab} and the "mass matrix" is nothing but the tensor $M_{a<b;c<d}$ defined in the (4.32). We need to study the inverse of this quadratic operator in order to obtain the value of the χ_4 susceptibility.
In principle, and as already discussed, the whole tensor M, with all indices running form 1 to $s+1$ (we always assume $m = 1$), has to be taken into account. However, here we are mostly interested with the most divergent part, and not on the finite corrections. As a result of this, we can again focus only on the tensor M restricted to the sector of s replicas, equation (4.36), that we had already studied in appendix C for locating the Gardner transition. The inversion of the tensor M^s is just a

matter of standard linear algebra, so we refer the interested reader to [2] and just quote the the final result

$$\chi_4^{\text{div}} = \frac{24}{\lambda_R}, \tag{5.29}$$

where λ_R is the replicon mode, equation (4.40). Unsurprisingly, the diverging susceptibility is inversely proportional to the critical mode at the transition.

5.2.4 Shear moduli

The appearance of a fRSB hierarchy within the glassy states has very interesting consequences in terms of shear modulus. The reason for this is the following: suppose that our system is into one of the bottom fRSB microstates, with MSD $\Delta(1) = \Delta_{EA}$. We now apply a small strain to the system. If the shear is small enough that the system does not leave the microstate, it will respond elastically with a shear modulus $\mu = \frac{1}{\Delta_{EA}}$. However, if the shear is large enough that the system is kicked out of the microstate, goes all the way to the top of the hierarchy, and then falls in another microstate (but anyway within the same glass basin), the response will be described by a modulus $\mu = 1/\Delta(0)$, where $\Delta(0)$ is the MSD of the whole metabasin as previously discussed. In summary, the presence of a hierarchy of sub-states makes it necessary to keep track of the fact that the strain may not only act as a deformation of the minimum the system is in (as it was the case above the Gardner transition where the glassy state has no structure), but may also cause the system to escape from the minimum and end up into another [215]. As a result of this, the response of the system will be described by a generalized, protocol-dependent shear modulus

$$\mu(x) \equiv \frac{1}{\Delta(x)} \tag{5.30}$$

where the relevant value of x depends on how high in the hierarchy the system has to go to make the jump. This fact is well known in the context of spin glasses where an external magnetic field and the magnetic susceptibility play the role of the strain and shear modulus, respectively, but the physical picture is the same [215].
It is obvious that the most important moduli correspond to the two extreme cases $\mu(0) = \frac{1}{\Delta(0)}$ and $\mu(1) = \frac{1}{\Delta_{EA}}$. We are interested in studying their behavior near the Gardner point. In order to achieve this, we just go for the easiest route and assume that near enough to the Gardner point, the full profile $\Delta(x)$ can be reasonably approximated with a two-step (1RSB) profile with two MSDs Δ_1 and Δ_2 and two shear moduli

$$\begin{aligned} \mu_1 &= \frac{1}{\Delta_1}, \\ \mu_2 &= \frac{1}{\Delta_2}. \end{aligned} \tag{5.31}$$

We are interested in the behavior of $\Delta_1 - \Delta_2$ as a function of the density $\widehat{\varphi}$ near the Gardner point $\widehat{\varphi}_G$, which requires the study of the saddle point equations for the replicated free energy truncated at cubic order, as done in paragraph C.1. The computations are just a matter of standard algebra and are again very similar to

the study of [156, sec. VII], so we skip again to the final result and refer to [2] for details. One gets:

$$\frac{1}{\mu_1} - \frac{1}{\mu_2} = \Delta_1 - \Delta_2 \propto \widehat{\varphi} - \widehat{\varphi}_G. \tag{5.32}$$

So the difference between the two moduli is linear in the distance from the Gardner point. This prediction should be easy to check numerically.

5.3 Discussion

In this chapter we have performed the computation of the Franz-Parisi entropy within the fRSB ansatz, describing a glassy minimum wherein a hierarchical, fractal structure of microstates manifests at the bottom of the glassy minimum, thereby making it a metabasin of fractal sub-minima [41]. Using this ansatz, we have been able to cure the unphysical spinodal points that appeared within the RS ansatz, making it possible to follow glassy states in compression, all the way to the jamming point. For what concerns yielding, we have been unable to follow the state all the way to the yielding point because of technical difficulties, but we are anyway able to detect a stress overshoot and the presence of a yielding point also within the fRSB ansatz appears to be irrefutable. We believe that the technical problems can be fixed simply by using a more refined code to solve our state following equations. Notice however that the fRSB equations (appendix E) are Partial Differential Equations (PDEs), so their numerical treatment is anyway a hard task and an open field of study in numerical analysis as of today. There may also be another possibility, namely that the equations near yielding develop a scaling regime as in the jamming case, with an associated set of critical exponents, rendering possible an analytic study near the yielding point. However, the presence of such a criticality near yielding is far from established, and still an open problem [189, 194, 195, 200], so more studies will be needed in the future.

There is one very important point to discuss. Throughout this thesis we have stated multiple times that the result we derive are valid on a timescale t_{exp} such that

$$\tau_\beta \ll t_{exp} \ll \tau_\alpha,$$

where τ_β is the time needed to equilibrate within the glassy states. Within state following with the two-replica potential, we are *always* looking at equilibrium within the glassy state, no matter which ansatz we use.
Now, in the stable glass phase above $\widehat{\varphi}_G$, relaxation within the glassy state is exponential [166] and the timescale τ_β is short enough that any reasonable protocol has a t_{exp} such that the above requirement is met. This however is not true anymore beyond the Gardner point. We recall the reader that the Gardner transition [249] is equivalent to the ferromagnetic transition in the SK model [57, 250]; this means that the dynamics of the system beyond the Gardner point will be characterized by an aging phenomenology [258] much like the one exhibited by the SK model [57]. This aging phenomenology is extremely rich and as of now still not fully understood. What is certain is that it is a lot more complicated than the aging phenomenology commonly exhibited by structural glasses. Instead of a two-timescale scenario like the one commonly found in RFOT models, a very complicated hierarchy of

timescales (and with them, effective temperatures) manifests within the dynamics of systems with a fRSB transition [21, 57, 160]; as a result of this, the system takes a long time (though not as large as τ_α of course) to attain equilibration, even within the glassy metabasin.
In such a situation, a theory aiming to reproduce a realistic laboratory protocol would focus on the state following of *a single fRSB microstate*, instead to the whole metabasin as we have done in this chapter. This is however extremely difficult (and maybe impossible) to realize in practice, because fRSB microstates merge, bifurcate, and cross even when the perturbation is infinitesimal, an effect well explained in [215]; as a result of this, a two-replica (or even a three-replica) potential is not sufficient for following a single microstate, and a continuous chain, with an infinite number of replicas as detailed in section 3.3, is in principle needed. However, a computation with a continuous replica chain within the fRSB ansatz looks extremely difficult and perhaps not even doable.
This effect can be easily understood by looking at the stress strain curves in figure 5.4, beyond the Gardner point, and comparing then with the ones in figure 2.10. The response in figure 2.10 is very rough, as one should expect from a system whose dynamics takes place in a very disordered landscape. The curves in 5.4, however, are smooth, despite the fact thet the system is now moving in a very rough FEL characterized by a fractal hierarchy of microstates. The reason for this is that in figure 5.4 we are are looking at equilibrium inside the metabasin, so we are effectively giving the system enough time to explore ergodically all the fRSB sub-minima after each strain step; from a practical point of view, we are taking various rough shear histories like the ones in figure 2.10 and we are averaging their stress-strain curves, getting back a smooth response.

In summary, beyond the Gardner point, our SF calculation is only an approximation of the real dynamics of the system. However, as the numerical results of [4] indicate, the deviations between theory and simulation, in compression-decompression protocols, are anyway very small. For what concerns shear, our approach is not able to reproduce the state following of a single inherent structure, as done in AQS protocols (paragraph 2.2.1), since it looks always at equilibrium within the metabasin. It is however well suited to the rheology of thermal systems like foams, pastes and soft matter in general.

5.3.1 Yielding within the fRSB ansatz

We conclude the chapter with some comments about the picture that emerges from our calculation for what concerns the yielding transition. As in the preceding chapter, the yielding point looks very much like a spinodal point whereupon the state loses stability and opens up along an unstable direction, becoming a saddle. This is signaled by a behavior of the intra-metabasin MSD $\Delta(0)$ that looks very much like the one exhibited at the onset transition (see figure 4.2, top left panel), with a square root singularity

$$\Delta_1 - \Delta_1^{max} = -C\sqrt{\gamma_Y - \gamma},$$

as already discussed. However, from figure 5.5 we can see that while $\Delta(0)$ shoots up, the behavior of the other MSDs is milder, and Δ_{EA} is even decreasing. Thus, as the metabasin is being widened more and more by the shear, the fractal hierarchy

of state within it survives, and the bottom states with $\Delta = \Delta_{EA}$ are even getting tighter. It is safe to assume that even when the basin finally opens and loses stability because of the shear, the bottonmost microstates anyway maintain their form.

This fact is very interesting if one views it in term of shear moduli instead of MSDs, as detailed in paragraph 5.2.4. As explained in paragraph 2.2.2, the onset of an instability (and with it, an avalanche) is signaled by a square root-like singularity in the shear modulus. We have also mentioned, figure 2.11, how the curves typically found in AQS protocols have a sort of scale-invariant structure, and are made of small segments which have a general trend similar to the whole stress-strain curve. This fact can be nicely interpreted in terms of the $\mu(1)$ and $\mu(0)$ shear moduli: the shear modulus $\mu(1)$ is the one relative to the small segments and to a single inherent structure, while the shear modulus $\mu(0)$ is the one relative to the "elastic" part of the whole stress-strain curve (see figure 2.10 for small γ). The small plastic events would then correspond to a loss of stability at fRSB microstate level and a singularity in the $\mu(1)$ modulus, while the yielding transition whereupon the system starts to flow corresponds to a loss of stability within the *whole metabasin* and a singularity in the $\mu(0)$ shear modulus. In addition to this, one can also see that the curves after yielding are on average flat (no $\mu(0)$ can be defined) but do show an elastic response on small scales ($\mu(1)$ can still be defined). This seems to be in accordance with the approach to the yielding point within our state following calculation, wherein only $\Delta(0)$ exhibits a square-root like behavior at yielding while $\Delta(1)$ stays finite.

It is worth of note that the basic phenomenology of yielding seems to be well captured by our HS model in the MF limit. This appears surprising since one of the defining traits of MF models is their lack of space structure, while the phenomenology of yielding (and in particular of avalanches) seems to be mainly ruled by local rearrangement modes (we remind the discussion in paragraph 2.2.2), which should be completely missed by the MF solution. We must however precise that the local modes are certainly relevant for small avalanches like the ones visible in figure 2.11, while there is no consensus about the localization properties of the rearrangement modes that separate the elastic part of stress-strain curves from the flowing, steady-state part. While Eshelby-like [199] modes still seem to be relevant, it is argued in [207] that a concatenation of many Eshelby modes is necessary to destroy the glass via a shear-banding process; in this case, the localization properties of the rearrangement modes may be much more complicated to figure out then how it would be in the case of a single, simple Eshelby mode, and an effective delocalization effect may appear. We remind the reader that from the discussion of paragraph 1.1.5, it transpires that a cooperative, delocalized rearrangement is necessary for glass relaxation. This may also be the case for driven glasses under shear.

In any case, more work is required to better understand the flow regime beyond the yielding point.

Chapter 6

Numerics in the Mari-Kurchan model

All the results we presented in the preceding two chapters are valid for hard spheres in the $d \to \infty$ limit. Despite the fact that the physics predicted by the State Following approach is in qualitative agreement with the general phenomenology of glasses reviewed in chapter 2, it would be anyway nice to get a quantitative comparison with numerical results. Such a program is however difficult to implement as the simulation of a particle system with many spatial dimensions is obviously an endeavor of considerable computational cost. In this chapter we report a workaround, centered around a special HS model which has a MF-like behavior also in finite dimension, in particular dimension three. The model has the advantage of being both analytically tractable with the replica method and of being very easy to implement numerically, allowing for a systematic comparison between theory and simulation.

6.1 Model

The model we employ is referred to as *Mari-Kurchan (MK) model* [259], and its Hamiltonian is

$$H_{MK} \equiv \sum_{i<j} V(\boldsymbol{x}_i - \boldsymbol{x}_j - \boldsymbol{A}_{ij}), \tag{6.1}$$

where V is any suitable interaction potential (in our case it will be the HS one). The $\boldsymbol{A}_{ij}$ are "random shifts", i.e. quenched, random d-dimensional vectors identically, independently and uniformly distributed in the d-dimensional cube:

$$P(\boldsymbol{A}) = \frac{1}{V};$$

and of course $\boldsymbol{A}_{ij} = \boldsymbol{A}_{ji}$.

This model can be seen as MF in multiple ways. First, we can notice that the model is devoid of any space structure: despite the fact that every particle interacts, given a certain realization of the $\boldsymbol{A}$s, with a finite number of "neighbors", those neighbors can be anywhere in the sample, since the shifts are uniformly distributed in the whole cube. From this point of view, the model is MF because the physical space the model is embedded into plays no role on the interactions.

A less intuitive, but more profound line of reasoning stems from considering the probability of having three particles, say i, j and k, interact with each other *at the same time*, i.e., each of them interacts with *both the other two* at the same time. For this to happen, we should have, for the HS potential,

$$\begin{aligned} |\boldsymbol{x}_i - \boldsymbol{x}_j - \boldsymbol{A}_{ij}| &\simeq D, \\ |\boldsymbol{x}_j - \boldsymbol{x}_k - \boldsymbol{A}_{jk}| &\simeq D, \\ |\boldsymbol{x}_k - \boldsymbol{x}_i - \boldsymbol{A}_{ki}| &\simeq D, \end{aligned} \tag{6.2}$$

which would imply

$$|\boldsymbol{A}_{ij} + \boldsymbol{A}_{jk} + \boldsymbol{A}_{ki}| \simeq D,$$

which is very unlikely (and, in the thermodynamic limit, outright impossible), since the shifts are $O(L)$[1]. In this model, three body interactions are effectively forbidden: if i interacts with j, and i interacts also with k, then k and j do not interact with each other. Thus, the MK model is mean-field in the sense that the network of interactions is tree-like, i.e., there are no *loops* [45]. Actually, it is indeed the disappearance of loops for $d \to \infty$ that gives high-d HSs their mean field nature. In that case, three-body interactions are made impossible for $d \to \infty$ by the high dimensionality itself [260].

Besides the fact that the model has a MF behavior also for finite d, it has two more big advantages. First, the presence of a quenched disorder in the form of the random shifts allows one to implement a procedure, dubbed the *planting* method [261], which allows one to obtain thermalized configurations also in the glass phase above φ_{MCT}, wherein it would normally be extremely time-consuming to do so, because of the glassy slowdown. So one can effectively implement an annealing protocol with arbitrary φ_g with a negligible computational cost.
The basic idea of planting is to invert the order according to which initial particle positions $\boldsymbol{r}_i$ and quenched random shifts $\boldsymbol{A}_{ij}$ are chosen: first one extracts a random configuration of particle positions $\boldsymbol{r}_i$, and afterwards the random shifts $\boldsymbol{A}_{ij}$ are chosen uniformly, with the sole requirement that spheres do not overlap. In the liquid phase $\varphi \in [\varphi_{MCT}, \varphi_K]$, this straightforward process produces an equilibrium configuration that automatically satisfies the liquid EOS (see [261] for more details). Since in the MK model the complexity never vanishes and consequently the ideal glass transition density φ_K goes to infinity, this procedure allows one to produce equilibrated configurations for any density, with negligible computational cost. A set of positions $\{\boldsymbol{r}_i\}$ and shifts $\{\boldsymbol{A}_{ij}\}$ identifies a *sample*.

Besides this numerical flexibility, the model can be also easily treated analytically, in the sense that its replicated entropy (section 3.1) can be computed using the techniques discussed in [153]; the result is exact only for infinite d [154], but for finite d it constitutes an anyway excellent approximation, as we are going to see and as discussed in [4]. The computation of the replicated entropy of the MK model is reported in full detail in [45], so we just report the final result, for an RS ansatz:

$$s[m, \varphi, A] = -\log \rho + \log N + S_{harm}(m, A) - 2^{d-1}\varphi[1 - G_m(A)], \tag{6.3}$$

[1] L is the side of the simulation cube.

where A is the *cage radius*, $A \equiv \frac{D^2}{2d}\Delta$, S_{harm} is defined as

$$S_{harm}(m, A) \equiv (m-1)\frac{d}{2}\log(2\pi A) - \frac{d}{2}\log m + d\frac{m-1}{2}, \tag{6.4}$$

and the function $G_m(A)$ is defined in [45, 153]. The reader is invited to appreciate the similarity with the expression (4.9) for $s \to 0$. Indeed, for $d \to \infty$ the (6.3) reduces to the (4.9) computed with the RS ansatz [154]. As the (4.9), this expression must be optimized over A to obtain the physical replicated entropy $\mathcal{S}(m, \varphi)$.

6.2 Results

The MK model defined above is a very convenient test-bed for the theory exposed in this thesis. We now report some results obtained with numerical simulations of the model, contained in references [3, 4]. Those studies have a larger scope and contain much more material than reported here, so we refer to them for further reading.
Simulations are always performed following the same basic guideline: first, an equilibrium configuration is produced through planting at a certain planting density φ_g (φ_0 in the notation of [3, 4]); then a compression (decompression) protocol is implemented by inflating (deflating) the spheres with the LS algorithm [135]. This way, a state following procedure in compression/decompression is reproduced. To our knowledge, a similar numerical procedure has not been implemented for State Following under quasi-static shear, though it is an obvious continuation of the studies [3, 4] that we leave for future work.

6.2.1 Isocomplexity

As a warm-up exercise we first derive the equations of state of the glass through the isocomplexity approximation [3], paragraph 3.1.2, also for the sake of comparison with the more refined State Following computation. We then compare the analytical results with numerical simulations of an MK model in $d = 3$ with $N = 800$ particles of diameter $D = 1$ and periodic boundary conditions. Since we focus only on thermodynamic, self-averaging observables (see the discussion of section 3.2), only a small number of samples, $N_s = 6$, is needed to perform ensemble averages. The dynamics is implemented through a Metropolis algorithm and compression-decompression is implemented through inflation-deflation of the spheres as in the LS [135] algorithm.

To perform the derivation of glassy EOS, one just needs to compute the complexity and in-state free energy using equations (3.7),(3.8) (we recall that the prescription is $\mathcal{S} = -\beta\Phi$) and then implement the isocomplexity approximation by solving the (3.12); more details are given in the SI of [3].
In figure 6.1 we report the results obtained; as in figure 4.4, we plot the inverse pressure $1/p$ versus the packing fraction φ for various planting densities φ_0. Notice that the quantities are not rescaled anymore as in chapters 4 and 5, as now we are in $d = 3$.

Overall, one can see that a good agreement with simulation is already visible, even with isocomplexity approximation. Despite the fact that it is a lot less flexible and rigorous than the SF formalism, the theory is anyway satisfactory enough, at least

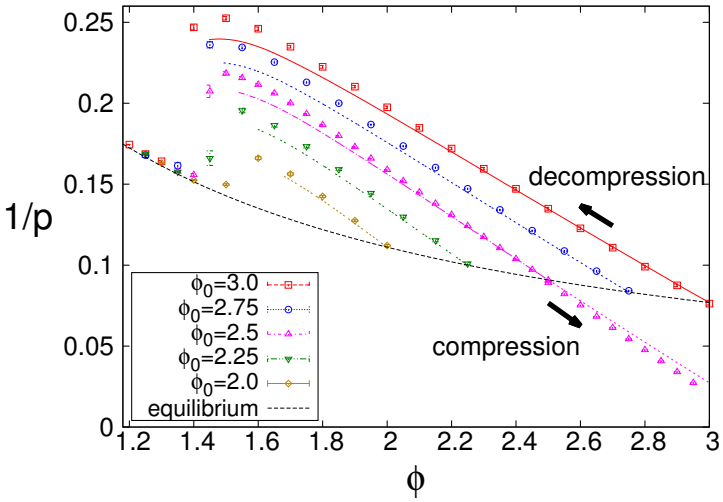

Figure 6.1. Equation of state of various glasses as in figure 4.4. The lines are theory and the dots are simulation data as described in [3]. A satisfactory agreement between theory and simulation can be observed already with the simplest isocomplexity computation.

at the level of thermodynamic observables.
Since the isocomplexity approximation (and the real replica method in general) are a lot less mathematically convoluted than the SF formalism, it is easy to study the singular behavior of the cage radius at the onset point whereupon the glass state melts back into the liquid. One gets:

$$A(\varphi) = A_{max} - C\sqrt{\varphi - \varphi_{on}}, \tag{6.5}$$

where the coefficient C depends on m and can be computed easily (see the SI of [3]).

6.2.2 State Following and the Gardner transition

As mentioned before, the MK model for $d \to \infty$ is quantitatively and qualitatively identical to mean-field HSs. In finite dimension, some corrections have to be taken into account with respect to the $\infty - d$ result. The most important finite-dimensional effect in the MK model lies in the fact that caging is not perfect in the glass phase, and particles are effectively free to move in a network of cages as well studied in [262]. This effect washes away the MCT singularity at φ_{MCT}, but since hopping is exponentially suppressed in φ, it produces relevant effects only for $\varphi_0 \simeq \varphi_{MCT}$. Once the effect of hopping has been removed by focusing on higher φ_0s, the corrections with respect to $\infty - d$ are effectively only quantitative in nature. So, for the sake of comparison, we can just take the SF results exposed in the preceding chapters, paying attention to rescaling the quantities in the correct way (for example $\varphi = \frac{d}{2^d}\widehat{\varphi}$).

The study of [4] is performed with the same basic numerical setup as the one of [3], though with the aim of verifying the prediction of the presence of a Gardner

transition in compression; comparison with the SF results reported in the preceding chapters is also reported (with the proper rescaling as discussed above). A first check of the SF procedure is reported in figure 6.2, where the effect of the compression rate on the measured glass EOS is also considered. Its effect on the pressure in a compression protocol is effectively negligible as one can see in the inset of figure 6.2. This is to be expected as the relaxation time within the state τ_β is expected to be very small as long as $\varphi < \varphi_G$.

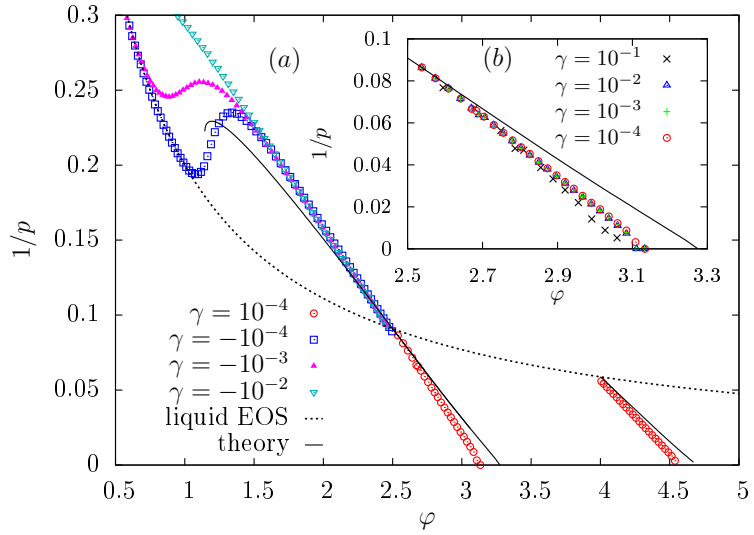

Figure 6.2. Equations of state of a glass planted art $\varphi_0 = 2.5$, ($\widehat{\varphi}_g = 6.667$ in $\infty - d$ units), and $\varphi_0 = 4$. Hopping effects are negligible in both cases. The lines are theory and the dots are simulation data as described in [4]. (*Inset*) though a larger compression rate smooths away the singular behavior at the onset point, its effects on the pressure in a compression protocol are effectively negligible as long as $\varphi < \varphi_G$.

Dynamics

A non-trivial and rich aging phenomenology manifests in the fRSB phase [258]. To better explore the complex free-energy landscape structure that is associated with the fRSB ansatz, it is convenient to define two instantaneous quantities. The first is the MSD between configurations at different times

$$\hat{\Delta}(t, t_w) \equiv \frac{1}{N} \sum_{i=1}^{N} |\boldsymbol{r}_i(t + t_w) - \boldsymbol{r}_i(t_w)|^2, \tag{6.6}$$

where the waiting time is the time elapsed since the end of the compression protocol, as in section 2.1. The second is the MSD between two different "cloned" configurations A and B

$$\hat{\Delta}_{AB}(t) \equiv \frac{1}{N} \sum_{i=1}^{N} |\boldsymbol{r}_i^A(t) - \boldsymbol{r}_i^B(t)|^2. \tag{6.7}$$

The "cloning" procedure works as follows: before the compression starts, an equilibrated planted configuration is duplicated ($\{\boldsymbol{r}_A(0)\} = \{\boldsymbol{r}_B(0)\}$), but each of the two instances is given a different set of initial velocities, randomly drawn from the Maxwell distribution. The two configurations are then compressed independently. This way, A and B will evolve inside the same glass metabasin (which as we recall from section 3.2 is selected by a single equilibrated configuration) but will have independent compression histories. They will thus serve as a probe of the metabasin structure, in the same fashion as the replicas discussed in section 5.1.1.
These instantaneous quantities are to be averaged over the statistical ensemble of samples:

$$\Delta(t,t_w) \equiv \overline{\left\langle \hat{\Delta}(t,t_w) \right\rangle} \qquad \Delta_{AB}(t) \equiv \overline{\left\langle \hat{\Delta}_{AB}(t) \right\rangle}. \tag{6.8}$$

The number of samples varies from $N_s = 500$ to $N_s = 15000$ depending on the statistical convergence properties of the observable under consideration. It is also convenient to define a quantity

$$\delta\Delta(t,t_w) \equiv \Delta_{AB}(t+t_w) - \Delta(t,t_w). \tag{6.9}$$

If the system is in restricted equilibrium (and so t_w is large enough) in the RS phase above the Gardner transition, we have basically the same caging picture of figure 1.4

$$\lim_{t\to\infty} \Delta(t) = \Delta, \tag{6.10}$$

where Δ is the Debye-Waller factor computed in chapter 4. The only difference is that in this case we are looking at the MSD inside the glass (as opposed to the supercooled liquid), and so we are unable to see the diffusive regime as in figure 1.4. Accordingly, since the system is able to explore ergodically the glass basin, one will have

$$\lim_{t\to\infty} \Delta_{AB}(t) = \Delta, \tag{6.11}$$

and as a result of this

$$\lim_{t\to\infty} \lim_{t_w\to\infty} \delta\Delta(t,t_w) = 0. \tag{6.12}$$

The picture changes in the fRSB phase $\varphi \gtrsim \varphi_G$, wherein aging manifests and equilibrium within the metabasin is out of computational reach (the time τ_{meta} needed to achieve restricted equilibration is expected to scale as $\exp(N^{1/3})$ [263], well beyond the length of simulations considered in [4]). In this case, the system will initially equilibrate in one microstate at the bottom of the fRSB hierarchy, so the MSD $\Delta(t,t_w)$ will reach a short plateau, $\Delta(t,t_w=0) = \Delta_{EA}$ for $t \ll \tau_{meta}(t_w)$ and $t > \tau_0$, where τ_0 is the typical timescale for the ballistic regime. Thereafter, the system will start to explore the fRSB hierarchy, visiting higher and higher levels of it and hopping over larger and larger free energy barriers. Since the hierarchy of sub-states is fractal ($k = \infty$), the system will continuously surmount barriers until equilibration is reached (*continuous aging*) instead of attaining it in a simple step-like manner as it would with a finite number of RSBs (section 1.1.3). As a consequence of this, $\Delta(t,t_w)$ will drift upwards for all observable times after leaving the initial plateau corresponding to Δ_{EA}.
For what concerns $\Delta_{AB}(t)$, the two copies have different compression histories, as we

already mentioned; this means that they will usually end up in different microstates, and so the long-time limit of $\Delta_{AB}(t)$ will correspond to the average distance $\langle\Delta\rangle$ between microstates. This means that in the Gardner phase

$$\lim_{t\to\infty}\lim_{t_w\to\infty}\delta\Delta(t,t_w)\neq 0, \tag{6.13}$$

which provides a dynamical order parameter for the Gardner transition. Notice that in general $\Delta_{AB}(t+t_w)>\Delta(t,t_w)$ for every t. However, since equilibration is never reached $\Delta_{AB}(t)$ as well slowly drifts (the drift can be observed for every simulation time) without ever reaching a plateau. In figure 6.3 we report the results obtained, which follow the basic phenomenology described above.

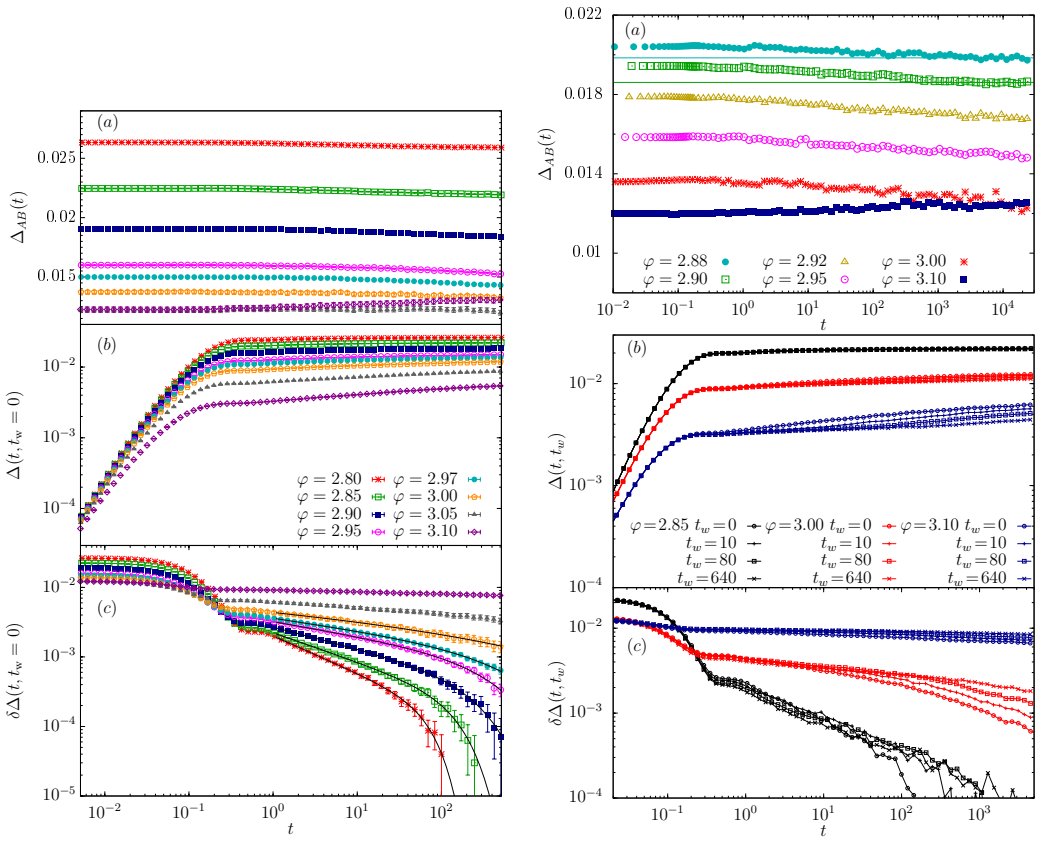

Figure 6.3. Dynamics in a glassy state planted at $\widehat{\varphi}_g=6.667$, for densities in the vicinity of the Gardner transition, for $t_w=0$ (*left panel*) and $t_w\neq 0$ and large times (*right panel*). When $\varphi<\varphi_G$ (here $\varphi_G\simeq 3.0$ as reported in the following), the MSDs $\Delta(t,t_w)$ and $\Delta_{AB}(t)$ rapidly attain their equilibrium value ($\Delta_{AB}(t)$ is effectively independent of time), $\delta\Delta(t,t_w)$ decays to zero at long times and no dependence on t_w is observed: the system is in restricted equilibrium (solid lines are fits to equation (6.15)). When $\varphi\gtrsim\varphi_G$, the MSDs drift for all observable times without ever attaining a plateau value, and $\delta\Delta(t,t_w)$ remains positive; a marked dependence on t_w is observed, especially for high density: the system is continuously aging inside the glassy metabasin, signature of a Gardner phase. Notice how the relaxation time $\tau_{meta}(t_w)$ grows with t_w, another typical signature of aging (fig. 2.1).

From this picture, it transpires that if one chooses t_s such that $\tau_0 < t_s \ll \tau_{meta}$, then $\Delta(t_s, t_w = 0)$ can be used as an estimator for Δ_{EA} and $\Delta_{AB}(t_s)$ for Δ_1, and then one can compare the so obtained results with the theoretical prediction for the bifurcation of MSDs presented in figure 5.3. In particular, one can verify if $\Delta(0)$ increases after φ_G as predicted. In figure 6.4 we report the results so obtained, with again a satisfactory agreement between theory and simulation.

Besides this, it certainly would be appropriate to get also a check of the behavior

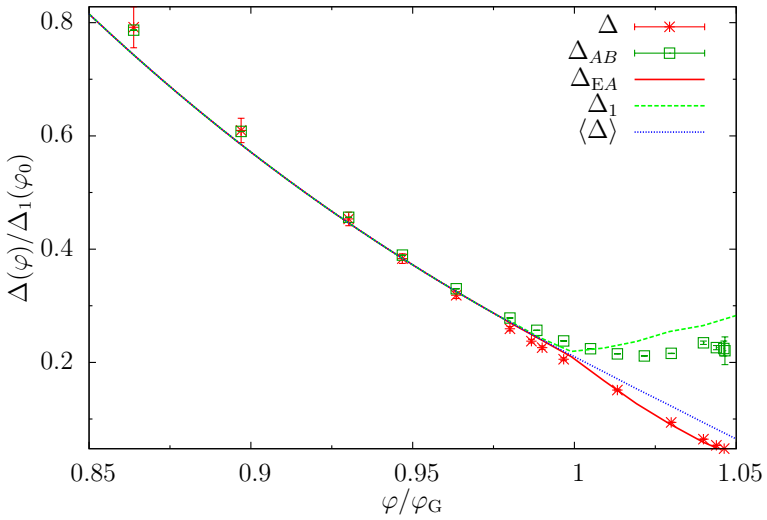

Figure 6.4. MSDs for the glass around the Gardner point for $\widehat{\varphi}_g = 6.667$. The lines are theory and the dots are simulation data as described in [4]. $\Delta_1 \equiv \Delta(0)$ in the notation of [4]. Both the theoretical and the numerical datasets have been rescaled with their value $\Delta(\varphi_0)$ on the equilibrium line.

in shear, figure 5.5, and in particular the decreasing of Δ_{EA} when $\gamma > \gamma_G$. We leave the issue for future work.

Locating the Gardner point

Apart from the check of the equations of state and dynamics of MSDs, the numerics of [4] are also able to robustly locate the Gardner points for various planting densities φ_0 and to verify that their position on the glass EOSs is compatible with the theoretical prediction in figure 4.4. Three different methods are used, here we just give the basic picture and refer to [4] for details.

The first focuses on dynamics above the Gardner point, in particular the power-law divergence of the relaxation time due to critical slowing down, paragraph 5.2.2. Besides the qualitative picture of the dynamics exposed in the preceding paragraph, one can also try a more quantitative analysis following the lines of the classic work [258] of Ogielski on spin glasses and the theoretical scheme for glassy dynamics developed in [264]. The basic idea is to extract the relaxation timescale τ_β from the decay of the $\delta\Delta(t, t_w)$ on approaching the Gardner transition from above. Since this timescale diverges as a power law in the distance $\delta\varphi \equiv |\varphi - \varphi_G|$ from the transition

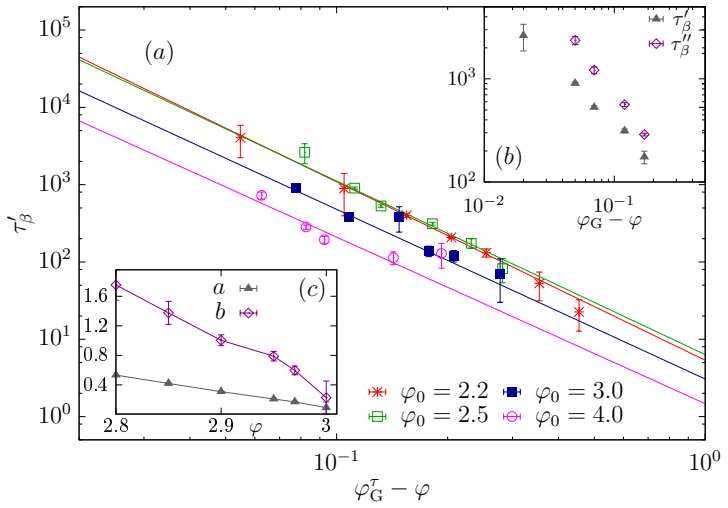

Figure 6.5. (a) Growth of τ'_β with $\delta\varphi$ for various planting densities φ_0. (b) The two estimates τ'_β e τ''_β as a function of $\delta\varphi$ for $\varphi_0 = 2.5$; both exhibit the same power-law scaling. (c) Evolution of the fitted a and b exponents with φ, again for $\varphi_0 = 2.5$.

as a consequence of critical slowing down, it can be used to locate the Gardner point φ_G as shown in the following. Notice that this scheme is then well defined only in the RS phase. According to the theory developed in [264], upon approaching the Gardner point from above while in restricted equilibrium in the RS phase, one must have

$$\delta\Delta(t) \simeq \delta\varphi \mathcal{F}(t/\tau_\beta), \qquad \tau_\beta \simeq \delta\varphi^{-\gamma}, \tag{6.14}$$

where $\mathcal{F}(x)$ is a function such that $\mathcal{F}(x \ll 1) \simeq x^{-a}$ while $\mathcal{F}(x \gg 1)$ decays exponentially, and the exponents a and $\gamma = 1/a$ are those defined in paragraph 5.2.2; notice how $\delta\Delta(t)$ does not depend on t_w here, as we are in the RS phase where aging is not present.
We can estimate τ_β by choosing the empirical form [258] $\mathcal{F}(x) \propto x^{-a} e^{-x^b}$, which means fitting $\delta\Delta(t, t_w = 0)$ to the form

$$\delta\Delta(t, t_w = 0) = c \frac{\exp[-(t/\tau'_\beta)^b]}{t^a}, \tag{6.15}$$

where all parameters will depend on φ and $\varphi_0 \equiv d/2^d \widehat{\varphi}_g$, and τ'_β offers a first estimate of τ_β. We fit the exponent a instead of fixing its value to the analytical prediction reported in table 5.1, since the value of a away from the transition is quite different from the critical value, as one can appreciate by looking at the linear part of the plots in the lower left panel of figure 6.3.
The relaxation time τ_β is then expected to scale as

$$\tau_\beta \propto |\varphi - \varphi_G^\tau|^{-\gamma},$$

which gives a first estimate of φ_G. This time, we fix the value of γ to the analytic prediction and we fit φ_G^τ to get a first estimate of the transition point (see figure 6.5

for the results). To get a better check on our result, we also estimate τ_β through the logarithmic decay of the $\delta\Delta(t)$ at long times (see figure 6.6):

$$\delta\Delta(t, t_w = 0) = k\left[1 - \frac{\ln(t)}{\ln(\tau''_\beta)}\right], \tag{6.16}$$

where in this case we fit τ''_β and k. From inset (b) in figure 6.5, one can see how the growth of both estimators τ'_β and τ''_β is compatible with the same power-law scaling, which supports our claim that the slowing down is a manifestation of an underlying second-order transition.

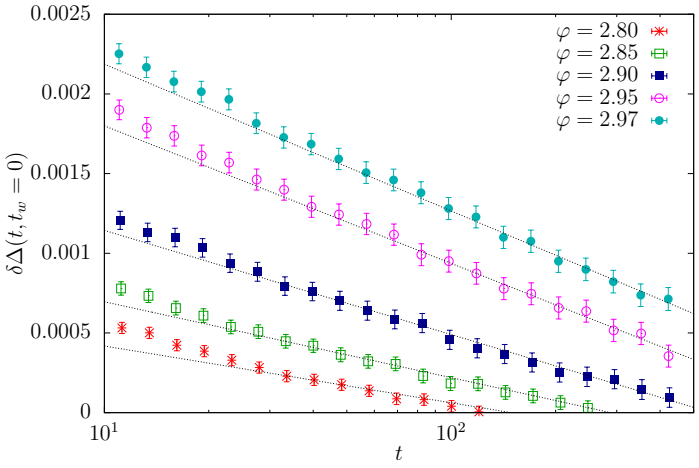

Figure 6.6. Logarithmic decay of $\delta\Delta(t, t_w = 0)$ for $\varphi_0 = 2.5$. The data are fitted to equation (6.16).

The second method focuses on static properties below the Gardner point. Let us suppose to prepare two initial configurations for the simulation, each of them identified by a $2Nd$-dimensional position-velocity couple $(\boldsymbol{r}, \boldsymbol{v})$. The configuration of the $\boldsymbol{r}$ is obtained though the planting method and is the same for both, while the velocities are extracted at random from the Maxwell distribution. This procedure defines two *clones* of the same initial configuration. One can then define a MSD between clones

$$\hat{\Delta}_{AB}(t) = \frac{1}{N}\sum_{i=1}^{N}\left|\boldsymbol{r}_i^A(t) - \boldsymbol{r}_i^B(t)\right|^2. \tag{6.17}$$

Since in the fRSB phase the glass state breaks up in a fractal hierarchy of sub-states, usually the two replicas will not end up in the same state. One can measure the long-time limit of $\Delta_{AB}(t)$ and construct an histogram $P(\Delta_{AB})$ which will describe the structure of the glass metabasin. Proven that finite-size effects are accounted for [4], the two replicas sample the Parisi probability distribution $P(\Delta)$ [250]. One can than prove that its variance χ_{AB} obeys

$$\chi_{AB} \equiv N\frac{\overline{\langle\Delta_{AB}^2\rangle} - \overline{\langle\Delta_{AB}\rangle}^2}{\overline{\langle\Delta_{AB}^2\rangle}^2} = \frac{\langle\Delta_{ab}^2\rangle - \langle\Delta_{ab}\rangle^2}{\langle\Delta_{ab}\rangle^2} = \frac{\chi_4}{\Delta^2}. \tag{6.18}$$

We recall that the divergent part of the χ_4 susceptibility is the $\chi_4^{div} = \frac{24}{\lambda^R}$ computed in paragraph 5.2.3. Thus, the numerical χ_{AB} is supposed to diverge as $\chi_{AB} \simeq (\varphi_G - \varphi_G^\chi)^{-1}$ since the replicon vanishes linearly at the Gardner point (see figure 4.3). This provides another estimator for φ_G, and also a way to measure the critical χ_4 susceptibility (see figure 6.7).

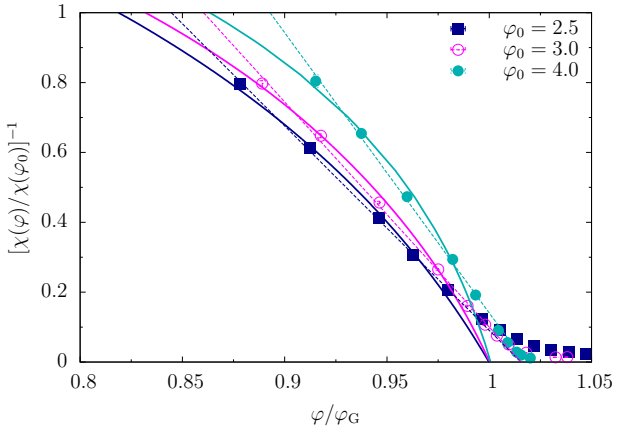

Figure 6.7. The critical susceptibility χ_4 near the Gardner point for three different planting densities. Lines are the theoretical prediction while the symbols are numerical data. $\varphi_0 \equiv d/2^d\widehat{\varphi}_g$ in the notation of [4].

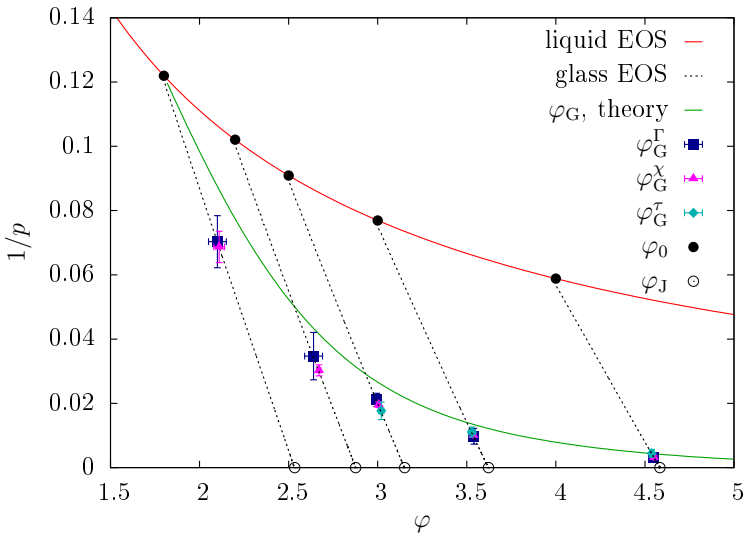

Figure 6.8. The Gardner transition points located with the three different estimators φ_G^τ, φ_G^χ and φ_G^Γ. The numerical estimate is robust and consistent with the theoretical prediction reported in chapter 4.

The third method uses again the $P(\Delta_{AB})$, but focuses on another parameter,

its *skewness* Γ whose definition is

$$\Gamma \equiv \frac{\overline{\left\langle (\Delta_{AB} - \overline{\langle \Delta_{AB} \rangle})^3 \right\rangle}}{\overline{\left\langle (\Delta_{AB} - \overline{\langle \Delta_{AB} \rangle})^2 \right\rangle}^{3/2}}, \tag{6.19}$$

this quantity is supposed to be maximal at the Gardner point, so one can get another estimate φ_G^{Γ}.

In figure 6.8 we finally report the results for the Gardner point obtained with these three estimates. The reader can appreciate how all three estimates give compatible values for different planting densities φ_0, and how those are compatible with the Gardner line reported in figure 4.4. Only the estimate for the $\varphi_0 = \varphi_{MCT}$ is off (although anyway very robust), which can be attributed to the hopping effects which show up prominently near φ_{MCT} and may spoil the numerical result.

In summary, the prediction of a Gardner transition in HS under compression [1, 41, 156] is validated at least for a MF glass former, in this case the infinite range MK model. Work is ongoing in this moment to prove its existence also for ordinary HSs in finite d, and a study in the same spirit for HS under shear will be the logical continuation of the research effort started in [3, 4].

Chapter 7

Conclusions

In this final chapter, we summarize our main results and predictions and give an assessment of the strengths and weaknesses of the state following construction, and RFOT as a whole. Finally, we conclude the thesis with some perspectives and proposals on further research inspired by the present work.

7.1 Summary of main predictions

Our state following approach is able to provide many interesting predictions which fit well within the phenomenology of glasses explored in the first two chapters. These include:

1. The basic phenomenology of the calorimetric glass transition (paragraph 1.1.1), with a jump in heat capacity (or equivalently, compressibility), is captured by out approach.

2. We are able to compute from first principles the equation of state of a generic glass prepared with a generic annealing protocol (paragraph 2.1), reproducing the basic phenomenology of glasses as observed in DSC experiments (paragraph 2.1.2), in particular those on ultrastable glasses [129–133]. We are able to observe hysteresis in agreement with the results of [7, 129, 130], and the onset transition whereupon the glass melts back into the liquid at high temperature is well reproduced.

3. The Gardner transition detected in [41, 156] is recovered within the state following approach, along with the results concerning the isostaticity and marginality of jammed packings and the critical exponents of the jamming transition (paragraph 2.1.3). We are also able to compute the jamming density φ_j for generic disordered packing constructed with an annealing-like (i.e. reasonably slow) procedure [140, 141].

4. We are able to compute from first principles stress-strain curves of the glass and obtain again a phenomenology in agreement with simulations and experiments (paragraph 2.2); our approach reproduces the presence of a stress overshoot [172, 184–186] and a yielding point (paragraph 2.2.2) whereupon the glassy state dies and the glass former starts to flow [172, 182]. We are able

to compute the Debye-Waller factor, the shear modulus [8] and the dilatancy [187, 188] everywhere in the glass phase.

These results indicate that the state following approach is at least a good starting point for a first principles theory of glasses prepared via slow coolings.

In addition to this, we can also provide some novel predictions which make for a good test bed of the theory and may allow one to validate/falsify it through simulations and experiments:

1. We detect the presence of a Gardner transition for high enough values γ_G of the strain perturbation (section 4.3.3), for *every* preparation density $\widehat{\varphi}_g$. From the practical point of view, this means that the response of a glass to the strain is elastic and solid-like only up to γ_G. Afterwards, the fRSB structure manifests within the state and the system will start to jump from a microstate to the other in a non-equilibrium fashion, producing a rough response with avalanches like the one that can be seen in figure 2.10 for athermal materials. In summary, we argue that an avalanche-dominated regime with energy dissipation is *bound to appear*, for high enough strains, also in thermal systems, no matter which their preparation temperature is. In this regime, as one can see from figure 5.5 the Debye-Waller factor Δ_{EA} decreases and consequently the $\mu(1)$ shear modulus (which is the slope of the small elastic segments between avalanches) increases. All of these are novel predictions that should be easily verifiable.

2. We predict the insurgence, in the Gardner phase, of a set $\mu(x)$ of shear moduli (paragraph 5.2.4), with a scaling relation $\mu(0) - \mu(1) \propto (\widehat{\varphi} - \widehat{\varphi}_G)$. It can be argued that the $\mu(1)$ modulus corresponds to the average slope of a stress strain curve, while the $\mu(0)$ corresponds to the slope of small elastic segments like in figure 2.11. This is true both for athermal systems (which are already in the Gardner phase when shear is applied) and thermal ones beyond the Gardner point induced by the strain itself.

3. We compute critical slowing down exponents and critical fluctuations around the Gardner Point for various preparation densities $\widehat{\varphi}_g$. A first encouraging test of these results can be found in [4], for the MK model discussed in the preceding chapter.

7.2 Strengths and weaknesses of our approach

The state following theory presented in this thesis has some very appealing traits. First of all, it allows one to perform theoretical physics calculations on glasses using only tools of standard statistical mechanics, like partition functions, free energies, large deviations and saddle-point methods, etc., and only requires, as an input, a microscopic interaction potential. In addition to this, it is also completely static in nature, which is a very welcome feature considering that the established theory for the first principle dynamics of glass formers has been, up to very recently, the Mode Coupling theory, whose flaws and weaknesses (especially in the low-temperature/high density regime) are well known. There is no need to employ

dynamics, or phenomenological arguments, or parameter tunings of any sort. The state following construction brings everything back to the definition of a suitable Gibbs measure for the statistical-mechanical study of metastable, out of equilibrium glassy states. In summary, it cleverly exploits the basic picture of RFOT to bring back the problem of describing out of equilibrium glass to an equilibrium formalism. And despite these aspects of theoretical "cleanliness", it still provides predictions in remarkable agreement with the phenomenology of glasses.

However, it also has some weaknesses, both technical and conceptual. On a conceptual level, the SF construction always assumes restricted equilibration of the glass former within a glassy state. As a result of this, is only able to provide predictions in regimes where such equilibration is effectively attained, i.e. when perturbations are *adiabatically* applied to the glass.
However, the experimental literature on glasses (see [7, 23] and references therein) is teeming with experiments and protocols which do not meet this requirement. This is particularly evident in the case of driven dynamics, wherein time dependent shear protocols are pretty much the norm. A steady shear rate $\dot{\gamma} = const$ must be employed for the determination of the flow curve, and oscillatory shear protocols are used for the determination of the storage and loss moduli $G'(\omega)$ and $G''(\omega)$ [8, 177]; in both these cases, the perturbation changes with time and is not applied adiabatically.
Also in the case of simple aging, one could for example consider applying AC currents to measure dielectric relaxation spectra as done for example in [265, 266]. All such situations cannot be described within the state following setting.
The main technical difficulty lies in the fact that the state following approach is quite heavy from the computational point of view (the size of the appendix is probably a giveaway on this point), already at two-replica level; performing calculations with the replica chain, for example, looks feasible only for the simplest spin glass models like the PSM. This is part of the reason why we had to focus on the mean-field limit $d \to \infty$; just by looking at the expression (3.17) of the Franz-Parisi potential one can understand how going beyond the MF calculation is a hard and perhaps impossible task; some proposals on how to do so are formulated in [1, 153], but there is no systematic perturbation scheme and it is very difficult to understand how big of an error one is committing in considering these approximations. This weakness is however shared also by other sectors of theoretical physics wherein a small perturbation parameter is difficult to identify [267].

7.2.1 The current status of RFOT

However, the reliance of RFOT on MF concepts is not only a technical, but also a conceptual problem. The RFOT is clearly an impressive piece of theoretical physics: it provides an elegant and easy to grasp picture of the glassy slowdown, and is able to make very different observations and theoretical inputs (in some cases produced by completely unrelated scientific communities, such as MCT [40] and spin glass theory [57]) fit together in a coherent way. It also comes with a set of tools, in the form of the replica method, for performing first principles calculations [45, 94] (a trait which is not shared by other approaches such as Dynamical Facilitation Theory and Frustration Limited Domains), and it has proven to be able to provide

quantitative predictions for problems which were, originally, outside of the domain wherein it was initially conceived, such as the jamming problem [42–44].

Despite these many strengths, RFOT is still struggling to break out of the mean-field domain wherein it originally appeared; as a matter of fact, much of the research work that is produced today by the RFOT community is aimed at understanding non-MF effects, and the strongest criticisms which are today moved to RFOT are centered around the claim that the theory cannot be valid beyond mean-field. Indeed, for much time there were no finite dimensional models wherein the RFOT picture could apply (the very first proposal for such a model is very recent [268]), a difficulty which is shared by the replica theory of spin glasses; in both cases, the existence beyond mean field of replica symmetry breaking, and the Parisi picture that comes with it, is still a matter of intense debate and simulations performed on finite-dimensional models are not conclusive. This MF-bound character of RFOT can be also found in the scenario where RFOT works best, namely the jamming problem. In [147], it is shown how the RFOT computation of [156] fails to account for localized excitations within packings, and as a result of this, localized excitations must be numerically removed in order to recover from simulations the predicted value of the exponent θ of the force distribution. This incapacity of taking into account localized excitations is very much to be expected from a MF theory. However, while in the case of jamming it is possible to disentagle localized and extended modes, this does not look easy in the case of yielding, whereupon the relevant modes really seem to be localized ones [200].

On a more technical side, importing non-MF effects within RFOT also amounts to understanding how the physics of the MCT and Gardner transitions are modified in finite dimension. In the case of MCT, it is still not very clear what is the actual mechanism that transforms the transition into a crossover; while there is consensus on the viewpoint that MCT is a MF-like theory [68, 257] unable to take into account activation mechanisms, there are indications that activation may be already at play in the regime above T_{MCT} [23, 106, 193]. Some attempts have been made to include activation effects within MCT, but their results are subject of debate, see for example [269]. It is even argued in [87] that the MCT transition is destroyed by critical fluctuations instead of activation, so the problem is still very much open. For what concerns the Gardner transition, its presence in finite dimensional systems is still to be proven. Since it is a second order critical point, a renormalization group study of the transition must be performed to understand how and if its physics changes in finite dimension. Such an attempt has been made in [270] using perturbative tools, but the results are quite odd. The upper critical dimension d_u, for example, appears to be model dependent; the only conclusive statement one can make is that if the Gardner transition survives, a perturbative RG approach is unable to predict this fact, requiring the use of non-perturbative RG tools. In any case, a solution to all these problems does not seem to be forthcoming.

7.3 Proposals for further research

We conclude the chapter with some proposals for further research on the field of glass physics. The reader will surely notice how they are all somewhat relative to

the yielding transition and related problems.

7.3.1 The Gardner transition in shear

The most novel prediction produced by the present work is the existence of a Gardner transition in shear strain. As we mentioned, this Gardner transition is related to the onset of energy dissipation within the system for large enough strain.
A possible way to test this prediction is the following. First of all, glassy configurations equilibrated at low temperature must be prepared, using for example the algorithms of [130] or [271]. Then a cycling shear strain protocol, like the one of [197], must be applied, for example implementing it with an affine transformation on particle coordinates like in [203]. The strain should be applied in small steps in such a way that the liquid is able to equilibrate at each step, i.e. one should always have $\dot{\gamma} < 1/\tau_\beta$. This condition should be easy to satisfy since τ_β is very low.
As soon as the amplitude of the cycle exceeds γ_G, the Gardner transition is met and energy starts to be dissipated, producing a closed hysteresis curve with nonzero surface like in [197]. The presence or not of a stress overshoot (which, if one believes figure 4.8, appears only within the Gardner phase) can be used to discriminate the Gardner transition from the yielding transition that happens at $\gamma_Y > \gamma_G$.
The behavior of the $\mu(1) = 1/\Delta_{EA}$ shear modulus can also be studied easily: if the prediction of figure 5.5 is true, the slope of the small elastic segments between avalanches is supposed to increase as γ_Y is approached. One could also measure the Debye-Waller factor (Δ for $\gamma < \gamma_G$, Δ_{EA} for $\gamma > \gamma_G$) in the whole glass phase in order to get a double check both on the numerics and the theory, and verify that it has a maximum for $\gamma = \gamma_G$ as reported in figure 5.5.

7.3.2 State following in AQS protocols

The protocols we reproduce in figure 4.8 are thermal protocols wherein a glass former is "annealed" down to a density $\widehat{\varphi}_g$ and then strain is applied. However, most literature on the subject considers Athermal Quasi Static protocols as detailed in paragraph 2.2.1. Since such a protocols are anyway quasi-static, they can be described within the state following setting. There are two possible ways to do this: one can either choose $m = 0$ in the expression (4.2) and then follow the state in γ (instantaneous quench to $T = 0$ followed by strain), or one can keep $m = 1$, compress a state all the way to φ_j and then follow it in strain (slow annealing to $T = 0$ followed by strain). This way, AQS stress-strain curves should be obtained. However, we must again stress that the SF approach looks at equilibrium within the glassy metabasin, so the stress strain curves will again be smooth curves corresponding to the average of many shear histories like the ones in figure 2.11, and no stress drops (avalanches) will be observed.

7.3.3 Avalanches

It is however possible to study avalanches. Within the fRSB approach, avalanches correspond to the rearrangement modes that take place when the system crosses over from a microstate to another. In spin glasses, one has a similar phenomenon with the hysteresis curve of magnetization M versus magnetic field H, that exhibits

an intermittent response (Barkhausen noise) much like the avalanche response seen in AQS protocols (see for example [272] for a study in stressed athermal packings). The statistics of these magnetization drops in the SK model has been extensively studied in [273, 274]. Their probability distribution has been found to have a power-law behavior

$$\rho(\Delta M) \propto \Delta M^{-\tau},$$

where the exponent τ has been computed in [273] ($\tau = 1$). A similar power law behavior is observed for avalanches in jammed packings [272] under stress control (γ vs. σ) with an exponent $\tau \simeq 1.46$, so one would like to compute again the exponent in the case of hard spheres.
The calculation of [273] can in principle be "translated" from spin glasses to hard spheres. In [273] the starting point of the calculation is the computation of the cumulants of the magnetization in different fields

$$\overline{\langle m_{h_1} m_{h_2} \dots m_{h_p} \rangle}^c \tag{7.1}$$

where $\overline{\bullet}$ denotes an average over the quenched disorder. In the case of HSs, one should consider the cumulants of the stress in different strains

$$\overline{\langle \sigma_{\gamma_1} \sigma_{\gamma_2} \dots \sigma_{\gamma_p} \rangle}^c, \tag{7.2}$$

where now the average over the "disorder" is the average over the configuration R as defined in the (3.17). The first step for performing the calculation is certainly understanding how the relevant quantities scale; in the case of the SK model it is known that the magnetic field should scale like $H = \frac{h}{\sqrt{N}}$ [273] for a magnetization drop of order $\sqrt{N}$ to happen. In the case of strain, it may be that the relevant scaling is $\gamma \simeq N^{\beta_{iso}}$, with $\beta_{iso} \simeq -0.62$ as reported in [195].
In any case, the study of [273, 274] is valid at zero temperature in the SK model and a scaling solution of the fRSB equations is needed to perform the calculation, so the computation in the case of spheres can be only made for the jammed, athermal case. An eventual extension to the case of yielding beyond γ_Y, wherein a scaling regime is not even guaranteed to exists, does not seem like an easy task.

7.3.4 Yielding

The picture that emerges from this work for what concerns the yielding transition is that of a spinodal point, akin the the onset transition found in decompression/heating (paragraph 2.1.2). Having a spinodal point within a replica theory means having a zero *longitudinal* mode in the Hessian matrix of the replica free energy $s[\hat{\alpha}]$ as discusses in section 4.2.1; intuitively, one should consider the longitudinal mode of the outermost block of the fRSB ansatz. A computation of the longitudinal mode of the fRSB solution of state following should probably be performed in order to better understand yielding.
The analogy between yielding and a spinodal point has led some authors to proposing a picture of yielding as a phenomenon akin to an inverse glass transition by raising the temperature (essentially, an onset transition), a point of view strongly criticized in [194]. While it is true, at least for what concerns this work, that the

yielding transition is a spinodal point, there is a big difference between it and the onset point: the onset transition *always* takes place at a temperature $T_{on} > T_{MCT}$ (see also figure 4.4), which means that when the glass former is kicked out of the state, the only thing it finds outside is a trivial FEL and an equilibrium measure dominated by the ergodic liquid. This need not be true in the case of yielding, which can take place at temperatures below T_{MCT}; this means that the system, when is kicked out the state because of strain, may still have a rough FEL to move in and may even end up in a different glassy state.
Understanding where the systems ends up after the spinodal point is an obvious question whose answer is related to the description of the steady flow regime beyond yielding. The bare-to-the-bone problem is essentially answering the question "Which is the thermodynamic state an RFOT system, with $T < T_d$, end up in when the glassy state it finds itself in is killed by an external perturbation? For example, is it another glassy state, or a liquid-like state?". Such a question could be in principle answered by numerical simulations of simple RFOT models such as the PSM [66], using a magnetic field to induce a spinodal point.

7.3.5 Non-linear rheology

We have mentioned how the state following construction is unable to reproduce time dependent shear protocols $\dot{\gamma}(t)$; the replica chain discussed in section 3.3 may provide a solution for this problem, at least if certain conditions are met. The idea is to consider a chain of replicas, all of them at the same temperature T_g, and apply upon each replica a shear strain in the following way

$$\gamma_a = \sum_{c<a} \delta\gamma, \tag{7.3}$$

in summary, we apply the strain progressively with a small increment $\delta\gamma$ on each replica, $\gamma_{a+1} - \gamma_a = \delta\gamma$. Such a construction can in principle be implemented for MF hard spheres using the expression (4.9) of the replicated entropy and implementing shear through the (B.15). If one is able to successfully perform the infinite-bond limit of the chain, a constitutive equation [8] for HS glasses prepared at $\widehat{\varphi}_g$ should in principle be obtained. It is very interesting to notice that since the temperature is constant, the chain will automatically yield a TTI dynamics when this construction is performed, in agreement with the phenomenon of rejuvenation.
However, besides the obvious technical difficulties, there is a big conceptual limit: pseudodynamics with the replica chain assumes quasi-equilibration, and as a result of this all details of the fast relaxation in the β-regime are hopelessly lost. Only the slow part of the dynamics is accounted for, as detailed in [242, 243].
It is therefore necessary to understand how much the fast part of relaxation matters for the rheology of glassy materials, for example for the determination of the flow curve. Intuitively, in the case of oscillatory protocols, the construction should be meaningful as long as the frequency ω is chosen in such a way that

$$\omega < 1/\tau_\beta,$$

which is not a particularly restrictive condition, unless the temperature is very low.

Appendix A

The infinite-d solution of hard spheres

In this appendix we sketch the derivation of the replicated entropy (4.9) for hard spheres in the $d \to \infty$ limit. We only give the broad strokes, referring to [154] for further details.

The starting point is a density functional theory [18] in the form [45]

$$\mathcal{S}[\rho(\overline{\boldsymbol{x}})] = \int d\overline{\boldsymbol{x}} \rho(\overline{\boldsymbol{x}})[1 - \log \rho(\overline{\boldsymbol{x}})] + \frac{1}{2} \int d\overline{\boldsymbol{x}}\, d\overline{\boldsymbol{y}}\ \rho(\overline{\boldsymbol{x}}) f(\overline{\boldsymbol{x}} - \overline{\boldsymbol{y}}) \rho(\overline{\boldsymbol{y}}), \tag{A.1}$$

where $\overline{\boldsymbol{x}} \equiv (\boldsymbol{x}_1, \dots, \boldsymbol{x}_m)$ is a "molecular coordinate" that specifies the position of a molecule made of m spheres, and $f(\overline{\boldsymbol{x}})$ is a replicated Mayer function [153]. The replicated liquid of HSs is nothing but a molecular liquid wherein each molecule is made up of m replicas[1] of the same original sphere. The equilibrium density profile $\rho(\boldsymbol{x})$ is required to minimize the functional

$$\frac{\delta \mathcal{S}}{\delta \rho(\overline{\boldsymbol{x}})} = 0 \Longrightarrow \log \rho(\overline{\boldsymbol{x}}) = \int d\overline{\boldsymbol{y}} f(\overline{\boldsymbol{x}} - \overline{\boldsymbol{y}}) \rho(\overline{\boldsymbol{y}}) \tag{A.2}$$

as usual. Normally, this density functional would be given by a diagrammatic expansion [18] whose first term would be the second one in the (A.1), but for $d \to \infty$, only the first diagram survives [260], yielding the (A.1). The $\mathcal{S}$ is essentially the analogue, for HSs and in the continuum, of the TAP free energy [46].

Passing from the (A.1) to the (4.9) amounts to nothing more than a change of coordinates in the integrals, which is done by exploiting the inherent symmetries of the problem. First of all, the liquids is homogeneous, so it is invariant by translations. More specifically, if one defines

$$X \equiv \frac{1}{m} \sum_{a=1}^{m} \boldsymbol{x}_a \qquad\qquad u_a \equiv \boldsymbol{x}_a - X$$

which are the center of mass of a molecule and the displacement of atom a with respect to it, then the density profile $\rho(\overline{\boldsymbol{x}})$ can only depend on the u_a. We can

[1] Of course we can choose m as we please.

exploit this fact by changing coordinates

$$d\overline{\boldsymbol{x}} = dX\ d\overline{u}\ m^d \delta\left(\sum_{a=1}^{m} u_a\right) \equiv dX \mathcal{D}\overline{u}, \tag{A.3}$$

so that we can rewrite the (A.1) as

$$\mathcal{S}[\rho(\overline{\boldsymbol{x}})] = V \int \mathcal{D}\overline{u}\rho(\overline{u})[1 - \log\rho(\overline{u})] + \frac{V}{2}\int \mathcal{D}\overline{u}\ \mathcal{D}\overline{v}\ \rho(\overline{u})\overline{f}(\overline{u}-\overline{v})\rho(\overline{v}) \tag{A.4}$$

where

$$\overline{f}(\overline{u}-\overline{v}) \equiv \int dX\ f(\overline{u}-\overline{v}+X). \tag{A.5}$$

Secondly, the liquid is also isotropic, i.e. it is rotationally invariant. So, if one defines new coordinates

$$q_{ab} \equiv u_a \cdot u_b \qquad p_{ab} \equiv v_a \cdot v_b \qquad r_{ab} \equiv u_a \cdot v_b, \tag{A.6}$$

then the density profile can only depend on the matrix $\hat{q} = q_{ab}$. We can write

$$\frac{\mathcal{S}[\rho(\overline{\boldsymbol{x}})]}{V} = \int d\hat{q}J(\hat{q})\rho(\hat{q})[1-\log\rho(\hat{q})] + \frac{1}{2}\int d\hat{q}d\hat{p}d\hat{r}K(\hat{q},\hat{p},\hat{r})\rho(\hat{q})\rho(\hat{p})\overline{f}(\hat{q}+\hat{p}-\hat{r}-\hat{r}^T). \tag{A.7}$$

We can now see that the integration is not anymore on md variables, but on $m(m-1)/2$ variables, all just by exploiting the symmetries of the problem. To proceed with the calculation, one must then compute the Jacobians J and K. For the Jacobian J, for example, one has

$$\begin{aligned} J(\hat{q}) &= \int \mathcal{D}\overline{u} \prod_{a\leq b}^{m} \delta(q_{ab} - u_a \cdot u_b), \\ &= m^d \int d\overline{u}\ \delta\left(\sum_{a=1}^{m} u_a\right) \prod_{a\leq b}^{m} \delta(q_{ab} - u_a \cdot u_b), \\ &= m^d \prod_{a=1}^{m} \delta\left(\sum_{b=1}^{m} q_{ab}\right) \int du_1 \dots du_{m-1} \prod_{a\leq b}^{m-1} \delta(q_{ab} - u_a \cdot u_b). \end{aligned} \tag{A.8}$$

Luckily, the last integral has been already computed. It is nothing but the Jacobian that one must compute to infer the probability distribution of a Wishart matrix $Q = U^\dagger U$ wherein U is a $M \times N$ matrix (whose probability distribution is known) with $M = d$ and $N = m - 1$; its value is just [275]

$$C_{m,d} \exp\left(\frac{d-m}{2} \log\det \hat{q}^{m,m}\right). \tag{A.9}$$

So the Jacobian is

$$J(\hat{q}) = m^d \prod_{a=1}^{m} \delta\left(\sum_{b=1}^{m} q_{ab}\right) C_{m,d} \exp\left(\frac{d-m}{2} \log\det \hat{q}^{m,m}\right), \tag{A.10}$$

where $C_{m,d}$ is a normalization constant (see [156, appendix A] for its computation); the calculation proceeds on similar lines for the Jacobian K. From this last equation

we can see that the integrand scales like e^d, so for $d \to \infty$ we can compute its value using the saddle point-method [86] on the three matrices $\hat{q}$, $\hat{p}$ and $\hat{r}$ as discussed in section 4.1.2. At the saddle point one finds [154]

$$\hat{q}_{ab} = \hat{p}_{ab} \qquad\qquad \hat{r}_{ab} = 0. \tag{A.11}$$

so that the entropy must be optimized only on the matrix $\hat{q}$. Afterwards, one defines

$$\hat{\alpha} \equiv \frac{d}{D_g}\hat{q}, \tag{A.12}$$

and after some more manipulations, one finally gets

$$\begin{aligned}\frac{\mathcal{S}[\rho(\boldsymbol{x})]}{N} = 1 - \log\rho + d\log(m) + \frac{(m-1)d}{2}\log(2\pi e D_g^2/d^2) \\ + \frac{d}{2}\log\det(\hat{\alpha}^{m,m}) - \frac{d}{2}\widehat{\varphi}_g\,\mathcal{F}\,(2\hat{\alpha})\ ,\end{aligned}$$

which is the (4.9). We stress again the fact that this derivation is completely exact, without any approximations.

Appendix B

Computation of the replicated entropy in the RS ansatz

B.1 Entropic term

We want to compute $\det \hat{\alpha}^{m+s,m+s}$, where we recall that $\hat{\alpha}^{a,a}$ is the matrix obtained from $\hat{\alpha}$ by deleting the a-th row and column, i.e. it is the (a,a)-cofactor of $\hat{\alpha}$. Being a Laplacian matrix, $\hat{\alpha}$ has a vanishing determinant. Also, the "Kirchhoff's matrix tree theorem" states that for Laplacian matrices, all the cofactors are equal, hence $\det \hat{\alpha}^{a,a}$ is independent of a. Therefore, if $\mathbf{1}$ is the identity in $m+s$ dimensions, we have

$$\det(\hat{\alpha}+\varepsilon\mathbf{1}) = \det\hat{\alpha}+\varepsilon\sum_{a=1}^{m+s}\det\hat{\alpha}^{a,a}+O(\varepsilon^2) \quad \Rightarrow \quad \det\hat{\alpha}^{a,a} = \lim_{\varepsilon\to 0}\frac{1}{\varepsilon(m+s)}\det(\hat{\alpha}+\varepsilon\mathbf{1})\,. \tag{B.1}$$

We then define $\hat{\beta}(\varepsilon) = \hat{\alpha}+\varepsilon\mathbf{1}$ and we note that

$$\hat{\beta}(\varepsilon) = \begin{pmatrix} A & B \\ B^T & D \end{pmatrix} \tag{B.2}$$

where A is a $m\times m$ matrix with components $A_{ab} = (\delta^g+\alpha^g+\varepsilon)\delta_{ab}-\alpha^g$, D is a $s\times s$ matrix with $D_{ab} = (\delta+\alpha+\varepsilon)\delta_{ab}-\alpha$, and B is a $m\times s$ matrix with $B_{ab}=\chi$.

We can use the following general formula

$$\det\hat{\beta}(\varepsilon) = (\det A)\det(D-B^TA^{-1}B)\,, \tag{B.3}$$

recalling that a $m\times m$ matrix $M_{ab} = M_1\delta_{ab}+M_2$ has determinant $\det M = M_1^{m-1}(M_1+mM_2)$ and its inverse is $M^{-1}_{ab} = (M^{-1})_1\delta_{ab}+(M^{-1})_2$ with

$$\begin{aligned}(M^{-1})_1 &= \frac{1}{M_1}\,,\\ (M^{-1})_2 &= -\frac{M_2}{M_1(M_1+mM_2)}\,.\end{aligned} \tag{B.4}$$

The matrix A^{-1} has this form, with

$$\begin{aligned}(A^{-1})_1 &= \frac{1}{\alpha^g + \delta^g + \varepsilon} \ , \\ (A^{-1})_2 &= \frac{\alpha^g}{(\alpha^g(1-m) + \delta^g + \varepsilon)(\alpha^g + \delta^g + \varepsilon)} \ , \\ \det A &= (\delta^g + \alpha^g + \varepsilon)^{m-1} \left(\delta^g + (1-m)\alpha^g + \varepsilon\right) \ .\end{aligned} \tag{B.5}$$

The matrix $\Omega = D - B^T A^{-1} B$ has the same form with

$$\begin{aligned}\Omega_1 &= \delta + \varepsilon + \alpha \ , \\ \Omega_2 &= -\alpha - \chi^2[m(A^{-1})_1 + m^2(A_2^{-1})] \ , \\ \det \Omega &= (\delta + \alpha + \varepsilon)^{s-1}\{\delta + \alpha(1-s) + \epsilon - s\chi^2[m(A^{-1})_1 + m^2(A_2^{-1})]\} \ .\end{aligned} \tag{B.6}$$

Using Eqs. (B.5), (B.6), (B.3) and (B.1), we obtain the final result

$$\det \hat{\alpha}^{(m+s,m+s)} = \chi(m\alpha^g + s\chi)^{m-1}(s\alpha + m\chi)^{s-1} \ . \tag{B.7}$$

By taking the logarithm and replacing the χ, α, α_g with Δ_g, Δ and Δ_f using the (4.12), we get the (4.13).

B.2 Interaction term

Here we compute the interaction function $\mathcal{F}(2\hat{\alpha})$. This function has been computed in [154], but only for $\eta = 0$ and $\gamma = 0$. Here we need to generalize the calculation to non-zero perturbations.

B.2.1 General expression of the replicated Mayer function

We follow closely the derivation of [154] which has been generalized in [215] to the presence of a strain. The replicated Mayer function is

$$\begin{aligned}\overline{f}(\bar{u}) &= \int dX \left\{ -1 + \prod_{a=1}^{m} \theta(|X + u_a| - D_g) \prod_{b=m+1}^{m+s} \theta(|S(\gamma)(X + u_b)| - D) \right\} \\ &= -\int dX \, \theta\left(\max_{a=1,m+s} \{D_a - |S(\gamma_a)(X + u_a)|\} \right) \ ,\end{aligned} \tag{B.8}$$

where we introduced $D_a = D_g(1 + \eta_a/d)$ with $\eta_a = \gamma_a = 0$ for $1 \leq a \leq m$, and $\eta_a = \eta$ and $\gamma_a = \gamma$ for $m+1 \leq a \leq m+s$.

The u_a are $m+s$ vectors in d dimensions and define a hyper-plane in the d-dimensional space. It is then reasonable to assume that this $(m+s)$-dimensional plane is orthogonal to the strain directions $\mu = 1, 2$ with probability going to 1 for $d \to \infty \gg m + s$. Hence, the vector X can be decomposed in a two dimensional vector $\{X_1, X_2\}$ parallel to the strain plane, a $(d - m - s - 2)$-component vector $X_\perp$, orthogonal to the plane $\mu = 1, 2$ and to the plane defined by u_a, and a $m + s$-component vector $X_\parallel$ parallel to that plane. Defining Ω_d as the d-dimensional solid

angle and recalling that $V_d = \Omega_d/d$, and following the same steps as in [154, Sec. 5], we have, calling $k = m + s$

$$\begin{aligned}
\overline{f}(\bar{u}) =& - \int dX_1 dX_2 \; d^k X_\parallel \; d^{d-k-2} X_\perp \\
& \times \theta\left(\max_a \{D_a^2 - (X_1 + \gamma_a X_2)^2 - X_2^2 - |X_\parallel + u_a|^2 - |X_\perp|^2\}\right) \\
=& - \Omega_{d-k-2} \int dX_1 dX_2 \; d^k X_\parallel \int_0^\infty dx \, x^{d-k-3} \\
& \times \theta\left(\max_a \{D_a^2 - x^2 - (X_1 + \gamma_a X_2)^2 - X_2^2 - |X_\parallel + u_a|^2\}\right) \\
=& - \Omega_{d-k-2} \int dX_1 dX_2 \; d^k X_\parallel \int_0^{\sqrt{\max_a \{D_a^2 - (X_1+\gamma_a X_2)^2 - X_2^2 - |X_\parallel + u_a|^2\}}} dx \, x^{d-k-3} \\
=& - V_{d-k-2} \int dX_1 dX_2 \; d^k X_\parallel \\
& \times \Theta_{d-k-2}\left(\max_a \{D_a^2 - (X_1 + \gamma_a X_2)^2 - X_2^2 - |X_\parallel + u_a|^2\}\right)
\end{aligned} \tag{B.9}$$

where we defined the function $\Theta_p(x) = x^{p/2}\theta(x)$.

It has been shown in [154] that the region where $\overline{f}(\bar{u})$ has a non-trivial dependence on the u_a is where $u_a \sim 1/\sqrt{d}$. Here we use D_g as the unit of length, hence we define $u_a = x_a D_g/\sqrt{d}$, $X_{1,2} = \zeta_{1,2} D_g/\sqrt{d}$ and $X_\parallel = \epsilon D_g/\sqrt{d}$. Using that $\lim_{n\to\infty} \Theta_n(1 + y/n) = e^{y/2}$, and that for large d and finite k we have $V_{d-k}/V_d \sim d^{k/2}/(2\pi)^{k/2}$, we have

$$\begin{aligned}
\overline{f}(\bar{u}) =& - \frac{V_{d-k-2}}{V_d} \frac{V_d D_g^d}{d^{(k+2)/2}} \int d\zeta_1 d\zeta_2 d^k\epsilon \\
& \times \Theta_{d-k-2}\left(1 - \frac{1}{d} \min_a \{-2\eta_a + (\zeta_1 + \gamma_a \zeta_2)^2 + \zeta_2^2 + |\epsilon + x_a|^2\}\right) \\
\sim& - V_d D_g^d \int \frac{d\zeta_1 d\zeta_2 d^k\epsilon}{(2\pi)^{(k+2)/2}} \, e^{-\frac{1}{2}\min_a \{-2\eta_a + (\zeta_1+\gamma_a\zeta_2)^2 + \zeta_2^2 + |\epsilon + x_a|^2\}} \\
\equiv& - V_d D_g^d \mathcal{F}(\bar{x}) \; ,
\end{aligned} \tag{B.10}$$

where the function $\mathcal{F}$ has been introduced following [154, 155].

We can then follow the same steps as in [155, Sec.V C] and in [215] to obtain

$$\begin{aligned}
\mathcal{F}(\bar{x}) =& \int \frac{d\zeta_1 d\zeta_2 d^k\epsilon}{(2\pi)^{(k+2)/2}} \, e^{-\frac{1}{2}\min_a \{-2\eta_a + (\zeta_1+\gamma_a\zeta_2)^2 + \zeta_2^2 + |\epsilon + x_a|^2\}} \\
=& \int \frac{d\zeta_1 d\zeta_2 d^k\epsilon}{(2\pi)^{(k+2)/2}} \lim_{n\to 0} \left(\sum_{a=1}^k e^{-\frac{1}{2n}[-2\eta_a + (\zeta_1+\gamma_a\zeta_2)^2 + \zeta_2^2 + |\epsilon + x_a|^2]}\right)^n \\
=& \lim_{n\to 0}{}^* \sum \int \frac{d\zeta_1 d\zeta_2 d^k\epsilon}{(2\pi)^{(k+2)/2}} e^{-\sum_a \frac{n_a}{2n}[-2\eta_a + (\zeta_1+\gamma_a\zeta_2)^2 + \zeta_2^2 + |\epsilon + x_a|^2]} \\
=& \lim_{n\to 0}{}^* \sum \; e^{\sum_{a=1}^k \frac{n_a}{n}\eta_a - \frac{1}{2}\sum_{a=1}^k \frac{n_a}{n}|x_a|^2 + \frac{1}{2}\sum_{a,b}^{1,k} \frac{n_a n_b}{n^2} x_a \cdot x_b} \int \frac{d\zeta_1 d\zeta_2}{2\pi} e^{-\sum_a \frac{n_a}{2n}[(\zeta_1+\gamma_a\zeta_2)^2 + \zeta_2^2]} \\
=& \lim_{n\to 0}{}^* \sum \; e^{\sum_{a=1}^k \frac{n_a}{n}\eta_a - \frac{1}{4}\sum_{a,b}^{1,k} \frac{n_a n_b}{n^2}(x_a - x_b)^2} \int \frac{d\zeta}{\sqrt{2\pi}} e^{-\frac{\zeta^2}{2}\left[1 + \frac{1}{2}\sum_{ab} \frac{n_a n_b}{n^2}(\gamma_a - \gamma_b)^2\right]} \; .
\end{aligned} \tag{B.11}$$

where

$$\sum^{*} \equiv \sum_{n_1,\ldots,n_k;\sum_{a=1}^{k} n_a = n} \frac{n!}{n_1!\ldots n_k!}. \tag{B.12}$$

We now introduce the matrix $\hat{\Delta}$ of mean square displacements between replicas

$$\Delta_{ab} = (x_a - x_b)^2 = \frac{d}{D_g^2}(u_a - u_b)^2 \ . \tag{B.13}$$

We should now recall that the Mayer function is evaluated in $\bar{u} - \bar{v}$, hence after rescaling the function $\mathcal{F}$ is evaluated in $\bar{x} - \bar{y}$. For $d \to \infty$, the interaction term is dominated by a saddle point on $\bar{u}$ and $\bar{v}$, such that $(x_a - x_b)^2 = (y_a - y_b)^2 = \Delta_{ab}$ and $x_a \cdot y_b = 0$ [154–156], hence $(x_a - y_a - x_b + y_b)^2 = (x_a - x_b)^2 + (y_a - y_b)^2 = 2\Delta_{ab}$. This is also why the function $\mathcal{F}$ is evaluated in $2\hat{\alpha}$ in Eq. (4.9). The contribution of the interaction term to the free energy (4.9) is [154]

$$\frac{1}{2}\frac{N}{V}\overline{f}(\bar{u} - \bar{v}) = -\frac{NV_d D_g^d}{2V}\mathcal{F}(\bar{x} - \bar{y}) = -2^{d-1}\varphi_g \mathcal{F}(2\hat{\alpha}) = -\frac{d\widehat{\varphi}_g}{2}\mathcal{F}(2\hat{\alpha}) \ . \tag{B.14}$$

With an abuse of notation, we now call $\mathcal{F}(\hat{\Delta}) = \mathcal{F}(2\hat{\alpha})$.

We therefore obtain at the saddle point

$$\begin{aligned}
\mathcal{F}(\hat{\Delta}) &= \lim_{n\to 0} \sum^{*} e^{\sum_{a=1}^{k} \frac{n_a}{n}\eta_a - \frac{1}{2}\sum_{a,b}^{1,k} \frac{n_a n_b}{n^2}\Delta_{ab}} \int \frac{d\zeta}{\sqrt{2\pi}} e^{-\frac{\zeta^2}{2}\left[1 + \frac{1}{2}\sum_{ab} \frac{n_a n_b}{n^2}(\gamma_a - \gamma_b)^2\right]} \\
&= \int \frac{d\zeta}{\sqrt{2\pi}} e^{-\frac{\zeta^2}{2}} \left[\lim_{n\to 0} \sum^{*} e^{\sum_{a=1}^{k} \frac{n_a}{n}\eta_a - \frac{1}{2}\sum_{a,b}^{1,k} \frac{n_a n_b}{n^2}\left(\Delta_{ab} + \frac{\zeta^2}{2}(\gamma_a - \gamma_b)^2\right)}\right] \\
&= \int \frac{d\zeta}{\sqrt{2\pi}} e^{-\frac{\zeta^2}{2}} \mathcal{F}_0\left(\Delta_{ab} + \frac{\zeta^2}{2}(\gamma_a - \gamma_b)^2\right) \ ,
\end{aligned} \tag{B.15}$$

where $\mathcal{F}_0(\hat{\Delta})$ is the interaction function in absence of strain and is given by

$$\mathcal{F}_0(\hat{\Delta}) = \lim_{n\to 0} \sum_{n_1,\ldots,n_k;\sum_{a=1}^{k} n_a = n} \frac{n!}{n_1!\ldots n_k!} e^{\sum_{a=1}^{k} \frac{n_a}{n}\eta_a - \frac{1}{2}\sum_{a,b}^{1,k} \frac{n_a n_b}{n^2}\Delta_{ab}} \ . \tag{B.16}$$

B.2.2 Computation of the interaction term for a RS displacement matrix

We now compute the function $\mathcal{F}_0(\hat{\Delta})$ for the replica structure encoded by the matrix (4.11). Defining $\Sigma_m = \sum_{a=1}^{m} \frac{n_a}{n}$ and $\Sigma_s = \sum_{a=m+1}^{m+s} \frac{n_a}{n}$, keeping in mind that $\Sigma_m + \Sigma_s = 1$, and recalling that $\eta_a = \eta$ for $m+1 \le a \le m+s$ and $\eta_a = 0$ otherwise, we can then write with some manipulations

$$\mathcal{F}_0(\hat{\Delta}) = \lim_{n\to 0} \sum^{*} e^{-\left(\frac{\Delta^g}{2} + \frac{\Delta^f}{2}\right)\Sigma_m - \left(\frac{\Delta}{2} - \eta\right)\Sigma_s + \frac{\Delta^f}{2}\Sigma_m^2 + \frac{\Delta^g}{2}\sum_{a=1}^{m} \frac{n_a^2}{n^2} + \frac{\Delta}{2}\sum_{a=m+1}^{m+s} \frac{n_a^2}{n^2}} \ . \tag{B.17}$$

We now introduce Gaussian multipliers (Hubbard-Stratonovich transformation [66]) to decouple the quadratic terms and introduce the notation $\mathcal{D}\lambda = \frac{d\lambda}{\sqrt{2\pi}} e^{-\lambda^2/2}$. Note that $\Delta^g \geq 0$ and $\Delta \geq 0$. *Under the assumption that* $2\Delta^f \geq 0$ (to be discussed later on), we get

$$\begin{aligned}\mathcal{F}_0(\hat{\Delta}) &= \int \mathcal{D}\lambda_a \mathcal{D}\mu \lim_{n\to 0} \left[\sum_{a=1}^{m} e^{-\frac{1}{n}\left(\frac{\Delta^g}{2}+\frac{\Delta^f}{2}+\lambda_a\sqrt{\Delta^g}+\mu\sqrt{\Delta^f}\right)} + \sum_{a=m+1}^{m+s} e^{-\frac{1}{n}\left(\frac{\Delta}{2}-\eta+\lambda_a\sqrt{\Delta}\right)} \right]^n \\ &= \int \mathcal{D}\lambda_a \mathcal{D}\mu\, e^{-\min\left\{\frac{\Delta^g}{2}+\frac{\Delta^f}{2}+(\min_{a\leq m}\lambda_a)\sqrt{\Delta^g}+\mu\sqrt{\Delta^f},\, \frac{\Delta}{2}-\eta+(\min_{a>m}\lambda_a)\sqrt{\Delta}\right\}}\end{aligned} \tag{B.18}$$

Now we use that for any function $f(x)$,

$$\begin{aligned}\int \mathcal{D}\lambda_a f\left(\min_{a\leq m}\lambda_a\right) &= m\int \mathcal{D}\lambda f(\lambda)\left(\int_\lambda^\infty \mathcal{D}\lambda'\right)^{m-1} \\ &= -\int d\lambda f(\lambda)\frac{d}{d\lambda}\Theta\left(-\frac{\lambda}{\sqrt{2}}\right)^m \\ &\equiv \int \overline{\mathcal{D}}_m[\lambda] f(\lambda)\end{aligned} \tag{B.19}$$

with

$$\overline{\mathcal{D}}_n[\lambda] = -d\lambda \frac{d}{d\lambda}\Theta\left(-\frac{\lambda}{\sqrt{2}}\right)^n. \tag{B.20}$$

We therefore obtain

$$\mathcal{F}_0(\hat{\Delta}) = \int \overline{\mathcal{D}}_m\lambda\, \overline{\mathcal{D}}_s\lambda'\, \mathcal{D}\mu\, e^{-\min\left\{\frac{\Delta^g}{2}+\frac{\Delta^f}{2}+\lambda\sqrt{\Delta^g}+\mu\sqrt{\Delta^f},\, \frac{\Delta}{2}-\eta+\lambda'\sqrt{\Delta}.\right\}} \tag{B.21}$$

The integral over μ can be done explicitly, and we obtain

$$\begin{aligned}K(\lambda,\lambda') &= \int \mathcal{D}\mu\, e^{-\min\left\{\frac{\Delta^g}{2}+\frac{\Delta^f}{2}+\lambda\sqrt{\Delta^g}+\mu\sqrt{\Delta^f},\, \frac{\Delta}{2}-\eta+\lambda'\sqrt{\Delta}\right\}} \\ &= e^{-\frac{\Delta}{2}+\eta-\sqrt{\Delta}\lambda'}\Theta\left(\frac{\eta+\frac{\Delta^f+\Delta^g-\Delta}{2}+\sqrt{\Delta^g}\lambda-\sqrt{\Delta}\lambda'}{\sqrt{2\Delta^f}}\right) \\ &\quad + e^{-\Delta^g/2-\sqrt{\Delta^g}\lambda}\Theta\left(\frac{-\eta+\frac{\Delta^f-\Delta^g+\Delta}{2}-\sqrt{\Delta^g}\lambda+\sqrt{\Delta}\lambda'}{\sqrt{2\Delta^f}}\right)\end{aligned} \tag{B.22}$$

Now, integrating by parts, we can write

$$\begin{aligned}\mathcal{F}_0(\hat{\Delta}) &= \int d\lambda \frac{d}{d\lambda}\left[1-\Theta\left(-\frac{\lambda}{\sqrt{2}}\right)^m\right]\int d\lambda' \frac{d}{d\lambda'}\left[1-\Theta\left(-\frac{\lambda'}{\sqrt{2}}\right)^s\right] K(\lambda,\lambda') \\ &= \int d\lambda \frac{d}{d\lambda}\left[1-\Theta\left(-\frac{\lambda}{\sqrt{2}}\right)^m\right]\left\{K(\lambda,\lambda'=\infty)\right. \\ &\quad \left. -\int d\lambda'\left[1-\Theta\left(-\frac{\lambda'}{\sqrt{2}}\right)^s\right]\frac{\partial K}{\partial\lambda'}(\lambda,\lambda')\right\} \\ &= \int d\lambda \frac{d}{d\lambda}\left[1-\Theta\left(-\frac{\lambda}{\sqrt{2}}\right)^m\right] e^{-\Delta^g/2-\sqrt{\Delta^g}\lambda}\end{aligned}$$

$$
\begin{aligned}
&- \int d\lambda' \left[1-\Theta\left(-\frac{\lambda'}{\sqrt{2}}\right)^s\right] \int d\lambda \frac{d}{d\lambda}\left[1-\Theta\left(-\frac{\lambda}{\sqrt{2}}\right)^m\right] \frac{\partial K}{\partial \lambda'}(\lambda,\lambda') \\
=&\sqrt{\Delta^g} \int d\lambda \left[1-\Theta\left(-\frac{\lambda}{\sqrt{2}}\right)^m\right] e^{-\Delta^g/2-\sqrt{\Delta^g}\lambda} \\
&- \int d\lambda' \left[1-\Theta\left(-\frac{\lambda'}{\sqrt{2}}\right)^s\right] \left\{\frac{\partial K}{\partial \lambda'}(\lambda=\infty,\lambda') \right. \\
&\left. - \int d\lambda \left[1-\Theta\left(-\frac{\lambda}{\sqrt{2}}\right)^m\right] \frac{\partial^2 K}{\partial\lambda\partial\lambda'}(\lambda,\lambda')\right\} \\
=&\sqrt{\Delta^g} \int d\lambda \left[1-\Theta\left(-\frac{\lambda}{\sqrt{2}}\right)^m\right] e^{-\Delta^g/2-\sqrt{\Delta^g}\lambda} \\
&+ \sqrt{\Delta} \int d\lambda' \left[1-\Theta\left(-\frac{\lambda'}{\sqrt{2}}\right)^s\right] e^{-\Delta/2+\eta-\sqrt{\Delta}\lambda'} \\
&+ \int d\lambda\, d\lambda' \left[1-\Theta\left(-\frac{\lambda}{\sqrt{2}}\right)^m\right] \left[1-\Theta\left(-\frac{\lambda'}{\sqrt{2}}\right)^s\right] \frac{\partial^2 K}{\partial\lambda\partial\lambda'}(\lambda,\lambda') \,.
\end{aligned}
$$

We also have

$$
\frac{\partial^2 K}{\partial\lambda\partial\lambda'}(\lambda,\lambda') = -\sqrt{\Delta^g\Delta}\, e^{\eta-\Delta/2-\sqrt{\Delta}\lambda'} \frac{e^{-\frac{1}{2\Delta^f}\left(-\eta+\frac{\Delta-\Delta^g-\Delta^f}{2}-\sqrt{\Delta^g}\lambda+\sqrt{\Delta}\lambda'\right)^2}}{\sqrt{2\pi\Delta^f}} \,. \tag{B.23}
$$

We remark that the function K does not depend explicitly on m and s, therefore the derivative with respect to s can be computed straightforwardly. Also, using Eq. (B.23) one can write

$$
\begin{aligned}
\mathcal{F}_0(\hat{\Delta}) =&\sqrt{\Delta^g} \int d\lambda \left[1-\Theta\left(-\frac{\lambda}{\sqrt{2}}\right)^m\right] e^{-\Delta^g/2-\sqrt{\Delta^g}\lambda} \\
&+ \sqrt{\Delta} \int d\lambda' \left[1-\Theta\left(-\frac{\lambda'}{\sqrt{2}}\right)^s\right] e^{-\Delta/2+\eta-\sqrt{\Delta}\lambda'} \\
&\times \int d\lambda\, \Theta\left(-\frac{\lambda}{\sqrt{2}}\right)^m \sqrt{\Delta^g} \frac{e^{-\frac{1}{2\Delta^f}\left(-\eta+\frac{\Delta-\Delta^g-\Delta^f}{2}-\sqrt{\Delta^g}\lambda+\sqrt{\Delta}\lambda'\right)^2}}{\sqrt{2\pi\Delta^f}} \,.
\end{aligned} \tag{B.24}
$$

We can also change to variables $y = -\Delta^g/2 - \sqrt{\Delta^g}\lambda$ and $y' = \eta - \Delta/2 - \sqrt{\Delta}\lambda'$, and $x = y' - y$. Then we have

$$
\begin{aligned}
\mathcal{F}_0(\Delta^g,\Delta,\Delta^f) = \int dy\, e^y &\left\{1-\Theta\left(\frac{y+\Delta^g/2}{\sqrt{2\Delta^g}}\right)^m \right. \\
&\left. \times \int dx\, \Theta\left(\frac{x+y-\eta+\Delta/2}{\sqrt{2\Delta}}\right)^s \frac{e^{-\frac{1}{2\Delta^f}\left(x-\Delta^f/2\right)^2}}{\sqrt{2\pi\Delta^f}}\right\} \,.
\end{aligned} \tag{B.25}
$$

From Eq. (B.15), recalling that $\gamma_a = \gamma$ for the s replicas and zero otherwise, we have

$$
\mathcal{F}(\Delta^g,\Delta,\Delta^f) = \int \frac{d\zeta}{\sqrt{2\pi}} e^{-\frac{\zeta^2}{2}} \mathcal{F}_0\left(\Delta^g,\Delta,\Delta^f+\zeta^2\gamma^2\right) \,. \tag{B.26}
$$

Which is the (4.14).

Appendix C

Computation of the replicon mode

In this appendix we discuss in detail the stability of the replica symmetric ansatz (4.11) for the calculation of the Franz-Parisi entropy. We want to compute the stability matrix of the small fluctuations around the RS solution and from that extract the replicon eigenvalue [155]. The calculation is very close to the one given in [155] and we will use many of the results reported in that work.

C.1 The structure of the unstable mode

The general stability analysis of the RS solution can be done on the following lines. In principle, we have to take the general expression (4.9) and compute the Hessian matrix obtained by varying at the second order the replicated entropy with respect to the full matrix $\hat{\alpha}$. We can then compute the Hessian on the RS saddle point. The task here is complicated by the fact that the entropy (4.9) is not symmetric under permutation of all replicas. The symmetries are restricted to arbitrary perturbations of the m replicas and the s replicas separately. Hence the structure of the Hessian matrix is more complicated than the one studied in [155].

However, here we are mostly interested in studying the problem when the m replicas are at equilibrium in the liquid phase, hence $m = 1$, and in that case we already know that the RS solution is stable in the sector of the m replicas [155]. Moreover, the m reference replicas only select the glass state and do not evolve when the state is followed, differently from the s replicas. Hence, on physical grounds, we expect that replica symmetry will be broken in the sector of the s replicas and that the unstable mode in that sector will have the form of a "replicon" mode similar to the one studied in [155]. Based on this reasoning, we conjecture the following form for the unstable mode:

$$\delta\hat{\Delta} = \begin{bmatrix} \delta\Delta^g(I^m_{ab} - \delta_{ab}) & \delta\Delta^r I^{m,s}_{ab} \\ \delta\Delta^r I^{s,m}_{ab} & \delta\Delta_R\, r_{ab} \end{bmatrix} , \tag{C.1}$$

where $\hat{I}^m$ is a $m \times m$ matrix and $\hat{I}^{m,s}$ is a $m \times s$ matrix with all elements equal to 1, and $\hat{r}$ is a $s \times s$ "replicon" matrix such that $\sum_{ab} r_{ab} = 0$ [155, 156]. In other words, we look for fluctuations around the RS matrix (4.11) where the matrix elements

of the m replicas Δ^g and the matrix elements connecting the m and s replicas Δ^r are varied uniformly, while in the s block we break replica symmetry following the replicon mode.

Let us write the variation of the entropy (4.9) around the RS solution, along the unstable mode (C.1). We have

$$\delta s = \frac{1}{2} \sum_{a\neq b, c\neq d} M_{ab;cd}\delta\Delta_{ab}\delta\Delta_{cd} + \frac{1}{6} \sum_{a\neq b, c\neq d, e\neq f} W_{ab;cd;ef}\delta\Delta_{ab}\delta\Delta_{cd}\delta\Delta_{ef} + \cdots \ . \quad \text{(C.2)}$$

The mass matrix $M_{ab;cd}$ and the cubic term $W_{ab;cd;ef}$ are derivatives of the entropy s (which is replica symmetric) computed in a RS point, and therefore they must satisfy certain symmetries which are simple extensions of the ones discussed in [155]. Let us call $(ab)^m$ a pair of indices $a \neq b$ that both belong to the m block. Similarly $(ab)^s$ belong to the s block, and $(ab)^r$ are such that one index belong to the m block and the other to the s block. At the quadratic order, we obtain

$$\begin{aligned} \delta s = {} & \frac{1}{2}(\delta\Delta^g)^2 \sum_{(ab)^m,(cd)^m} M_{ab;cd} + \frac{1}{2}(\delta\Delta^r)^2 \sum_{(ab)^r,(cd)^r} M_{ab;cd} \\ & + \frac{1}{2}\delta\Delta_R^2 \sum_{(ab)^s,(cd)^s} M_{ab;cd} r_{ab} r_{cd} + \delta\Delta^g\delta\Delta^r \sum_{(ab)^m,(cd)^r} M_{ab;cd} \\ & + \delta\Delta^g\delta\Delta_R \sum_{(ab)^m,(cd)^s} M_{ab;cd} r_{cd} + \delta\Delta^r\delta\Delta_R \sum_{(ab)^r,(cd)^s} M_{ab;cd} r_{cd} \ . \end{aligned} \quad \text{(C.3)}$$

It is easy to show that the cross-terms involving the replicon mode vanish. In fact, the sum $\sum_{(ab)^m} M_{ab;cd}$ must be a constant independent of the choice of indices $(cd)^s$, which are all equivalent due to replica symmetry in the s-block. Hence $\sum_{(ab)^m,(cd)^s} M_{ab;cd} r_{cd} = const. \sum_{(cd)^s} r_{cd} = 0$ because of the zero-sum property of the matrix $\hat{r}$. The same property applies to the other cross-term. The quadratic term has therefore the form

$$\delta s^{(2)} = \frac{1}{2}A(\delta\Delta^g)^2 + \frac{1}{2}B(\delta\Delta^r)^2 + C\delta\Delta^g\delta\Delta^r + \frac{1}{2}\delta\Delta_R^2 \sum_{(ab)^s,(cd)^s} M_{ab;cd} r_{ab} r_{cd} \ , \quad \text{(C.4)}$$

and the stability analysis of the replicon mode in the s-block can be done independently of the presence of the m replicas.

A similar reasoning can be applied to the cubic terms. Let us write only the terms that involve the replicon mode:

$$\begin{aligned} \delta s^{(3)} = {} & \frac{1}{6}\delta\Delta_R^3 \sum_{(ab)^s,(cd)^s,(ef)^s} W_{ab;cd;ef} r_{ab} r_{cd} r_{ef} \\ & + \frac{1}{2}\delta\Delta_R^2\delta\Delta^g \sum_{(ab)^s,(cd)^s,(ef)^m} W_{ab;cd;ef} r_{ab} r_{cd} \\ & + \frac{1}{2}\delta\Delta_R^2\delta\Delta^r \sum_{(ab)^s,(cd)^s,(ef)^r} W_{ab;cd;ef} r_{ab} r_{cd} \\ & + \delta\Delta_R\delta\Delta^r\delta\Delta^g \sum_{(ab)^s,(cd)^r,(ef)^m} W_{ab;cd;ef} r_{ab} \end{aligned}$$

$$
\begin{aligned}
&+ \frac{1}{2}\delta\Delta_R(\delta\Delta^r)^2 \sum_{(ab)^s,(cd)^r,(ef)^r} W_{ab;cd;ef} r_{ab} \\
&+ \frac{1}{2}\delta\Delta_R(\delta\Delta^g)^2 \sum_{(ab)^s,(cd)^m,(ef)^m} W_{ab;cd;ef} r_{ab} \\
&+ \text{terms without } \delta\Delta_R
\end{aligned}
$$

Clearly, all terms that are linear in $\delta\Delta_R$ vanish. In fact, for example

$$
\sum_{(ab)^s,(cd)^r,(ef)^m} W_{ab;cd;ef} r_{ab} = \sum_{(ab)^s} r_{ab} \sum_{(cd)^r,(ef)^m} W_{ab;cd;ef} = \text{const.} \times \sum_{(ab)^s} r_{ab} = 0 \ , \tag{C.5}
$$

because once again $\sum_{(cd)^r,(ef)^m} W_{ab;cd;ef}$ must be a constant independent of the choice of $(ab)^s$ which are all equivalent thanks to replica symmetry in the s-block. Collecting all non-vanishing terms that involve the replicon mode, we obtain

$$
\begin{aligned}
\delta s = &\frac{1}{2}A(\delta\Delta^g)^2 + \frac{1}{2}B(\delta\Delta^r)^2 + C\delta\Delta^g\delta\Delta^r + \frac{1}{2}\delta\Delta_R^2 \sum_{(ab)^s,(cd)^s} M_{ab;cd} r_{ab} r_{cd} \\
&+ \frac{1}{6}\delta\Delta_R^3 \sum_{(ab)^s,(cd)^s,(ef)^s} W_{ab;cd;ef} r_{ab} r_{cd} r_{ef} + \frac{1}{2}\delta\Delta_R^2\delta\Delta^g \sum_{(ab)^s,(cd)^s,(ef)^m} W_{ab;cd;ef} r_{ab} r_{cd} \\
&+ \frac{1}{2}\delta\Delta_R^2\delta\Delta^r \sum_{(ab)^s,(cd)^s,(ef)^r} W_{ab;cd;ef} r_{ab} r_{cd} \ .
\end{aligned} \tag{C.6}
$$

This perturbative entropy must be optimized over $\delta\Delta^g, \delta\Delta^r, \delta\Delta_R$, in order to check if one can construct a perturbative saddle point solution with more RSBs [155]. The above equation clearly shows that for a fixed $\delta\Delta_R$, the optimization over $\delta\Delta^g, \delta\Delta^r$ given $\delta\Delta^g \sim \delta\Delta^r \sim \delta\Delta_R^2$. Hence we conclude that all the terms that involve $\delta\Delta^g$ and $\delta\Delta^r$ are at least of order $\delta\Delta_R^4$ and can be neglected in the linear stability analysis. We finally obtain at the leading order

$$
\delta s = \frac{1}{2}\delta\Delta_R^2 \sum_{(ab)^s,(cd)^s} M_{ab;cd} r_{ab} r_{cd} + \frac{1}{6}\delta\Delta_R^3 \sum_{(ab)^s,(cd)^s,(ef)^s} W_{ab;cd;ef} r_{ab} r_{cd} r_{ef} \tag{C.7}
$$

and all the couplings between the s-block and the m-block disappear. This shows that the stability analysis of the replicon mode can be performed by restricting all the derivatives to the s-block, both at the quadratic and cubic orders. The Gardner transition corresponds to the appearance of a negative mode in the quadratic term for a particular choice of the matrix r_{ab} that corresponds to a 1RSB structure in the s-block, characterized by a Parisi parameter s_1, as discussed in [156, Sec. VII]. The unstable quadratic mode is stabilized by the cubic term leading to a fullRSB phase [156, 276]. Note that, according to the analysis of [156, 276], in the "typical state" calculation done with m replicas with $m \in [0, 1]$ taken as a free parameter, the fullRSB phase can only be stabilized if the parameter $m_1 > m$, and this only happens at low enough temperature or large enough densities, hence the fullRSB phase can only exist at sufficiently low temperatures and high densities [156, 276]: unless these conditions are met, the replicon instability only means that the replica

calculation is generally unstable and only the liquid phase exists.
However, the situation is crucially different here because the state following construction requires $s \to 0$. The perturbative analysis gives $s_1 = \lambda(s)$, where $\lambda(s) > 0$ is the MCT parameter discussed in paragraph 5.2.2, hence one always has $s_1 = \lambda(s) > s = 0$ and the fullRSB phase exist at all temperatures and densities when the RS phase becomes unstable. This a big difference between the State Following calculation and the real replica one.

Summarizing, we have shown that one can define the following stability matrix

$$M^s_{a\neq b;c\neq d} = M_1\left(\frac{\delta_{ac}\delta_{bd}+\delta_{ad}\delta_{bc}}{2}\right) + M_2\left(\frac{\delta_{ac}+\delta_{ad}+\delta_{bc}+\delta_{bd}}{4}\right) + M_3 \tag{C.8}$$

where the indices $a,\ b,\ c,\ d$ run between $m+1$ and $m+s$. The fact that the replica structure of this stability matrix is the one defined in eq. (4.36) is due to replica symmetry under permutation of the s replicas as already discussed. When a zero mode appears in this matrix, the RS solution becomes unstable and transform continuously in a fullRSB one, signaling that the glass state sampled by the s replicas undergoes a Gardner transition.

We now compute the replicon mode. We divide the problem of computing that stability matrix in the part coming from the derivatives of the entropic term and the part relative to the interaction term. We will first derive the stability matrix in the case of absence of shear, and the generalize it to a shear-strain situation.

C.2 Entropic term

We want to compute the contribution of the entropic term to the stability matrix. Note that under a variation of $\delta\alpha_{ab}$, we have an identical variation of $\delta\alpha_{ba} = \delta\alpha_{ab}$, and the diagonal terms vary by minus the same amount, $\delta\alpha_{aa} = \delta\alpha_{bb} = -\delta\alpha_{ab}$ to maintain the Laplacian condition of $\hat{\alpha}$. Hence we have

$$\frac{\delta}{\delta\alpha_{a<b}} = \frac{\delta}{\delta\alpha_{ab}} + \frac{\delta}{\delta\alpha_{ba}} - \frac{\delta}{\delta\alpha_{aa}} - \frac{\delta}{\delta\alpha_{bb}}\ . \tag{C.9}$$

From Eq. (B.1), recalling that $\hat{\beta}(\varepsilon) = \hat{\alpha} + \varepsilon\mathbf{1}$, we have $\log\det\hat{\alpha}^{m+s,m+s} = \log\det\hat{\beta} - \log(\varepsilon) - \log(m+s) + O(\varepsilon)$, therefore, using (for symmetric matrices)

$$\frac{\delta}{\delta\beta_{ab}}\log\det\hat{\beta} = \beta^{-1}_{ab}, \longrightarrow \frac{\delta^2}{\delta\beta_{ab}\delta\beta_{cd}}\log\det\hat{\beta} = \frac{\delta\beta^{-1}_{ab}}{\delta\beta_{cd}} = -\beta^{-1}_{ac}\beta^{-1}_{bd}\ , \tag{C.10}$$

we obtain

$$\begin{aligned} M^{(E)}_{ab;cd} &= \frac{\delta^2}{\delta\alpha_{a<b}\delta\alpha_{c<d}}\log\det\hat{\alpha}^{m+s,m+s} = \lim_{\varepsilon\to 0}\frac{\delta^2}{\delta\beta_{a<b}\delta\beta_{c<d}}\log\det\hat{\beta} \\ &= \lim_{\varepsilon\to 0}\Big[-2\beta^{-1}_{ac}\beta^{-1}_{bd} - 2\beta^{-1}_{ad}\beta^{-1}_{bc} + 2\beta^{-1}_{ac}\beta^{-1}_{bc} + 2\beta^{-1}_{ad}\beta^{-1}_{bd} + 2\beta^{-1}_{ac}\beta^{-1}_{ad} + 2\beta^{-1}_{bc}\beta^{-1}_{bd} \\ &\qquad -(\beta^{-1}_{ac})^2 - (\beta^{-1}_{bc})^2 - (\beta^{-1}_{ad})^2 - (\beta^{-1}_{bd})^2\Big]\ . \end{aligned} \tag{C.11}$$

Based on the discussion above, we are only interested in the matrix elements corresponding to a, b, c, d belonging to the block of s replicas. The matrix $\hat{\beta}$ has the

form (B.2), and using the block-inversion formula, its inverse in the s block is $\Omega^{-1} = (D - BA^{-1}B^T)^{-1}$. Hence, for $a, b \in [m+1, m+s]$ we have $\beta_{ab}^{-1} = \Omega_{ab}^{-1} = (\Omega^{-1})_1 \delta_{ab} + (\Omega^{-1})_2$ where the coefficients are obtained from equations (B.6) and (B.4). In particular we have $(\Omega^{-1})_1 = 1/(\delta + \alpha + \varepsilon) = 1/(\Delta/2 + \varepsilon)$.

Plugging this form of β_{ab}^{-1} in equation (C.11), one can check that all terms involving $(\Omega^{-1})_2$ disappear (as it should, because this term is divergent when $\varepsilon \to 0$), and one gets (recalling that $a \neq b$ and $c \neq d$):

$$\begin{aligned} M^{(E)}_{ab;cd} &= M_1^{(E)} \left(\frac{\delta_{ac}\delta_{bd} + \delta_{ad}\delta_{bc}}{2} \right) + M_2^{(E)} \left(\frac{\delta_{ac} + \delta_{ad} + \delta_{bc} + \delta_{bd}}{4} \right) + M_3^{(E)} \\ &= -\frac{16}{\Delta^2} \left(\frac{\delta_{ac}\delta_{bd} + \delta_{ad}\delta_{bc}}{2} \right) - \frac{16}{\Delta^2} \left(\frac{\delta_{ac} + \delta_{ad} + \delta_{bc} + \delta_{bd}}{4} \right) . \end{aligned} \tag{C.12}$$

C.3 Interaction term

We define the interaction part of the stability matrix in absence of shear as

$$\begin{aligned} M^{(I)}_{ab;cd} &= \left. \frac{\delta^2 \mathcal{F}_0[\hat{\upsilon}]}{\delta \upsilon_{a<b} \delta \upsilon_{c<d}} \right|_{\hat{\upsilon} = 2\hat{\alpha}_{RS}} \\ &= M_1^{(I)} \left(\frac{\delta_{ac}\delta_{bd} + \delta_{ad}\delta_{bc}}{2} \right) + M_2^{(I)} \left(\frac{\delta_{ac} + \delta_{ad} + \delta_{bc} + \delta_{bd}}{4} \right) + M_3^{(I)} \end{aligned} \tag{C.13}$$

so that the expression for the matrix coefficients M_i of the full stability matrix is given by

$$M_i = M_i^{(E)} - 4\widehat{\varphi} M_i^{(I)} . \tag{C.14}$$

The calculation of the derivatives of the interaction term can be done on the same lines and following the same tricks of [155]. Let us start by writing the general expression for the derivatives using the representation (B.16) of the function $\mathcal{F}_0$. We have

$$\begin{aligned} M^{(I)}_{ab;cd} = \lim_{n\to 0} \sum^{*} f(n_a, n_b) f(n_c, n_d) \exp \Bigg[&- \left(\frac{\Delta^g}{2} + \frac{\Delta^f}{2} \right) \Sigma_m - \left(\frac{\Delta}{2} - \eta \right) \Sigma_s \\ &+ \frac{\Delta^f}{2} \Sigma_m^2 + \frac{\Delta^g}{2} \sum_{a=1}^{m} \frac{n_a^2}{n^2} + \frac{\Delta}{2} \sum_{a=m+1}^{m+s} \frac{n_a^2}{n^2} \Bigg] , \end{aligned} \tag{C.15}$$

where the function f is defined in [155, eq. (45)]. As a variant of [155, eq.(46)], we can introduce the following notation

$$\begin{aligned} \langle O \rangle = \lim_{n\to 0} \sum^{*} O \exp \Bigg[&- \left(\frac{\Delta^g}{2} + \frac{\Delta^f}{2} \right) \Sigma_m - \left(\frac{\Delta}{2} - \eta \right) \Sigma_s \\ &+ \frac{\Delta^f}{2} \Sigma_m^2 + \frac{\Delta^g}{2} \sum_{a=1}^{m} \frac{n_a^2}{n^2} + \frac{\Delta}{2} \sum_{a=m+1}^{m+s} \frac{n_a^2}{n^2} \Bigg] . \end{aligned} \tag{C.16}$$

The stability matrix can thus be rewritten as [155, Eq.(47)] where the replica indices run from $m+1$ to $m+s$. Then we have to compute monomials of the form

$\langle n_{a_1} \dots n_{a_k}/n^k \rangle$, which can be done in the following way

$$\begin{aligned}
\langle \frac{n_{a_1} \dots n_{a_k}}{n^k} \rangle =& \lim_{n\to 0} \sum^{*} \frac{n_{a_1} \dots n_{a_k}}{n^k} \int_{-\infty}^{\infty} \frac{\mathrm{d}\mu}{\sqrt{2\pi}} e^{-\mu^2/2} \int_{-\infty}^{\infty} \left(\prod_{a=1}^{m+s} \frac{\mathrm{d}\lambda_a}{\sqrt{2\pi}} e^{-\lambda_a^2/2} \right) \\
& \times \exp\left[-\left(\frac{\Delta^g}{2} + \frac{\Delta^f}{2} \right) \Sigma_m - \left(\frac{\Delta}{2} - \eta \right) \Sigma_s - \mu \sqrt{\Delta^f} \Sigma_m \right. \\
& \left. -\sqrt{\Delta}^g \sum_{a=1}^{m} \frac{n_a \lambda_a}{n} - \sqrt{\Delta} \sum_{a=m+1}^{m+s} \frac{n_a \lambda_a}{n} \right] \\
=& \frac{1}{\Delta^{k/2}} \int_{-\infty}^{\infty} \mathcal{D}\mu \int_{-\infty}^{\infty} \left(\prod_{a=1}^{m} \mathcal{D}\lambda_a \right) \int_{-\infty}^{\infty} \left(\prod_{a=m+1}^{m+s} \frac{\mathrm{d}\lambda_a}{\sqrt{2\pi}} \right) \\
& \times \frac{\partial^k}{\partial\lambda_{a_1} \dots \partial\lambda_{a_k}} e^{-\frac{1}{2}\sum_{a=m+1}^{m+s} \lambda_a^2} \\
& \times e^{-\min\left\{ \frac{\Delta^g}{2} + \frac{\Delta^f}{2} + (\min_{a\le m} \lambda_a)\sqrt{\Delta^g} + \mu\sqrt{\Delta^f},\, \frac{\Delta}{2} - \eta + (\min_{a>m} \lambda_a)\sqrt{\Delta} \right\}} .
\end{aligned} \tag{C.17}$$

If O is a function that depends only on the λ_a with $a \in [m+1, m+s]$, then we can define

$$\begin{aligned}
\langle O \rangle =& \int_{-\infty}^{\infty} \mathcal{D}\mu \int_{-\infty}^{\infty} \left(\prod_{a=1}^{m+s} \mathcal{D}\lambda_a \right) \\
& \times O\, e^{-\min\left\{ \frac{\Delta^g}{2} + \frac{\Delta^f}{2} + (\min_{a\le m} \lambda_a)\sqrt{\Delta^g} + \mu\sqrt{\Delta^f},\, \frac{\Delta}{2} - \eta + (\min_{a>m} \lambda_a)\sqrt{\Delta} \right\}} \\
=& \int_{-\infty}^{\infty} \left(\prod_{a=1}^{m+s} \mathcal{D}\lambda_a \right) O\, K(\min_{a\le m} \lambda_a, \min_{a>m} \lambda_a) = \int_{-\infty}^{\infty} \left(\prod_{a=m+1}^{m+s} \mathcal{D}\lambda_a \right) O\, G\left(\min_{a>m} \lambda_a \right) ,
\end{aligned} \tag{C.18}$$

where

$$G(\lambda') = \int_{-\infty}^{\infty} \overline{\mathcal{D}}_m \lambda\, K(\lambda, \lambda') . \tag{C.19}$$

In this way we obtain a generalization of [155, Eq.(48)], in the form

$$\langle n_{a_1} \dots n_{a_k}/n^k \rangle = \frac{1}{\Delta^{k/2}} \left\langle e^{\frac{1}{2}\sum_{a=m+1}^{m+s} \lambda_a^2} \frac{\partial^k}{\partial\lambda_{a_1} \dots \partial\lambda_{a_k}} e^{-\frac{1}{2}\sum_{a=m+1}^{m+s} \lambda_a^2} \right\rangle . \tag{C.20}$$

The interaction part of the stability matrix is then given by the same reasoning as in [155, Eq.(50, 51, 53, 54, 56)] where the replica indices must be all shifted by m. The only difference with respect to [155] is the definition of the measure used to take the average over the variables λs. In fact instead of having [155, Eq.(52)] we have

$$\langle O(\lambda) \rangle = \int_{-\infty}^{\infty} \mathcal{D}\lambda\, G(\lambda) O(\lambda) = \int_{-\infty}^{\infty} \mathcal{D}\lambda \bar{\mathcal{D}}_m \lambda'\, K(\lambda', \lambda)\, O(\lambda) . \tag{C.21}$$

This completes the calculation of the stability matrix without shear.

The stability matrix in presence of shear

The result of the previous section is valid when $\gamma = 0$. Here we generalize the calculation to the case in which also the shear is present. The presence of a non vanishing γ is detectable only in the interaction part of the replicated entropy. This means that the expression of the entropic term does not change, and we need to compute only the new interaction part of the stability matrix. This can be done using the following line of reasoning. The interaction part of the stability matrix can be written in presence of shear as

$$M^{(I,\gamma)}_{ab;cd} = \frac{\delta^2}{\delta\upsilon_{a<b}\delta\upsilon_{c<d}} \int \mathcal{D}\zeta \mathcal{F}_0[\Delta_{ab} + \frac{\zeta^2}{2}\gamma^2\Gamma_{ab}]\Big|_{\hat{\upsilon}=2\hat{\alpha}_{RS}} \tag{C.22}$$

where the matrix $\Gamma_{ab} = 1$ if a belongs to the m-block and b to the s-block or viceversa, and zero otherwise. Recalling that $\Delta_{ab} = \alpha_{aa} + \alpha_{bb} - 2\alpha_{ab}$, we have that the relation between $\hat{\Delta}$ and $\hat{\alpha}$ is linear, therefore a constant shift of $\hat{\Delta}$ induces a constant shift in $\hat{\alpha}$, which does not affect the derivatives. We deduce that

$$M^{(I,\gamma)}_{ab;cd} = \int \mathcal{D}\zeta\, M^{(I,\gamma=0)}_{ab;cd}[\Delta_{ab} + \frac{\zeta^2}{2}\gamma^2\Gamma_{ab}] = \int \mathcal{D}\zeta\, M^{(I,\gamma=0)}_{ab;cd}[\Delta^g, \Delta, \Delta^f + \zeta^2\gamma^2]\ . \tag{C.23}$$

Because Δ^f appears only in the kernel K, shifting Δ^f amounts to nothing more than a change in definition for the measure for the average of monomials of λ, which will contain a modified kernel

$$\begin{aligned} K^\gamma(\lambda,\lambda') &= \int \mathcal{D}\zeta K(\lambda,\lambda';\Delta^g,\Delta,\Delta^f+\zeta^2\gamma^2) \\ &= \int \mathcal{D}\zeta \left[e^{-\frac{\Delta}{2}+\eta-\sqrt{\Delta}\lambda'}\Theta\left(\frac{\eta + \frac{\Delta^f+\zeta^2\gamma^2+\Delta^g-\Delta}{2} + \sqrt{\Delta^g}\lambda - \sqrt{\Delta}\lambda'}{\sqrt{2(\Delta^f+\zeta^2\gamma^2)}}\right)\right. \\ &\qquad \left. + e^{-\Delta^g/2-\sqrt{\Delta^g}\lambda}\Theta\left(\frac{-\eta + \frac{\Delta^f+\zeta^2\gamma^2-\Delta^g+\Delta}{2} - \sqrt{\Delta^g}\lambda + \sqrt{\Delta}\lambda'}{\sqrt{2(\Delta^f+\zeta^2\gamma^2)}}\right)\right]\ , \end{aligned} \tag{C.24}$$

and the functional expression of the interaction part of the stability matrix has the same form of the $\gamma = 0$ case.

Appendix D

Computation of the replicated entropy in the fRSB ansatz

We perform here the computation of the replicated entropy and the FP entropy for the fRSB ansatz. As for the RS case, we take care separately of the entropic and interaction terms.

D.1 Entropic term

The entropic term for the replicated entropy has the following expression in terms of the MSD matrix $\hat{\Delta}$ [277]:

$$\frac{2}{d}s_{entr} \equiv \log\det\hat{\alpha}^{m+s,m+s} = \log\left[-\frac{2}{(m+s)^2}\left(\sum_{ab}(\hat{\Delta})^{-1}_{ab}\right)\det(-\hat{\Delta}/2)\right]. \tag{D.1}$$

Let us now compute separately the two terms

$$\log\det\hat{\Delta} \qquad\qquad \sum_{a,b=1}^{m+s}\left[\hat{\Delta}^{-1}\right]_{ab}. \tag{D.2}$$

$m\times s$ matrix whose elements are all equal to Δ^r, and $\Delta^{\infty RSB}$ is a generic hierarchical matrix. Let us start from the first one that can be rewritten as

$$\det\hat{\Delta} = \left(\det\hat{\Delta}^g\right)\det\left(\hat{\Delta}^s - \hat{\Delta}^r(\hat{\Delta}^g)^{-1}(\hat{\Delta}^r)^T\right). \tag{D.3}$$

Using the fact that for a $m\times m$ replica symmetric matrix of the form $q_{ab} = \delta_{ab} + (1-\delta_{ab})q$, the expression of the determinant is [66]

$$\det\hat{q} = (1-q)^{m-1}[1+(m-1)q] \tag{D.4}$$

then for $\hat{\Delta}^g$ we have that

$$\begin{aligned}\det\hat{\Delta}^g &= \lim_{\epsilon\to 0}\left(\hat{\Delta}^g + \epsilon\mathbb{1}_m\right) = \lim_{\epsilon\to 0}\epsilon^m\left(1-\frac{\Delta^g}{\epsilon}\right)^{m-1}\left[1+(m-1)\frac{\Delta^g}{\epsilon}\right] \\ &= (1-m)(-\Delta^g)^m\end{aligned} \tag{D.5}$$

where $\mathbb{1}_m$ is the m dimensional identity matrix. Moreover we have [66]

$$(\Delta^g)^{-1}_{ab} = -\frac{1}{\Delta^g}\left(\delta_{ab} + \frac{1}{1-m}\right) \tag{D.6}$$

so that

$$\left[\hat{\Delta}^r(\hat{\Delta}^g)^{-1}(\hat{\Delta}^r)^T\right]_{ab} = -\frac{(\Delta^r)^2}{\Delta^g}\frac{m}{1-m} \tag{D.7}$$

This means that the matrix $\hat{\Omega} = \hat{\Delta}^s - \hat{\Delta}^r(\hat{\Delta}^g)^{-1}(\hat{\Delta}^r)^T$ will be parametrized within the fullRSB ansatz by

$$\hat{\Omega} \to \{\Omega_d, \Omega(x)\} \qquad x \in [s,1] \tag{D.8}$$

where

$$\begin{aligned} \Omega_d &\equiv \frac{(\Delta^r)^2}{\Delta^g}\frac{m}{1-m}, \\ \Omega(x) &\equiv \Delta(x) + \frac{(\Delta^r)^2}{\Delta^g}\frac{m}{1-m}\,. \end{aligned} \tag{D.9}$$

In this way we can use the result of [156, 254] to obtain

$$\log\det\hat{\Omega} = s\log(\Omega_d - \langle\Omega\rangle) - s\int_s^1 \frac{\mathrm{d}y}{y^2}\log\left(\frac{\Omega_d - \langle\Omega\rangle - [\Omega](y)}{\Omega_d - \langle\Omega\rangle}\right) \tag{D.10}$$

where

$$[\Omega](x) = x\Omega(x) - \int_0^x \mathrm{d}y\,\Omega(y)\;, \qquad \langle\Omega\rangle = \int_0^1 \mathrm{d}x\,\Omega(x)\;, \tag{D.11}$$

and we are assuming $\Omega(x) = 0 \;\; \forall x < s$. By inserting the fullRSB parametrization for $\hat{\Omega}$ we get the computation of the first term of (D.2).
We now turn to the computation of the second term. We need to compute the inverse of the matrix $\hat{\Delta}$. We thus consider a general matrix of the following form

$$\hat{G} = \begin{pmatrix} \hat{q}_g & \hat{q}_r^{(1)} \\ \hat{q}_r^{(2)} & \hat{q} \end{pmatrix} \tag{D.12}$$

where the fullRSB structure is only inside the sub-block $\hat{q} \to \{\tilde{q}, q(x)\}$, the entries of the matrices $\hat{q}_r^{(1)}$ and $\hat{q}_r^{(2)}$ are all equal respectively to $q_r^{(1)}$ and $q_r^{(2)}$, and the matrix $\hat{q}_g$ has an RS form. Again we assume that $q(x) = 0$ for $x \in [0,s]$. We want to solve the inverse matrix problem, namely we want to find the matrix

$$\hat{G}^{-1} = \begin{pmatrix} \hat{p}_g & \hat{p}_r^{(1)} \\ \hat{p}_r^{(2)} & \hat{p} \end{pmatrix} \tag{D.13}$$

such that $\hat{G}\hat{G}^{-1} = \mathbb{1}_{m+s}$. We assume the matrix G^{-1} to have the same general form of the G and be likewise parametrized. Using this form of G^{-1}, the equations for the inverse are

$$q_d p_d + (m-1)q_g p_g + s q_r^{(1)} p_r^{(2)} \;=\; 1 \tag{D.14}$$

$$
\begin{aligned}
q_d p_g + q_g p_d + (m-2) q_g p_g + s q_r^{(1)} p_r^{(2)} &= 0 && \text{(D.15)}\\
q_r^{(2)} p_d + (m-1) p_g q_r^{(2)} + p_r^{(2)} (\tilde{q} - \langle q \rangle) &= 0 && \text{(D.16)}\\
q_d p_r^{(1)} + (m-1) q_g p_r^{(1)} + q_r^{(1)} (\tilde{p} - \langle p \rangle) &= 0 && \text{(D.17)}\\
m q_r^{(2)} p_r^{(1)} + \tilde{q}\tilde{p} - \int_s^1 \mathrm{d}x q(x) p(x) &= 1 && \text{(D.18)}\\
m q_r^{(2)} p_r^{(1)} - s p(x) q(x) + (\tilde{q} - \langle q \rangle) p(x) + (\tilde{p} - \langle p \rangle) q(x) & \\
- \int_s^x \mathrm{d}y (q(y) - q(x))(p(y) - p(x)) &= 0 && \text{(D.19)}
\end{aligned}
$$

These equations can be solved exactly. Let us focus first on the last two equations and let us call $A(x)$ the right hand side of eq. (D.19). This equation holds for all x in the interval $[0, 1]$. If we consider its derivative with respect to x we get

$$
0 = \dot{A}(x) = (\tilde{p} - \langle p \rangle)\dot{q}(x) + (\tilde{q} - \langle q \rangle)\dot{p}(x) - \dot{p}(x)[q](x) - \dot{q}(x)[p](x) \tag{D.20}
$$

Let us now consider the following quantity:

$$
B(x) = (\tilde{p} - \langle p \rangle - [p](x))\,(\tilde{q} - \langle q \rangle - [q](x)) \tag{D.21}
$$

It is simple to show that $\dot{A}(x) = -x\dot{B}(x)$ so that we obtain

$$
(\tilde{p} - \langle p \rangle - [p](x))\,(\tilde{q} - \langle q \rangle - [q](x)) = \aleph \tag{D.22}
$$

where $\aleph$ is a independent of x. Computing (D.22) in $x = 1$ and using eq. (D.18) we get

$$
(\tilde{p} - p(1))\,(\tilde{q} - q(1)) = \aleph \tag{D.23}
$$

Moreover let us consider again eq. (D.19) evaluated in $x = 1$. We get

$$
1 = (\tilde{p} - p(1))\,(\tilde{q} - q(1)) \tag{D.24}
$$

so that we have $\aleph = 1$. Let us consider again the equation (D.22) evaluated in $x = s$. We get

$$
\tilde{p} - \langle p \rangle - s p(s) = \frac{1}{\tilde{q} - \langle q \rangle - s q(s)}, \tag{D.25}
$$

and using again eq. (D.19) evaluated at $x = s$ we get

$$
0 = m p_r^{(1)} q_r^{(2)} - s p(s) q(s) + (\tilde{p} - \langle p \rangle) q(s) + (\tilde{q} - \langle q \rangle) p(s) \tag{D.26}
$$

By solving the last two equations with respect to $\tilde{p} - \langle p \rangle$ and $p(s)$ we get

$$
\begin{aligned}
\tilde{p} - \langle p \rangle &= -\frac{s}{\tilde{q} - \langle q \rangle}\left[m p_r^{(1)} q_r^{(2)}\right] + \frac{1}{\tilde{q} - \langle q \rangle}\\
p(s) &= -\frac{1}{\tilde{q} - \langle q \rangle}\left[m p_r^{(1)} q_r^{(2)} + \frac{q(s)}{\tilde{q} - \langle q \rangle - s q(s)}\right]
\end{aligned} \tag{D.27}
$$

from which we obtain

$$
[p](x) = -\frac{[q](x)}{(\tilde{q} - \langle q \rangle)(\tilde{q} - \langle q \rangle - [q](x))} - \frac{s m p_r^{(1)} q_r^{(2)}}{\tilde{q} - \langle q \rangle}\,. \tag{D.28}
$$

Taking the derivative with respect to x we get

$$\dot{p}(x) = -\frac{1}{x}\frac{\mathrm{d}}{\mathrm{d}x}\frac{[q](x)}{(\tilde{q}-\langle q\rangle)(\tilde{q}-\langle q\rangle-[q](x))} \tag{D.29}$$

so that we have

$$\begin{aligned} p(x) &= p(s) - \int_s^x \mathrm{d}y \frac{1}{y}\frac{\mathrm{d}}{\mathrm{d}y}\frac{[q](y)}{(\tilde{q}-\langle q\rangle)(\tilde{q}-\langle q\rangle-[q](y))} \\ &= -\frac{1}{\tilde{q}-\langle q\rangle}\left[mp_r^{(1)}q_r^{(2)} + \frac{1}{x}\frac{[q](x)}{\tilde{q}-\langle q\rangle-[q](x)} + \int_s^x \frac{\mathrm{d}y}{y^2}\frac{[q](y)}{\tilde{q}-\langle q\rangle-[q](y)}\right] \end{aligned} \tag{D.30}$$

and finally, we get the solution for $\hat{p}$

$$\begin{aligned} \langle p\rangle &= -mp_r^{(1)}q_r^{(2)}\frac{1-s}{\tilde{q}-\langle q\rangle} - \frac{1}{\tilde{q}-\langle q\rangle}\int_s^1 \frac{\mathrm{d}y}{y^2}\frac{[q](y)}{\tilde{q}-\langle q\rangle-[q](y)} \\ \tilde{p} &= \frac{1}{\tilde{q}-\langle q\rangle}\left[1 - mp_r^{(1)}q_r^{(2)} - \int_s^1 \frac{\mathrm{d}y}{y^2}\frac{[q](y)}{\tilde{q}-\langle q\rangle-[q](y)}\right]. \end{aligned} \tag{D.31}$$

Let us now go back to the first four equations (D.14-D.17). We can use eq. (D.17) together with (D.27) to solve for $p_r^{(1)}$, and the remaining three equations (D.14)-(D.16) can be used to get p_d, p_g and $p_r^{(2)}$:

$$\begin{aligned} p_r^{(1)} &= -\frac{q_r^{(1)}}{q_d+(m-1)q_g}\left(\tilde{q}-\langle q\rangle - \frac{smq_r^{(1)}q_r^{(2)}}{q_d+(m-1)q_g}\right)^{-1} \\ p_r^{(2)} &= -\frac{q_r^{(2)}}{q_d+(m-1)q_g}\left(\tilde{q}-\langle q\rangle - \frac{smq_r^{(1)}q_r^{(2)}}{q_d+(m-1)q_g}\right)^{-1} \\ p_g &= -\frac{1}{q_d+(m-1)q_g}\left[\frac{q_g}{q_d-q_g} - \frac{sq_r^{(1)}q_r^{(2)}}{q_d+(m-1)q_g}\left(\tilde{q}-\langle q\rangle - \frac{smq_r^{(1)}q_r^{(2)}}{q_d+(m-1)q_g}\right)^{-1}\right] \\ p_d &= \frac{1}{q_d-q_g} - \frac{1}{q_d+(m-1)q_g} \\ &\quad\times\left[\frac{q_g}{q_d-q_g} - \frac{sq_r^{(1)}q_r^{(2)}}{q_d+(m-1)q_g}\left(\tilde{q}-\langle q\rangle - \frac{smq_r^{(1)}q_r^{(2)}}{q_d+(m-1)q_g}\right)^{-1}\right] \end{aligned} \tag{D.32}$$

Note that the inverse of a symmetric matrix ($q_r^{(1)} = q_r^{(2)}$) is symmetric as well. By inserting the expression of $p_r^{(1)}$ inside $\tilde{p}$ and $p(x)$ we end up with

$$\begin{aligned} \tilde{p} &= \frac{1}{\tilde{q}-\langle q\rangle}\left[1 + mq_r^{(2)}\frac{q_r^{(1)}}{q_d+(m-1)q_g}\left(\tilde{q}-\langle q\rangle - \frac{smq_r^{(1)}q_r^{(2)}}{q_d+(m-1)q_g}\right)^{-1}\right. \\ &\quad\left. - \int_s^1 \frac{\mathrm{d}y}{y^2}\frac{[q](y)}{\tilde{q}-\langle q\rangle-[q](y)}\right] \\ p(x) &= -\frac{1}{\tilde{q}-\langle q\rangle}\left[-mq_r^{(2)}\frac{q_r^{(1)}}{q_d+(m-1)q_g}\left(\tilde{q}-\langle q\rangle - \frac{smq_r^{(1)}q_r^{(2)}}{q_d+(m-1)q_g}\right)^{-1}\right. \\ &\quad\left. + \frac{1}{x}\frac{[q](x)}{\tilde{q}-\langle q\rangle-[q](x)} + \int_s^x \frac{\mathrm{d}y}{y^2}\frac{[q](y)}{\tilde{q}-\langle q\rangle-[q](y)}\right] \end{aligned} \tag{D.33}$$

and this completes the calculation of the inverse. We can now collect all the results. Firstly we have that

$$\log\det(\hat{\Delta}) = \log\det(\hat{\Delta}^g) + \log\det(\hat{\Omega})\,. \tag{D.34}$$

Using (D.5), the first term of the previous equation is easy and we get

$$\log\det\hat{\Delta}^g = \log(1-m) + m\log(-\Delta^g). \tag{D.35}$$

To evaluate the second term of the right hand side of eq (D.34), we use the expression (D.10). We have

$$\begin{aligned} \Omega_d - \langle\Omega\rangle &= s\frac{(\Delta^r)^2}{\Delta^g}\frac{m}{1-m} - \langle\Delta\rangle\,, \\ [\Omega]\,(y) &= s\frac{(\Delta^r)^2}{\Delta^g}\frac{m}{1-m} + [\Delta]\,(y), \end{aligned} \tag{D.36}$$

so that

$$\log\det(\hat{\Omega}) = s\log\left(s\frac{(\Delta^r)^2}{\Delta^g}\frac{m}{1-m} - \langle\Delta\rangle\right) - s\int_s^1 \frac{\mathrm{d}y}{y^2}\log\left(\frac{\langle\Delta\rangle + [\Delta](y)}{\langle\Delta\rangle - s\frac{(\Delta^r)^2}{\Delta^g}\frac{m}{1-m}}\right). \tag{D.37}$$

We now need to perform the sum of the elements of $\hat{\Delta}^{-1}$. By parametrizing the entries of $\hat{\Delta}^{-1}$ with the same form of (D.13) we get

$$\sum_{a,b=1}^{m+s}\left[\hat{\Delta}^{-1}\right]_{ab} = msp_r^{(1)} + msp_r^{(2)} + mp_d + m(m-1)p_g + s(\tilde{p} - \langle p\rangle). \tag{D.38}$$

Now, using eqs. (D.32) and (D.33) with

$$\begin{aligned} q_d &= 0, \\ q_g &= \Delta^g, \\ q_r^{(1)} &= q_r^{(2)} = \Delta_r, \\ \tilde{q} &= 0, \\ q(x) &= \Delta(x), \end{aligned} \tag{D.39}$$

we get

$$msp_r^{(1)} + msp_r^{(2)} = 2ms\left[\frac{\Delta^r}{(m-1)\Delta^g}\left(\langle\Delta\rangle + s\frac{(\Delta^r)^2}{\Delta^g}\frac{m}{m-1}\right)^{-1}\right], \tag{D.40}$$

while

$$mp_d = -\frac{m}{\Delta^g} - \frac{m}{(m-1)\Delta^g}\left[-1 + \frac{s(\Delta^r)^2}{(m-1)\Delta^g}\left(\langle\Delta\rangle + s\frac{(\Delta^r)^2}{\Delta^g}\frac{m}{m-1}\right)^{-1}\right], \tag{D.41}$$

and

$$m(m-1)p_g = -\frac{m(m-1)}{(m-1)\Delta^g}\left[-1 + \frac{s(\Delta^r)^2}{(m-1)\Delta^g}\left(\langle\Delta\rangle + s\frac{(\Delta^r)^2}{\Delta^g}\frac{m}{m-1}\right)^{-1}\right]. \tag{D.42}$$

The last term is then given by

$$s(\tilde{p} - \langle p \rangle) = -\frac{s}{\langle \Delta \rangle + s\frac{(\Delta^r)^2}{\Delta^g}\frac{m}{m-1}}. \tag{D.43}$$

And summing everything we finally obtain, with some trivial algebra

$$\sum_{a,b=1}^{m+s} \left[\hat{\Delta}^{-1}\right]_{ab} = \frac{m}{(m-1)\Delta^g} - s\left(\frac{m\Delta^r}{(m-1)\Delta^g} - 1\right)^2 \left(\langle \Delta \rangle + s\frac{(\Delta^r)^2}{\Delta^g}\frac{m}{m-1}\right)^{-1}. \tag{D.44}$$

The final expression of the entropic term for the replicated entropy is thus given by

$$\begin{aligned}
\frac{2}{d}s_{entr} &= (1-m-s)\log 2 - 2\log(m+s) + \log\left[\frac{m}{(1-m)\Delta^g}\right. \\
&\quad \left. + s\left(\frac{m\Delta^r}{(m-1)\Delta^g} - 1\right)^2 \left(\langle \Delta \rangle - s\frac{(\Delta^r)^2}{\Delta^g}\frac{m}{1-m}\right)^{-1}\right] \\
&\quad + \log(1-m) + m\log(\Delta^g) + s\log\left(\langle \Delta \rangle - s\frac{(\Delta^r)^2}{\Delta^g}\frac{m}{1-m}\right) \\
&\quad - s\int_s^1 \frac{\mathrm{d}y}{y^2}\log\left(\frac{\langle \Delta \rangle + [\Delta](y)}{\langle \Delta \rangle - s\frac{(\Delta^r)^2}{\Delta^g}\frac{m}{1-m}}\right) \\
&= (1-m-s)\log 2 - 2\log(m+s) + (m-1)\log\Delta^g \\
&\quad + \log[m\langle \Delta \rangle + 2ms\Delta^r + (1-m)s\Delta^g] - s\int_s^1 \frac{\mathrm{d}y}{y^2}\log\left[\langle \Delta \rangle + [\Delta](y)\right]
\end{aligned} \tag{D.45}$$

This completes the calculation of the entropic term. One can easily check that this expression reverts back to the result of appendix B when a RS profile $\Delta(x) = \Delta$ is chosen for the s block [2]. Taking the linear order in s of this expression (with some caution, remember for example that $\langle \Delta \rangle \equiv \int_s^1 dx\ \Delta(x)$, so it depends on s as well), one gets the first row of the (5.5).

D.2 Interaction term

We turn to the interaction term. The general expression we need to compute is the (B.16), which we recall here

$$\mathcal{F}_0(\hat{\Delta}) = \lim_{n\to 0} \sum_{n_1,\dots,n_k;\sum_{a=1}^k n_a = n} \frac{n!}{n_1!\dots n_k!} e^{\sum_{a=1}^k \frac{n_a}{n}\eta_a - \frac{1}{2}\sum_{a,b}^{1,k}\frac{n_a n_b}{n^2}\Delta_{ab}}.$$

By introducing Gaussian integrals, we can rewrite this term as [156]

$$\mathcal{F}_0(\hat{\Delta}) = \int_{-\infty}^{\infty} \mathrm{d}h\, e^h \frac{\mathrm{d}}{\mathrm{d}h}\left\{\exp\left[-\frac{1}{2}\sum_{a,b=1}^k \Delta_{ab}\frac{\partial^2}{\partial h_a \partial h_b}\right]\prod_{a=1}^{m+s}\theta(h_a)\right\}_{\{h_a = h-\eta_a\}}. \tag{D.46}$$

where $k = m+s$ and $\theta(x)$ is again the step Heaviside function [233]. Now we assume that the s-sector of the displacement matrix has a generic kRSB structure. Thus we have, following the derivation of [278] for the s block

$$\begin{aligned}
\mathcal{F}_0(\hat{\Delta}) = & \int_{-\infty}^{\infty} \mathrm{d}h\, \mathrm{e}^{h} \frac{\mathrm{d}}{\mathrm{d}h} \left\{ \exp\left[-\frac{1}{2} \sum_{a,b=1}^{m} \Delta_{ab} \frac{\partial^2}{\partial h_a \partial h_b} - \frac{1}{2} \sum_{a=1}^{m} \sum_{b=m+1}^{m+s} \Delta_{ab} \frac{\partial^2}{\partial h_a \partial h_b} \right.\right. \\
& \left.\left. -\frac{1}{2} \sum_{a=m+1}^{m+s} \sum_{b=1}^{m} \Delta_{ab} \frac{\partial^2}{\partial h_a \partial h_b} - \frac{1}{2} \sum_{a,b=m+1}^{m+s} \Delta_{ab} \frac{\partial^2}{\partial h_a \partial h_b} \right] \prod_{a=1}^{k} \theta(h_a) \right\}_{\{h_a = h - \eta_a\}} \\
= & \int_{-\infty}^{\infty} \mathrm{d}h\, \mathrm{e}^{h} \frac{\mathrm{d}}{\mathrm{d}h} \left\{ \exp\left[-\frac{1}{2} \Delta_g \left(\sum_{a=1}^{m} \frac{\partial}{\partial h_a} \right)^2 + \frac{\Delta_g}{2} \sum_{a=1}^{m} \frac{\partial^2}{\partial h_a^2} \right.\right. \\
& \left.\left. -\Delta_r \left(\sum_{a=1}^{m} \frac{\partial}{\partial h_a} \right) \left(\sum_{b=m+1}^{m+s} \frac{\partial}{\partial h_b} \right) - \frac{1}{2} \sum_{a,b=m+1}^{m+s} \Delta_{ab} \frac{\partial^2}{\partial h_a \partial h_b} \right] \prod_{a=1}^{k} \theta(h_a) \right\}_{\{h_a = h - \eta_a\}} \\
= & \int_{-\infty}^{\infty} \mathrm{d}h\, \mathrm{e}^{h} \frac{\mathrm{d}}{\mathrm{d}h} \left\{ \exp\left[-\frac{1}{2} \Delta_g \left(\sum_{a=1}^{m} \frac{\partial}{\partial h_a} \right)^2 - \Delta_r \left(\sum_{a=1}^{m} \frac{\partial}{\partial h_a} \right) \left(\sum_{b=m+1}^{m+s} \frac{\partial}{\partial h_b} \right) \right.\right. \\
& \left.\left. -\frac{1}{2} \sum_{a,b=m+1}^{m+s} \Delta_{ab} \frac{\partial^2}{\partial h_a \partial h_b} \right] \left(\prod_{a=1}^{m} \Theta\left(\frac{h_a}{\sqrt{2\Delta_g}} \right) \right) \left(\prod_{b=m+1}^{m+s} \theta(h_b) \right) \right\}_{\{h_a = h - \eta_a\}} \\
= & \int_{-\infty}^{\infty} \mathrm{d}h\, \mathrm{e}^{h} \frac{\mathrm{d}}{\mathrm{d}h} \left\{ \exp\left[-\frac{1}{2} \Delta_g \frac{\partial^2}{\partial h'^2} - \Delta_r \frac{\partial}{\partial h'} \frac{\partial}{\partial h''} - \frac{1}{2} \Delta_1 \frac{\partial^2}{\partial h''^2} \right] \right. \\
& \left. \times \left(\Theta\left(\frac{h'}{\sqrt{2\Delta_g}} \right) \right)^m g^{s/s_1}(s_1, h'' - \eta) \right\}_{h' = h'' = h}
\end{aligned} \tag{D.47}$$

where the function $g(x,h)$ is defined in terms of $f(x,h)$ as

$$f(x,h) \equiv \frac{1}{x} \log g(x,h) \tag{D.48}$$

Note that we have defined $\Delta(s) = \Delta_1$. At this point we can manipulate the last expression to do the final integrals by parts, giving an integral representation for the exponential of differential operators. We consider the differential operator

$$\hat{O} \equiv -\frac{1}{2} \Delta_g \frac{\partial^2}{\partial h'^2} - \Delta_r \frac{\partial}{\partial h'} \frac{\partial}{\partial h''} - \frac{1}{2} \Delta_1 \frac{\partial^2}{\partial h''^2} \tag{D.49}$$

and we introduce also

$$\hat{H} \equiv \frac{\partial}{\partial h'} + \frac{\partial}{\partial h''}; \tag{D.50}$$

we have then

$$\hat{O} = \frac{1}{2} \Delta_f \left(\frac{\partial}{\partial h''} \right)^2 - \frac{1}{2} (\Delta_f + \Delta_1) \hat{H} \frac{\partial}{\partial h''} - \frac{\Delta_g}{2} \hat{H} \frac{\partial}{\partial h'} \tag{D.51}$$

where we have defined $\Delta_f = 2\Delta_r - \Delta_1 - \Delta_g$. By plugging this expression into the interaction term we get

$$\mathcal{F}_0(\hat{\Delta}) = \int_{-\infty}^{\infty} \mathrm{d}h\, \mathrm{e}^h \frac{\mathrm{d}}{\mathrm{d}h} \left\{ \exp\left[\frac{1}{2}\Delta_f \left(\frac{\partial}{\partial h''} \right)^2 - \frac{1}{2}(\Delta_f + \Delta_1)\hat{H}\frac{\partial}{\partial h''} - \frac{\Delta_g}{2}\hat{H}\frac{\partial}{\partial h'} \right] \right. \\ \left. \times \left(\Theta\left(\frac{h'}{\sqrt{2\Delta_g}} \right) \right)^m g^{s/s_1}(s_1, h'' - \eta) \right\}_{h'=h''=h} . \tag{D.52}$$

Let us consider now a simple term of the form

$$\begin{aligned} &\int_{-\infty}^{\infty} \mathrm{d}h\, \mathrm{e}^h \frac{\mathrm{d}}{\mathrm{d}h} \left\{ \exp\left[A\hat{H}\frac{\partial}{\partial h''} \right] f(h', h'') \right\}_{h'=h''=h} \\ &= \int_{-\infty}^{\infty} \mathrm{d}h\, \mathrm{e}^h \frac{\mathrm{d}}{\mathrm{d}h} \sum_{k=0}^{\infty} \frac{1}{k!} A^k \hat{H}^k \frac{\partial^k}{\partial h''^k} f(h', h'') \Big|_{h'=h''=h} . \end{aligned} \tag{D.53}$$

By integrating by parts all the terms of the series expansion we get

$$\begin{aligned} &\int_{-\infty}^{\infty} \mathrm{d}h\, \mathrm{e}^h \frac{\mathrm{d}}{\mathrm{d}h} \left\{ \exp\left[A\hat{H}\frac{\partial}{\partial h''} \right] f(h', h'') \right\}_{h'=h''=h} \\ &= \int_{-\infty}^{\infty} \mathrm{d}h\, \mathrm{e}^h \frac{\mathrm{d}}{\mathrm{d}h} \sum_{k=0}^{\infty} \frac{1}{k!} (-A)^k \frac{\partial^k}{\partial h''^k} f(h', h'') \Big|_{h'=h''=h} \\ &= \int_{-\infty}^{\infty} \mathrm{d}h\, \mathrm{e}^h \frac{\mathrm{d}}{\mathrm{d}h} \left\{ \exp\left[-A\frac{\partial}{\partial h''} \right] f(h', h'') \right\}_{h'=h''=h} \\ &= \int_{-\infty}^{\infty} \mathrm{d}h\, \mathrm{e}^h \frac{\mathrm{d}}{\mathrm{d}h} \left\{ f(h', h - A) \right\}_{h'=h''=h} . \end{aligned} \tag{D.54}$$

Using this result we finally get for the entropic term

$$\begin{aligned} \mathcal{F}_0(\hat{\Delta}) = &\int_{-\infty}^{\infty} \mathrm{d}h\, \mathrm{e}^h \frac{\mathrm{d}}{\mathrm{d}h} \left\{ \exp\left[-\frac{1}{2}(\Delta_f + \Delta_1)\hat{H}\frac{\partial}{\partial h''} - \frac{\Delta_g}{2}\hat{H}\frac{\partial}{\partial h'} \right] \right. \\ &\left. \times \left(\Theta\left(\frac{h'}{\sqrt{2\Delta_g}} \right) \right)^m \gamma_{\Delta_f} \star g^{s/s_1}(s_1, h'' - \eta) \right\}_{h'=h''=h} = \\ = &\int_{-\infty}^{\infty} \mathrm{d}h\, \mathrm{e}^h \frac{\mathrm{d}}{\mathrm{d}h} \left\{ \left(\Theta\left(\frac{h + \Delta_g/2}{\sqrt{2\Delta_g}} \right) \right)^m \gamma_{\Delta_f} \star g^{s/s_1}(s_1, h - \eta + (\Delta_f + \Delta_1)/2) \right\} = \\ = &\int_{-\infty}^{\infty} \mathrm{d}h\, \mathrm{e}^h \left\{ 1 - \left(\Theta\left(\frac{h + \Delta_g/2}{\sqrt{2\Delta_g}} \right) \right)^m \gamma_{\Delta_f} \star g^{s/s_1}(s_1, h - \eta + (\Delta_f + \Delta_1)/2) \right\} . \end{aligned} \tag{D.55}$$

where we have used the definitions [156]

$$\mathrm{e}^{\frac{a}{2}\frac{\partial^2}{\partial h^2}} f(h) \equiv \gamma_a \star f(h) \qquad \gamma_a \star f(h) \equiv \int_{-\infty}^{\infty} \frac{\mathrm{d}z}{\sqrt{2\pi a}} \mathrm{e}^{-\frac{z^2}{2a}} f(h - z).. \tag{D.56}$$

We now have to take again the the linear order in s. We just have to expand the function g in the following way

$$g(s_1, h)^{s/s_1} \simeq 1 + \frac{s}{s_1} \log g(s_1, h) + O(s^2).$$

and then we have to send $s \to 0$. In doing so $k \to \infty$ as well, and both $\Delta(x)$ and $f(x, h)$ become continuous functions of x. The function f can then be shown [57, 278] to obey the equation (5.9)

$$\frac{\partial f}{\partial x} = \frac{1}{2}\frac{\mathrm{d}\Delta(x)}{\mathrm{d}x}\left[\frac{\partial^2 f}{\partial h^2} + x\left(\frac{\partial f}{\partial h}\right)^2\right],$$

with the boundary condition (5.10)

$$f(1, h) = \log\Theta\left(\frac{h}{\sqrt{2\Delta(1)}}\right),$$

and we get the interaction part of the (5.5).

D.3 Simplifications for $m = 1$

Before proceeding with the variational equations for $\hat{\Delta}$ we want to show that in the case in which the master replicas are taken at equilibrium, namely when $m = 1$, the form of the state-followed entropy can be much simplified. Indeed in this case Δ^g disappears from the equations.
It is quite easy to see this in the case of the entropic term of eq. (5.5) by remembering that $\Delta^f \equiv 2\Delta^r - \Delta(s) - \Delta^g$. It remains to verify that Δ^g disappears also from the interaction term. For $m = 1$ its general form is given by

$$\mathcal{F}(\widehat{\Delta}) = \int_{-\infty}^{\infty}\mathcal{D}\zeta\int_{-\infty}^{\infty}\mathrm{d}y\,\mathrm{e}^y\left\{1 - \Theta\left(\frac{y + \Delta^g/2}{\sqrt{2\Delta^g}}\right)\int_{-\infty}^{\infty}\mathrm{d}x\,\sigma(x + y)\frac{\mathrm{e}^{-\frac{1}{2\Delta_\gamma(\zeta)}(x - \Delta_\gamma(\zeta)/2)^2}}{\sqrt{2\pi\Delta_\gamma(\zeta)}}\right\},$$

where in our case the function $\sigma(x)$ is given by

$$\sigma(x) = g^{s/s_1}\left(s_1, x - \eta + \frac{\Delta_1}{2}\right). \tag{D.57}$$

This general form is valid for every replica-symmetry-breaking ansatz (the only difference is in the specific form of $\sigma(x)$). We then express the Θ function with its integral representation

$$\Theta\left(\frac{h + \Delta^g/2}{\sqrt{2\Delta^g}}\right) = \int_{-\infty}^{\infty}\frac{\mathrm{d}\lambda}{\sqrt{2\pi\Delta^g}}\mathrm{e}^{-\lambda^2/(2\Delta^g)}\theta\left(h + \frac{\Delta^g}{2} - \lambda\right) \tag{D.58}$$

to get

$$\mathcal{F}(\widehat{\Delta}) = \int_{-\infty}^{\infty}\mathcal{D}\zeta\int_{-\infty}^{\infty}\mathrm{d}x\mathrm{d}y\mathrm{d}\lambda\;\mathrm{e}^y\frac{\mathrm{e}^{-\frac{(\lambda + \Delta^g/2)^2}{2\Delta^g}}}{\sqrt{2\pi\Delta^g}}\frac{\mathrm{e}^{-\frac{(x - \Delta_\gamma(\zeta)/2)^2}{2\Delta_\gamma(\zeta)}}}{\sqrt{2\pi\Delta_\gamma(\zeta)}}\left[1 - \theta(y - \lambda)\sigma(x + y)\right]. \tag{D.59}$$

We now change integration variables in the following way:

$$\begin{cases} u = y + x \\ v = \lambda + x \\ w = x\,. \end{cases} \tag{D.60}$$

Note that the Jacobian of this change of coordinates is one so that we get

$$\mathcal{F}(\widehat{\Delta}) = \int_{-\infty}^{\infty} \mathcal{D}\zeta \int_{-\infty}^{\infty} \mathrm{d}u\mathrm{d}v\mathrm{d}w \; \mathrm{e}^{u-w} \frac{\mathrm{e}^{-\frac{(v-w+\Delta^g/2)^2}{2\Delta^g}}}{\sqrt{2\pi\Delta^g}} \frac{\mathrm{e}^{-\frac{(w-\Delta_\gamma(\zeta)/2)^2}{2\Delta_\gamma(\zeta)}}}{\sqrt{2\pi\Delta_\gamma(\zeta)}} [1-\theta(u-v)\sigma(u)]. \tag{D.61}$$

The integral on w can be easily done analytically, since it is just a convolution of two Gaussians. We obtain

$$\mathcal{F}(\widehat{\Delta}) = \int_{-\infty}^{\infty} \mathcal{D}\zeta \int_{-\infty}^{\infty} \mathrm{d}u\mathrm{d}v \; \mathrm{e}^{u} \frac{\mathrm{e}^{-\frac{(v+\Delta^g/2+\Delta_\gamma(\zeta)/2)^2}{2(\Delta^g+\Delta_\gamma(\zeta))}}}{\sqrt{2\pi(\Delta^g+\Delta_\gamma(\zeta))}} [1-\theta(u-v)\sigma(u)]\,. \tag{D.62}$$

Remembering that $\Delta_g + \Delta_f = 2\Delta_r - \Delta_1$, we get that Δ_g disappears from the expression. Using again (D.58) we get finally

$$\mathcal{F}(\widehat{\Delta}) = \int_{-\infty}^{\infty} \mathcal{D}\zeta \int_{-\infty}^{\infty} \mathrm{d}u \; \mathrm{e}^{u} \left\{ 1 - \Theta\left(\frac{u + (2\Delta_r + \gamma^2\zeta^2 - \Delta_1)/2}{\sqrt{2(2\Delta_r + \gamma^2\zeta^2 - \Delta_1)}} \right) \sigma(u) \right\}. \tag{D.63}$$

This expression is much simpler than the corresponding one with $m \neq 1$. We conclude by recalling that with a 1RSB ansatz the function σ would be given by

$$\sigma_{\mathrm{1RSB}}(u) = \Theta\left(\frac{u - \eta + \Delta_1/2}{\sqrt{2\Delta_1}} \right)^s, \tag{D.64}$$

and for the more general fullRSB case it is given by (D.57).

Appendix E

Variational equations in the fRSB ansatz

In this appendix we derive the variational equations for the optimization of the (5.5) with respect to $\Delta(x)$. Two routes are possible: one can start from the entropy of the $m+s$ replicas for a finite number of RSBs k, take the derivatives with respect to the Δ_i, and then take the $k \to \infty$ limit at the end to get the fRSB equations; alternatively, one can start directly from the (5.5), and obtain the equations by taking functional derivatives with respect to $\Delta(x)$. Here we use only this last procedure, introduced by Sommers and Dupont in [279], and refer to [2] for the computation for finite k.

E.1 Lagrange multipliers

In the formalism of [279], one introduces Lagrange multipliers in the expression of the entropy in order to enforce the Parisi equation (5.9) and its boundary condition (5.10). These Lagrange multipliers are called $P(x,h)$ and $P(1,h)$; we rewrite the relevant part of the free energy of the followed system (5.5) (we omit constant terms), adding the Lagrange multipliers

$$\begin{aligned}
\mathcal{S}_\infty = & \frac{1}{2}\log\left(\frac{\pi\langle\Delta\rangle}{d^2}\right) - \frac{1}{2}\int_0^1 \frac{dx}{x^2}\log\left(\frac{G(x)}{\langle\Delta\rangle}\right) + \frac{1}{2}\frac{m\Delta^f + \Delta^g}{m\langle\Delta\rangle} \\
& + \frac{\widehat{\varphi}_g}{2}\int_{-\infty}^{\infty} dh\; e^h \Theta\left(\frac{h+\Delta^g/2}{\sqrt{2\Delta^g}}\right)^m \\
& \times \int dx'\, f(0, x'+h-\eta+\Delta(0)/2)\frac{e^{-\frac{1}{2\Delta^f}\left(x'-\Delta^f/2\right)^2}}{\sqrt{2\pi\Delta^f}} \\
& + \frac{\widehat{\varphi}_g}{2}\int_0^1 dx \int_{-\infty}^{\infty} dh\; P(x,h)\left\{\dot{f}(x,h) - \frac{\dot{G}(x)}{2x}\left[f''(x,h) + x f'(x,h)^2\right]\right\} \\
& - \frac{\widehat{\varphi}_g}{2}\int_{-\infty}^{\infty} dh\; P(1,h)\left\{f(1,h) - \log\Theta\left(\frac{h}{\sqrt{2G(1)}}\right)\right\},
\end{aligned} \tag{E.1}$$

where we have defined the function

$$G(x) \equiv x\Delta(x) + \int_x^1 dy\ \Delta(y). \tag{E.2}$$

We start from the equation for Δ_f. We easily get

$$\begin{aligned} 0 = &\frac{1}{\langle\Delta\rangle} + \frac{\widehat{\varphi}_g}{2}\int dh\, e^h \Theta\left(\frac{h+\Delta^g/2}{\sqrt{2\Delta^g}}\right)^m \\ &\times \int dx\, f'(0, x+h-\eta+\Delta(0)/2)\left(\frac{x+\Delta_f/2}{\Delta_f}\right)\frac{e^{-\frac{1}{2\Delta^f}\left(x-\Delta^f/2\right)^2}}{\sqrt{2\pi\Delta^f}}. \end{aligned} \tag{E.3}$$

We must now take the functional derivatives of the $\mathcal{S}_\infty$. Taking the ones with respect to $P(x,h)$ and $f(x,h)$ we get

$$\dot{f}(x,h) = \frac{\dot{G}(x)}{2x}\left[f''(x,h) + xf'(x,h)^2\right], \tag{E.4}$$

$$\dot{P}(x,h) = -\frac{\dot{G}(x)}{2x}\left[P''(x,h) - 2x(P(x,h)f'(x,h))'\right], \tag{E.5}$$

where we have used the apex to denote the derivative with respect to h, and the dot for the one with respect to x. We must now differentiate with respect to $f(0,h)$, which is contained in the third line and in the boundary term of the fourth line (we can make it explicit with an integration by parts over x). We get the initial condition for the function $P(x,h)$:

$$P(0,h) = e^{h+\eta-\Delta(0)/2}\int_{-\infty}^{\infty} dx \frac{e^{-\frac{(x+\Delta_f/2)^2}{2\Delta_f}}}{\sqrt{2\pi\Delta_f}}\Theta\left(\frac{h-x+\eta-\Delta(0)/2+\Delta_g/2}{\sqrt{2\Delta_g}}\right)^m. \tag{E.6}$$

for generic m. For $m=1$ we can use the results of section D.3 to get

$$P(0,h) = e^{h+\eta-\Delta(0)/2}\Theta\left(\frac{h+\eta+\Delta_r-\Delta(0)}{\sqrt{2(2\Delta_r-\Delta(0))}}\right), \tag{E.7}$$

while in presence of shear we get, using the (4.14).

$$P(0,h) = e^{h+\eta-\Delta(0)/2}\int_{-\infty}^{\infty} d\zeta\ \frac{e^{-\frac{\zeta^2}{2}}}{\sqrt{2\pi}}\Theta\left(\frac{h+\eta+\Delta_r+\zeta^2\gamma^2/2-\Delta(0)}{\sqrt{2(2\Delta_r+\zeta^2\gamma^2-\Delta(0))}}\right) \tag{E.8}$$

We now differentiate with respect to $G(x)$, $x\neq 0$, $x\neq 1$. We must integrate by parts the term proportional to $\dot{G}(x)$ in the fourth line, and use equations (E.4) and (E.5). We must not forget that the second line depends as well on $G(x)$ through $\Delta(0)$, as [156]

$$\Delta(x) = \frac{G(x)}{x} - \int_x^1 dz\ \frac{G(z)}{z^2}. \tag{E.9}$$

Surprisingly, the terms which contain $\langle\Delta\rangle$ give no contribution since $\frac{\delta\langle\Delta\rangle}{\delta G(x)} = 0$, as can be checked using the (E.9):

$$\begin{aligned}\frac{\delta\langle\Delta\rangle}{\delta G(x)} &= \frac{\delta}{\delta G(x)}\left(\int_0^1 dy\frac{G(y)}{y} - \int_0^1 dy\int_y^1\frac{dz}{z^2}G(z)\right)\\ &= \frac{\delta}{\delta G(x)}\left(\int_0^1 dy\frac{G(y)}{y} - \int_0^1 dy\int_0^1\frac{dz}{z^2}G(z)\theta(z-y)\right)\\ &= \frac{1}{x} - \frac{1}{x^2}\int_0^1 dy\ \theta(x-y) = \frac{1}{x} - \frac{1}{x^2}x = 0.\end{aligned} \tag{E.10}$$

So we get

$$\begin{aligned}\frac{1}{G(x)} =& -\frac{\widehat{\varphi}_g}{2}\int_{-\infty}^{\infty} dh\ P(x,h)f''(x,h) - \frac{\widehat{\varphi}_g}{2}\int_{-\infty}^{\infty} dh\ e^h\Theta\left(\frac{h+\Delta^g/2}{\sqrt{2\Delta^g}}\right)^m\\ &\times\int dy\, f'(0,y+h-\eta+\Delta(0)/2)\frac{e^{-\frac{1}{2\Delta^f}\left(y-\Delta^f/2\right)^2}}{\sqrt{2\pi\Delta^f}}\\ =& -\frac{\widehat{\varphi}_g}{2}\int_{-\infty}^{\infty} dh\ P(x,h)f''(x,h) - \frac{\widehat{\varphi}_g}{2}\int_{-\infty}^{\infty} dh\ P(0,h)f'(0,h),\end{aligned} \tag{E.11}$$

where we have made a translational change of coordinates over h and used the definition of $P(0,h)$ in the second term. Finally, we focus on the boundary term at $x = 0$ and we differentiate with respect to $G(0) = \langle\Delta\rangle$. We remember the reader that

$$\frac{\delta G(x)}{\delta G(y)} = \delta(x-y). \tag{E.12}$$

Let us start with the entropic term. We get

$$\begin{aligned}\frac{\delta\mathcal{S}_\infty^{entr}}{\delta G(0)} &= \left[\frac{1}{G(0)} + \int_0^1\frac{dx}{x^2}\frac{1}{G(0)} - \frac{m\Delta_f+\Delta_g}{mG(0)^2}\right]\delta(0)\\ &= \left[\lim_{x\to 0^+}\frac{1}{xG(0)} - \frac{m\Delta_f+\Delta_g}{mG(0)^2}\right]\delta(0).\end{aligned} \tag{E.13}$$

We stress the fact that the boundary term for $x = 0$ in the integral part of the entropic term does not depend on $G(0)$, so it gives no contribution.
For what concerns the interaction term, we must first differentiate the third line with respect to $G(0)$ through its dependence on $\Delta(0)$. We have, using the (E.9):

$$\frac{\delta\Delta(0)}{\delta G(0)} = \lim_{x\to 0^+}\frac{1}{x}\delta(0). \tag{E.14}$$

then we have to take the boundary term for $x = 0$ in the fourth line, again integrating it by parts. The final result is, for the interaction term

$$\begin{aligned}\frac{\delta\mathcal{S}_\infty^{int}}{\delta G(0)} =& \left[\lim_{x\to 0^+}\frac{\widehat{\varphi}_g}{2x}\int_{-\infty}^{\infty} dh\ P(0,h)f'(0,h) + \lim_{x\to 0^+}\frac{\widehat{\varphi}_g}{2x}\int_{-\infty}^{\infty} dh\ P(0,h)f''(0,h)\right.\\ &\left.+\frac{\widehat{\varphi}_g}{2}\int_{-\infty}^{\infty} dh\ P(0,h)f'(0,h)^2\right]\delta(0).\end{aligned} \tag{E.15}$$

We can now put the two terms together. Using the (E.3) (or equivalently, the (E.11) for $x = 0$) to eliminate the term in $\frac{1}{G(0)}$, we finally get

$$\frac{m\Delta_f + \Delta_g}{m \langle \Delta \rangle^2} = \frac{\widehat{\varphi}_g}{2} \int_{-\infty}^{\infty} dh P(0,h) f'(0,h)^2. \tag{E.16}$$

This completes the derivation of the variational equations. We now have an equation to fix every variable.

In summary, the equations we have to use are

$$\dot{f}(x,h) = \frac{\dot{G}(x)}{2x} \left[f''(x,h) + x f'(x,h)^2 \right], \tag{E.17}$$

$$\dot{P}(x,h) = -\frac{\dot{G}(x)}{2x} \left[P''(x,h) - 2x(P(x,h)f'(x,h))' \right] \tag{E.18}$$

$$\frac{1}{G(x)} = -\frac{\widehat{\varphi}_g}{2} \int_{-\infty}^{\infty} dh \; [P(x,h)f''(x,h) + P(0,h)f'(0,h)], \tag{E.19}$$

$$\frac{m\Delta_f + \Delta_g}{m \langle \Delta \rangle^2} = \frac{\widehat{\varphi}_g}{2} \int_{-\infty}^{\infty} dh \; P(0,h) f'(0,h)^2. \tag{E.20}$$

The procedure to solve them is as follows:

- One starts from a guess for Δ_f and $G(x)$.
- Then we solve the (E.4) and (E.5), with the boundary conditions (5.10) and (E.6).
- Then we compute the new $G(x)$ and Δ_f using the (E.16) and (E.11).
- Repeat until the procedure converges.

E.2 A different equation for $G(x)$

We show here that the equation for $G(x)$ can be recast in the form:

$$\begin{aligned} \frac{1}{G(x)} &= \frac{1}{\langle \Delta \rangle} + \frac{\widehat{\varphi}_g}{2} \int_{-\infty}^{\infty} dh \; \left[x P(x,h) f'(x,h)^2 - \int_0^x dz \; P(z,h) f'(z,h)^2 \right], \\ \frac{1}{G(x)} &= \frac{1}{\langle \Delta \rangle} + x\kappa(x) - \int_0^x dy \; \kappa(y), \end{aligned} \tag{E.21}$$

where we have defined

$$\kappa(x) \equiv \frac{\widehat{\varphi}_g}{2} \int_{-\infty}^{\infty} \mathrm{d}h \, P(x,h) \left(f'(x,h) \right)^2 , \tag{E.22}$$

which is more convenient for the purpose of the scaling analysis near jamming, paragraph E.3. As in [156], we show that equations (E.11) and (E.21) are the same for $x = 0$ and then we show that their derivatives of every order with respect to x coincide. For $x = 0$ it is trivial as the integral term in the (E.21) is zero, so that

$$-\frac{\widehat{\varphi}_g}{2} \int_{-\infty}^{\infty} dh \; [P(0,h)f''(0,h) + P(0,h)f'(0,h)] = \frac{1}{\langle \Delta \rangle}, \tag{E.23}$$

which is just the (E.19) for $x = 0$. For what concerns the derivative, we proceed and use the same notation as in [156]. From the (E.11) we get

$$\dot{P}f'' + P\dot{f}'' \sim \dot{P}f'' + P''\dot{f} \sim \frac{\dot{G}}{2x}[(2x(Pf')' - P'')f'' + P''(f'' + xf'^2)] \sim \dot{G}P(f'')^2, \tag{E.24}$$

and from the (E.21) we get

$$x\dot{P}f'^2 + 2xPf'\dot{f}' \sim \frac{\dot{G}}{2}[(2x(Pf')' - P'')f'^2 + 2Pf'(f''' + 2xf'f'')] \sim -\dot{G}P(f'')^2. \tag{E.25}$$

Where $a \sim b \implies \int dh\ a(x,h) = \int dh\ b(x,h)$ and we have used the equations for f and P. We have thus proven that equations (E.21) and (E.11) are equivalent.

E.3 Scaling analysis near jamming

We show now that once the glass state is followed in compression up to the jamming point, the solution on the fullRSB equations develops a scaling regime characterized by a set of critical exponents that coincide with the ones computed in [156]. The proof will be given by showing that the scaling equations close to jamming, and the asymptotic behavior of their initial conditions are the same as those that had been obtained in [156]; the values of the critical exponents follow directly from these requirements.

E.3.1 Scaling form of the equations

On approaching the jamming point, the mean square displacement $\Delta_{EA} \equiv \Delta(1)$ of the fRSB microstates at the bottom of the hierarchy goes to zero. We thus define the jamming limit as $\Delta(1) \equiv \Delta_{EA} \to 0$. Moreover we expect that Δ^f stays finite. We want to show that the fullRSB equations develop a scaling regime. At jamming the pressure diverges as $1/p \propto \Delta_{EA}^{1/\kappa}$ [149, 156] and we want to determine κ. We thereby define the following scaling variables and functions (we omit the subscript EA to lighten the notation):

$$y \equiv \Delta_{EA}^{-\frac{1}{\kappa}} x, \tag{E.26}$$

$$\widehat{f}(y,h) \equiv \Delta^{\frac{1}{\kappa}} f(\Delta^{\frac{1}{\kappa}} y, h), \tag{E.27}$$

$$\gamma(y) \equiv \frac{G(\Delta^{\frac{1}{\kappa}} y)}{\Delta^{\frac{1}{\kappa}}}, \tag{E.28}$$

$$\widehat{P}(y,h) \equiv e^{-h-\eta} P(\Delta^{\frac{1}{\kappa}} y, h)\,. \tag{E.29}$$

The initial conditions for the new functions $\widehat{f}$ and $\widehat{P}$ are therefore

$$\widehat{P}(0,h) = e^{-\Delta(0)/2} \int_{-\infty}^{\infty} dx \frac{e^{-\frac{(x+\Delta_f)^2}{2\Delta_f}}}{\sqrt{2\pi\Delta_f}} \Theta\left(\frac{h - x + \eta - \Delta(0)/2 + \Delta_g/2}{\sqrt{2\Delta_g}}\right)^m,$$

$$\widehat{f}(1/\Delta^{\frac{1}{\kappa}}, h) = \Delta^{\frac{1}{\kappa}} \log \Theta\left(\frac{h}{\sqrt{2\Delta^{\frac{1}{\kappa}}\gamma(1/\Delta^{\frac{1}{\kappa}})}}\right),$$

and the relation between $\Delta(y)$ and $\gamma(y)$ becomes

$$\Delta(y) = \frac{\gamma(y)}{y} - \int_y^{1/\Delta^{\frac{1}{\kappa}}} \frac{dz}{z^2}\gamma(z). \tag{E.30}$$

Using the same reasoning, the variational equations for the scaling functions are:

$$\begin{aligned}
\frac{\partial \widehat{f}(y,h)}{\partial y} &= \frac{\dot{\gamma}(y)}{2y}\left[\frac{\partial^2 \widehat{f}(y,h)}{\partial h^2} + y\left(\frac{\partial \widehat{f}(y,h)}{\partial h}\right)^2\right], \\
\frac{\partial \widehat{P}(y,h)}{\partial y} &= -e^{-h}\frac{\dot{\gamma}(y)}{2y}\left[\frac{\partial^2 [e^h \widehat{P}(y,h)]}{\partial h^2} - 2y\frac{\partial}{\partial h}\left(e^h \widehat{P}(y,h)\frac{\partial \widehat{f}(y,h)}{\partial h}\right)\right] \\
\frac{1}{\gamma(y)} &= \frac{1}{\langle\Delta\rangle} + y\kappa(y) - \int_0^y dz\ \kappa(z) \\
\frac{m\Delta_f + \Delta_g}{m\langle\Delta\rangle^2} &= \kappa(0) \\
\kappa(y) &= \frac{\widehat{\varphi}_g e^{\eta}}{2}\int_{-\infty}^{\infty} dh\ e^h \widehat{P}(y,h)\widehat{f}'(y,h)^2,
\end{aligned}$$

which are very close to those obtained in [156]. The entropy, for its part, is rephrased in

$$\begin{aligned}
\mathcal{S} = \frac{1}{2}\log\left(\frac{\pi\langle\Delta\rangle}{d^2}\right) + \frac{1}{2}\log(\Delta^{\frac{1}{\kappa}}) + \frac{1}{\Delta^{\frac{1}{\kappa}}}\Bigg[-\frac{1}{2}\int_0^{1/\Delta^{\frac{1}{\kappa}}}\frac{dy}{y^2}\log\left(\frac{\gamma(y)}{\langle\Delta\rangle}\right) \\
+\frac{1}{2}\frac{m\Delta_f + \Delta_g}{m\langle\Delta\rangle} + \frac{\widehat{\varphi}_g e^{\eta}}{2}\int_{-\infty}^{\infty} dh\ e^h \widehat{P}(0,h)\widehat{f}(0,h)\Bigg],
\end{aligned} \tag{E.31}$$

where now $\langle\Delta\rangle$ is defined as

$$\langle\Delta\rangle = \int_0^{1/\Delta^{\frac{1}{\kappa}}} dy\ \Delta(y). \tag{E.32}$$

We expect that the entropy diverges as $\log 1/p \simeq \log \Delta^{\frac{1}{\kappa}}$. This means that the term between square parentheses on the right hand side of (E.32) must vanish. This gives a condition for the jamming point η_J as in the RS case (paragraph 4.3.1).

E.3.2 Asymptotes and scaling of $\widehat{P}$ and $\widehat{f}$

In order to show that the scaling equations (E.31) have the same critical exponents as the ones derived in [156] we need to show that the asymptotic behavior for $h \to \pm\infty$ of the initial conditions for $\widehat{f}$ and $\widehat{P}$ coincides with the one of [156]. We start from the $\widehat{f}$. Since the boundary condition for $\widehat{f}$ is the same as the one in [156], it trivially follows that also the asymptotic behavior is the same. Indeed we have

$$\widehat{f}(1/\Delta^{\frac{1}{\kappa}}, h \to -\infty) = -h^2/(2\gamma(1/\Delta^{\frac{1}{\kappa}})), \tag{E.33}$$

$$\widehat{f}(1/\Delta^{\frac{1}{\kappa}}, h \to \infty) = 0, \tag{E.34}$$

and by inserting this asymptotes in the equation for $\widehat{f}$ we get,

$$\widehat{f}(y, h \to -\infty) = -h^2/(2\gamma(y)), \tag{E.35}$$
$$\widehat{f}(y, h \to \infty) = 0, \tag{E.36}$$

as in [156]. Conversely, the boundary condition for $\widehat{P}$ is not the same as in [156]. However one can easily see that the asymptotic behavior is still the same. In fact, we have for $y = 0$

$$\widehat{P}(0, h \to -\infty) = A(0)e^{B(0)h - D(0)h^2} \tag{E.37}$$
$$\widehat{P}(0, h \to \infty) = e^{-\Delta(0)/2}, \tag{E.38}$$

thanks to the fact that our $\widehat{P}(0, h)$ is the convolution of a Θ function with a normalized Gaussian. We can again plug these asymptotes (and those of $\widehat{f}$) in the equation for $\widehat{P}$ in (E.31), to get

$$\widehat{P}(0, h \to -\infty) = A(y)e^{B(y)h - D(y)h^2} \tag{E.39}$$
$$\widehat{P}(0, h \to \infty) = e^{-\Delta(y)/2}, \tag{E.40}$$

where the equations for A, B and D are the same as in [156].

We now look for a solution for $\widehat{P}$ and $\widehat{f}$ at large y. We conjecture that $\Delta(y) \simeq \Delta_\infty y^{-\kappa}$ for large y, which through the (E.30) implies that $\gamma(y) \simeq \gamma_\infty y^{-c}$ with $c = \kappa - 1$ and $\gamma_\infty = \frac{\kappa}{\kappa-1}\Delta_\infty$. We can then solve the equations for A, B and D for large y, and we get for $h \to -\infty$

$$\widehat{P}(y, h) = A_\infty y^c e^{B_\infty h^c y^c - D_\infty h^2 y^{2c}} = y^c p_0(hy^c). \tag{E.41}$$

We can thus conjecture for $\widehat{P}$ the same exact scaling that was used in [156]:

$$\widehat{P}(y, h) \simeq \begin{cases} y^c p_0(hy^c) & h \simeq -y^{-c} \\ y^a p_1(hy^b) & |h| \simeq y^{-b} \\ p_2(h) & h \gg y^{-b}\,. \end{cases} \tag{E.42}$$

This scaling in turn requires that the function $p_1(z)$ must obey the boundary conditions

$$p_1(z) = \begin{cases} z^\theta & z \to \infty \\ z^{-\alpha} & z \to -\infty \end{cases} \tag{E.43}$$

where $\theta \equiv \frac{c-a}{b-c}$ and $\alpha = \frac{a}{b}$, as in [156] and [280].

For what concerns the $\widehat{f}$, we define as in [156] a function

$$\widehat{j}(y, h) \equiv \widehat{f}(y, h) + \frac{h^2\theta(-h)}{2\gamma(y)}. \tag{E.44}$$

Using the equation for $\widehat{f}$ it is easy to see that, for all y

$$\widehat{j}(y, h \to -\infty) = \int_y^\infty \frac{du}{2u}\frac{\dot{\gamma}(u)}{\gamma(u)}, \tag{E.45}$$
$$\widehat{j}(y, h \to \infty) = 0. \tag{E.46}$$

For large y, again $\gamma(y) \simeq \gamma_\infty y^{-c}$, which means $\widehat{j}(y, h \to -\infty) \simeq -c/(2y)$. So we can again conjecture the scaling form

$$\widehat{j}(y,h) = -\frac{c}{2y} J(hy^b/\sqrt{\gamma_\infty}). \tag{E.47}$$

with the boundary conditions $J(-\infty) = 1$ and $J(\infty) = 0$.

Now that we have the boundary conditions for the functions J and p_1, all that we have to do is to plug them into the equations for $\widehat{P}$ and $\widehat{f}$ in order to get the equations for p_1 and J: since the scaling equations are the same as in [156] we get the same equations for p_1 and J. The final step to show that the critical exponents here are the same as in [156] is to show that the *marginal stability* equation for the replicon mode is the same [156]. In order to achieve this we can start from equation (E.21) and consider the quantity

$$\kappa(x) = \frac{\widehat{\varphi}_g}{2} \int_{-\infty}^{\infty} \mathrm{d}h \, P(x,h) \left(f'(x,h)\right)^2 \, . \tag{E.48}$$

By taking the derivative with respect to x and assuming that we are in a fullRSB region such that $x > 0$ and $\dot{G}(x) \neq 0$ we get

$$1 = \frac{\widehat{\varphi}_g}{2} \int_{-\infty}^{\infty} \mathrm{d}h \, P(x,h) \left(G(x) f''(x,h)\right)^2 \tag{E.49}$$

This equation is the same as the starting point that has been used in [156] in order to close the system of equations for the critical exponents at jamming, and it can be shown [156] that implies both the marginality of the replicon mode everywhere in the fRSB phase [247], and the isostaticity of jammed packings [156].
We conclude that the scaling behavior of the solution of (E.31) is the same as the one found in [156], thus proving that the critical exponents a, b and c and κ, θ and γ are the same as in [156].

Bibliography

[1] C. Rainone, P. Urbani, H. Yoshino, F. Zamponi, "Following the Evolution of Hard Sphere Glasses in Infinite Dimensions under External Perturbations: Compression and Shear Strain", *Phys. Rev. Lett.* **2015**, *114*, 015701.

[2] C. Rainone, P. Urbani, "Following the evolution of glassy states under external perturbations: the full replica symmetry breaking solution", *ArXiv e-prints* **Dec. 2015**.

[3] M. S. Mariani, G. Parisi, C. Rainone, "Calorimetric glass transition in a mean-field theory approach", *Proceedings of the National Academy of Sciences* **2015**, *112*, 2361–2366.

[4] P. Charbonneau et al., "Numerical detection of the Gardner transition in a mean-field glass former", *Phys. Rev. E* **2015**, *92*, 012316.

[5] A. Cavagna, "Supercooled liquids for pedestrians", *Physics Reports* **2009**, *476*, 51 –124.

[6] C. Angell, P. Poole, J. Shao, "Glass-forming liquids, anomalous liquids, and polyamorphism in liquids and biopolymers", English, *Il Nuovo Cimento D* **1994**, *16*, 993–1025.

[7] J. C. Dyre, "Colloquium: The glass transition and elastic models of glass-forming liquids", *Rev.Mod.Phys.* **2006**, *78*, 953.

[8] M. Cates, English in *Slow Relaxations and nonequilibrium dynamics in condensed matter*, (Eds.: J.-L. Barrat, M. Feigelman, J. Kurchan, J. Dalibard), Les Houches-École d'Été de Physique Theorique, Springer Berlin Heidelberg, **2003**, pp. 75–129.

[9] F Sausset, G Biroli, J Kurchan, "Do solids flow?", *Journal of Statistical Physics* **2010**, *140*, 718–727.

[10] H. Vogel, "Das temperaturabhängigkeitsgesetz der viskosität von flüssigkeiten", *Phys. Z* **1921**, *22*, 645–646.

[11] G. S. Fulcher, "Analysis of recent measurements of the viscosity of glasses", *Journal of the American Ceramic Society* **1925**, *8*, 339–355.

[12] G. Tammann, W Hesse, "Die Abhängigkeit der Viscosität von der Temperatur bie unterkühlten Flüssigkeiten", *Zeitschrift für anorganische und allgemeine Chemie* **1926**, *156*, 245–257.

[13] F Stickel, E. W. Fischer, R. Richert, "Dynamics of glass-forming liquids. I. Temperature-derivative analysis of dielectric relaxation data", *The Journal of chemical physics* **1995**, *102*, 6251–6257.

[14] Y. S. Elmatad, D. Chandler, J. P. Garrahan, "Corresponding states of structural glass formers", *The Journal of Physical Chemistry B* **2009**, *113*, 5563–5567.

[15] H Bässler, "Viscous flow in supercooled liquids analyzed in terms of transport theory for random media with energetic disorder", *Physical review letters* **1987**, *58*, 767.

[16] E. A. A. Pogna et al., "Probing equilibrium glass flow up to exapoise viscosities", *Proceedings of the National Academy of Sciences* **2015**, *112*, 2331–2336.

[17] T. Hecksher, A. I. Nielsen, N. B. Olsen, J. C. Dyre, "Little evidence for dynamic divergences in ultraviscous molecular liquids", *Nature Physics* **2008**, *4*, 737–741.

[18] J.-P. Hansen, I. R. McDonald, *Theory of Simple Liquids, Third Edition*, Academic Press, 3rd ed., **Apr. 2006**.

[19] W. Kob, English in *Slow Relaxations and nonequilibrium dynamics in condensed matter*, (Eds.: J.-L. Barrat, M. Feigelman, J. Kurchan, J. Dalibard), Les Houches-École d'Été de Physique Theorique, Springer Berlin Heidelberg, **2003**, pp. 199–269.

[20] J. Zinn-Justin, *Quantum field theory and critical phenomena*, Oxford University Press, Oxford, **2002**.

[21] L. F. Cugliandolo in *Slow Relaxations and nonequilibrium dynamics in condensed matter*, Springer, **2003**, pp. 367–521.

[22] W. Kob, H. C. Andersen, "Testing mode-coupling theory for a supercooled binary Lennard-Jones mixture. II. Intermediate scattering function and dynamic susceptibility", *Physical Review E* **1995**, *52*, 4134.

[23] L. Berthier, G. Biroli, "Theoretical perspective on the glass transition and amorphous materials", *Rev. Mod. Phys.* **2011**, *83*, 587–645.

[24] W. Kob, H. C. Andersen, "Testing mode-coupling theory for a supercooled binary Lennard-Jones mixture I: The van Hove correlation function", *Phys. Rev. E* **1995**, *51*, 4626–4641.

[25] G. Biroli, J. Bouchaud in Structural Glasses and Supercooled Liquids: Theory, Experiment and Applications, (Eds.: P.G.Wolynes, V.Lubchenko), Wiley & Sons, **2012**.

[26] T. Kirkpatrick, D Thirumalai, "Comparison between dynamical theories and metastable states in regular and glassy mean-field spin models with underlying first-order-like phase transitions", *Physical Review A* **1988**, *37*, 4439.

[27] C Dasgupta, A. Indrani, S. Ramaswamy, M. Phani, "Is there a growing correlation length near the glass transition?", *EPL: Europhysics Letters* **1991**, *15*, 307–312.

[28] S. Franz, C. Donati, G. Parisi, S. C. Glotzer, "On dynamical correlations in supercooled liquids", *Philosophical Magazine B* **1999**, *79*, 1827–1831.

[29] C. Toninelli et al., "Dynamical susceptibility of glass formers: Contrasting the predictions of theoretical scenarios", *Physical Review E* **2005**, *71*, 041505.

[30] L. Berthier et al., "Direct experimental evidence of a growing length scale accompanying the glass transition", *Science* **2005**, *310*, 1797–1800.

[31] E. Flenner, G. Szamel, "Dynamic Heterogeneity in a Glass Forming Fluid: Susceptibility, Structure Factor, and Correlation Length", *Phys. Rev. Lett.* **2010**, *105*, 217801.

[32] S. Karmakar, C. Dasgupta, S. Sastry, "Growing length and time scales in glass-forming liquids", *Proceedings of the National Academy of Sciences* **2009**, *106*, 3675–3679.

[33] M. D. Ediger, "Spatially heterogeneous dynamics in supercooled liquids", *Annual review of physical chemistry* **2000**, *51*, 99–128.

[34] L. Berthier et al., *Dynamical heterogeneities in glasses, colloids, and granular media*, Oxford University Press, **2011**.

[35] M. D. Ediger, C. A. Angell, S. R. Nagel, "Supercooled liquids and glasses", *J.Phys.Chem.* **1996**, *100*, 13200–13212.

[36] W Götze, J. Hansen, D Levesque, J Zinn-Justin, Liquids, freezing and the glass transition, **1991**.

[37] P. G. Debenedetti, *Metastable liquids: concepts and principles*, Princeton University Press, **1996**.

[38] K. Binder, W. Kob, *Glassy materials and disordered solids: An introduction to their statistical mechanics*, World Scientific, **2005**.

[39] L. Leuzzi, T. M. Nieuwenhuizen, *Thermodynamics of the glassy state*, Taylor & Francis, New York, **2008**.

[40] W. Götze, *Complex dynamics of glass-forming liquids: a mode-coupling theory*, Oxford University Press, Oxford, **2009**.

[41] P. Charbonneau et al., "Fractal free energies in structural glasses", *Nature Communications* **2014**, *5*, 3725.

[42] A. Liu, S. Nagel, W. Van Saarloos, M. Wyart in Dynamical Heterogeneities and Glasses, (Eds.: L. Berthier et al.), Oxford University Press, **2011**.

[43] A. J. Liu, S. R. Nagel, "Nonlinear dynamics: Jamming is not just cool any more", *Nature* **1998**, *396*, 21–22.

[44] G. Biroli, "Jamming: A new kind of phase transition?", *Nature Physics* **2007**, *3*, 222–223.

[45] C. Rainone, "The replica method in liquid theory: from the basics to explicit computations", *arXiv preprint arXiv:1411.3941* **2014**.

[46] D. J. Thouless, P. W. Anderson, R. G. Palmer, "Solution of 'Solvable model of a spin glass'", *Philosophical Magazine* **1977**, *35*, 593–601.

[47] J. P. Stoessel, P. G. Wolynes, "Linear excitations and the stability of the hard sphere glass", *The Journal of Chemical Physics* **1984**, *80*, 4502–4512.

[48] Y. Singh, J. P. Stoessel, P. G. Wolynes, "Hard-Sphere Glass and the Density-Functional Theory of Aperiodic Crystals", *Phys. Rev. Lett.* **1985**, *54*, 1059–1062.

[49] P. Chaudhuri et al., "Equilibrium Glassy Phase in a Polydisperse Hard-Sphere System", *Physical Review Letters* **2005**, *95*, 248301.

[50] P. Chaudhuri, S. Karmakar, C. Dasgupta, "Signatures of dynamical heterogeneity in the structure of glassy free-energy minima", *Physical review letters* **2008**, *100*, 125701.

[51] U. Bengtzelius, W Gotze, A Sjolander, "Dynamics of supercooled liquids and the glass transition", *Journal of Physics C: solid state Physics* **1984**, *17*, 5915.

[52] E Leutheusser, "Dynamical model of the liquid-glass transition", *Physical Review A* **1984**, *29*, 2765.

[53] R. Zwanzig, *Nonequilibrium statistical mechanics*, Oxford University Press, USA, **2001**.

[54] J. Bouchaud, L. Cugliandolo, J. Kurchan, M. Mézard, "Mode-coupling approximations, glass theory and disordered systems", *Physica A: Statistical Mechanics and its Applications* **1996**, *226*, 243 –273.

[55] D. R. Reichman, P. Charbonneau, "Mode-coupling theory", *Journal of Statistical Mechanics: Theory and Experiment* **2005**, *2005*, P05013.

[56] T. R. Kirkpatrick, D. Thirumalai, "p-spin interaction spin-glass models: Connection with the structural glass problem", *Physical Review B* **1987**, *36*, 5388–5397.

[57] M. Mézard, G. Parisi, M. A. Virasoro, *Spin glass theory and beyond*, *Vol. v. 9*, World Scientific, Singapore, **1987**.

[58] D. J. Gross, M. Mézard, "The simplest spin glass", *Nucl. Phys. B* **1984**, *240*, 431.

[59] T. R. Kirkpatrick, P. G. Wolynes, "Connections between some kinetic and equilibrium theories of the glass transition", *Phys. Rev. A* **1987**, *35*, 3072–3080.

[60] T. R. Kirkpatrick, P. G. Wolynes, "Stable and metastable states in mean-field Potts and structural glasses", *Phys. Rev. B* **1987**, *36*, 8552–8564.

[61] T. R. Kirkpatrick, D. Thirumalai, "Comparison between dynamical theories and metastable states in regular and glassy mean-field spin models with underlying first-order-like phase transitions", *Phys. Rev. A* **1988**, *37*, 4439–4448.

[62] T. R. Kirkpatrick, D. Thirumalai, P. G. Wolynes, "Scaling concepts for the dynamics of viscous liquids near an ideal glassy state", *Phys. Rev. A* **1989**, *40*, 1045–1054.

[63] A. Crisanti, H.-J. Sommers, "The spherical p-spin interaction spin glass model: the statics", English, *Zeitschrift für Physik B* **1992**, *87*, 341–354.

[64] A. Crisanti, H. Horner, H. J. Sommers, "The spherical p-spin interaction spin-glass model - the dynamics", *Zeitschrift für Physik B* **1993**, *92*, 257–261.

[65] A. Cavagna, I. Giardina, G. Parisi, "Stationary points of the Thouless-Anderson-Palmer free energy", *Phys. Rev. B* **1998**, *57*, 11251–11257.

[66] T. Castellani, A. Cavagna, "Spin-Glass theory for pedestrians", *Journal of Statistical Mechanics: Theory and Experiment* **2005**, *2005*, P05012.

[67] T. Maimbourg, J. Kurchan, F. Zamponi, "Solution of the dynamics of liquids in the large-dimensional limit", *arXiv preprint arXiv:1507.03421* **2015**.

[68] A. Andreanov, G. Biroli, J.-P. Bouchaud, "Mode coupling as a Landau theory of the glass transition", *Europhysics Letters* **2009**, *88*, 16001.

[69] S. Franz, G. Parisi, F. Ricci-Tersenghi, T. Rizzo, "Field theory of fluctuations in glasses", *The European Physical Journal E: Soft Matter and Biological Physics* **2011**, *34*, 1–17.

[70] M. Goldstein, "Viscous Liquids and the Glass Transition: A Potential Energy Barrier Picture", *The Journal of Chemical Physics* **1969**, *51*, 3728–3739.

[71] T. B. Schrøder, S. Sastry, J. C. Dyre, S. C. Glotzer, "Crossover to potential energy landscape dominated dynamics in a model glass-forming liquid", *The Journal of Chemical Physics* **2000**, *112*, 9834–9840.

[72] A. Sokolov, "The glass transition: general scenario and crossover temperature", *Journal of non-crystalline solids* **1998**, *235*, 190–195.

[73] A. Cavagna, I. Giardina, G. Parisi, "Role of saddles in mean-field dynamics above the glass transition", *Journal of Physics A: Mathematical and General* **2001**, *34*, 5317.

[74] L Angelani et al., "Saddles in the energy landscape probed by supercooled liquids", *Physical review letters* **2000**, *85*, 5356.

[75] K. Broderix et al., "Energy landscape of a Lennard-Jones liquid: statistics of stationary points", *Physical review letters* **2000**, *85*, 5360.

[76] T. S. Grigera, A. Cavagna, I. Giardina, G. Parisi, "Geometric approach to the dynamic glass transition", *Physical review letters* **2002**, *88*, 055502.

[77] G. Biroli, R. Monasson, "From inherent structures to pure states: Some simple remarks and examples", *EPL (Europhysics Letters)* **2000**, *50*, 155.

[78] W. Kauzmann, "The glassy state and the behaviour of liquids at low temperature", *Chem Rev* **1948**, *43*, 219–256.

[79] B. J. Alder, T. E. Wainwright, "Phase Transition for a Hard Sphere System", *The Journal of Chemical Physics* **1957**, *27*, 1208–1209.

[80] L.-M. Martinez, C. Angell, "A thermodynamic connection to the fragility of glass-forming liquids", *Nature* **2001**, *410*, 663–667.

[81] P. G. Debenedetti, F. H. Stillinger, "Supercooled liquids and the glass transition", *Nature* **2001**, *410*, 259–267.

[82] H. Tanaka, "Relation between thermodynamics and kinetics of glass-forming liquids", *Physical review letters* **2003**, *90*, 055701.

[83] F. H. Stillinger, "Supercooled liquids, glass transitions, and the Kauzmann paradox", *The Journal of chemical physics* **1988**, *88*, 7818–7825.

[84] J. P. Garrahan, "Transition in coupled replicas may not imply a finite-temperature ideal glass transition in glass-forming systems", *Phys. Rev. E* **2014**, *89*, 030301.

[85] M. Talagrand, "Rigorous low-temperature results for the mean field p-spins interaction model", *Probability Theory and Related Fields* **2000**, *117*, 303–360.

[86] C. M. Bender, S. A. Orszag, *Advanced Mathematical Methods for Scientists and Engineers I*, Springer Science & Business Media, **1999**.

[87] T. Rizzo, "Long-wavelength fluctuations lead to a model of the glass crossover", *EPL (Europhysics Letters)* **2014**, *106*, 56003.

[88] V. Lubchenko, P. G. Wolynes, "Theory of Structural Glasses and Supercooled Liquids", *Annual Review of Physical Chemistry* **2007**, *58*, 235–266.

[89] G. Adam, J. H. Gibbs, "On the temperature dependence of cooperative relaxation properties in glass-forming liquids", *The journal of chemical physics* **1965**, *43*, 139–146.

[90] B. Gaveau, L. Schulman, "Theory of nonequilibrium first-order phase transitions for stochastic dynamics", *Journal of Mathematical Physics* **1998**, *39*, 1517–1533.

[91] G. Biroli, J. Kurchan, "Metastable states in glassy systems", *Physical Review E* **2001**, *64*, 016101.

[92] J. P. Bouchaud, G. Biroli, "On the Adam-Gibbs-Kirkpatrick-Thirumalai-Wolynes scenario for the viscosity increase in glasses", *J. Chem. Phys.* **2004**, *121*, 7347.

[93] G. Biroli et al., "Thermodynamic signature of growing amorphous order in glass-forming liquids", *Nature Physics* **2008**, *4*, 771–775.

[94] M. Mezard, G. Parisi in Structural Glasses and Supercooled Liquids: Theory, Experiment and Applications, (Eds.: P.G.Wolynes, V.Lubchenko), Wiley & Sons, **2012**.

[95] P. G. Wolynes, V. Lubchenko, *Structural Glasses and Supercooled Liquids: Theory, Experiment, and Applications*, John Wiley & Sons, **2012**.

[96] P. Debenedetti, *Metastable liquids: concepts and principles*, Princeton Univ Press, **1996**.

[97] F. Sciortino, "Potential energy landscape description of supercooled liquids and glasses", *Journal of Statistical Mechanics: Theory and Experiment* **2005**, *2005*, P05015.

[98] D. Chandler, J. P. Garrahan, "Dynamics on the Way to Forming Glass: Bubbles in Space-Time", *Annual Review of Physical Chemistry* **2010**, *61*, PMID: 20055676, 191–217.

[99] F. Ritort, P. Sollich, "Glassy dynamics of kinetically constrained models", *Advances in Physics* **2003**, *52*, 219–342.

[100] J. Garrahan, P. Sollich, C. Toninelli in Dynamical Heterogeneities and Glasses, (Eds.: L. Berthier et al.), Oxford University Press, **2011**.

[101] S. H. Glarum, "Dielectric relaxation of isoamyl bromide", *The Journal of Chemical Physics* **1960**, *33*, 639–643.

[102] W. Kob, H. C. Andersen, "Kinetic lattice-gas model of cage effects in high-density liquids and a test of mode-coupling theory of the ideal-glass transition", *Physical Review E* **1993**, *48*, 4364.

[103] G. H. Fredrickson, H. C. Andersen, "Kinetic ising model of the glass transition", *Physical review letters* **1984**, *53*, 1244.

[104] J Jäckle, S Eisinger, "A hierarchically constrained kinetic ising model", *Zeitschrift für Physik B Condensed Matter* **1991**, *84*, 115–124.

[105] C. Toninelli, G. Biroli, D. S. Fisher, "Jamming percolation and glass transitions in lattice models", *Physical review letters* **2006**, *96*, 035702.

[106] L. Berthier, J. P. Garrahan, "Real space origin of temperature crossovers in supercooled liquids", *Physical Review E* **2003**, *68*, 041201.

[107] P. Harrowell, "Visualizing the collective motions responsible for the α and β relaxations in a model glass", *Physical Review E* **1993**, *48*, 4359.

[108] S Franz, R Mulet, G Parisi, "Kob-Andersen model: A nonstandard mechanism for the glassy transition", *Physical Review E* **2002**, *65*, 021506.

[109] Y. Jung, J. P. Garrahan, D. Chandler, "Excitation lines and the breakdown of Stokes-Einstein relations in supercooled liquids", *Physical Review E* **2004**, *69*, 061205.

[110] R Candelier, O Dauchot, G Biroli, "Dynamical facilitation decreases when approaching the granular glass transition", *EPL (Europhysics Letters)* **2010**, *92*, 24003.

[111] J. P. Garrahan, "Glassiness through the emergence of effective dynamical constraints in interacting systems", *Journal of Physics: Condensed Matter* **2002**, *14*, 1571.

[112] G. Tarjus, S. A. Kivelson, Z Nussinov, P. Viot, "The frustration-based approach of supercooled liquids and the glass transition: a review and critical assessment", *Journal of Physics: Condensed Matter* **2005**, *17*, R1143.

[113] F. Frank, "Supercooling of liquids", *Proceedings of the Royal Society of London. Series A Mathematical and Physical Sciences* **1952**, 43–46.

[114] D. Kivelson et al., "A thermodynamic theory of supercooled liquids", *Physica A: Statistical Mechanics and its Applications* **1995**, *219*, 27–38.

[115] P. Viot, G. Tarjus, D. Kivelson, "A heterogeneous picture of α relaxation for fragile supercooled liquids", *The Journal of Chemical Physics* **2000**, *112*, 10368–10378.

[116] D. R. Nelson, *Defects and geometry in condensed matter physics*, Cambridge University Press, **2002**.

[117] L Chayes et al., "Avoided critical behavior in a uniformly frustrated system", *Physica A: Statistical Mechanics and its Applications* **1996**, *225*, 129–153.

[118] S. Brazovskii, "Phase transition of an isotropic system to a nonuniform state", *Zh. Eksp. Teor. Fiz* **1975**, *68*, 175.

[119] C. P. Royall, S. R. Williams, "The role of local structure in dynamical arrest", *Physics Reports* **2015**, *560*, 1–75.

[120] S Mossa, G Tarjus, "An operational scheme to determine the locally preferred structure of model liquids", *Journal of non-crystalline solids* **2006**, *352*, 4847–4850.

[121] D Coslovich, G Pastore, "Understanding fragility in supercooled Lennard-Jones mixtures. I. Locally preferred structures", *The Journal of chemical physics* **2007**, *127*, 124504.

[122] H. Tanaka, "Bond orientational order in liquids: Towards a unified description of water-like anomalies, liquid-liquid transition, glass transition, and crystallization", *The European Physical Journal E* **2012**, *35*, 1–84.

[123] F. Sausset, G. Tarjus, P. Viot, "Tuning the fragility of a glass-forming liquid by curving space", *Physical review letters* **2008**, *101*, 155701.

[124] J. Schmalian, P. G. Wolynes, "Stripe Glasses: Self-Generated Randomness in a Uniformly Frustrated System", *Phys. Rev. Lett.* **2000**, *85*, 836–839.

[125] L. Struik, *Physical aging in polymers and other amorphous materials*, Elsevier, Amsterdam, **1978**.

[126] A. Kovacs, "Glass transition in amorphous polymers: a phenomenological study", *Adv. Polym. Sci* **1963**, *3*, 394–508.

[127] A. Q. Tool, "Relation between inelastic deformability and thermal expansion of glass in its annealing range", *Journal of the American Ceramic society* **1946**, *29*, 240–253.

[128] G. Parisi, F. Sciortino, "Structural glasses: Flying to the bottom", *Nature materials* **2013**, *12*, 94–95.

[129] S. F. Swallen et al., "Organic glasses with exceptional thermodynamic and kinetic stability", *Science* **2007**, *315*, 353–356.

[130] S. Singh, M. Ediger, J. J. de Pablo, "Ultrastable glasses from in silico vapour deposition", *Nature Materials* **2013**, *12*, 139–144.

[131] S. Singh, M. Ediger, J. J. de Pablo, "Corrigendum: Ultrastable glasses from in silico vapour deposition", *Nature materials* **2014**, *13*, 662–662.

[132] I. Lyubimov, M. D. Ediger, J. J. de Pablo, "Model vapor-deposited glasses: Growth front and composition effects", *The Journal of chemical physics* **2013**, *139*, 144505.

[133] A. Sepúlveda et al., "Role of Fragility in the Formation of Highly Stable Organic Glasses", *Phys. Rev. Lett.* **2014**, *113*, 045901.

[134] G. D. Scott, D. M. Kilgour, "The density of random close packing of spheres", *Brit. J. Appl. Phys.* **1969**, *2*, 863.

[135] B. D. Lubachevsky, F. H. Stillinger, "Geometric properties of random disk packings", *J. Stat. Phys.* **1990**, *60*, 561–583.

[136] C. S. O'Hern, S. A. Langer, A. J. Liu, S. R. Nagel, "Random Packings of Frictionless Particles", *Phys. Rev. Lett.* **2002**, *88*, 075507.

[137] C. S. O'Hern, L. E. Silbert, A. J. Liu, S. R. Nagel, "Jamming at zero temperature and zero applied stress: The epitome of disorder", *Phys. Rev. E* **2003**, *68*, 011306.

[138] S. Torquato, F. H. Stillinger, "Jammed hard-particle packings: From Kepler to Bernal and beyond", *Rev. Mod. Phys.* **2010**, *82*, 2633–2672.

[139] M. Van Hecke, "Jamming of soft particles: geometry, mechanics, scaling and isostaticity", *Journal of Physics: Condensed Matter* **2010**, *22*, 033101.

[140] M. Skoge, A. Donev, F. H. Stillinger, S. Torquato, "Packing hyperspheres in high-dimensional Euclidean spaces", *Physical Review E (Statistical Nonlinear and Soft Matter Physics)* **2006**, *74*, 041127.

[141] P. Chaudhuri, L. Berthier, S. Sastry, "Jamming Transitions in Amorphous Packings of Frictionless Spheres Occur over a Continuous Range of Volume Fractions", *Phys. Rev. Lett.* **2010**, *104*, 165701.

[142] C. F. Moukarzel, "Isostatic Phase Transition and Instability in Stiff Granular Materials", *Phys. Rev. Lett.* **1998**, *81*, 1634–1637.

[143] J.-N. Roux, "Geometric origin of mechanical properties of granular materials", *Phys. Rev. E* **2000**, *61*, 6802–6836.

[144] J. C. Maxwell, "L. on the calculation of the equilibrium and stiffness of frames", *The London Edinburgh and Dublin Philosophical Magazine and Journal of Science* **1864**, *27*, 294–299.

[145] E. Lerner, G. During, M. Wyart, "Low-energy non-linear excitations in sphere packings", *Soft Matter* **2013**, *9*, 8252–8263.

[146] P. Charbonneau, E. I. Corwin, G. Parisi, F. Zamponi, "Universal Microstructure and Mechanical Stability of Jammed Packings", *Phys. Rev. Lett.* **2012**, *109*, 205501.

[147] P. Charbonneau, E. I. Corwin, G. Parisi, F. Zamponi, "Jamming Criticality Revealed by Removing Localized Buckling Excitations", *Phys. Rev. Lett.* **2015**, *114*, 125504.

[148] M. Wyart, "Marginal Stability Constrains Force and Pair Distributions at Random Close Packing", *Phys. Rev. Lett.* **2012**, *109*, 125502.

[149] A. Ikeda, L. Berthier, G. Biroli, "Dynamic criticality at the jamming transition", *J. Chem. Phys.* **2013**, *138*, 12A507.

[150] L. Silbert, A. Liu, S. Nagel, "Vibrations and Diverging Length Scales Near the Unjamming Transition", *Physical Review Letters* **2005**, *95*, 098301.

[151] M. Wyart, S. Nagel, T. Witten, "Geometric origin of excess low-frequency vibrational modes in weakly connected amorphous solids", *Europhysics Letters* **2005**, *72*, 486–492.

[152] C. Brito, M. Wyart, "Geometric interpretation of previtrification in hard sphere liquids", *The Journal of Chemical Physics* **2009**, *131*, 024504.

[153] G. Parisi, F. Zamponi, "Mean-field theory of hard sphere glasses and jamming", *Rev. Mod. Phys.* **2010**, *82*, 789–845.

[154] J. Kurchan, G. Parisi, F. Zamponi, "Exact theory of dense amorphous hard spheres in high dimension. I. The free energy", *JSTAT* **2012**, *2012*, P10012.

[155] J. Kurchan, G. Parisi, P. Urbani, F. Zamponi, "Exact Theory of Dense Amorphous Hard Spheres in High Dimension. II. The High Density Regime and the Gardner Transition", *J. Phys. Chem. B* **2013**, *117*, 12979–12994.

[156] P. Charbonneau et al., "Exact theory of dense amorphous hard spheres in high dimension. III. The full replica symmetry breaking solution", *JSTAT* **2014**, *2014*, P10009.

[157] L. F. Cugliandolo, J. Kurchan, "Analytical solution of the off-equilibrium dynamics of a long-range spin-glass model", *Physical Review Letters* **1993**, *71*, 173–176.

[158] J. Kurchan, L. Laloux, "Phase space geometry and slow dynamics", *Journal of Physics A: Mathematical and General* **1996**, *29*, 1929.

[159] L. F. Cugliandolo, J. Kurchan, L. Peliti, "Energy flow, partial equilibration, and effective temperatures in systems with slow dynamics", *Physical Review E* **1997**, *55*, 3898.

[160] S Franz, M. A. Virasoro, "Quasi-equilibrium interpretation of ageing dynamics", *Journal of Physics A: Mathematical and General* **2000**, *33*, 891.

[161] J.-L. Barrat, W. Kob, "Aging and the fluctuation dissipation ratio in a Lennard-Jones fluid", *Journal of Physics: Condensed Matter* **1999**, *11*, A247.

[162] L. Berthier, "Efficient measurement of linear susceptibilities in molecular simulations: Application to aging supercooled liquids", *Physical review letters* **2007**, *98*, 220601.

[163] J. Kurchan, "In and out of equilibrium", *Nature* **2005**, *433*, 222–225.

[164] A Crisanti, F Ritort, "Violation of the fluctuation–dissipation theorem in glassy systems: basic notions and the numerical evidence", *Journal of Physics A: Mathematical and General* **2003**, *36*, R181.

[165] N. Greinert, T. Wood, P. Bartlett, "Measurement of effective temperatures in an aging colloidal glass", *Physical review letters* **2006**, *97*, 265702.

[166] A Barrat, R Burioni, M Mézard, "Dynamics within metastable states in a mean-field spin glass", *Journal of Physics A: Mathematical and General* **1996**, *29*, L81.

[167] G. Biroli, "Dynamical TAP approach to mean field glassy systems", *Journal of Physics A: Mathematical and General* **1999**, *32*, 8365.

[168] S. Léonard et al., "Non-equilibrium dynamics of spin facilitated glass models", *Journal of Statistical Mechanics: Theory and Experiment* **2007**, *2007*, P07017.

[169] P. Mayer et al., "Activated aging dynamics and negative fluctuation-dissipation ratios", *Physical review letters* **2006**, *96*, 030602.

[170] A. S. Keys, J. P. Garrahan, D. Chandler, "Calorimetric glass transition explained by hierarchical dynamic facilitation", *Proceedings of the National Academy of Sciences* **2013**, *110*, 4482–4487.

[171] A. Liu, S. Nagel, *Jamming and Rheology: Constrained Dynamics on Microscopic and Macroscopic Scales*, Taylor & Francis, **2001**.

[172] D. Rodney, A. Tanguy, D. Vandembroucq, "Modeling the mechanics of amorphous solids at different length scale and time scale", *Modelling and Simulation in Materials Science and Engineering* **2011**, *19*, 083001.

[173] A. Ikeda, L. Berthier, P. Sollich, "Unified study of glass and jamming rheology in soft particle systems", *Phys. Rev. Lett.* **2012**, *109*, 018301.

[174] C. Maloney, A. Lemaître, "Amorphous systems in athermal, quasistatic shear", *Phys. Rev. E* **2006**, *74*, 016118.

[175] A. Nicolas, K. Martens, J.-L. Barrat, "Rheology of athermal amorphous solids: Revisiting simplified scenarios and the concept of mechanical noise temperature", *EPL (Europhysics Letters)* **2014**, *107*, 44003.

[176] A. Nicolas, K. Martens, L. Bocquet, J.-L. Barrat, "Universal and non-universal features in coarse-grained models of flow in disordered solids", *Soft Matter* **2014**, *10*, 4648–4661.

[177] R. G. Larson, *The structure and rheology of complex fluids*, *Vol. 33*, Oxford university press New York, **1999**.

[178] V. Dailidonis, V. Ilyin, P. Mishra, I. Procaccia, "Mechanical properties and plasticity of a model glass loaded under stress control", *Physical Review E* **2014**, *90*, 052402.

[179] H. Princen, A. Kiss, "Rheology of foams and highly concentrated emulsions: IV. An experimental study of the shear viscosity and yield stress of concentrated emulsions", *Journal of colloid and interface science* **1989**, *128*, 176–187.

[180] A. Lemaître, C. Caroli, "Rate-dependent avalanche size in athermally sheared amorphous solids", *Physical review letters* **2009**, *103*, 065501.

[181] L. Berthier, J.-L. Barrat, J. Kurchan, "A two-time-scale, two-temperature scenario for nonlinear rheology", *Phys. Rev. E* **2000**, *61*, 5464–5472.

[182] N. Koumakis et al., "Yielding of hard-sphere glasses during start-up shear", *Phys.Rev.Lett.* **2012**, *108*, 098303.

[183] G. Petekidis, D. Vlassopoulos, P. N. Pusey, "Yielding and flow of colloidal glasses", *Faraday Discuss.* **2003**, *123*, 287–302.

[184] M Laurati, S. Egelhaaf, G Petekidis, "Nonlinear rheology of colloidal gels with intermediate volume fraction", *Journal of Rheology (1978-present)* **2011**, *55*, 673–706.

[185] Y. Wang, S.-Q. Wang, "Exploring stress overshoot phenomenon upon startup deformation of entangled linear polymeric liquids", *Journal of Rheology (1978-present)* **2009**, *53*, 1389–1401.

[186] M. Falk, J. Langer, L Pechenik, "Thermal effects in the shear-transformation-zone theory of amorphous plasticity: comparisons to metallic glass data", *Physical Review E* **2004**, *70*, 011507.

[187] O. Reynolds, "On the dilatancy of media composed of rigid particles. With experimental illustrations", *Philosophical magazine* **1885**, *20*, 469–481.

[188] B. P. Tighe, "Shear dilatancy in marginal solids", *Granular Matter* **2014**, *16*, 203–208.

[189] S. Karmakar, E. Lerner, I. Procaccia, J. Zylberg, "Statistical physics of elastoplastic steady states in amorphous solids: Finite temperatures and strain rates", *Physical Review E* **2010**, *82*, 031301.

[190] A. Lemaître, C. Maloney, "Sum rules for the quasi-static and visco-elastic response of disordered solids at zero temperature", *Journal of statistical physics* **2006**, *123*, 415–453.

[191] L. D. Landau, E. M. Lifshitz, *Course of Theoretical Physics Vol 7: Theory of Elasticity*, Pergamon Press, **1959**.

[192] M. Born, K. Huang, *Dynamical theory of crystal lattices*, Oxford university press, **1998**.

[193] A. Heuer, "Exploring the potential energy landscape of glass-forming systems: from inherent structures via metabasins to macroscopic transport", *Journal of Physics: Condensed Matter* **2008**, *20*, 373101.

[194] V. Ilyin, I. Procaccia, C. Shor, M. Singh, "The yield of Amorphous Solids Under Stress Control at Low Temperatures", *ArXiv e-prints* **Apr. 2015**.

[195] S. Karmakar, E. Lerner, I. Procaccia, "Statistical physics of the yielding transition in amorphous solids", *Phys. Rev. E* **2010**, *82*, 055103.

[196] J. Lin, E. Lerner, A. Rosso, M. Wyart, "Scaling description of the yielding transition in soft amorphous solids at zero temperature", *Proceedings of the National Academy of Sciences* **2014**, *111*, 14382–14387.

[197] D. Fiocco, G. Foffi, S. Sastry, "Oscillatory athermal quasistatic deformation of a model glass", *Physical Review E* **2013**, *88*, 020301.

[198] A. Argon, "Plastic deformation in metallic glasses", *Acta Metallurgica* **1979**, *27*, 47 –58.

[199] J. D. Eshelby, "The Determination of the Elastic Field of an Ellipsoidal Inclusion, and Related Problems", *Proceedings of the Royal Society of London A: Mathematical Physical and Engineering Sciences* **1957**, *241*, 376–396.

[200] H. G. E. Hentschel, S. Karmakar, E. Lerner, I. Procaccia, "Do athermal amorphous solids exist?", *Phys. Rev. E* **2011**, *83*, 061101.

[201] C. Maloney, A. Lemaître, "Subextensive Scaling in the Athermal, Quasistatic Limit of Amorphous Matter in Plastic Shear Flow", *Phys. Rev. Lett.* **2004**, *93*, 016001.

[202] G. I. Taylor, "The Mechanism of Plastic Deformation of Crystals. Part I. Theoretical", *Proceedings of the Royal Society of London A: Mathematical Physical and Engineering Sciences* **1934**, *145*, 362–387.

[203] O. Gendelman et al., "Shear Transformation Zones: State determined or protocol dependent?", *EPL (Europhysics Letters)* **2015**, *109*, 16002.

[204] M. L. Manning, A. J. Liu, "Vibrational Modes Identify Soft Spots in a Sheared Disordered Packing", *Phys. Rev. Lett.* **2011**, *107*, 108302.

[205] W. L. Johnson, "Bulk glass-forming metallic alloys: Science and technology", *MRS bulletin* **1999**, *24*, 42–56.

[206] M. Ashby, A. Greer, "Metallic glasses as structural materials", *Scripta Materialia* **2006**, *54*, 321–326.

[207] R. Dasgupta, H. G. E. Hentschel, I. Procaccia, "Microscopic Mechanism of Shear Bands in Amorphous Solids", *Phys. Rev. Lett.* **2012**, *109*, 255502.

[208] R. Dasgupta et al., "Shear localization in three-dimensional amorphous solids", *Phys. Rev. E* **2013**, *88*, 032401.

[209] K. Miyazaki, D. R. Reichman, "Molecular hydrodynamic theory of supercooled liquids and colloidal suspensions under shear", *Phys. Rev. E* **2002**, *66*, 050501.

[210] M. Fuchs, M. E. Cates, "A mode coupling theory for Brownian particles in homogeneous steady shear flow", *Journal of Rheology (1978-present)* **2009**, *53*, 957–1000.

[211] J. M. Brader, M. E. Cates, M. Fuchs, "First-Principles Constitutive Equation for Suspension Rheology", *Phys. Rev. Lett.* **2008**, *101*, 138301.

[212] J. M. Brader et al., "Glass rheology: From mode-coupling theory to a dynamical yield criterion", *Proceedings of the National Academy of Sciences* **2009**, *106*, 15186–15191.

[213] K. Miyazaki, H. M. Wyss, D. A. Weitz, D. R. Reichman, "Nonlinear viscoelasticity of metastable complex fluids", *EPL (Europhysics Letters)* **2006**, *75*, 915.

[214] H. Yoshino, M. Mézard, "Emergence of Rigidity at the Structural Glass Transition: A First-Principles Computation", *Phys. Rev. Lett.* **2010**, *105*, 015504.

[215] H. Yoshino, F. Zamponi, "Shear modulus of glasses: Results from the full replica-symmetry-breaking solution", *Physical Review E* **2014**, *90*, 022302.

[216] H. Yoshino, "Replica theory of the rigidity of structural glasses", *The Journal of Chemical Physics* **2012**, *136*, 214108.

[217] P. Sollich, F. Lequeux, P. Hébraud, M. E. Cates, "Rheology of soft glassy materials", *Physical review letters* **1997**, *78*, 2020.

[218] P. Sollich, "Rheological constitutive equation for a model of soft glassy materials", *Physical Review E* **1998**, *58*, 738.

[219] J.-P. Bouchaud, "Weak ergodicity breaking and aging in disordered systems", *Journal de Physique I* **1992**, *2*, 1705–1713.

[220] C. Monthus, J.-P. Bouchaud, "Models of traps and glass phenomenology", *Journal of Physics A: Mathematical and General* **1996**, *29*, 3847.

[221] M. L. Falk, J. S. Langer, "Dynamics of viscoplastic deformation in amorphous solids", *Phys. Rev. E* **1998**, *57*, 7192–7205.

[222] P. Hébraud, F. Lequeux, "Mode-Coupling Theory for the Pasty Rheology of Soft Glassy Materials", *Phys. Rev. Lett.* **1998**, *81*, 2934–2937.

[223] G. Picard, A. Ajdari, F. Lequeux, L. Bocquet, "Slow flows of yield stress fluids: Complex spatiotemporal behavior within a simple elastoplastic model", *Phys. Rev. E* **2005**, *71*, 010501.

[224] V. V. Bulatov, A. S. Argon, "A stochastic model for continuum elasto-plastic behavior. I. Numerical approach and strain localization", *Modelling and Simulation in Materials Science and Engineering* **1994**, *2*, 167.

[225] L. Berthier, "Trend: Dynamic Heterogeneity in Amorphous Materials", *Physics* **2011**, *4*, 42.

[226] R. Monasson, "Structural Glass Transition and the Entropy of the Metastable States", *Phys. Rev. Lett.* **1995**, *75*, 2847–2850.

[227] F. Zamponi, "Mean field theory of spin glasses", *ArXiv e-prints* **Aug. 2010**.

[228] A. Lopatin, L. Ioffe, "Structural glass on a lattice in the limit of infinite dimensions", *Physical Review B* **2002**, *66*, 174202.

[229] A. Montanari, F. Ricci-Tersenghi, "Cooling-schedule dependence of the dynamics of mean-field glasses", *Phys. Rev. B* **2004**, *70*, 134406.

[230] M. Mézard, A. Montanari, *Information, Physics, and Computation*, Oxford University Press, Inc., New York, NY, USA, **2009**.

[231] M. Mézard, G. Parisi, "A first-principle computation of the thermodynamics of glasses", *The Journal of Chemical Physics* **1999**, *111*, 1076–1095.

[232] M. Mézard, G. Parisi, "Thermodynamics of Glasses: A First Principles Computation", *Phys. Rev. Lett.* **1999**, *82*, 747–750.

[233] H. Abramowitz, I. Segun, *Handbook of Mathematical Functions*, Dover, New York, **1965**.

[234] H. Ritland, "Limitations of the fictive temperature concept", *Journal of the American Ceramic Society* **1956**, *39*, 403–406.

[235] S. Franz, G. Parisi, "Recipes for Metastable States in Spin Glasses", *J. Phys. I France* **1995**, *5*, 1401–1415.

[236] A. Barrat, S. Franz, G. Parisi, "Temperature evolution and bifurcations of metastable states in mean-field spin glasses, with connections with structural glasses", *Journal of Physics A: Mathematical and General* **1997**, *30*, 5593–5612.

[237] F. Krzakala, L. Zdeborová, "Following Gibbs states adiabatically - The energy landscape of mean-field glassy systems", *EPL* **2010**, *90*, 66002.

[238] L. Zdeborová, F. Krzakala, "Generalization of the cavity method for adiabatic evolution of Gibbs states", *Phys. Rev. B* **2010**, *81*, 224205.

[239] F. Krzakala, L. Zdeborová, "Performance of simulated annealing in p-spin glasses", *Journal of Physics: Conference Series* **2013**, *473*, 12022–12028.

[240] A. Cavagna, I. Giardina, G. Parisi, "Structure of metastable states in spin glasses by means of a three replica potential", *Journal of Physics A: Mathematical and General* **1997**, *30*, 4449.

[241] F. Krzakala, J. Kurchan, "Landscape analysis of constraint satisfaction problems", *Physical Review E* **2007**, *76*, 021122.

[242] S. Franz, G. Parisi, P. Urbani, "Quasi-equilibrium in glassy dynamics: a liquid theory approach", *Journal of Physics A: Mathematical and Theoretical* **2015**, *48*, 19FT01.

[243] S. Franz, G. Parisi, "Quasi-equilibrium in glassy dynamics: an algebraic view", *Journal of Statistical Mechanics: Theory and Experiment* **2013**, *2013*, P02003.

[244] Y. Sun et al., "Following states in temperature in the spherical s+ p-spin glass model", *Journal of Statistical Mechanics: Theory and Experiment* **2012**, *2012*, P07002.

[245] G. Szamel, "Dynamic glass transition: Bridging the gap between mode-coupling theory and the replica approach", *EPL (Europhysics Letters)* **2010**, *91*, 56004.

[246] G. Parisi, "A sequence of approximated solutions to the S-K model for spin glasses", *Journal of Physics A: Mathematical and General* **1980**, *13*, L115.

[247] A. J. Bray, M. A. Moore, "Evidence for massless modes in the 'solvable model' of a spin glass", *Journal of Physics C: Solid State Physics* **1979**, *12*, L441.

[248] U. Ferrari, L. Leuzzi, G. Parisi, T. Rizzo, "Two-step relaxation next to dynamic arrest in mean-field glasses: Spherical and Ising p-spin model", *Phys. Rev. B* **2012**, *86*, 014204.

[249] E. Gardner, "Spin Glasses with p-Spin Interactions", *Nuclear Physics B* **1985**, *257*, 747–765.

[250] G. Parisi, "The order parameter for spin glasses: a function on the interval 0-1", *Journal of Physics A: Mathematical and General* **1980**, *13*, 1101.

[251] P. Charbonneau, A. Ikeda, G. Parisi, F. Zamponi, "Glass Transition and Random Close Packing above Three Dimensions", *Phys. Rev. Lett.* **2011**, *107*, 185702.

[252] D. Sherrington, S. Kirkpatrick, "Solvable Model of a Spin-Glass", *Physical Review Letters* **1975**, *35*, 1792–1796.

[253] D. J. Thouless, J. R. L. de Almeida, J. M. Kosterlitz, "Stability and susceptibility in Parisi's solution of a spin glass model", *Journal of Physics C: Solid State Physics* **1980**, *13*, 3271.

[254] M. Mézard, G. Parisi, "Replica field theory for random manifolds", *Journal de Physique I* **1991**, *1*, 809–836.

[255] G. Parisi, T. Rizzo, "Critical dynamics in glassy systems", *Phys. Rev. E* **2013**, *87*, 012101.

[256] S. Franz, G. Parisi, "On non-linear susceptibility in supercooled liquids", *Journal of Physics: Condensed Matter* **2000**, *12*, 6335.

[257] S. Franz et al., "Quantitative field theory of the glass transition", *Proceedings of the National Academy of Sciences* **2012**, *109*, 18725–18730.

[258] A. T. Ogielski, "Dynamics of three-dimensional Ising spin glasses in thermal equilibrium", *Physical Review B* **1985**, *32*, 7384.

[259] R. Mari, J. Kurchan, "Dynamical transition of glasses: From exact to approximate", *The Journal of Chemical Physics* **2011**, *135*, 124504.

[260] H. L. Frisch, J. K. Percus, "High dimensionality as an organizing device for classical fluids", *Phys. Rev. E* **1999**, *60*, 2942–2948.

[261] F. Krzakala, L. Zdeborová, "Hiding Quiet Solutions in Random Constraint Satisfaction Problems", *Phys. Rev. Lett.* **2009**, *102*, 238701.

[262] P. Charbonneau, Y. Jin, G. Parisi, F. Zamponi, "Hopping and the Stokes–Einstein relation breakdown in simple glass formers", *Proceedings of the National Academy of Sciences* **2014**, *111*, 15025–15030.

[263] T. Aspelmeier, R. A. Blythe, A. J. Bray, M. A. Moore, "Free-energy landscapes, dynamics, and the edge of chaos in mean-field models of spin glasses", *Phys. Rev. B* **2006**, *74*, 184411.

[264] G. Parisi, T. Rizzo, "Critical dynamics in glassy systems", *Phys. Rev. E* **2013**, *87*, 012101.

[265] R. L. Leheny, S. R. Nagel, "Frequency-domain study of physical aging in a simple liquid", *Physical Review B* **1998**, *57*, 5154.

[266] L. Bellon, S. Ciliberto, C. Laroche, "Memory in the aging of a polymer glass", *EPL (Europhysics Letters)* **2000**, *51*, 551.

[267] E. Witten, "Quarks, atoms, and the $1/N$ expansion", *Physics Today* **1980**, *33*, 38.

[268] M. C. Angelini, G. Biroli, "Super-Potts glass: A disordered model for glass-forming liquids", *Phys. Rev. B* **2014**, *90*, 220201.

[269] M. Cates, S. Ramaswamy, "Do current-density nonlinearities cut off the glass transition?", *Physical review letters* **2006**, *96*, 135701.

[270] P. Urbani, G. Biroli, "Gardner transition in finite dimensions", *Physical Review B* **2015**, *91*, 100202.

[271] T. S. Grigera, G. Parisi, "Fast Monte Carlo algorithm for supercooled soft spheres", *Physical Review E* **2001**, *63*, 045102.

[272] G. Combe, J.-N. Roux, "Strain versus stress in a model granular material: a Devil's staircase", *Physical Review Letters* **2000**, *85*, 3628.

[273] P. Le Doussal, M. Müller, K. J. Wiese, "Equilibrium avalanches in spin glasses", *Physical Review B* **2012**, *85*, 214402.

[274] P. Le Doussal, M. Müller, K. J. Wiese, "Avalanches in mean-field models and the Barkhausen noise in spin-glasses", *EPL (Europhysics Letters)* **2010**, *91*, 57004.

[275] S. N. Majumdar, M. Vergassola, "Large Deviations of the Maximum Eigenvalue for Wishart and Gaussian Random Matrices", *Phys. Rev. Lett.* **2009**, *102*, 060601.

[276] T. Rizzo, "Replica-symmetry-breaking transitions and off-equilibrium dynamics", *Phys. Rev. E* **2013**, *88*, 032135.

[277] J. Kurchan, T. Maimbourg, F. Zamponi, "To appear".

[278] B Duplantier, "Comment on Parisi's equation for the SK model for spin glasses", *Journal of Physics A: Mathematical and General* **1981**, *14*, 283.

[279] H.-J. Sommers, W. Dupont, "Distribution of frozen fields in the mean-field theory of spin glasses", *Journal of Physics C: Solid State Physics* **1984**, *17*, 5785.

[280] S. Franz, G. Parisi, "The simplest model of jamming", *ArXiv e-prints* **Jan. 2015**.